University of Nevada, Reno

STRATIGRAPHY OF THE SANDMAN LOW SULFIDATION AU DEPOSITS, WINNEMUCCA, NEVADA

A thesis submitted in partial fulfillment of the
requirements for the degree in Masters of Sciences in
Geology

by

Robert Mitchell Anderson Jr.

Dr. Tommy B. Thompson/Thesis Advisor

May 13, 2013

University of Nevada, Reno
Statewide • Worldwide

THE GRADUATE SCHOOL

We recommend that the thesis
prepared under our supervision by

ROBERT MITCHELL ANDERSON JR.

entitled

Stratigraphy of the Sandman Low Sulfidation Deposits, Winnemucca, Nevada

be accepted in partial fulfillment of the
requirements for the degree of

MASTER OF SCIENCE

Dr. Tommy B. Thompson, Advisor

Dr. Christopher D. Henry, Committee Member

Dr. Victor R. Vasquez , Graduate School Representative

Marsha H. Read, Ph. D., Dean, Graduate School

May, 2013

THESIS ABSTRACT

STRATIGRAPHY OF THE SANDMAN LOW SULFIDATION AU DEPOSITS, WINNEMUCCA, NEVADA

Newmont Mining Corporation's Sandman Au project consists of five recognized, mid-Miocene low-sulfidation epithermal deposits hosted primarily in mid-Tertiary volcanic, volcaniclastic, and fluvial rocks, and to a lesser degree within basement Triassic rocks and late Mesozoic intrusions. These deposits include North Hill, Silica Ridge, Southeast Pediment, Abel Knoll and Ten Mile. Hosted entirely within mid-Tertiary volcanic, epiclastic, and fluvial rocks, the deposits of North Hill, Silica Ridge, and Southeast Pediment are both structurally and stratigraphically controlled. Abel Knoll is hosted within a mid-Tertiary polylithic breccia body composed of trachy-andesite to andesite, basement phyllites and trace granodiorite, and tuffaceous wall rocks. In the southeast of the project area, the Ten Mile deposit is structurally controlled and hosted dominantly within a late Mesozoic granodiorite stock.

Excluding the Ten Mile deposit, which is controlled by northeast-striking faults, deposits occur along north to north-northwest extensional structures. Intersections with northeast structures and the presence of Early Miocene mafic dikes also played a role as fluid conduits. Post-mineral structural offset affects all deposits. Older fault reactivation and movement along younger Basin and Range structures resulted in the development of north-south-striking grabens and half grabens and lesser intervening northeast grabens.

Basement lithologies consist of Triassic metasedimentary rocks dominated by phyllitic mudstones and siltstones with lesser degrees of quartzites and rare limestone units interbedded. Regional foliations strike northeast and dip moderately to the northwest. Basement rocks have been intruded by late Mesozoic granitic stocks to the east and southeast of the project in addition to local diking in phyllites on the flanks of Blue Mountain to the west. Lying unconformably on basement rocks is an approximately 700->1300 foot thick package of Tertiary volcanic, epiclastic, and fluvial rocks. Lithologies consist of northeast striking, gently southeast dipping dacitic to rhyolitic airfall tuffs, pyroclastics and distally sourced ash flow tuffs with interbedded fluvial and lacustrine volcaniclastic siltstones, sandstones, and conglomerates. The presence of thick, distally sourced fluvial rocks in the northern portions of the property represent a major east-west (?) Oligocene to early Miocene paleodrainage. These rocks may be related to the inferred Cretaceous age Pansy Lee Conglomerate to the east, although this remains to be definitively proved. Additionally, further to the south drill intercepts have encountered approximately two hundred feet of organic and sulfur-rich, varved and laminated lacustrine sediments. Early Miocene basaltic trachy-andesite, trachy-andesite, and andesite sills and dikes intrude and cap the Sandman stratigraphic section.

Subtle topography limits outcrop exposures of mid-Tertiary rocks to capping mafic flows within the Basalt and Little Basalt Hills and more resistant quartz-adularia altered ridges occurring in the northwest of the Sandman project area. Additionally, extensive Quaternary deposits of the Crescent Dune Field cover much of the northern part of the property. Three field seasons were spent mapping surface exposures and trenches and logging drill core and reverse circulation chips from the project area leading to the

recognition of three distinct tuff units within the Sandman stratigraphic section. Petrography, trace element geochemistry, and radiometric age dating was used to create a detailed stratigraphic column linking variable stratigraphy from deposit to deposit.

Within the northwest of the property, mapping and drilling has indicated a paleodrainage-controlled, marker fiamme unit—dated at ~25.4 Ma—linking the stratigraphic section across Silica Ridge, Adularia Hill, and North Hill. Outcrop appearance with abundant large fiamme, a sparse phenocryst assemblage of sanidine-plagioclase-anorthoclase-beta quartz-biotite, radiometric age dating, and trace element geochemistry confirm this marker fiamme unit to be the regionally widespread rhyolitic Nine Hill Tuff. Named for the type locality in the Sierra Nevada foothills just north of Carson City, this pyroclastic unit is widespread and has been correlated with the "D" unit of the Bates Mountain Tuff in central Nevada near Austin. The Sandman project area is the furthest north documented location of the Nine Hill Tuff. No source caldera has yet been identified, though through regional distribution it has been suggested to lie beneath sediments within the Carson Sink.

Lower in section, a distinctive rhyolite tuff with coarse-grained sanidine-anorthoclase crystal fragments and abundant pumice ± fiamme has been dated at ~26.0 Ma. With a similar age, the Ashdown tuff—exposed to the west of the Sandman project in the Pine Forest and Black Ranges—is petrographically similar with abundant coarse-grained sanidine and pumice fragments; however, the two have differing trace element geochemistry, with the Ashdown Tuff being significantly enriched in Zr and Nb compared to the unnamed tuff found in outcrop at Adularia Hill and encountered in drill core at Silica Ridge and Southeast Pediment.

A dacitic to rhyolitic tuff of older—but unconfirmed age—has been encountered in drill core at Abel Knoll, Southeast Pediment, and Silica Ridge. Recognized by a distinctive, moderately welded, basal polylithic volcanic breccia, the Red-Green Breccia tuff package is composed of repetitive lapilli-lithic, fiamme, and vitric airfall tuffs. Excluding rare plagioclase and biotite within the basal polylithic breccia, crystal fragments are largely absent. A lack of datable phenocrysts combined with extensive propylitic, argillic, and quartz-adularia overprints has hindered dating of this tuff unit.

The youngest rocks exposed within the Sandman project area include capping mafic flows and related sills and dikes of basaltic trachy-andesite, trachy-andesite, and lesser andesite. These rocks have been dated at ~22.5 Ma. Rocks of a similar age and composition have been documented to the northeast of the Sandman project area within the Bloody Run Hills and Santa Rosa Range. Similar rocks are also exposed to the east in the hills between Winnemucca Mountain and the Bloody Run Hills, and to the north in isolated exposures along the east flank of the Slumbering Hills. With abundant clasts of andesite, the Abel Knoll breccia body is also likely of a similar age. The spatial association of early Miocene dikes, sills, and mafic breccia bodies to middle Miocene low sulfidation Au mineralization may provide a useful tool for future exploration within and outside the project area.

TABLE OF CONTENTS

LIST OF FIGURES

LIST OF TABLES

INTRODUCTION

The Sandman Au project is located approximately 15 miles northwest of Winnemucca, Nevada (Fig. 1), just south of the Slumbering Hills, to the east of the Krum and Ten Mile Hills, and to the northeast of Blue Mountain. Topographically, the project area consists of low to moderate hills and relatively flat, fault bounded valleys. Elevations range from approximately 4400 to 5100 feet. Extensive Quaternary sands of the Crescent Dune Fields cover much of the northern part of the property. Primary access to the project is via driving west from Winnemucca 9 miles along Jungo Road. The project can also be accessed to the east via Barrett Springs Road and also through a network of dirt roads linking the project to US 95 via Sand Pass.

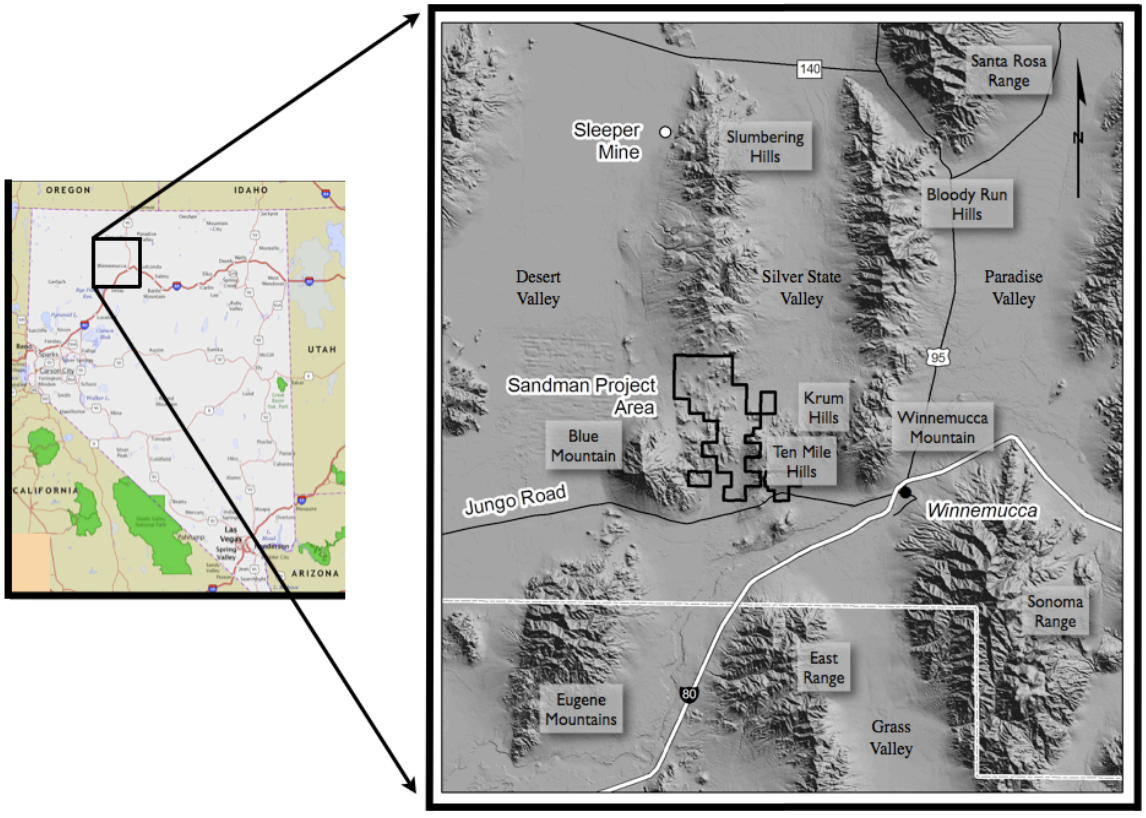

Figure 1: Location map for the Sandman Au Project.

The Sandman project was initiated as a joint venture between Fronteer Development Corporation and Newmont Mining Corporation in 2008. In spring of 2011, Newmont Mining Corporation became the sole operator with the acquisition of Fronteer Development Corporation. Exploration and development activities including drilling, surface trenching and mapping, feasibility studies and metallurgical testing continued through until fall of 2012. Mine permitting activities are currently ongoing.

Mineralization consists of five recognized, mid-Miocene low-sulfidation epithermal deposits hosted primarily in mid-Tertiary volcanic, volcaniclastic, and fluvial rocks, and to a lesser degree within basement Triassic rocks and late Mesozoic intrusions. These deposits include North Hill, Silica Ridge, Southeast Pediment, Abel Knoll and Ten Mile. Hosted entirely by mid-Tertiary volcanics, the deposits of North Hill, Silica Ridge, and Southeast Pediment are both structurally and stratigraphically controlled. Abel Knoll is hosted by a mid-Tertiary polylithic breccia body composed of andesite, basement phyllites and tuffaceous wall rocks, while Ten Mile is structurally controlled and hosted dominantly by a late Mesozoic granodiorite stock. These deposits are relatively small with a combined measured and inferred resource of approximately 272,000 ounces Au excluding the Ten Mile deposit (Table 1); however, mineralization is near surface, variably high grade, and dominantly oxidized.

SANDMAN GOLD RESOURCES - MAY 2007												
	MEASURED			INDICATED			MEASURED AND INDICATED			INFERRED		
DEPOSIT	Tons	Grade (oz Au/ton)	Au Ounces	Tons	Grade (oz Au/ton)	Au Ounces	Tons	Grade (oz Au/ton)	Au Ounces	Tons	Grade (oz Au/ton)	Au Ounces
Southeast Pediment	644,000	0.070	45,300	1,300,000	0.034	44,500	1,944,000	0.046	89,000	109,000	0.026	2,800
North Hill	387,000	0.037	14,400	2,684,000	0.029	78,400	3,071,000	0.030	92,800	294,000	0.021	6,200
Silica Ridge	511,000	0.032	16,200	1,382,000	0.028	39,000	1,893,000	0.029	55,200	518,000	0.014	7,400
Abel Knoll	168,000	0.037	6,200	957,000	0.029	27,900	1,125,000	0.030	34,100	497,000	0.027	21,600
Totals	1,710,000	0.048	82,100	6,323,000	0.030		8,033,000	0.034	271,900	1,418,000	0.027	38,000

Note: 0.010 oz Au/ton cutoff for Abel Knoll, North Hill, and Silica Ridge
0.010 oz Au/ton cutoff for SE Pediment above 4,200 ft elevation
0.020 oz Au/ton cutoff for SE Pediment below 4,200 ft elevation

Table 1: Sandman Au resources (Gustin et al., 2007).

METHODOLOGY

Field Work

Beginning in the summer of 2010, three summers in addition to time over semester breaks were spent conducting fieldwork for this study. This work included detailed geologic logging of diamond drill core and reverse circulation chips, a review of historical drill hole logs, photos, and skeletonized core, and detailed surface and trench mapping. Surface maps, deposit cross sections, and stratigraphic columns were compiled from my observations and work by Newmont geologists. Regional mapping by Newmont geologist Clay Postlethwaite greatly aided in these efforts.

Petrography

One hundred forty-seven standard and polished thin sections were examined in this study. These include a review of 30 historical reverse circulation chip mounts, 56 thin sections prepared for the prior thesis work by Gopon (2010), and 87 thin sections prepared for this study to characterize and correlate variable stratigraphy from deposit to deposit. Thin sections were dominantly prepared from diamond drill core with a few from outcrop exposure. Select billets were stained by sodium cobaltinitrite to determine the degree of potassic alteration for determining samples for geochemical analysis and age dating.

Geochemistry

A total of 76 geochemical samples were utilized in this study. Most rocks within

the project area have undergone some degree of alteration including propylitic, argillic, supergene argillic, quartz-adularia, or some combination of all. Least altered samples were collected from drill core and outcrop exposures and submitted to ALS Chemex Labs Inc. for analyses of major oxides and trace elements. See Appendix 1 for analytical methods.

Using Excel, normalized 100% volatile free oxide weight % was plotted in total alkali vs silica and Harker diagram plots to characterize and compare variable felsic and mafic rocks across the project area. For trace element data, modified spider diagrams were used for comparison. Values were chondrite-normalized using values from McDonough and Sun (1995). Additional data for comparisons to regional volcanics were attained through literature review and provided by Chris Henry at the Nevada Bureau of Mines and Geology and Mathew Brueseke at the University of Nebraska.

Geochronology

Four new age dates are presented in this study. These include two $^{40}Ar/^{39}Ar$ sanidine ages on tuffs collected from outcrop at Adularia Hill and to the east of Silica Ridge, and two $^{40}Ar/^{39}Ar$ groundmass ages on mafic units collected from drill core at North Hill and Southeast Pediment. Sanidine separates were prepared by Chris Henry with the Nevada Bureau of Mines and Geology and analyzed at the New Mexico Geochronology Research Laboratory. Two drill core samples were submitted to the University of Auburn Nobel Isotope Mass Analysis Lab where groundmass separates were prepared and analyzed by Willis Hames. See Appendices 23 through 25.

EXPLORATION HISTORY

Historical mining in the region (Fig. 2) began around 1910 with the discovery of the Alabama Mine on the eastern side of the Slumbering Hills. In the Awakening Mining District, production from the Alabama Mine along with other smaller properties was intermittent until the discovery of the Jumbo Mine in 1935 (Vanderburg, 1938a). Located on the western side of the Slumbering Hills—within sight of the future bonanza Sleeper Deposit discovery—the Jumbo Mine produced through to 1958 and accounts for most of production in the district. Total production information is limited, although Willden (1964) reports total production at approximately $1,000,000 for the Jumbo deposit and gives a total production for the district through 1963 at 26,262 oz. Au, 36,948 oz. Ag, 3,100 lbs. Cu and 42,704 lbs. Pb. Recorded base metal production for the district is not related to the mid-Miocene low-sulfidation systems discussed herein and is likely associated with Mesozoic granitic intrusions (see later discussion on the Pansy Lee Mine). The epithermal deposits of the Awakening District consist of narrow, northerly trending, quartz-adularia ± Au-dominant veins and veinlets occurring along high-angle bedding planes, bedding perpendicular joints, and fractures in Triassic metasedimentary rocks. Given fracture mechanic characteristics, quartzites prove more favorable host rocks than phyllites in the district.

Further south, additional historical production from this time period came from several operations in the Ten Mile and Krum Hills. Properties in the Ten Mile District were small and include the Golden Amethyst, Eldorado, and Ten Mile Mines. Total production for the district is believed to be approximately 20,000 oz. Au from 1900 through 1942 (Bowell et al., 2000). These deposits all consist of narrow, northeast

striking, Au-bearing quartz-adularia veins and veinlets in Triassic metasedimentary rocks, while at the Ten Mile Mine, mineralization is dominantly hosted by a small, late Mesozoic granodiorite stock and associated hornfels.

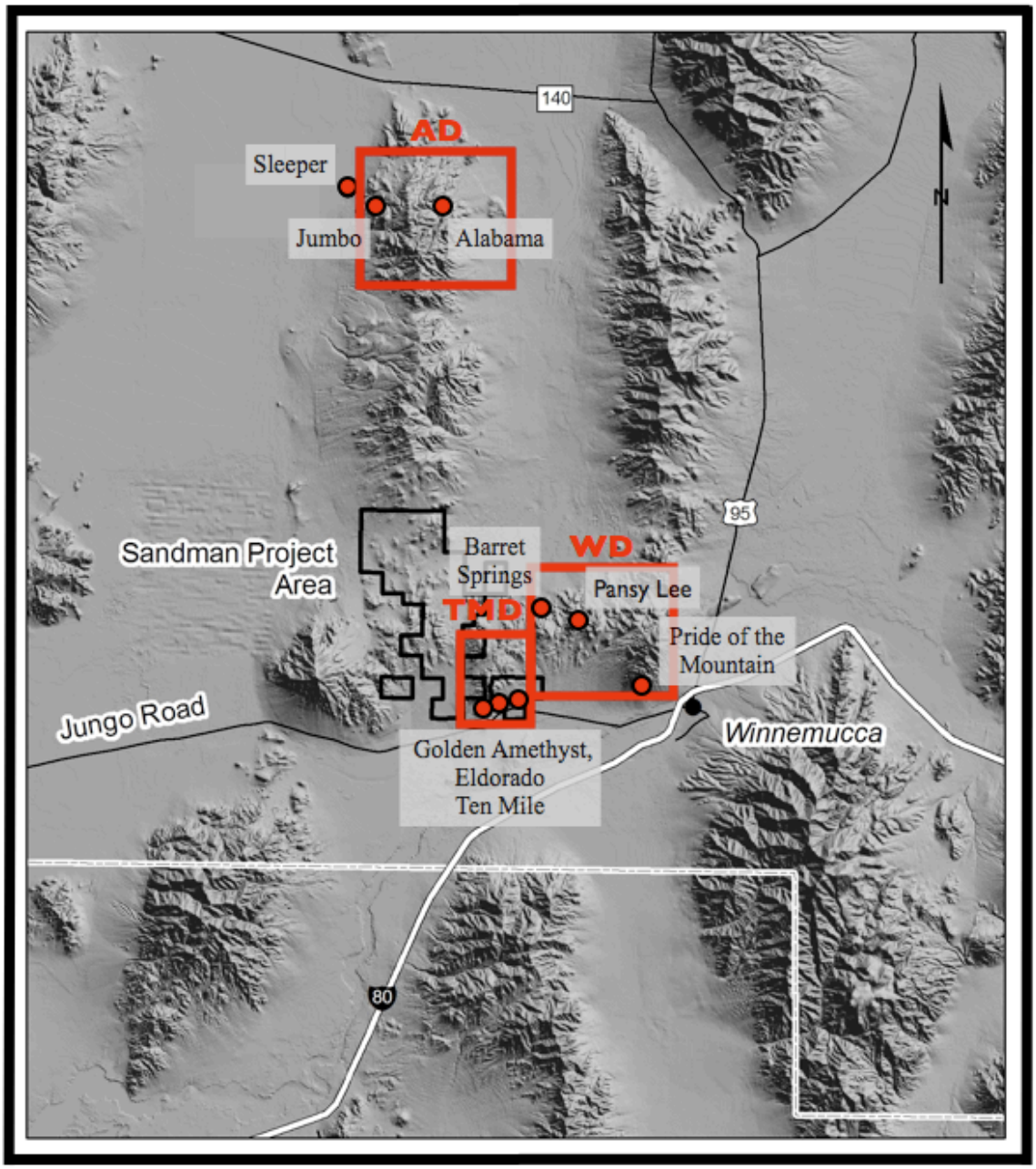

Figure 2: Location map for historic producers in the vicinity of the Sandman Project. AD = Awakening Mining District, WD = Winnemucca Mining District, TMD = Ten Mile Mining District. Deposits for Ten Mile Mining District are listed west to east.

Located just to the east of the Sandman project is the Winnemucca Mining District, including both mid-Miocene precious-metal rich, low-sulfidation deposits and precious and base metal shear-hosted vein and replacement ores likely associated with Mesozoic intrusions. An Indian named Winnemucca made the first notable discovery in the district in 1863. The most significant early producer was the Pride of the Mountain Mine — also referred to as the Pride of the West Mine—producing an estimated $1,000,000 in metals (Vanderburg, 1938a); however, later work by Willden (1964) reports this amount is not supported by other data. Additionally, a short-lived rush occurred during the early 1900's with the discovery of discontinuous, high-grade Au±Ag epithermal veins near Barrett Springs. (Vanderburg, 1938a). Activity resumed in the district between 1937-1943, mainly at the Pansy Lee Mine, also known as the West Coast Mine. The deposit is associated with small Jurassic-Cretaceous (?) quartz-diorite stocks and consists of discontinuous, shear-hosted quartz-calcite-pyrite veins plus Ag-dominant precious-metal mineralization with elevated base metals including Zn, Pb, and Cu-bearing sulfides and sulfosalts (Bonham et al., 1985). Given the style of mineralization at the Pansy Lee, this deposit is likely not associated with mid-Miocene low sulfidation mineralization in the region and is likely the result of Mesozoic intrusive activity. Total production data for the district is incomplete for the early years. From 1910 to 1935, a total of $132,433—dominantly from Au and Ag credits ± Cu and Pb—was produced (Vanderburg, 1938a), and during 1935 to 1959, about 10,070 ounces of gold was produced. Total gold production through 1959, including early production from the Pride of the Mountain mine, was probably 35,000 ounces (Koschmann and Bergendahl, 1968).

Modern exploration in the region was minimal prior to Amax's 1984 discovery of

the Sleeper deposit. In line of sight of the Jumbo Mine to the southeast, the Sleeper deposit is hosted in Tertiary volcanic rocks preserved in the down-to-the-west pediment along the western slopes of the Slumbering Hills. The deposit was originally concealed beneath 30 to 150 feet of alluvium. Stratigraphy of the Sleeper deposit consists of a basal package of volcaniclastic rocks overlain by intermediate composition lava flows and lapilli tuffs (Conrad et al., 1993). The major host of the Sleeper deposit, a rhyolite porphyry, was emplaced between 16.4 and 16.3 Ma and immediately predates high-grade Au-Ag epithermal veins emplaced at 16.1 Ma (Conrad and McKee, 1996).

With the bonanza nature of Sleeper suggesting potential for other high-grade deposits hosted in mid-Tertiary rocks, Kennecott Exploration conducted a helicopter supported exploration program in the fall of 1986. Initial geochemical sampling of a quartz-adularia flooded conglomerate outcrop did not return anomalous values (internal Kennecott Report, 1987). Later reconnaissance sampling of the iron oxide stained, quartz-adularia flooded basaltic trachy-andesite to trachy-andesites of North Hill returned initial values of 3 ppm Au. Further outcrop sampling yielded higher values up to 2.2 oz/ton Au. Following these results, Kennecott and Santa Fe Pacific Gold Corporation formed a joint venture in 1987. Exploration activities including geologic mapping, surface sampling, geophysical surveying, trenching, drilling and metallurgical testing continued through 1994. The joint venture drilled 275 reverse-circulation and three diamond-drill core holes, in addition to 4,000 feet of shallow auger holes sampling bedrock beneath extensive sand cover. U.S. Borax also drilled 37 reverse-circulation holes on a block of claims in the project area—acquired by the Kennecott-Santa Fe joint venture in 1989 (Gustin et al., 2007). Following the merger of Newmont Mining

Corporation with Santa Fe, Western States Minerals—later Fronteer—gained controlling interest in 1996 by acquiring BLM sections and leasing the remaining private JV sections from Newmont. In June of 2008, Newmont Mining Corporation regained interest through a joint venture agreement with Fronteer Development Group (Lauha et al., 2010), later acquiring full ownership of the property through acquisition of Fronteer Development Corporation in spring of 2011.

STRATIGRAPHY

Early middle-Miocene, low-sulfidation Au mineralization at the Sandman project is hosted dominantly by Oligocene to early Miocene volcanic, volcaniclastic, and fluvial rocks, and to a lesser degree by Triassic basement rocks and late Mesozoic granodiorite intrusions. The project area is characterized by low to moderate topographic relief, with outcrops limited to basement exposures to the north, south, and east of the project area, resistant knobs of quartz-adularia flooded mid-Tertiary fluvial and tuffaceous rocks in the northwest part of the project area, and extensive trachy-andesite flows covering approximately 8 square miles in the Basalt and Little Basalt Hills. Extensive Quaternary sands of the Crescent Dune Field cover much of the north part of the project area.

Basement Rocks

Basement rocks consist of Triassic metasedimentary rocks dominated by slate and phyllitic mudstones and siltstones with lesser degrees of quartzites and rare limestone units. Within the vicinity of the property, basement rocks have been mapped as the Triassic Raspberry and O'Neill formations of the Auld Lang Syne Group after Willden (1964) and also as undifferentiated Triassic-Jurassic greenschist metamorphosed-sediments of the Auld Lang Syne Group by Burke & Silberling (1973). These units are well exposed to the east, west, and north of the Sandman property (See Figs. 3 and 4 for distribution). Units of the Raspberry Formation dominate in the Ten Mile Hills to the southeast as well as to the southwest of the Basalt Hills and along the flanks of Blue Mountain. These include phyllite, discontinuous lenses of laminated, massive and locally cross-bedded quartzites, and rare limestone. Isolated exposures of basement phyllite are

also present just to the west of Adularia Hill. Quartzite of the O'Neill Formation is the dominant lithology to the north—forming prominent ridges along the southern slopes of the Slumbering Hills (Lauha et al., 2010).

Regionally, this package of rocks has been considered part of the Jungo terrane by Silberling et al. (1987) and also referred to as the Fencemaker allochthon by Oldow (1995). Numerous investigations (Speed, 1978; Lupe and Silberling, 1985, Wyld, 2000) show that these rocks were deposited in a deep marine back-arc basinal terrane with more carbonate-rich shelf rocks to the east and shallower volcaniclastic marine rocks associated with oceanic arcs to the west. Individual units within this basinal terrane were first defined in the Santa Rosa Range and Bloody Run Hills (Compton, 1960; Lupe and Silberling, 1985), and have since been inferred to correlate with units to the southwest in

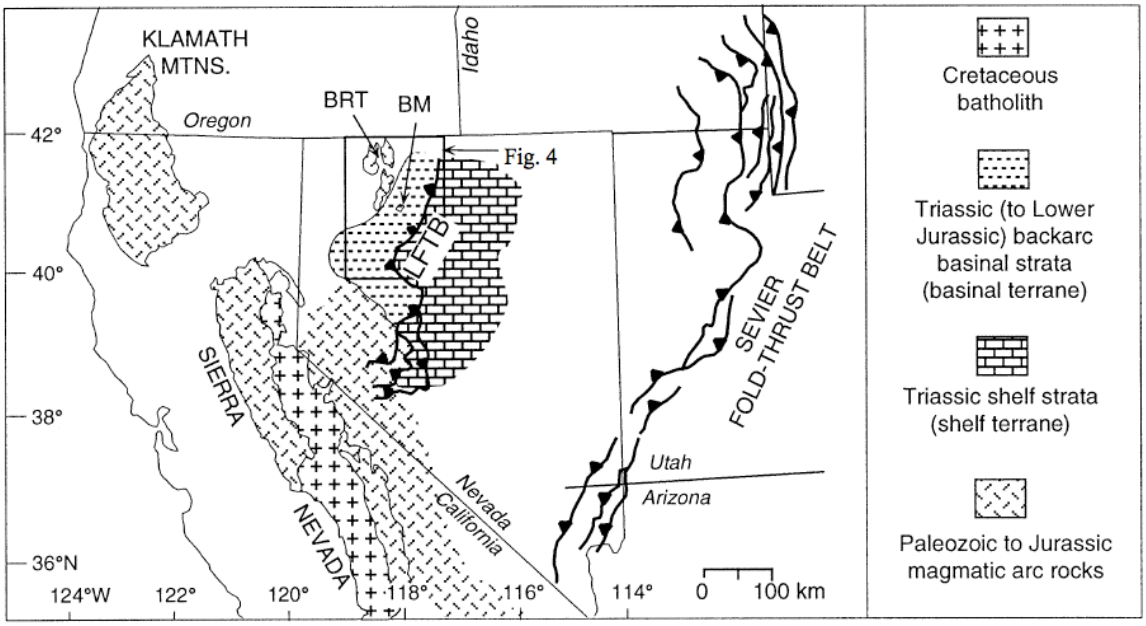

Figure 3: Map of the western U.S. Cordillera, showing distribution of lower Mesozoic rocks, Cretaceous batholith belt, and locations of major Mesozoic fold-and-thrust belts. The Luning-Fencemaker fold-and-thrust-belt (LFTB) encompasses the entire basinal terrane; only frontal thrusts are shown (Oldow, 1984). BM = Blue Mountain, BRT = Black Rock terrane (Wyld, 2002).

the Eugene Mountains (Thole and Prihar, 1998) and Blue Mountain (Wyld, 2002). These rocks have undergone numerous deformational events, with the first and most pronounced resulting from basin closure during the Jurassic and the generation of the Luning-Fencemaker fold-and-thrust belt.

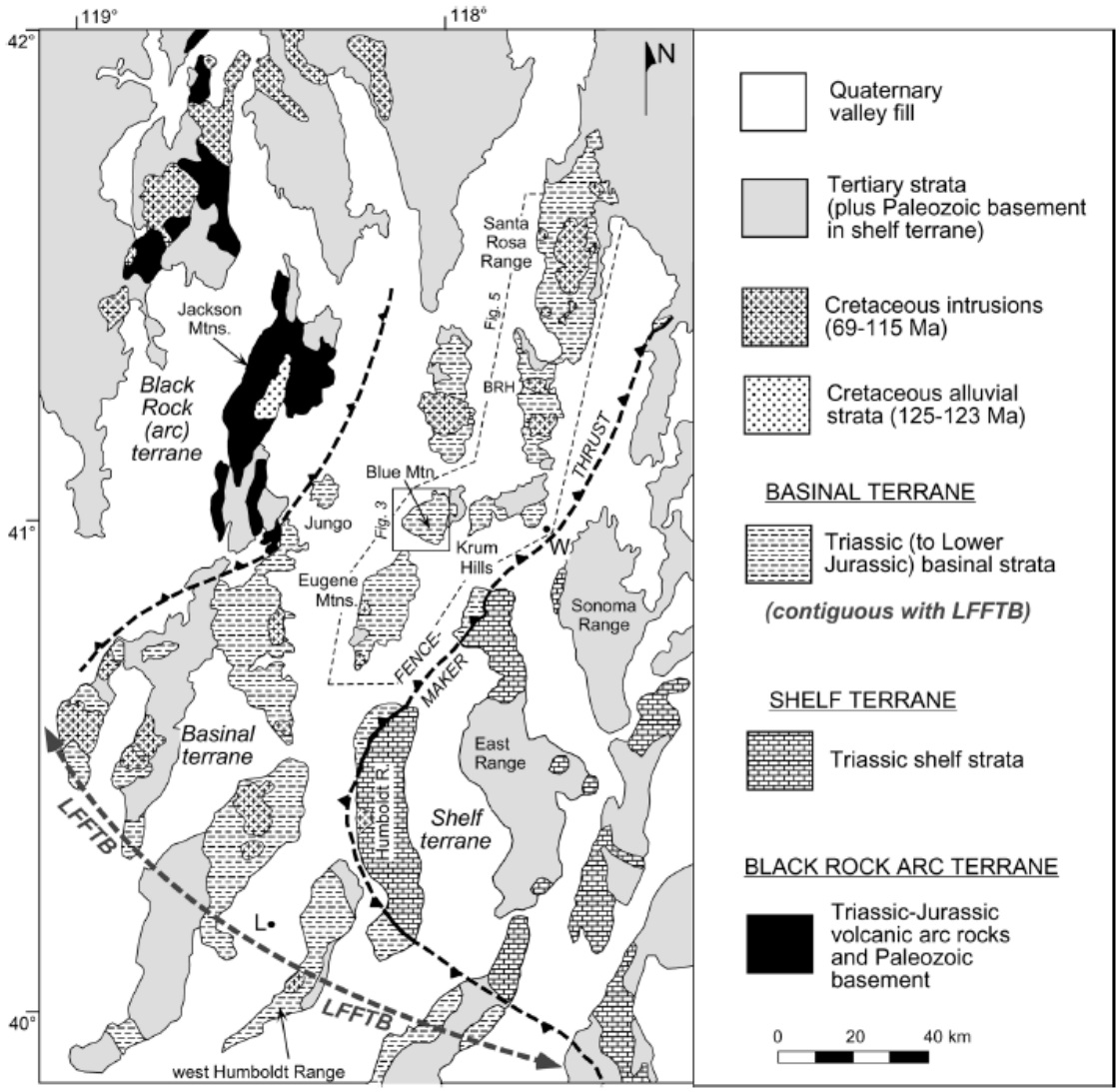

Figure 4: Location map showing mountain ranges in north-central Nevada (see Fig. 3 for location) and distribution of lower Mesozoic arc, basinal, and shelf terranes. Modified from Willden (1964), Oldow (1984), Elison and Speed (1989), Wyld (1996, 2000), and Quinn et al. (1997). BRH—Bloody Run Hills; LFFTB—Luning-Fencemaker Fold and Thrust Belt; L and W—towns of Lovelock and Winnemucca, respectively (Wyld, 2002).

The following discussion of basement stratigraphy and structure is based on early work by Compton (1960) and more recent work by Ciavarella and Wyld (2008), Wyld (2000, 2002) and Wyld et al., (2001). D_1 structures developed during Jurassic southeast-directed basinal closure include a pervasive S_1 cleavage, abundant folds, and inferred reverse faulting. All structures strike north-northeast with S_1 cleavage dipping steeply (~45-60 degrees) to the northwest. F_1 folds are tight to isoclinal, gently plunge to the northeast and have variable amplitudes from centimeters to greater than 50 meters. Reverse faults have been mapped at Blue Mountain and within the Santa Rosa Range.

Later basement structures are locally discontinuous, with variable orientations depending on their location within the Luning-Fencemaker Belt. D_2 and D_3 deformational events associated with minor northwest-southeast shortening have been mapped within the Santa Rosa Range and have similar orientations to those associated with major shortening of the D_1 deformational event; however, these later events record smaller degrees of crustal strain. D_4 deformation is also observed within the Santa Rosa Range and is coeval with the emplacement of mid-Cretaceous granitic stocks. These structural fabrics indicate minor northeast-southwest regional shortening probably related to the mid-Cretaceous development of the Sevier fold-and-thrust belt further to the east.

Illustrating regional variability, equivalent D_2 and D_3 structures as recorded in the Santa Rosa Range are absent at Blue Mountain to the southwest of the Sandman project. Mid-Cretaceous structural fabrics equivalent to D_4 deformation within the Santa Rosas do affect D_1 structures here and include open folds, crenulations, and spaced cleavage. These structures all strike north-northwest to northwest and dip relatively steeply to the southwest.

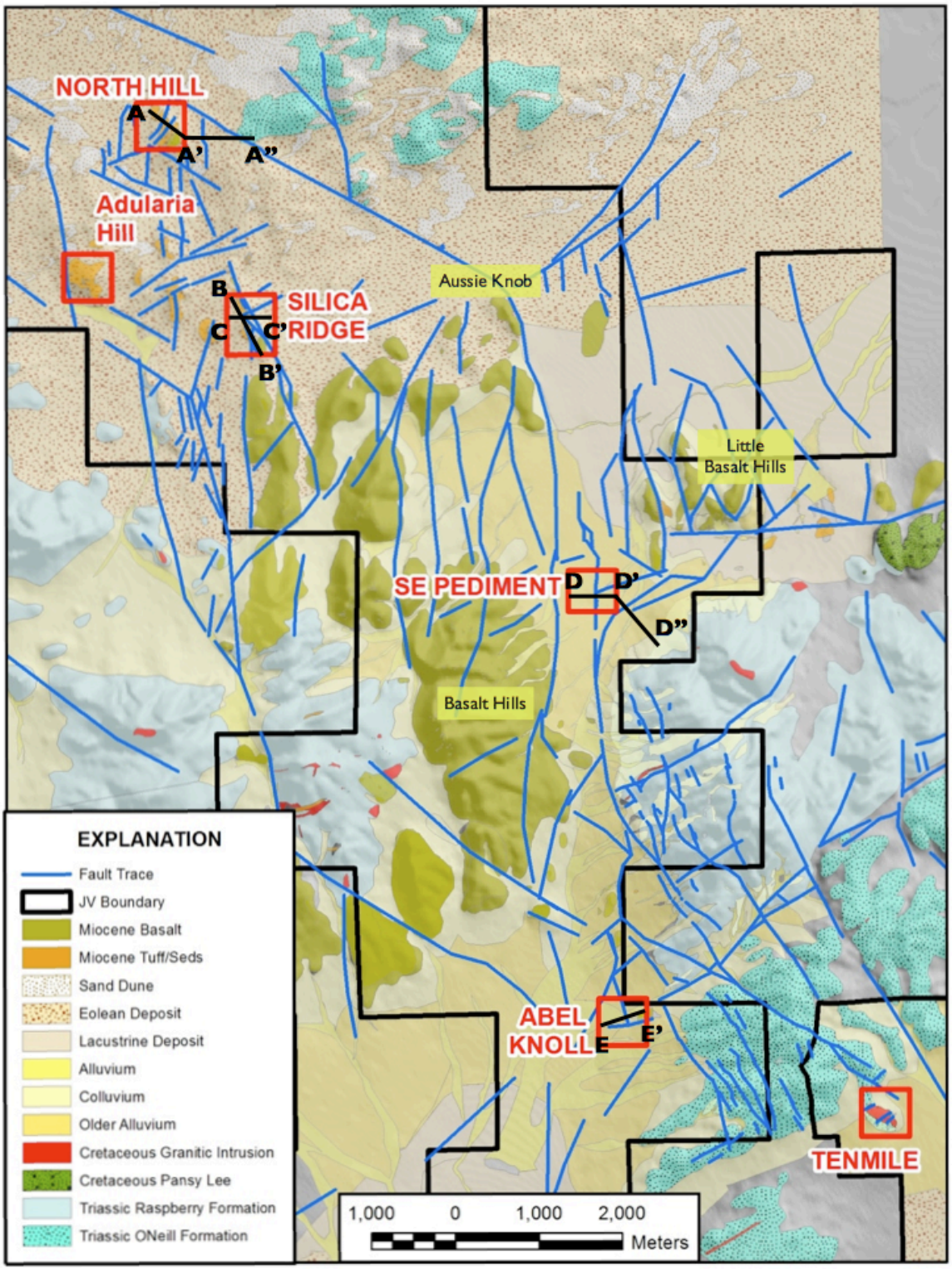

Figure 5: Geologic map for the Sandman project area showing deposit locations, cross sections, and locations mentioned in the text. See Figs. 23 through 32 for detailed deposit surface maps and cross sections. Map by Newmont geologist Clay Postlethwaite.

Late Mesozoic Intrusions

Numerous late Mesozoic granitic plutons, stocks, and dikes intrude basement rocks in most ranges of northwestern Nevada (Fig. 4). U-Pb zircon geochronology has established a late Cretaceous emplacement ranging between 116 and 91 Ma (Wyld, 2000; Wyld et al., 2001; Wyld and Wright, 2005, Colgan et al., 2006). In vicinity of the Sandman Project, granitic rocks in the Slumbering Hills are 116 Ma, and 98 Ma in the Bloody Run Hills (Colgan et al., 2006). Establishing depths of emplacement, metamorphic mineral assemblages within contact aureoles indicate that stocks and plutons within the Santa Rosa Range and Bloody Run Hills to the north of the Sandman project were emplaced at a depth of approximately 7-9 km (Compton, 1960; Maffei, 1992; Rogers, 1999; Wyld et al., 2001; Ciavarella, 2003). Due to southeastward tilting during Cenozoic Basin and Range normal faulting, depth of emplacement is not uniform across these ranges, increasing by approximately 2 km from southeast to northwest in the Bloody Run Hills, and by up to 4 km from southeast to northwest within the Santa Rosa Range (Colgan et al., 2006).

Within the Sandman property, there is a prominent granodiorite intrusive body exposed in outcrop in the Ten Mile Hills just to the southeast of Southeast Pediment. Additional inferred Cretaceous stocks included those at the Ten Mile Mine to the south-southeast and the Pansy Lee Mine to the east-southeast. A number of small intrusive bodies and dikes within basement rocks have also been mapped on the eastern flanks of Blue Mountain and within the Ten Mile Hills (Fig. 5). These dikes tend to be discontinuous in nature and are aligned preferentially along regional northeast basement foliations.

Pansy Lee Conglomerate (Cretaceous vs. Tertiary ?)

Exposed to the east of the property in the Krum Hills is the type location for the Pansy Lee conglomerate. First described by Willden (1958, 1963, 1964), here the Pansy Lee conglomerate unconformably overlays the Triassic Raspberry Formation and is composed of distally sourced clasts from outside backarc rocks of the Luning Fencemaker fold-and-thrust belt. Ranging between 400 and 500 feet thick, the Pansy Lee conglomerate is a buff to reddish-gray, pebble to cobble conglomerate grading upward into coarse-grained sandstone. The base of the Pansy Lee is typified by numerous clast supported, basal beds of gravel to cobble conglomerate, with clasts comprised of near-white, well-sorted, exceptionally pure quartzite, black to dark green chert ± mafic metavolcanics. Upsection, overall average clast size decreases with a transition from gravel ± cobble conglomerate, to pebble and gravel conglomerate and increasing course-grained sandstone. Temporal variations in clast composition are also observed with quartzites and mafic metavolcanics decreasing, while diversity in cherts (black, gray, light and dark green, red in color) increases upsection. Variable percentages of tuff clasts are present within middle and upper beds and are inferred as Tertiary in age within this study (see later discussion on age of Pansy Lee Conglomerate regarding tuffaceous clasts).

Rocks mapped as Pansy Lee conglomerate also crop out widely in the Jackson Mountains to the west of the Sandman project. Here, Willden (1964) describes the Pansy Lee conglomerate as similar to conglomerates within the Krum Hills, although distinguishing gravel ± cobble conglomerate horizons are less abundant and finer grained siltstones are more common. While resting unconformably on Triassic backarc rocks in

the Krum Hills, Willden indicates a conformable basal contact in the Jackson Mountains, resting on the Cretaceous King Lear Formation.

Defined as Lower Cretaceous arc-derived clastic sedimentary rocks uncomformably overlaying Jurassic igneous rocks, the presence of rare limestone beds containing freshwater gastropods indicate an age of middle Early Cretaceous for the King Lear Formation (Willden, 1958). Russel (1984) later added the Pansy Lee Conglomerate (as defined in the Jackson Mountains) to the King Lear Formation, recognizing that deposition of the two units was quasi-continuous. The definition of the King Lear Formation was further expanded by Maher (1989) to include felsic intrusive and volcaniclastic rocks in the southern portions of the King Lear basin. These rocks were previously thought to be Tertiary in age (Willden, 1963, 1964; Russell, 1981, 1984); however, U/Pb dating of zircons from a felsic tuff inter-bedded within the formation gives an age of 125 ± 1 Ma, and zircons within intrusive rocks yield an age of 123 ± 1 Ma, confirming Mahers interpretation of an Early Cretaceous age for these rocks, which they named the Clover Creek igneous complex (Quinn, 1996; Quinn et al., 1997).

Work by Martin et al. (2009) has expanded on the definition of the King Lear Formation, subdividing it into three members based on differences in clast lithologies and sourced provenance (Fig. 6). At the base of the section, the Jackson Creek Member is composed of conglomerates and sandstones sourced entirely from local, older arc sources ± rare inter-bedded limestone. The central Quartzite-Chert Member consists of conglomerate, sandstone, and siltstone dominantly sourced from outside the arc, with clasts dominated by gray, exceptionally pure quartzite and a mixture of cherts ± locally sourced rock. This member is described as equivalent to the Pansy Lee Conglomerate

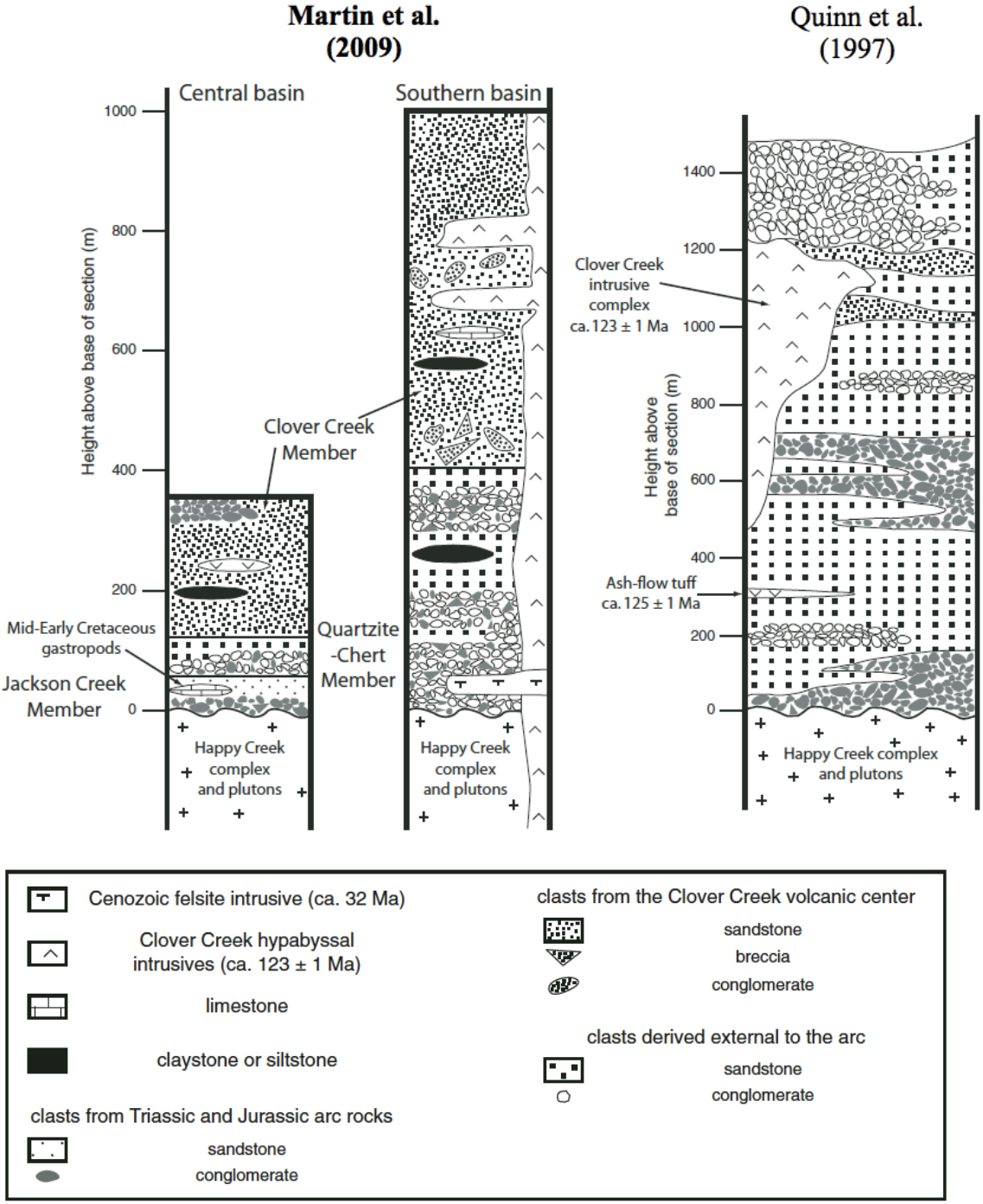

Figure 6: Composite stratigraphy of the King Lear Formation in the Jackson Mountains from Quinn et al. (1997) and Martin et al. (2009). Happy Creek igneous complex is latest Triassic to Early Jurassic.

described by Willden (1958, 1963) within the Jackson Mountains. Martin et al.'s upper member of the King Lear Formation is the Clover Creek Member, composed mostly of sandstones and siltstones ± rare felsic ash-flow tuff, limestone, and conglomerate beds. These rocks were locally sourced from the Early Cretaceous Clover Creek volcanic complex, composed dominantly of hypabyssal porphyritic dacite and related volcaniclastic rocks (Quinn et al., 1997).

Similar clast compositions between the Pansy Lee of the Krum Hills and the Quartzite-Chert Member of the King Lear Formation within the Jackson Mountains led Martin et al. to correlate these sedimentary rocks across ranges, suggesting an Early Cretaceous (>123 ±1 Ma) age for the Pansy Lee Conglomerate in the Krum Hills, with clasts sourced from the southeast and east (Table 2). With abundant quartzite and chert ± mafic metavolcanics, the Ordovician Valmy Formation was first suggested by Willden (1958) as a potential source rock for clasts within the Pansy Lee. The closest exposures are approximately 25 miles to the southeast in the Sonoma Range and approximately 35 miles to the east in the Osgood Mountains. Other potential source rocks for clasts include the Upper Paleozoic Golconda allochthon to the east and the Cambrian Osgood Mountains quartzite exposed in the Sonoma Range and Osgood Mountains.

While Martin et al.'s work provides a greater understanding of rocks mapped as the Pansy Lee in the Jackson Mountains, correlation of these sedimentary rocks to the those exposed in the Krum Hills (approximately 35 miles east-southeast of the Jackson Mountains) based solely on clast composition and sourced provence does not provide definitive proof for an Early Cretaceous age for the Pansy Lee Conglomerate type location. I question this age based on field relationships in the Krum Hills. These

include similar attitudes to rocks of an established Tertiary age, the proximal juxtaposition of the Pansy Lee Conglomerate against a late Mesozoic granodiorite, and the presence of inferred Tertiary tuff clasts in middle and upper beds.

Rock units	Location	Principal lithologies
Triassic Auld Lang Syne Group (shelf terrane)	ER, SR, TR	Mostly shale, slate, and siltstone, with minor quartzite. Locally abundant carbonate.
Triassic Star Peak Group (shelf terrane)	ER, SR, TR	Mostly carbonate.
Triassic Koipato Formation (shelf terrane)	ER, SR	Mostly rhyolitic volcanic rocks. Not widely exposed.
Upper Paleozoic Golconda allochthon	BM, ER, SR, TR	Mostly greenstone, chert, and argillite, with less common quartzite, carbonate, and conglomerate.
Upper Devonian to Mississippian Harmony Formation	BM, ER, SR	Mostly feldspathic and arkosic sandstone with less common shale, conglomerate, and limestone. Sandstones are poorly sorted and medium to coarse grained, with ≤80% quartz grains.
Ordovician Valmy Formation	BM, ER, SR	Interbedded quartzite, argillite, chert, and greenstone. Quartzites are fine to medium grained, with ≥95% quartz grains, well sorted and well rounded, and occur in layers up to 150 m thick.
Cambrian Preble Formation	SR	Mostly shale, less common limestone, minor quartzite.
Cambrian Osgood Mountains Quartzite	SR	Mostly fine- to medium-grained quartzite, with 90%–95% quartz grains, in layers from 30 cm to 15 m. Less common shale and impure quartzite.

Note: BM—Battle Mountain, ER—East Range, SR—Sonoma Range, TR—Tobin Range. References: Ferguson et al. (1959, 1976), Willden (1964), Gilluly (1967), Erikson and Marsh (1974), Whitebread (1994), and Ketner et al. (2005).

Table 2: Geologic units exposed in ranges southeast of the Krum Hills (Martin et al., 2009).

In the Krum Hills, attitudes for beds in the Pansy Lee are similar to attitudes of Tertiary strata to the west, striking north to northeast with east to southeast dips between 20 and 30 degrees. Measured dips at the base of the Pansy Lee section are as great as 37 degrees; however the basal unconformity was not observed here and it is possible this outcrop is a large slide-block. Additionally, Tertiary basaltic trachy-andesite to trachy-andesite flows to the south and southeast of the Pansy Lee are tilted approximately 25 degrees to the east (Fig. 7).

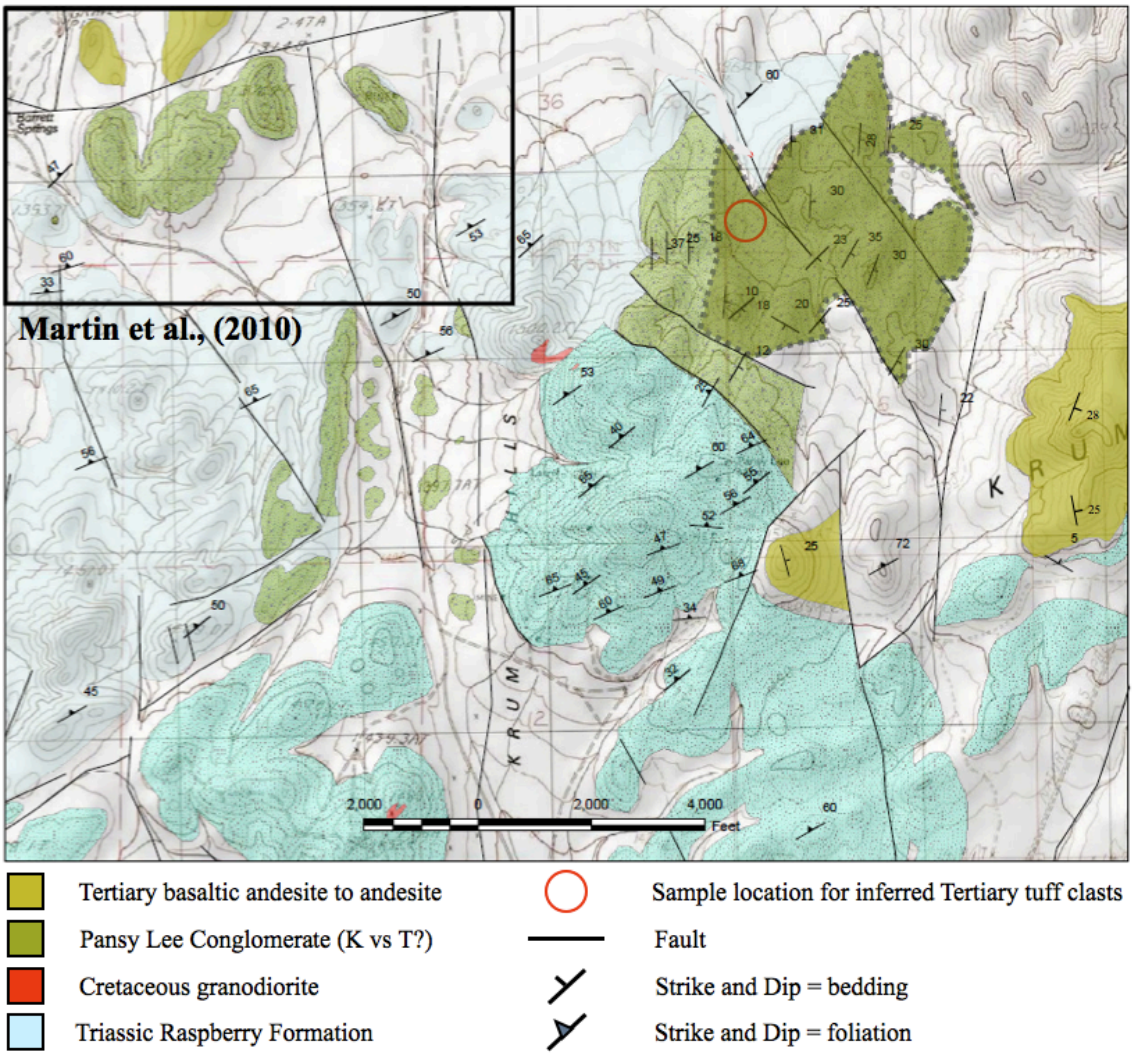

Figure 7: Geologic map of the Pansy Lee Conglomerate type location in the Krum Hills. Rock distributions, attitudes, and location of sampled tuffaceous clasts shown. Dashed outlines show distribution of inferred Tertiary tuffaceous clasts. Note proximity of inferred Cretaceous granodiorite to exposures of Pansy Lee. Modified from unpublished map by Clay Postlethwaite, Newmont geologist. Inset shows mapped area by Martin et al. (2010).

The spatial juxtaposition of the Pansy Lee to inferred late Mesozoic granodiorite also questions an Early Cretaceous age for these sedimentary rocks. Small granodiorite bodies intrude the Triassic Raspberry Formation to the southeast of the Pansy Lee—the closest within approximately 1000 feet (Fig. 7). In northwest Nevada, late Mesozoic granitic intrusions have an age range between 116 and 91 Ma. This range predates the

Clover Creek Igneous complex—providing an upper age constraint for the King Lear Formation of 123 ± 1 Ma—by a minimum of 6 million years and a maximum of 31 million years (Fig. 6). Metamorphic contact aureoles do not affect rocks of the Pansy Lee, therefore, if the Pansy Lee is correlatable to the Cretaceous Quartzite-Chert Member of the King Lear Formation, intrusive rocks within the Krum and Ten Mile Hills would have to be older than Cretaceous. Jurassic plutonic rocks are present to the west in the Jackson Mountains, and range in composition from quartz diorite to quartz monzodiorite with only rare late granodiorite to granite aplite dikes (Maher, 1989). The only other Jurassic plutonic rocks close to the Sandman Project—approximately 35 miles to the southeast—are quartz monzonite to porphyritic syenite of the Buffalo Mountain Pluton (Neff, 1973). Jurassic plutonic rocks in both the Jackson Mountains and Buffalo Mountain are compositionally unlike intrusive rocks in the Krum and Ten Mile Hills. Their location within the Cretaceous arc also suggests that they are of a similar age to other local granitic bodies.

The presence of tuffaceous clasts in the Pansy Lee Conglomerate type location leads to further doubt for an Early Cretaceous age for these rocks. Tuffaceous clasts increase in abundance upsection—upwards to 20% locally—and are inferred as Tertiary in this study. Early Cretaceous volcanogenic clasts—namely supracrustal andesite breccia, rare felsic ash flow tuffs, and hypabyssal porphyritic dacite—are present within the Clover Creek Member of the King Lear Formation (Quinn et al., 1997). This Member lies conformably above the Quartzite-Chert Member correlated to the Pansy Lee by Martin et al. These volcanogenic clasts are likely not equivalent to tuffaceous clasts in upper sections of the Pansy Lee as sourced provences for clasts within the Pansy Lee

occur to the east and southeast of the Krum Hill, not to the west within the Jackson Mountains (Table 2). Additionally, average clast size within these two sedimentary packages decreases from east to west—indicating east-west transport—assuming the two units are correlatable. Tuffaceous clasts are thus inferred to be Tertiary in age.

Whole rock and trace element geochemical analyses for four tuffaceous clasts within the Pansy Lee suggest two—and likely more—ash flow tuff sources (Fig. 8). Petrographic analyses from two of these samples, 8-09-12-1 and 8-09-12-3, confirms these observations. Both samples show intense potassic alteration and moderate to strong silicification. Only quartz and sanidine remain fresh. Throughout the Pansy Lee, quartz-adularia alteration is evident in outcrop and indicates the presence of a diffuse hydrothermal system within these clastic rocks. Indicative of this hydrothermal alteration, K_2O values range between 8 and 13 percent, and Ba values range between 2700 and 4900 ppm within these tuffaceous clasts. Subtracting for excess hydrothermal potassium and silica, tuffaceous clasts likely all plot within the dacite to low silica rhyolite field (Fig. 9).

Petrographically, 8-09-12-1 is a weakly welded tuff composed of approximately 40% crystal fragments of quartz-sanidine-plagioclase-biotite-amphibole ± accessory zircon and abundant pumice. Sample 8-09-12-3 is a weakly welded, slightly more mafic tuff based on a mineral assemblage of approximately 25% crystal fragments dominated by plagioclase and amphibole with only subordinate amounts of biotite, sanidine and quartz, accessory zircon, and minor pumice. Amphibole species was not determined in either of these samples due to the degree of alteration. Variable lithic fragments are present in both samples, although obscured by alteration.

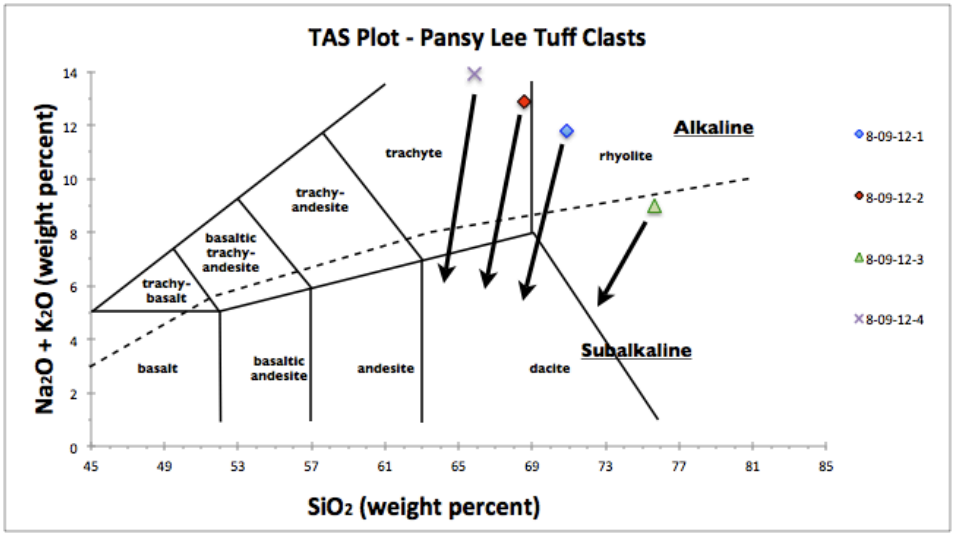

Figure 8: Total alkali versus silica for tuffaceous clasts of the Pansy Lee. Conglomerate beds from sample locations have undergone adularization and silicification. Based on crystal fragment assemblages, arrows indicate likely composition prior to addition of hydrothermal potassium and silica. See Appendix 12 for all geochemical data. Division between alkaline and subalkaline from Irvin and Baragar (1971).

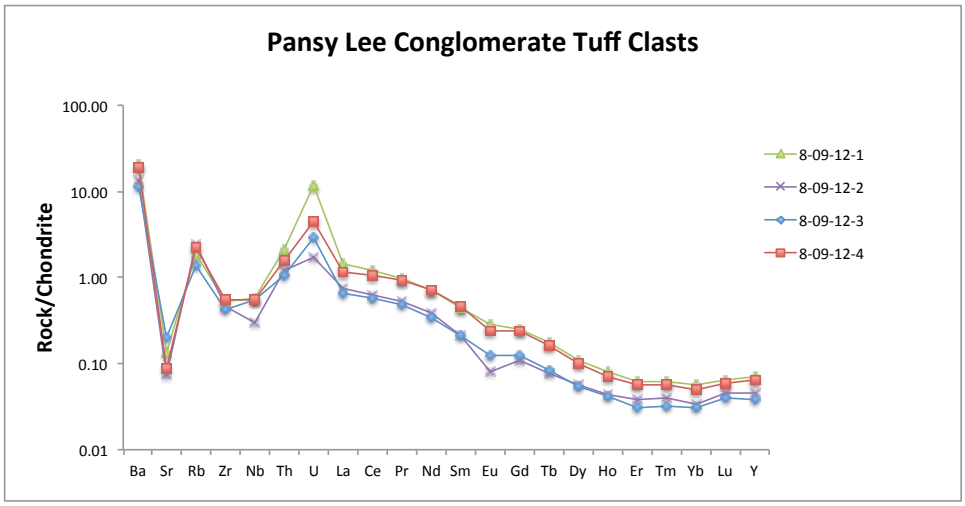

Figure 9: Modified spider diagram for select trace element and REE geochemistry for inferred Tertiary tuffaceous clasts of the Pansy Lee Conglomerate. Patterns suggest two distinct ash flow tuff sources.

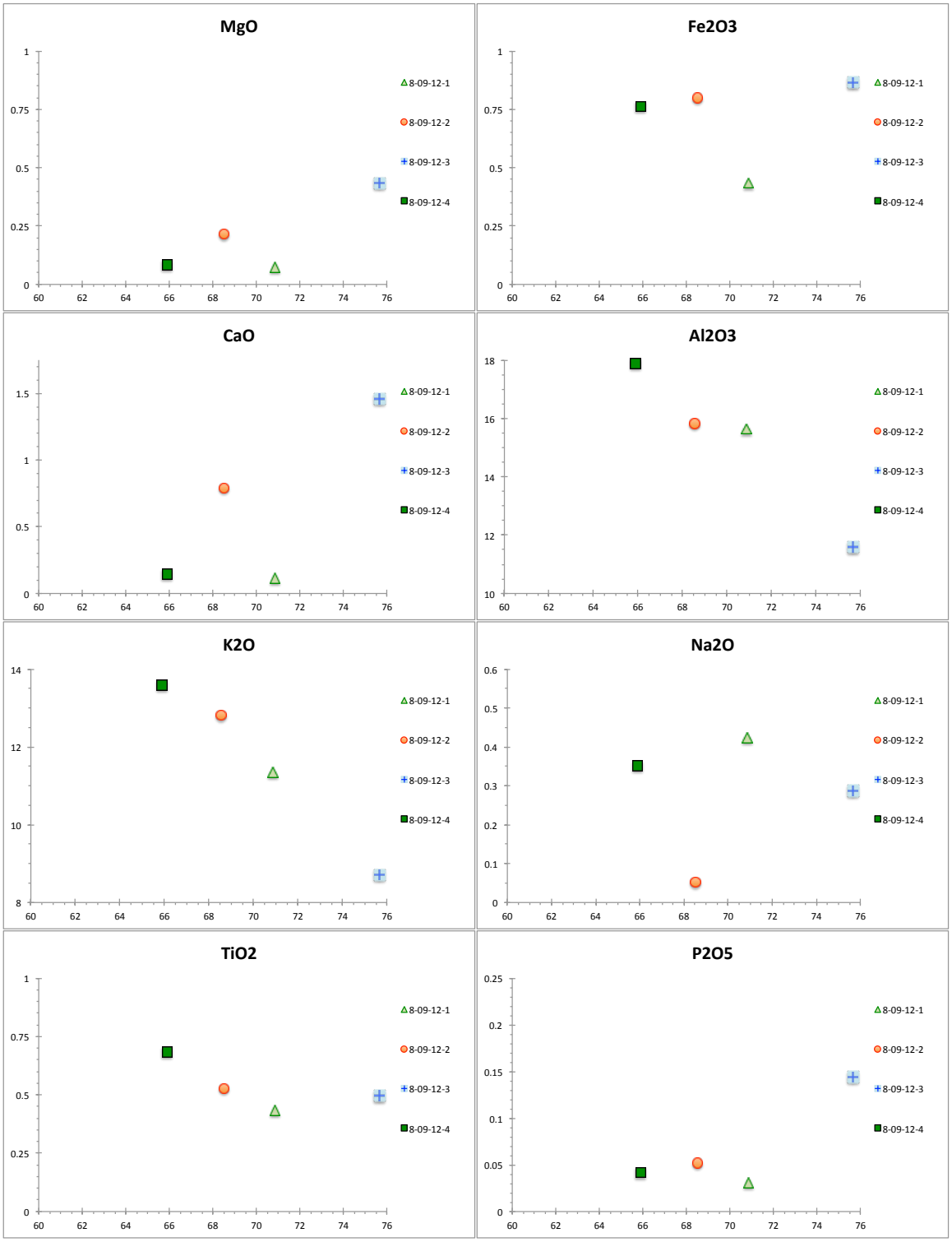

Figure 10: Harker diagrams for whole rock oxides of inferred Tertiary tuffaceous clasts contained within the Pansy Lee Conglomerate type location.

Possible sources of tuff clasts in the in the Pansy Lee include the 39.8-39.7 Ma Tuscarora Volcanic Field approximately 55 miles to the east of the Krum Hills (Henry et al., 1999), the 33.8 Ma Caetano Tuff and the older 34.2 Ma tuff of Cove Mine, approximately 50 miles to the southeast, and the 24.7 Ma Fish Creek Mountains Caldera (John et al., 2008) (See Fig. 11). Given that Tertiary drainage was east to west (Henry, 2008) (See Fig. 42), the Tuscarora Volcanic Field is the most likely source. In that field, the 39.9 Ma tuff of Nelson Creek, a plagioclase-biotite>hornblende-quartz-sanidine-rich, weakly welded, pumice-rich, trachy-dacite to rhyolite, is a possible source (Henry et al., 1999; Wallace, 2003a). Other tuffs in the Tuscarora field are unlike Pansy Lee clasts. The 39.8-39.7 Ma, small volume, dacitic tuff of Mount Blitzen, is densely to poorly welded, lithic and pumice rich, composd dominantly of plagioclase and minor biotite, lacks sanidine and rarely contains quartz. The 39.7 Ma tuff of Big Cottonwood Canyon, the most widespread ash-flow tuff in the Tuscaroa Volcanic Field, has phenocrysts of quartz, sanidine, plagioclase, and biotite but lacks amphibole (Henry et al., 1999)

Other Eocene dacitic tuffs to the east include the tuff of Coal Mine Canyon—a highly silica dacite characterized by abundant crystal fragments of plagioclase-biotite-and hornblende—and the plagioclase-biotite tuff dominated by plagioclase and biotite with lesser and variable degrees of hornblende, pyroxene, quartz, and sanidine (Henry, 2008). While biotite is present within tuffaceous clasts of the Pansy Lee, it occurs in subordinate amounts and the plagioclase-biotite tuff is not likely a source for observed clasts.

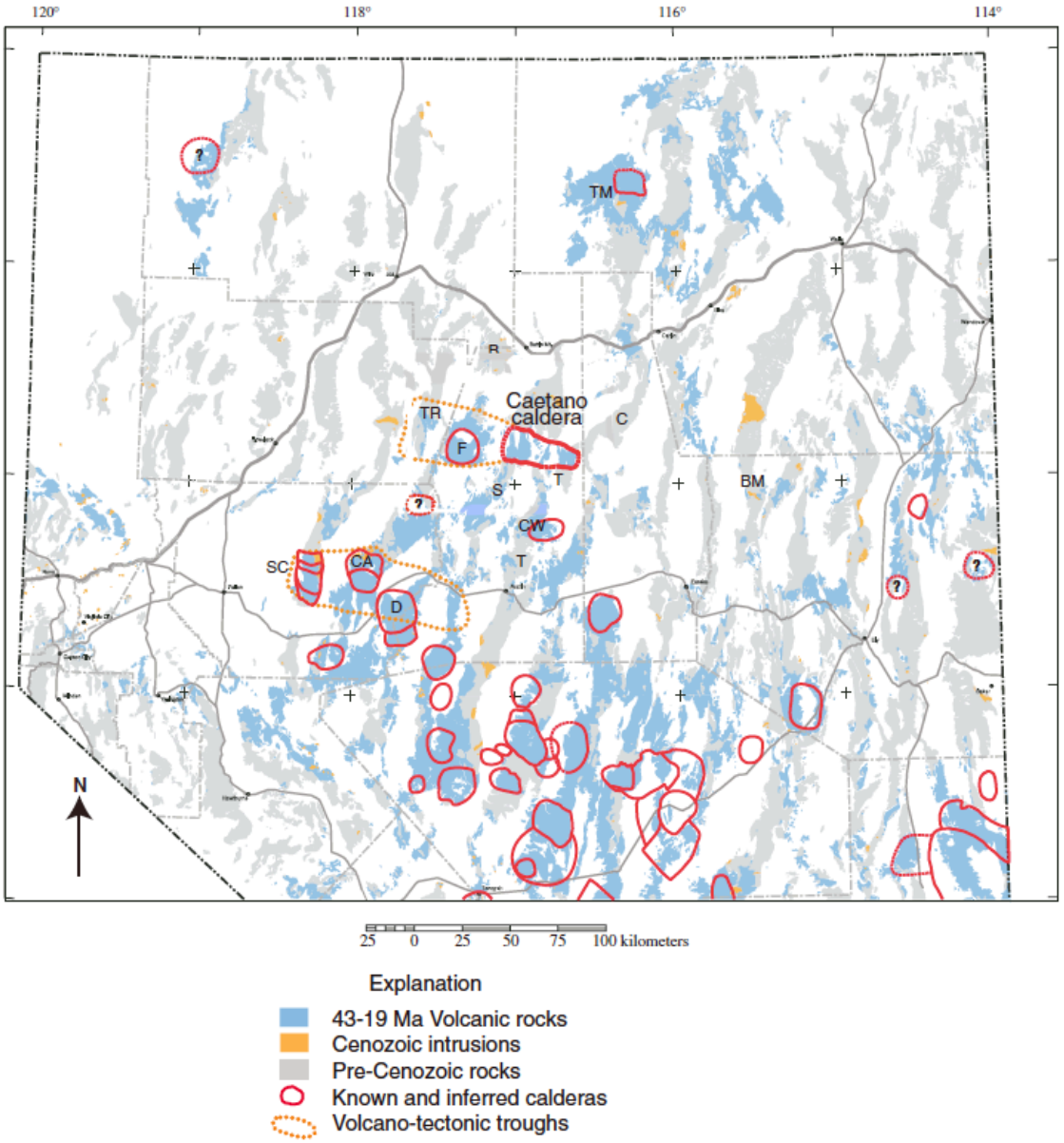

Figure 11: Map showing mid-Cenozoic (43–19 Ma) volcanic rocks and intrusions in northern Nevada and calderas (modified from Ludington et al. [1996]) and volcano-tectonic troughs of Burke and McKee (1979). B—Battle Mountain; BM—Bald Mountain; C—Cortez Range; CA—Clan Alpine Range calderas; CW—Cowboys Rest; D—Desatoya Mountains calderas; F—Fish Creek Mountains caldera; S—Shoshone Range; SC—Stillwater caldera complex; T—Toiyabe Range; TM—Tuscarora volcanic field; TR—Tobin Range (John et al., 2008).

While numerous lines of evidence have been proposed questioning an inferred Early Cretaceous age for the Pansy Lee Conglomerate, additional work is necessary to definitively prove or disprove this assumption. Additional geochemical and petrological comparisons between Tertiary ash-flow tuffs and tuffaceous clasts contained within the Pansy Lee would provide supporting evidence; however, U-Pb dating of detrital zircons may provide the strongest evidence. The presence of Tertiary crystallization ages from detrital zircons sourced from regional ash flows would provide definitive proof that the Pansy Lee Conglomerate type location within the Krum Hills is not correlative to the Quartzite-Chert Member of the King Lear Formation. Elizabeth Cassel at the University of Texas at Austin has recently collected bulk samples from outcrops of the Pansy Lee for detrital zircon analyses which should shed more light on the age of the Pansy Lee conglomerate type location. Additional samples for detrital zircon analyses have also been collected from deep drill core piercing the Sandman fluvial sequence between the North Hill and Silica Ridge deposit (see Fig. 15 and next section on mid-Tertiary fluvial rocks of the Sandman project).

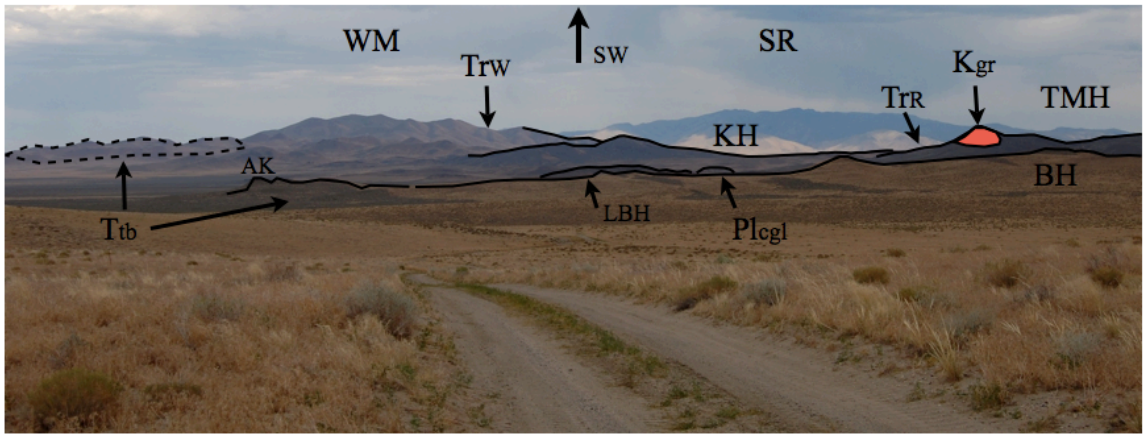

Figure 12: Photo taken from the road to North Hill looking southwest across the Sandman project area. Note sublte topographic excpressions and limited Tertiary outcrops. Wm = Winnemucca Mountain, SR = Sonoma Range, AK = Aussie Knob; KH = Krum Hills, TMH = Ten Mile Hills, BH = Basalt Hills, LBH = Little Basalt Hills; TrW = Triassic Winnemucca Formation, TrR = Triassic Rhaspbery Formation, Kgr = Cretaceous granodiorite, Plcgl = Pansy Lee conglomerate, Ttb = Tertiary basaltic trachy-andesite to trachy-andesite.

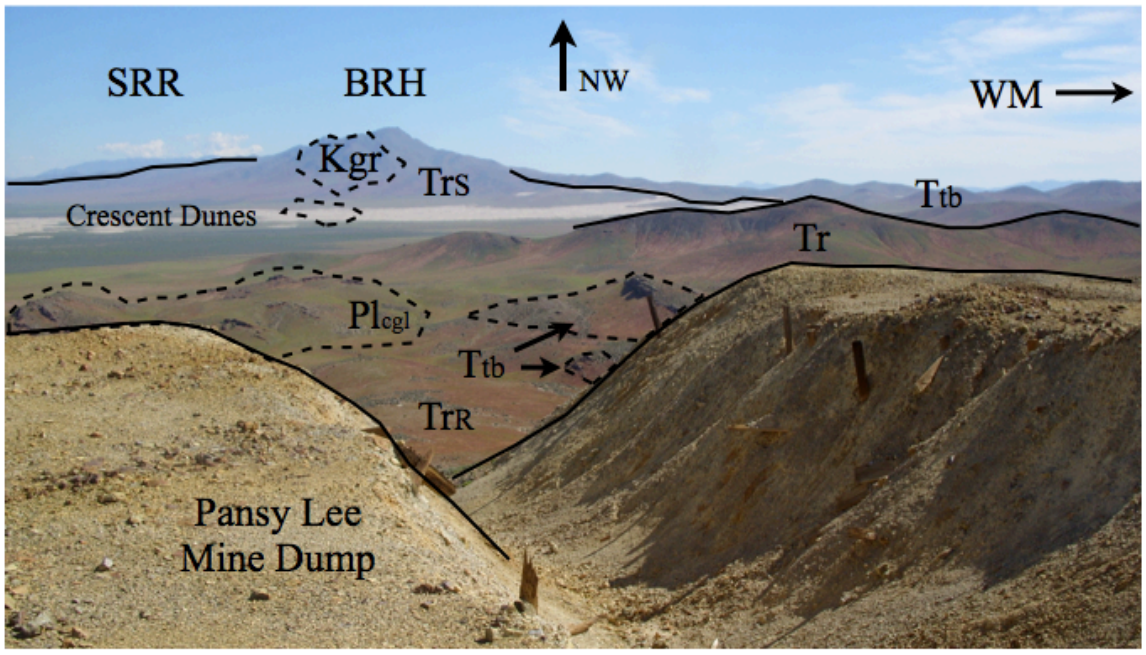

Figure 13: Photo taken from the Pansy Lee Mine dumps looking northwest across outcrops of the Pansy Lee conglomerate east of the Sandman project area. SRR = Santa Rosa Range, BRH = Bloody Run Hills, WM = Winnemucca Mountain, TrS = Triassic Singas Formation, Tr = Triassic undivided, TrR = Triassic Raspberry Formation, Kgr = Cretaceous granodiorite, Plcgl = Pansy Lee conglomerate, Ttb = Tertiary basaltic tracy-andesite to trachy-andesite.

Figure 14: Outcrop exposures of the Pansy Lee conglomerate. Images A-C are from the type location. See Fig 13. A.) Basement dominant gravel to boulder conglomerate overlying tuffaceous sandstones and conglomerates. B.) Tuffaceous clast rich conglomerate bed. C.) Closeup of tuffaceous clasts. Basement dominant gravel to boulder conglomerate in limited outcrops to the south of Adularia Hill.

Mid-Tertiary Fluvial, Volcanic, and Epiclastic Rocks

An approximately 700 to greater than 1350 foot thick package of Oligocene to early Miocene, dacitic to rhyolitic air-fall, pyroclastic, and epiclastic tuffs, and interbedded fluvial and lacustrine volcaniclastic siltstones, sandstones, and conglomerates rests unconformably on basement rocks. The stratigraphic package is capped by flows, and locally intruded by feeder dikes and sills, of basaltic trachy-andesite to trachy-andesite. Overall, mid-Tertiary rocks strike north-northeast and dip gently, 15 to 25 degrees, to the east-southeast; however, attitudes within flows of the Basalt Hills are highly variable. Here they show a general north-south progressive dip pattern from NE-E-SE, skirting a subtle inferred east-northeast striking basement arch in the central part of the property. Additionally, a large phreatic, polylithic breccia body dominated by clasts of andesite to trachy-andesite, basement phyllite and trace Mesozoic granodiorite ± tuffaceous wall rocks cross cuts the stratigraphic section and is the host for mineralization at Abel Knoll.

This mid-Tertiary stratigraphic package has informally been referred to as the Comforter Basin Formation (Newmont nomenclature). Thicknesses of this package increase from west to east and range from a thin veneer just to the west of Adularia Hill to greater than 1350 feet beneath the Little Basalt Hills. Within the deposit areas of North Hill, Silica Ridge, Southeast Pediment and Abel Knoll, this package averages between 650 and 800 feet thick. As a result of both variability in deposition and preservation, rock types are distributed irregularly across the project area; however, the recognition of two distinctive tuffs allows correlation of strata from deposit to deposit (Fig. 15).

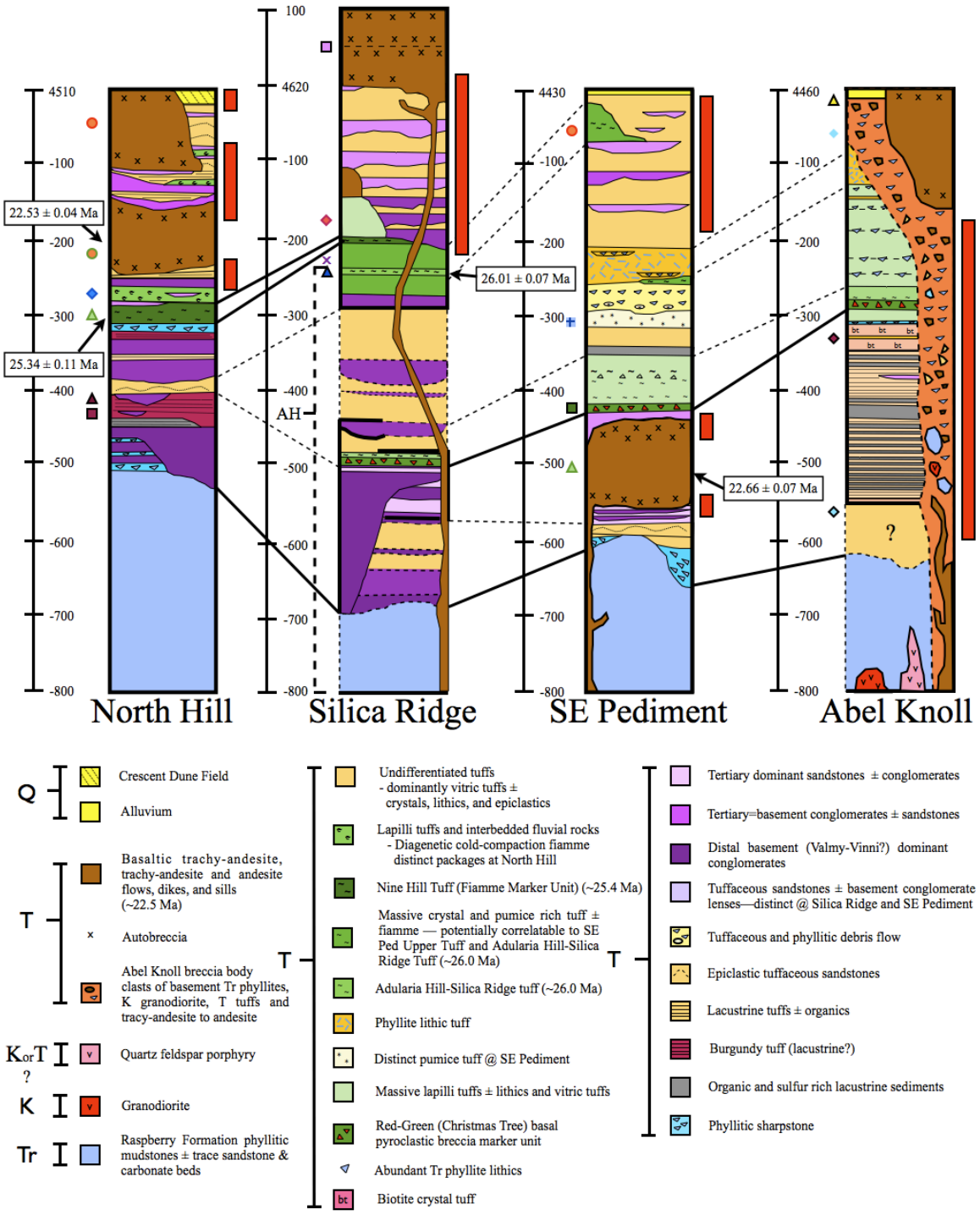

Figure 15: Oligocene to early Middle Miocene stratigraphy for Sandman epithermal deposits. Ten Mile deposit excluded as it is hosted predominantly within Cretaceous granodiorite. Dashed lines indicate stratigraphy loosely constrained by reverse circulation drilling. Red columns show stratigraphic horizon hosting quartz-adularia alteration and Au mineralization. Symbols to left of columns show location for geochemical data. Some symbols duplicated for mafic and felsic geochemical data. Age dates from this study given. AH with solid line indicates probable stratigraphy for Adularia Hill. See Fig. 5 for deposit locations and Fig. 23 through Fig. 32 for deposit surface maps and cross sections.

Sedimentary Rocks

Sedimentary rocks vary in distribution and composition both spatially and temporally within the stratigraphic section and include conglomerate, sandstone, siltstone, mudstone and sharpstone. Spatially, the distribution of these sedimentary rocks indicates the presence of a well established paleodrainage in the north of the property at North Hill, Adularia Hill, and Silica Ridge, a more epiclastic environment of deposition at Southeast Pediment, and a persistent lacustrine environment at Abel Knoll lower in the section. Temporal variations within these sedimentary rocks reflect changes in clast source rock, with the base of the section dominated by local Triassic basement phyllites and more distally derived quartzites, cherts, and metavolcanics. Upsection, fluvial rocks become increasingly dominated by clasts of Tertiary volcanic rocks, phyllite clasts are largely absent, and quartzite and chert clast percentages are variable given the proximity to major drainage channels.

Sharpstone

The base of the section is composed of locally sourced phyllitic sharpstone inter-bedded with more distally derived conglomerates and sandstones ± tuffaceous deposits. Sharpstone has been encountered in drill core at the base of both the North Hill and Southeast Pediment deposits, and is likely present at the base of the section at Silica Ridge and Abel Knoll; however, deep drilling is limited to reverse circulation within these deposits. Within drill cuttings, sharpstone is indistinguishable from basement phyllite. Sharpstone beds range from less than one to three feet in thickness and are composed of chaotic to imbricated, angular to subangular, pebble to gravel with trace cobble sized clasts of phyllites ± milky-white, metamorphic bull-quartz fragments

sourced from the Triassic Raspberry Formation within a fine-grained phyllitic-derived matrix. While imbrication suggests some fluvial transport, the chaotic nature and angularity of clasts within these beds indicates very limited transport, probably related to mass wasting associated with inferred basement topographic highs.

Sharpstones Higher in Section and the Southeast Pediment Debri Flow

Phyllitic sharpstone is also present in the middle of the section at North Hill and Southeast Pediment. At North Hill sharpstone occurs as thin beds just beneath the ~24.4 Ma Nine Hill Tuff. Tuffaceous clasts and matrix are absent from these sharpstone beds. Within the middle of the section at southeast Pediment, drill holes have intercepted a massive phyllite and tuffaceous rich fluvial debri flow deposit. Approximately 40 feet thick, this deposit is massive to weakly bedded and consists of 5-75 percent chaotic to imbricated phyllite clasts ranging from 1-6cm, trace metamorphic quartz vein fragments found within Triassic basement phyllites, and abundant tuffaceous clasts in a tuffaceous matrix. Tuffaceous clasts are subrounded to rounded, range from pebble to cobble in size, and are sourced from a distinct pumice rich tuff bed directly beneath the deposit (see Fig. 15). The base of the deposit and rare, thin beds within the package are dominated by clasts of imbricated phyllite; however, erosional channel scour is only recognized at the base of the package, indicating rapid deposition of the Southeast Pediment debri flow. An upper age for the Southeast Pediment debri flow is constrained by a crystal and pumice rich tuff occurring approximately 200 feet upsection at Southeast Pediment. This tuff has been dated at ~26.0 Ma from outcrop at Adularia Hill and petrographically and geochemically correlated to tuffaceous deposits at Silica Ridge and Southeast Pediment (see section Silica Ridge–Adularia Hill Tuff Package and Southeast Pediment Upper Tuff

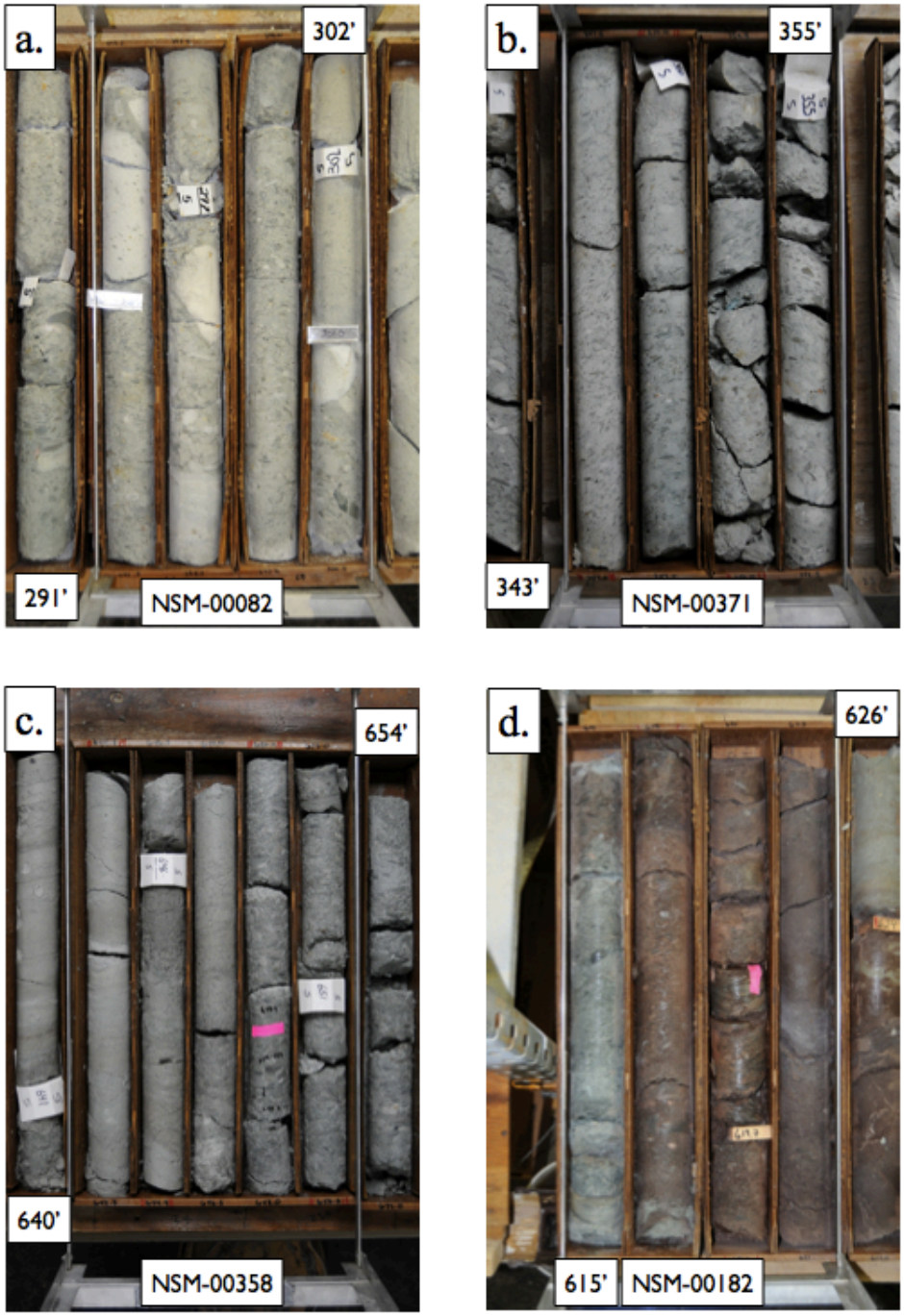

Figure 16: Diamond drill core photos of variious sharpstone units. A.) Fluvial debri flow deposit from Southeast Pediment composed of chaotic to imbricated phyllite and pumice tuff gravel to boulders in a tuffaceous matrix. B.) Southeast Pediment fluvial debri flow lacking large tuffaceous clasts. C.) Basal phylltic shapstone overlain by tuffaceous sandstone from Southeast Pediment. D.) Variably oxidized and reduced basal phyllitic sharpstone at North Hill.

Fig. 38 through 41). Given the absence of tuffaceous clasts and matrix in sharpstone beds within the middle of the section at North Hill, the two deposits are not likely related.

Phyllite clasts are largely absent in fluvial rocks — excluding the base of the section — and the presence of sharpstone beds in the middle of the section has tectonic implications for the region. As within sharpstone beds found lower in the section, the chaotic and angular nature of phyllitic clasts indicates limited transport. The presence of sharpstone beds higher in the section could be related to channel degradation and erosion of the Triassic basement or more likely the exposure of these rocks through local tectonic uplift sometime proximal to 26.0 Ma.

Conglomerate and Sandstone

Exploration and development drill holes in the northern part of the property have intercepted thick horizons of distally sourced basement dominant conglomerate and sandstone beds transitioning to more Tertiary dominant fluvial rocks up section. This package of rocks ranges between 90 and 330 feet thick within the project area — with the presence of clastic units decreasing to the south — and indicates the presence of a major paleodrainage channel (see Figs. 15 and 17). Individual conglomerate beds range from less than one to three feet in thickness, are massive to cross-bedded, typically clast supported, and often fine upward into medium to course grained sandstone. Clasts are sub-angular to sub-rounded and range in size from pebble to gravel ± trace cobbles at the base of the section. Overall average clast size decreases up section, and clasts show temporal variability through the section with changing input source rock.

At the base of the section, these fluvial rocks are interbedded with phyllitic sharpstone and are composed of clasts of black, gray and dark green chert, white to gray

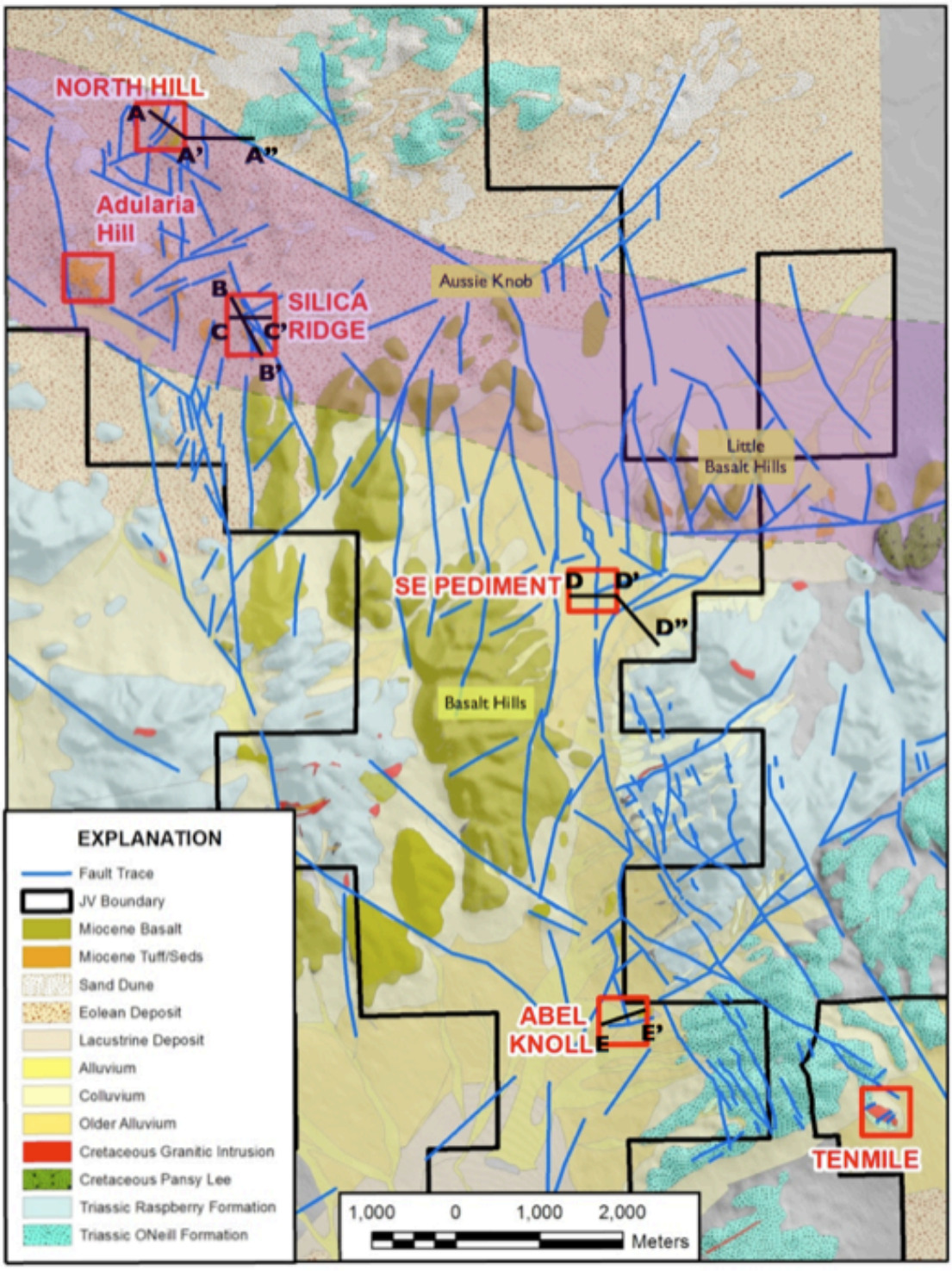

Figure 17: Sandman geologic map showing inferred location of mid-Tertiary paleodrainage in purple. Southern boundary is constrained by diamond and reverse circulation drill holes in addition to outcrop exposures. No constraint on northern boundary due to limited drill hole data and lack of outcrops.

quartzite, local phyllite ± trace metavolcanics. Phyllite clast percentages rapidly decrease up section, indicating overall burial of the Triassic basement. Clasts of Tertiary tuffs are largely absent at the base of the section; however, limited, discontinuous, thin tuffaceous horizons are present interbedded within these basal, basement dominant conglomerates ± sandstones. Progressing up section, white quartzite and metavolcanic clast percentages decrease and cherts become a mixture of black, gray, dark and light green, and red in color. Quartzites, cherts and metavocanics were most likely derived from the Ordovician Valmy Formation, while quartzite also may be sourced from the Cambrian Osgood Mountains Quartzite, both of which crop out in the Osgood Mountains ~35 miles to the east and the Sonoma Range ~25 miles to the southeast. With increasing Tertiary volcanic input, tuff clasts increase upsection, becoming dominant mid-section above the Nine Hill Tuff. Clasts of Tertiary basaltic andesite to andesite are absent except for thin sandstone horizons interbedded within mafic flows present at Aussie Knob. Within the project area, the lower basement dominated fluvial sequence only outcrops along the southwest flank of Adularia Hill with the inferred base exposed in isolated outcrops to the south of Adularia Hill. Mid section fluvial units consisting of Tertiary volcanics ± distally derived basement clasts outcrop both at North Hill and Silica Ridge, and inferred upper fluvial units dominated by Tertiary volcanics are exposed just north of the water well along the road to Silica Ridge.

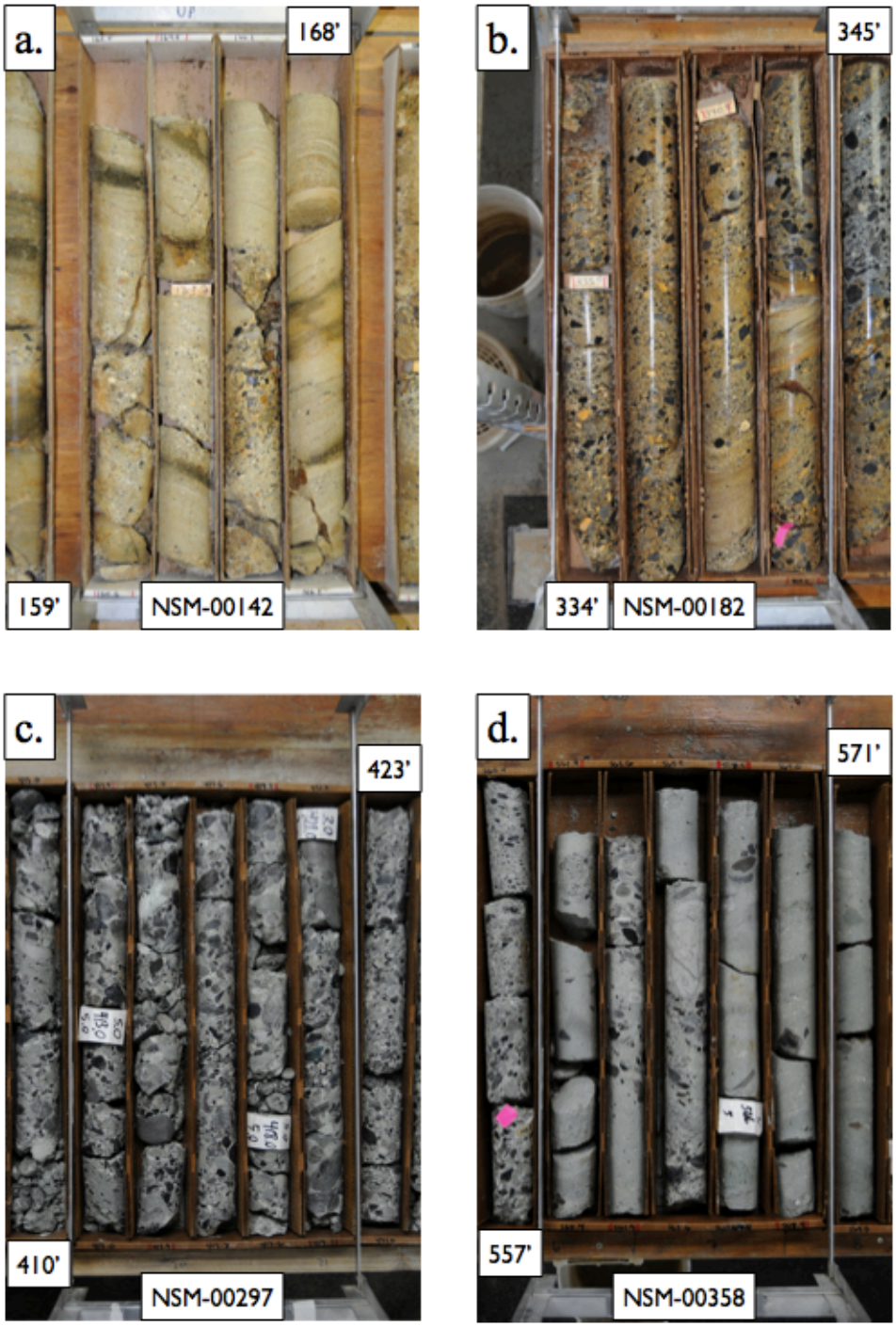

Figure 18: Core photos showing variations in fluvial rocks within the Sandman project area. A.) Oxidized tuffaceous sandstone and conglomerate ± distal basement clasts from Silica Ridge. B.) Oxidized and intensely quartz-adularia altered tuffaceous sandstone and conglomerate + distal basement clasts from North Hill. C.) Unoxidized distal basement dominant conglomerate north of Silica Ridge. D.) Unoxidized distal basement rich conglomerate lenses interbedded with tuffaceous sandstone from Southeast Pediment.

Lacustrine Mudstones and Siltstones

Additional sedimentary rocks in and around the Sandman deposits include thin and discontinuous lacustrine deposits encountered intermittently in drill core and exposed in exploration trenches both at North Hill and Ten Mile. These rocks are thinly laminated, beige to tan, tuffaceous mudstone and siltstone ± fine grained tuffaceous sandstone. Trenches at the Ten Mile Mine expose an approximately ten foot stacked sequence of water lain ash with some layers containing abundant leaf fossils and detrital organic material. Here, conifers include *Chamaecyparis* and *Tsuga* (long slender needles) and dicots consist of *Quercus pollardiana* and/or *Q. simulata*, *Cercocarpus,* or *Ceanothus*? (See Fig. 20). Tertiary rocks within the Ten Mile Mine area are poorly exposed except within trenches and have not been correlated with stratigraphy elsewhere on the property; however, the fossil leaf assemblage indicates an age range of Early to Middle Miocene (Dianne Erwin personal communication).

Organic rich, sedimentary horizons have also been encountered in drill core at North Hill, Southeast Pediment, and Abel Knoll. At North Hill, these intercepts include an approximately ten foot thick package of thinly laminated, dark gray to black, carbonaceous and sulfur rich mudstones and siltstones interbedded with basal conglomerates towards the base of the section. These rocks were deposited in a lacustrine and/or floodplain environment. Directly above these organic rich mudstones and siltstones occurs an approximately fifty foot thick package of finely varved and laminated ash that is also likely lacustrine in origin (Fig. 15). Given the distinct color, this package has been referred to as the Burgundy Tuff by Newmont geologist. A thin, biotite rich tuff interbedded with lacustrine ash of the Burgundy Tuff plots in the dacitic

field on a TAS diagram (refer to Fig. 33), as do samples of the Burgundy Tuff. The distinct burgundy color of this horizon is a result of oxidation of these more mafic rich tuffaceous units.

Higher in the section at North Hill occur thinly laminated, beige to tan, tuffaceous siltstone ± mudstone, interbedded with fine grained tuffaceous sandstone. These intervals range from less than one foot to as much as 15 feet in thickness and often contain horizons abundant in detrital organic material including conifer needles and bark fragments (Fig. 20). Organic rich sedimentary horizons encountered in drill core are also present at Southeast Pediment. These include thin and discontinuous organic horizons interbedded within limited fluvial sandstones and conglomerates higher in the section. Also, within the middle of the section is a one to five foot thick interval of carbonaceous and sulfur rich mudstone that occurs at the upper extent of the Red Green Breccia Tuff Package (Fig. 15, see later section on tuffs).

Sedimentary features within these rocks include preserved ripple marks and soft-sediment deformation including slumping, micro-growth faults, and ball-and-pillow structures. Additionally, desiccation cracks indicating subaerial exposure have also been observed in lacustrine horizons higher in the section at North Hill. While many of these lacustrine deposits likely represent seasonal or intermittent bodies of water, a more persistent lacustrine environment existed at Abel Knoll lower in the section. Here, drill core intercepts approximately 200 feet of lacustrine sediments, including numerous varved, organic and sulfur-rich horizons.

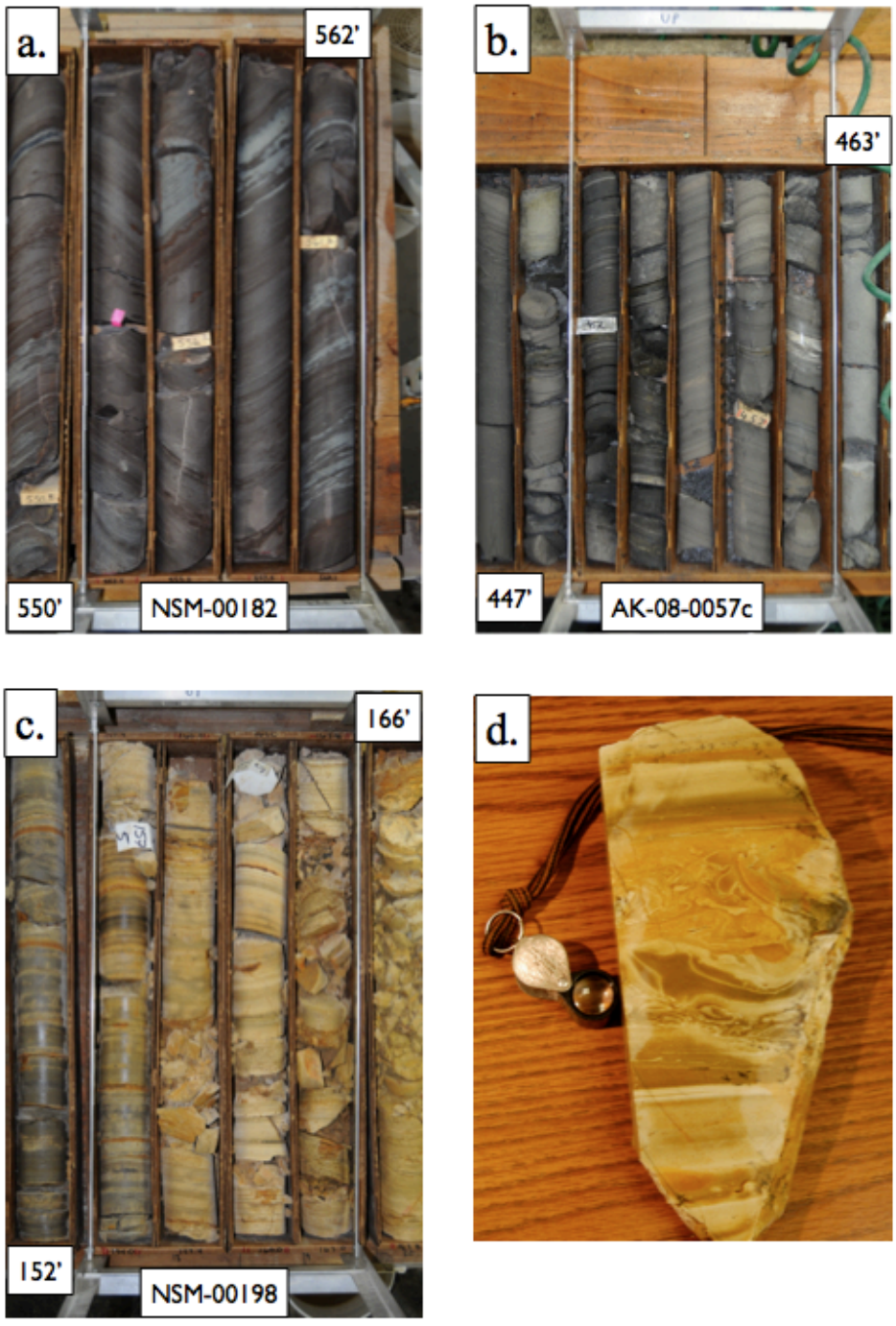

Figure 19: Core photos showing variations in lacustrine rocks within the Sandman project area. A.) Lacustrine (?) burgundy tuff from North Hill. B.) Tuffaceous volcanic sediments and carbonaceous rich horizons from Abel Knoll. C.) Varved tuffaceous lacustrine sediments with beds rich in detriatial organic material at North Hill. D.) Slabbed sample of adularized and silicified lacustrine deposit with turbulent rip up clast from trenches at North Hill.

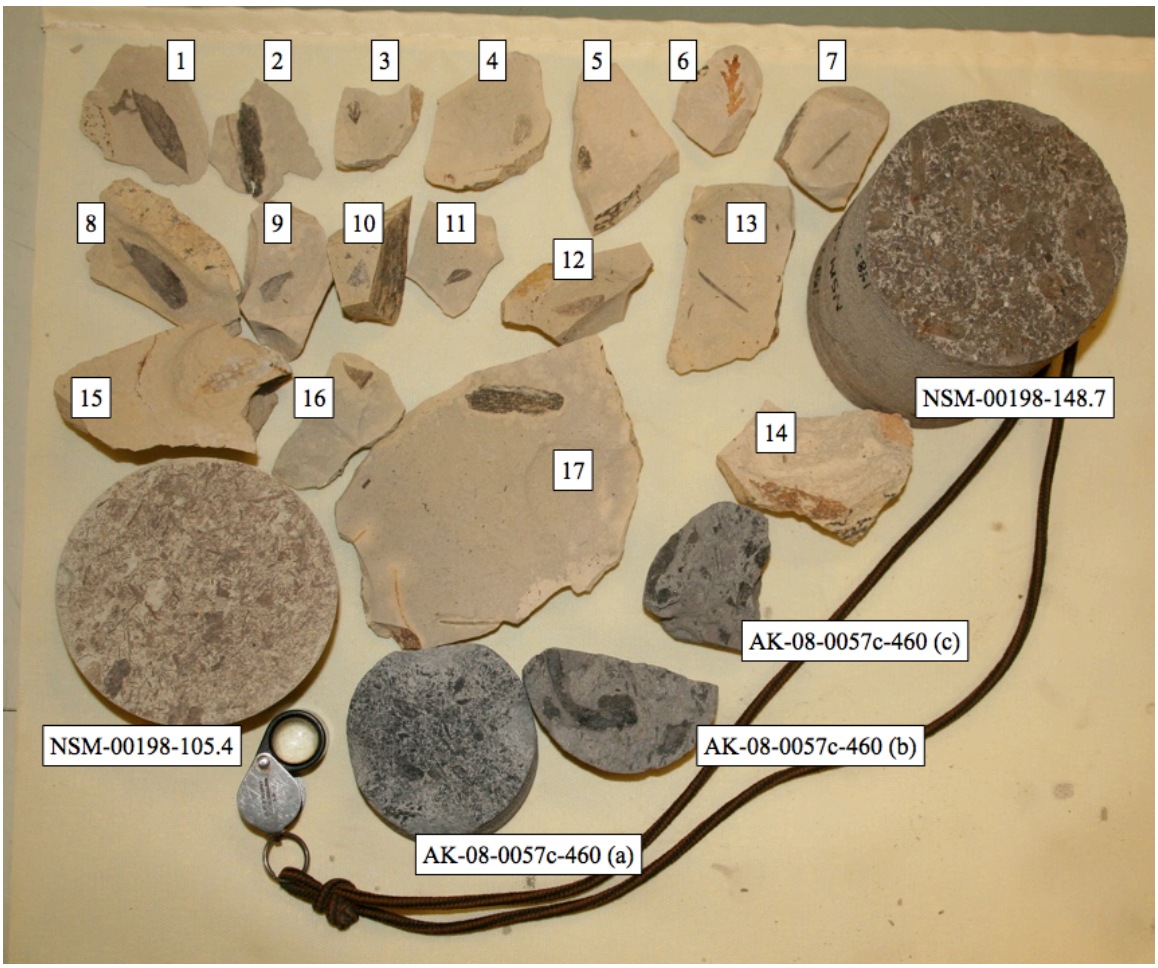

Figure 20: Fossil specimens and organic rich drill core from the Sandman project area. Samples 1 through 14 are from lacustrine tuffs exposed in trenches at the Ten Mile Mine. NSM-00198-xxx are drill core samples from the North Hill deposit (see Fig. 23). AK-08-0057c-460 (x) are drill core samples from the Abel Knoll deposit (see Fig. 31). Samples from the Ten Mile Mine include the conifers *Chamaecyparis* and *Tsuga* (long slender needles) and dicots consist of *Quercus pollardiana* and/or *Q.simulata*, *Cercocarpus,* or *Ceanothus*? This fossil leaf assemblage indicates an age range of Early to Middle Miocene (Dianne Erwin personal communication). North Hill samples consist of abundant conifer needles and bark, while Abel Knoll samples are dominated by detrital organic material. Samples from North Hill and Abel Knoll have not been identified.

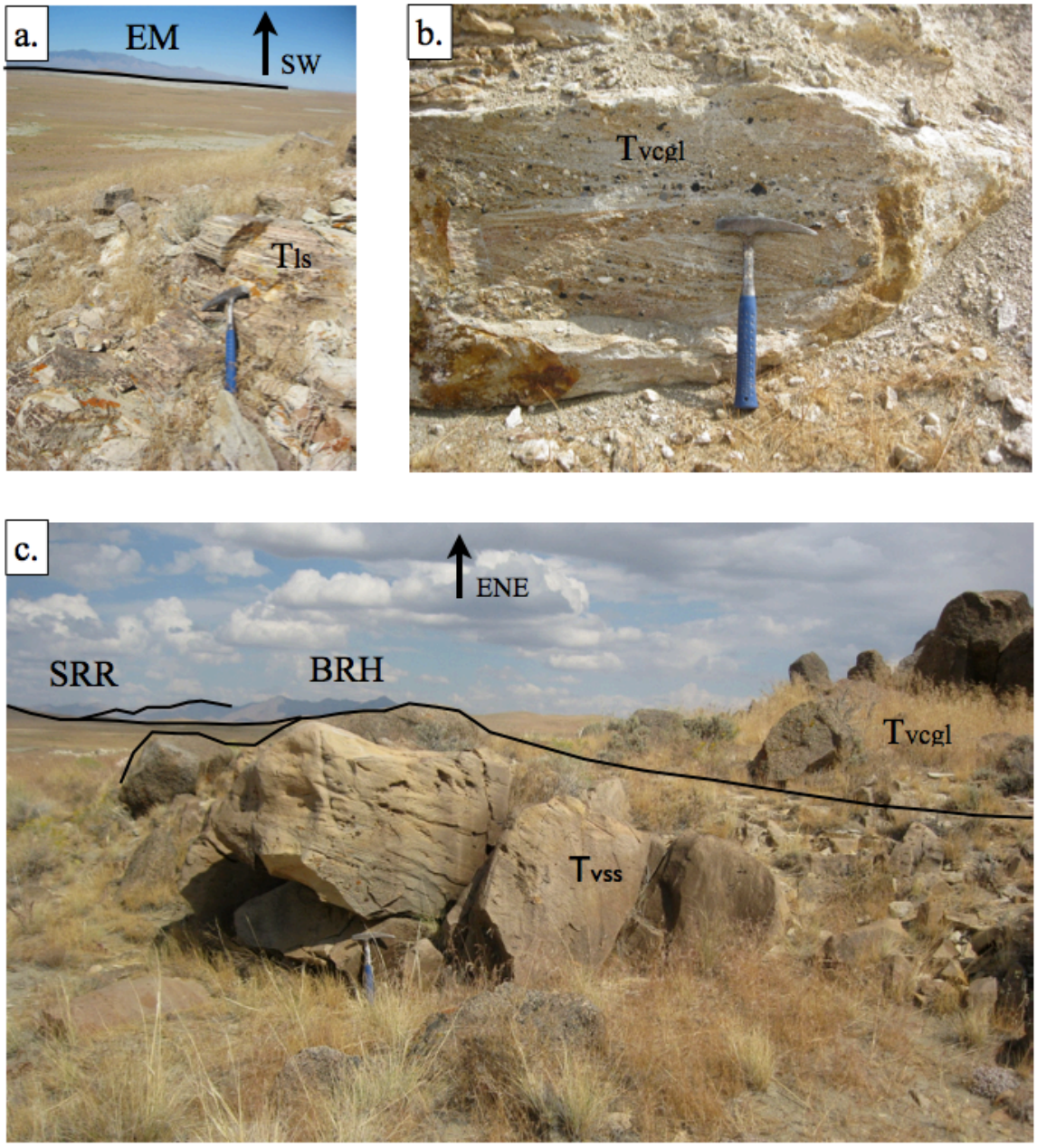

Figure 21: Outcrop exposures of Tertiary tuffaceous lacustrine and fluvial deposits. A.) Lacustrine and epiclastic tuffs beneath a 26.0 unnamed tuff at Adularia Hill. B.) Cross-bedded Tertiary volcanic conglomerate from trench exposure at North Hill. C.) Outcrop exposure of Tertiary volcanic conglomerate and sandstone at North Hill. EM = Eugene Mountains, Tls = Tertiary lacustrine sediments, Tvcgl = Tertiary volcanic conglomerate, Tvss = Tertiary volcanic sandstone, SRR = Santa Rosa Range, BRH = Bloody Run Hills.

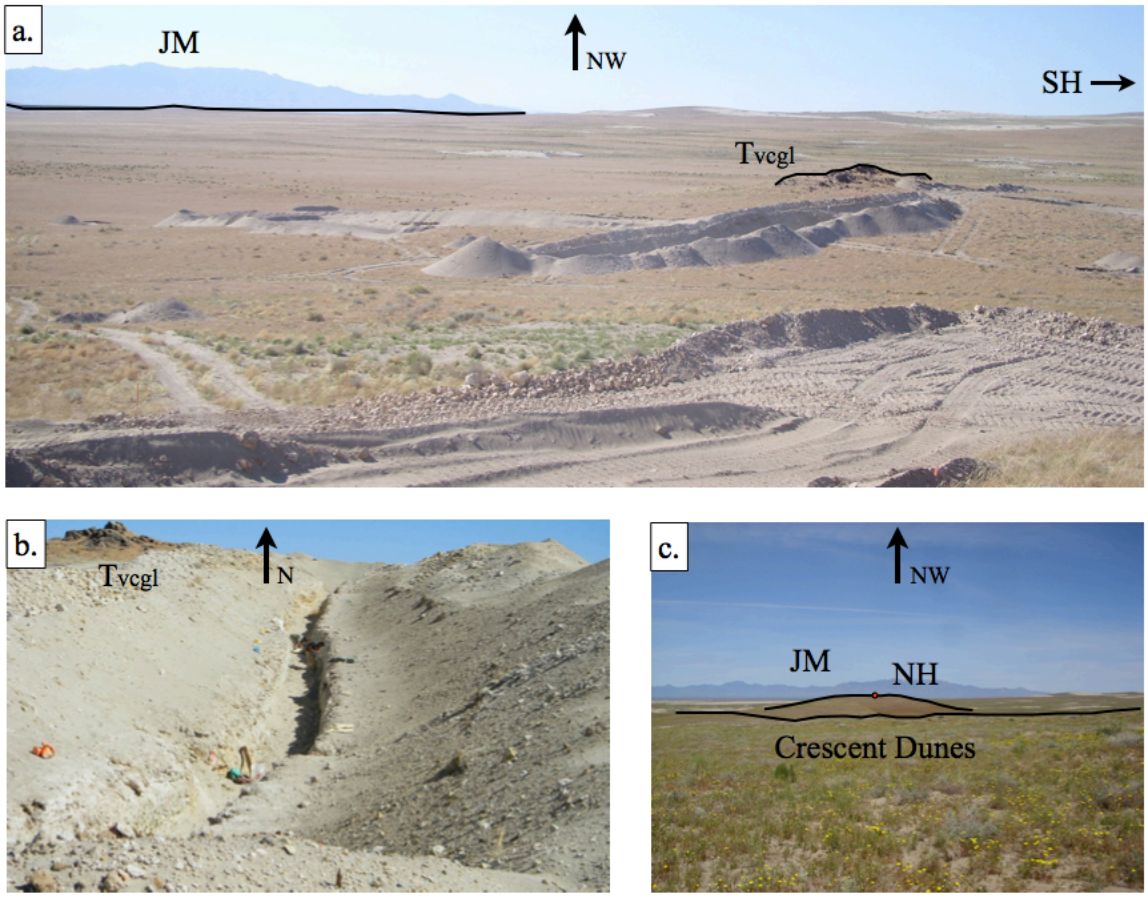

Figure 22: Photos from the North Hill Deposit. A.) Photo looking northwest from the top of North Hill across drill pads and trenches of 2010. B.) Close up image of trench illustrating extensive cover of the Quaternary Crescent Dune Field. Image looking north in trench shown in Fig. 22a. C.) Photo looking northwest towards Nine Hill. JM = Jackson Mountains, SH = Slumbering Hills, NH = North Hill, Tvcgl = Tertiary volcanic conglomerate.

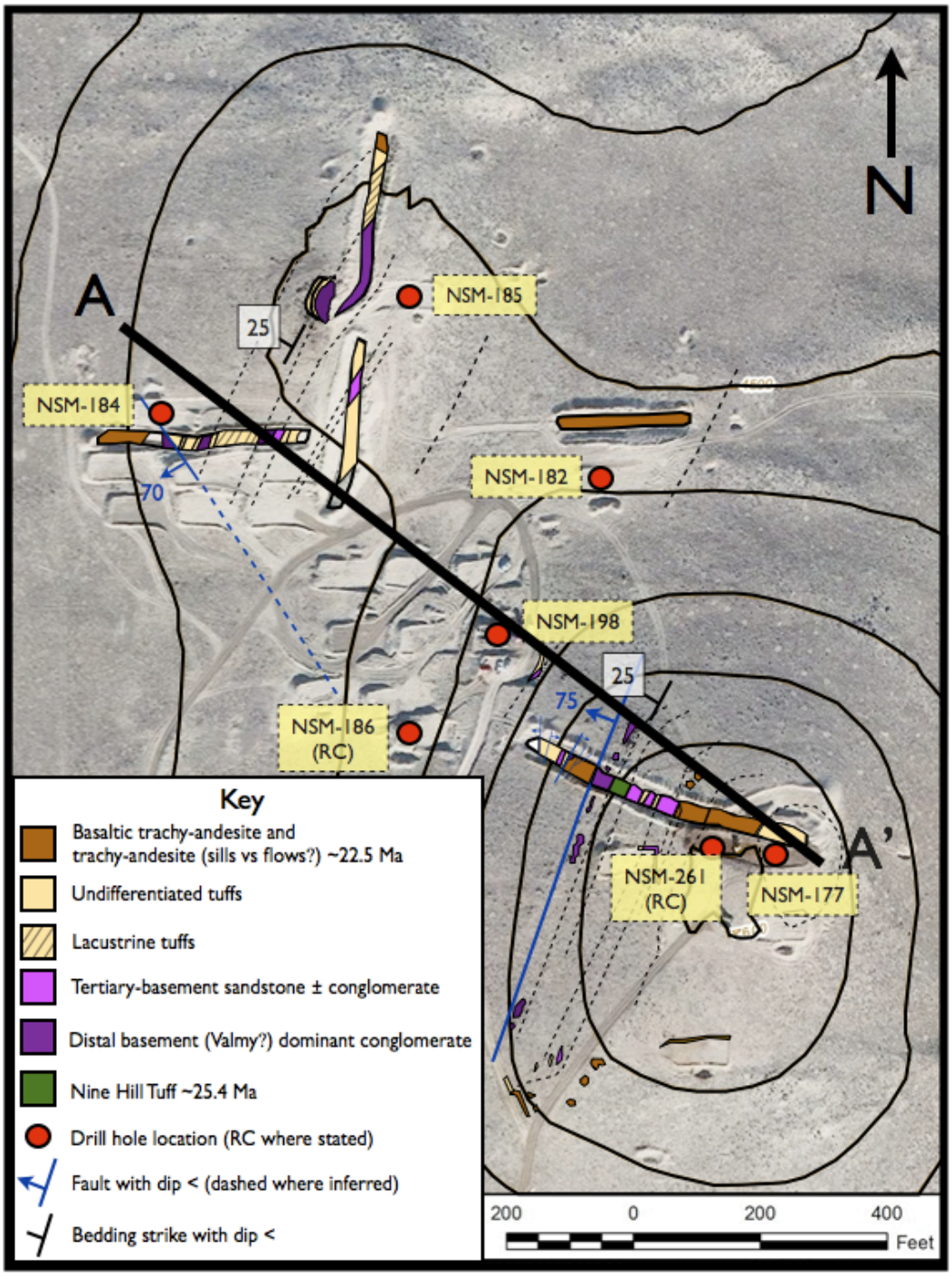

Figure 23: Geologic map of outcrop and trenches from North Hill deposit. See Fig. 5 for location and Figs. 24 and 25 for detailed cross sections. Given strike and dip of bedding, only approximately 150 feet of section are exposed west of the main fault and approximately 100 feet of section east of the main fault. Drill holes utilized in cross sections are given.

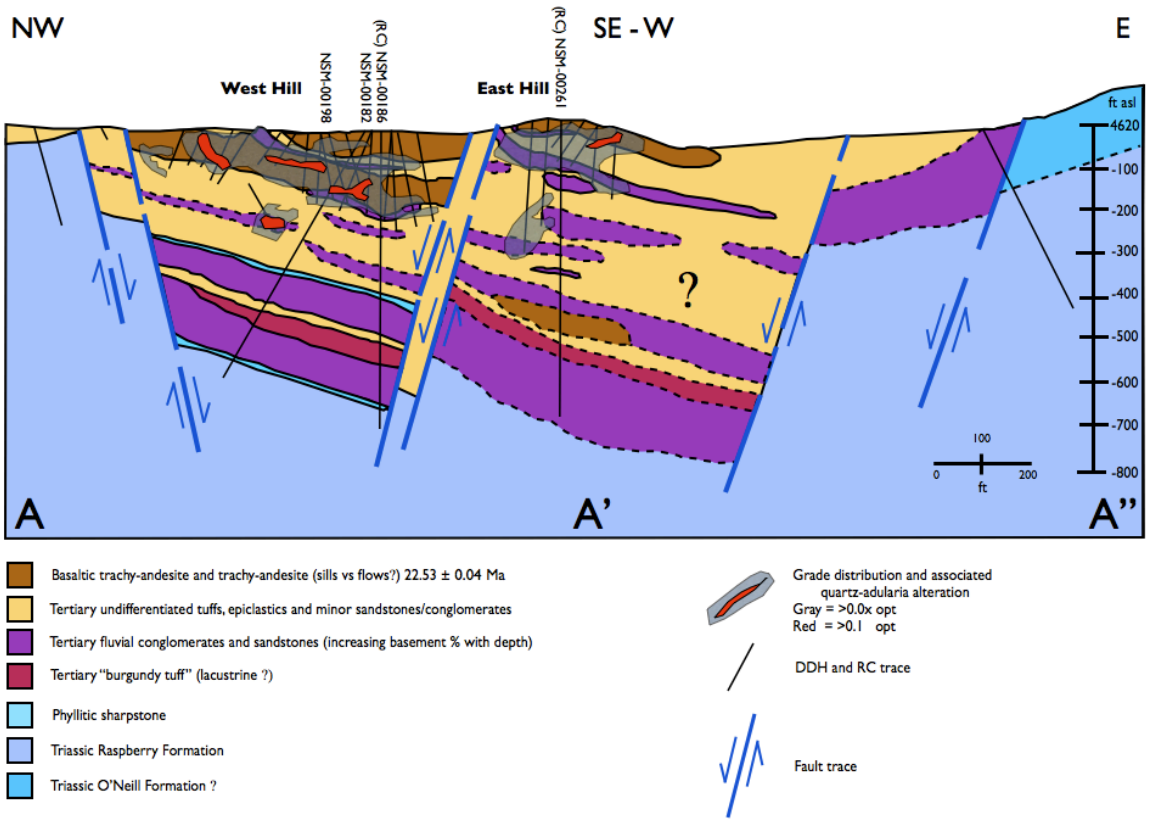

Figure 24: Generalized geologic cross section for the North Hill deposit showing rock distributions, structural features, grade distribution, and drill hole density in the vicinity of North Hill. Color differs slightly between key and figure for grade distribution and associated quartz-adularia alteration. See Fig. 5 for location, Fig. 15 for stratigraphic column, Fig. 23 for surface geologic map, and Fig. 25 for detailed stratigraphic cross section of North Hill. Modified from unpublished work by Newmont geologist Eric Lauha, Reed Kofeod, and Clay Postlethwaite.

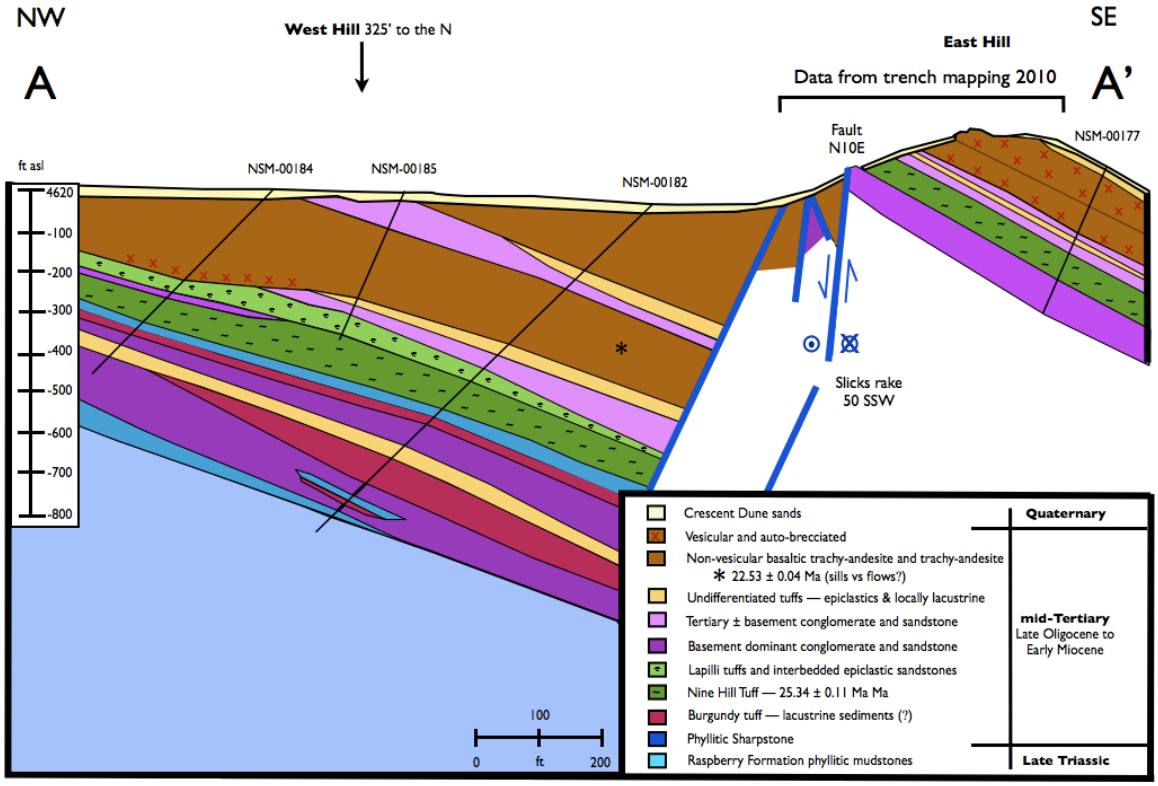

Figure 25: Detailed geologic cross section for the North Hill deposit showing structural offset along main structure as determined from position of Nine Hill Tuff. Note section is slightly oblique to Fig. 24 cross section. See Fig. 5 for location, Fig. 15 for stratigraphic column, and Fig. 24 for generalized cross section with structural features and grade distribution in the vicinity of North Hill.

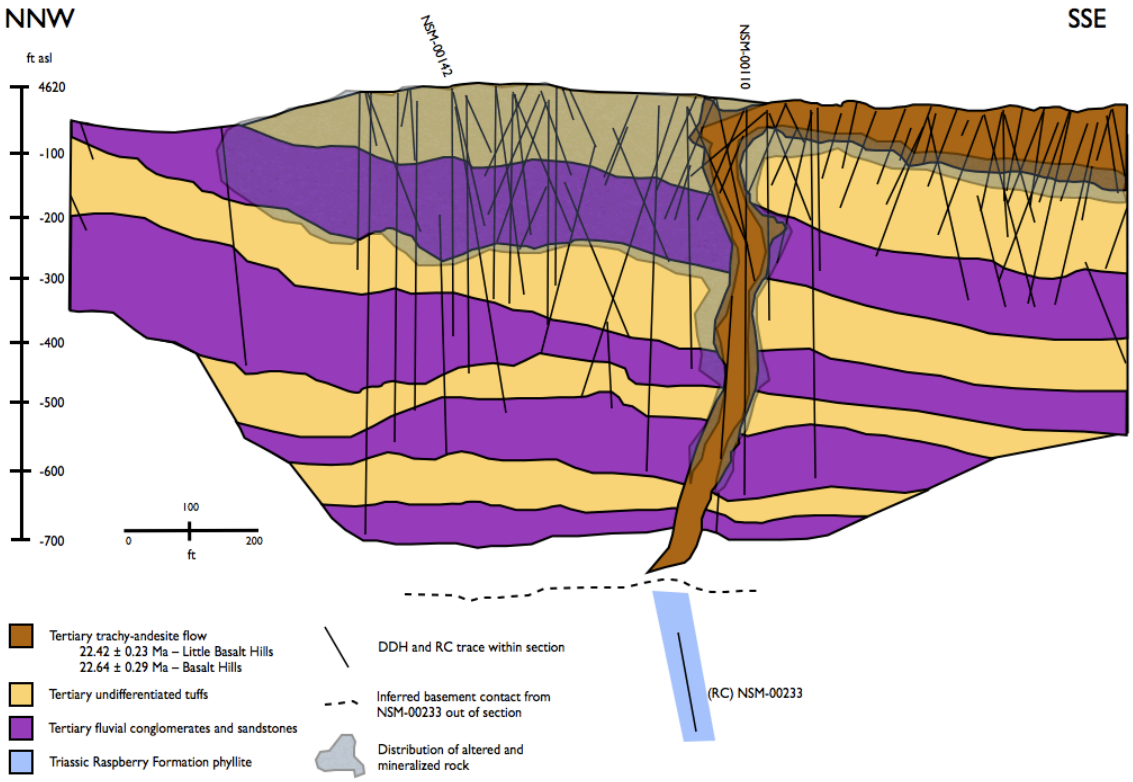

Figure 26: Generalized geologic long section for the Silica Ridge deposit. Section shows repetitive nature of fluvial channel deposits, location of mafic dike and surface flow, grade distribution, and drill hole density. The second tuff package down section constituents the Silica Ridge Tuff Package composed of the ~25.4 Ma Nine Hill Tuff, and an unnamed ~26.0 Ma crystal and pumice rich Tuff. Color differs slightly between key and figure for grade distribution and associated quartz-adularia alteration. See Fig. 5 for location, Fig. 15 for stratigraphic column and Fig. 27 for detailed stratigraphic cross section. Modified from unpublished work by Newmont geologist Eric Lauha.

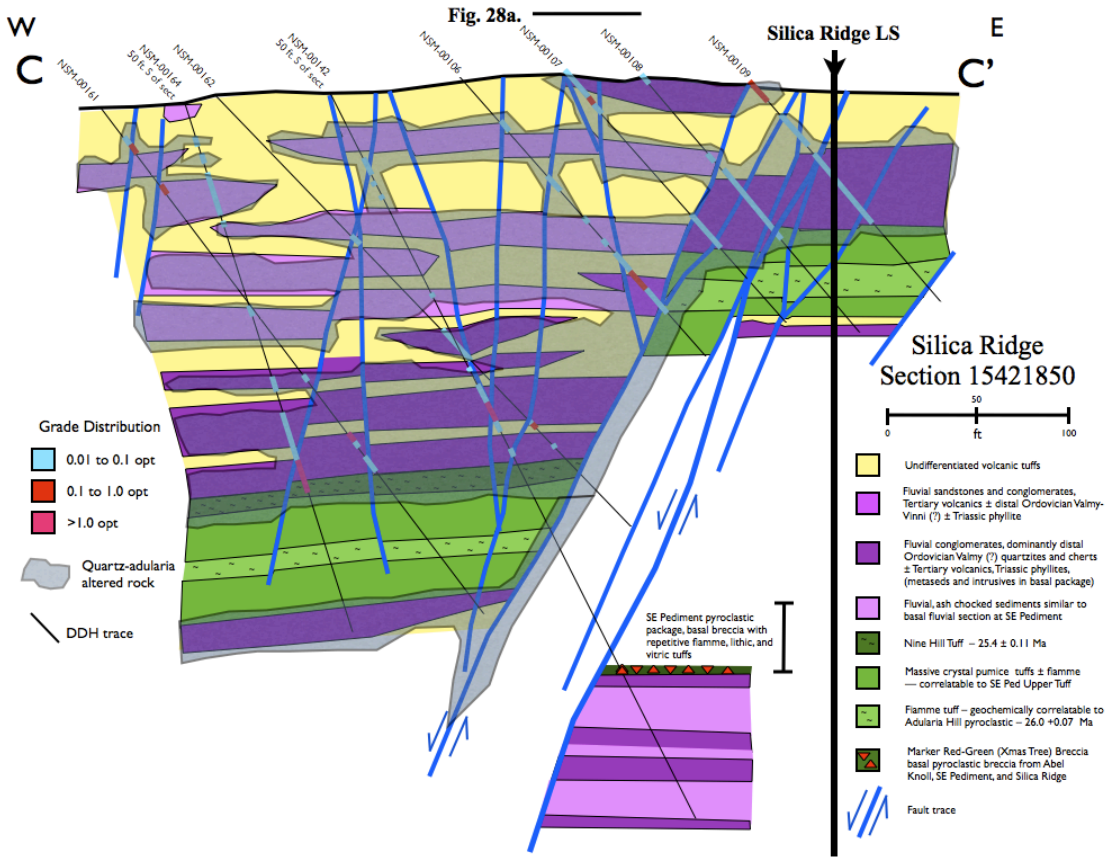

Figure 27: Detailed geologic cross section for the Silica Ridge deposit showing structural offset along main structure as determined from position of Silica Ridge Tuff Package. Note erosional removal of the Nine Hill Tuff in the eastern fault block. The Red-Green Breccia Tuff has only been encountered in two deep drill holes in the vicinity of Silica Ridge. Color differs slightly between key and figure for grade shell distribution and associated quartz-adularia alteration. See Fig. 5 for location, Fig. 15 for stratigraphic column, Fig. 26 for generalized geologic long section of the Silica Ridge deposit and Fig. 28a. for outcrop vein expression. Modified from Lauha et al. (2010).

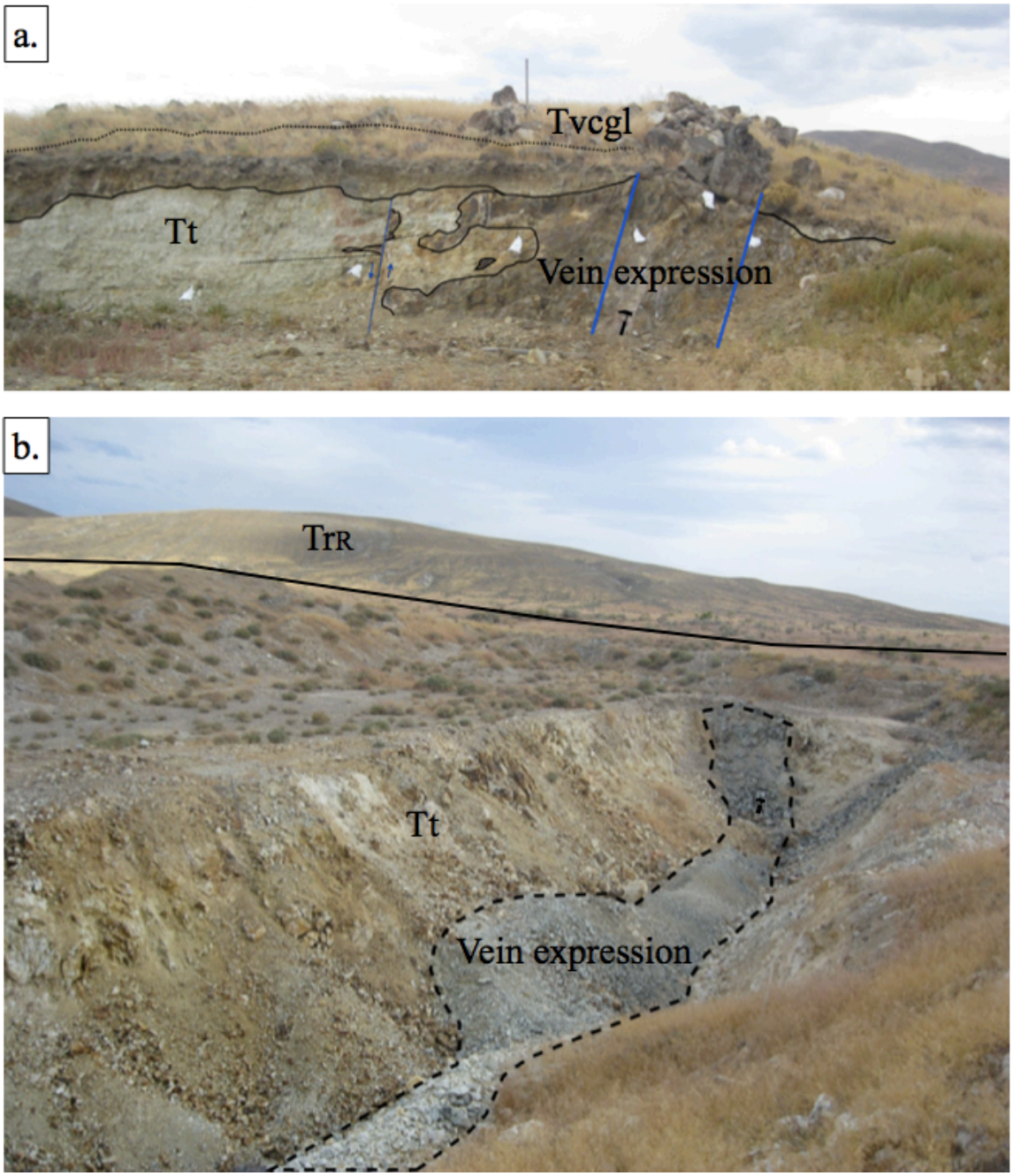

Figure 28: Outcrop expressions of intense adularization and silicification along vein structures at Silica Ridge and Southeast Pediment deposits. A.) Drill pad cut of vein at Silica Ridge. Photo is looking south. See Fig. 27 for cross section. B.) Bulk sample test pit exposure of Southeast Pediment vein. Photo is looking south-southeast. See Fig. 29 for vein surface projection and Fig. 30 for cross section. TrR = Triassic Raspberry Formation, Tt = Tertiary tuff, Tvcgl = Tertiary conglomerate. Rock hammer for scale.

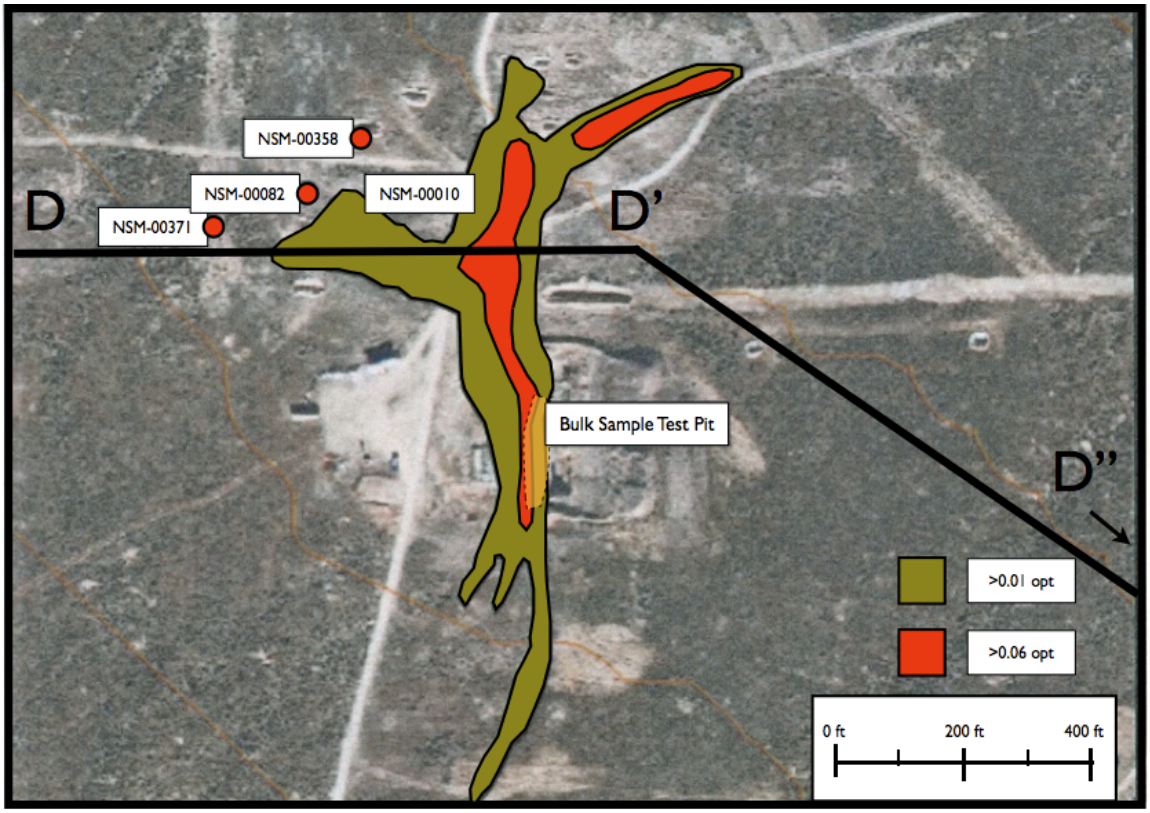

Figure 29: Grade distribution projected to surface for the Southeast Pediment deposit. Highest grades are found at the intersection of north striking and east-northeast striking faults. Mineralized lobe to the west of the main ore trend is hosted in porous and permeable fluvial channel deposits. Location of bulk sample test pit and drill holes used in the generation of generalized cross section are also shown. See Fig. 5 for location, Fig. 15 for stratigraphic column, and Fig. 30 for generalized geologic cross section. Modified from unpublished work by Newmont geologists.

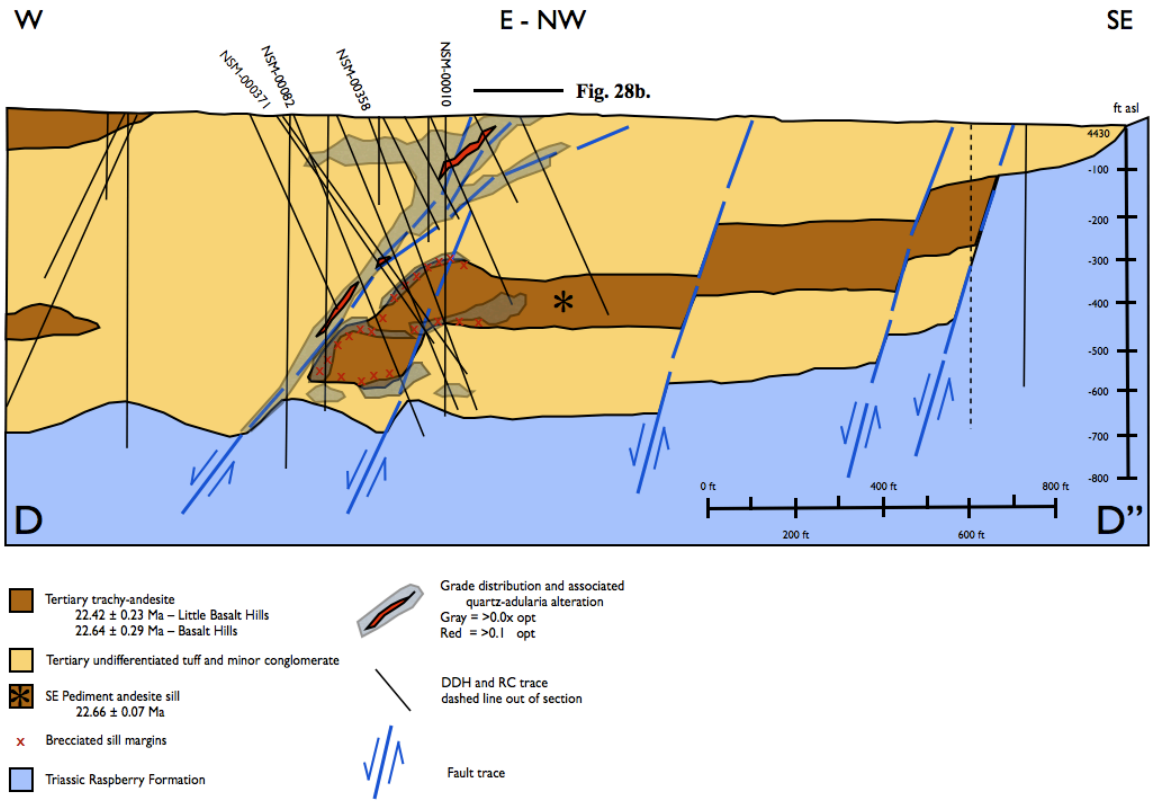

Figure 30: Generalized geologic cross section for the Southeast Pediment deposit. Note down to the west structural offset as shown by mafic sill. The Red-Green Breccia Tuff has been shown by relative stratigraphic positions to be greater than ~26.0 Ma at the Silica Ridge deposit. The mafic sill below this marker horizon has been dated at 22.66 ± 0.07 Ma. Note mineralized lobe to the west of the main mineralized structure is hosted in porous and permeable fluvial channel deposits. Color differs slightly between key and figure for grade distribution and associated quartz-adularia alteration. See Fig. 5 for location, Fig. 15 for stratigraphic column, Fig 28b. for outcrop vein expression and Fig. 29 for grade distribution plotted to surface. A detailed stratigraphic cross section was not compiled as the figure becomes to busy. Modified from unpublished work by Newmont geologist Eric Lauha, Reed Kofoed, and Clay Postlethwaite.

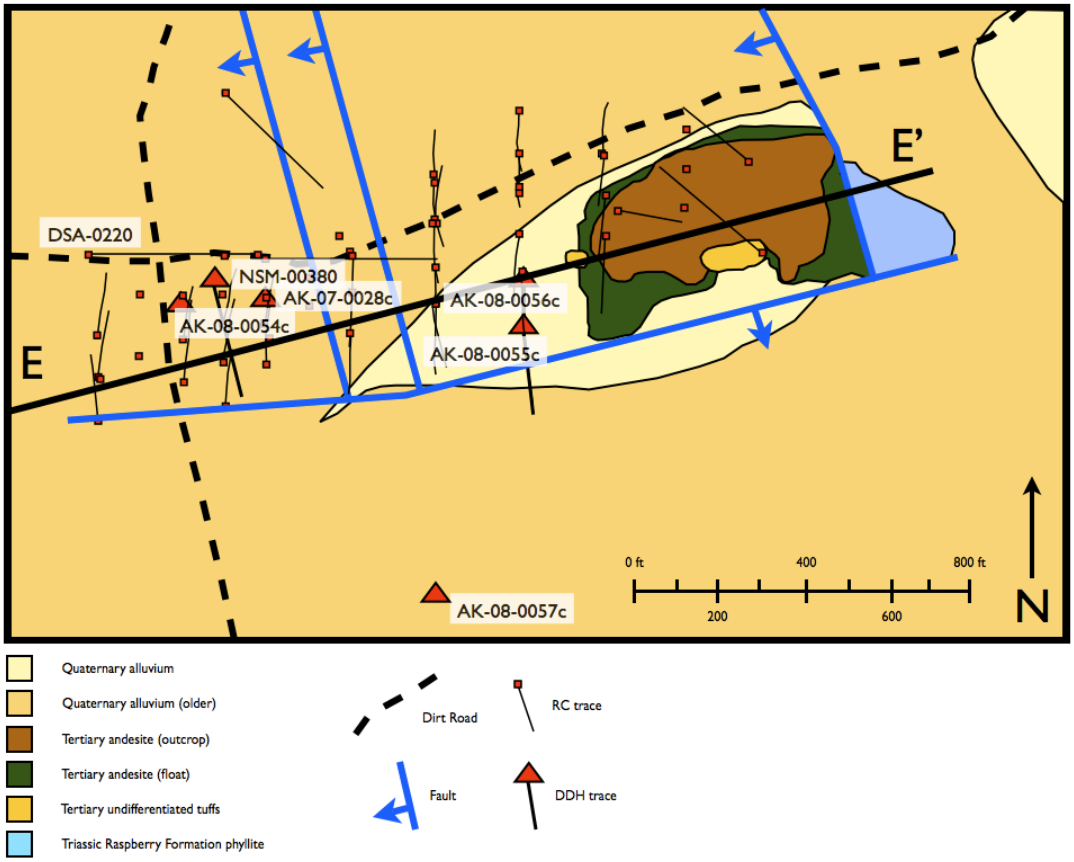

Figure 31: Geologic map of the Abel Knoll deposit. Structural features determined based on geophysics and subsurface drilling. Drill holes used in the generation of Fig. 32 are shown. As AK-08-0057c is outside of the main breccia body, it was used in the generation of a detailed stratigraphic section for the deposit. Note basement pierce points in AK-08-0056c (north of east striking fault) and AK-08-0055c (cross fault) indicate approximately 350 feet of down to the south displacement. See Fig 5 for location, Fig. 15 for stratigraphic column, and Fig. 32 for generalized geologic cross section. Modified from unpublished map by Newmont geologist Clay Postlethwaite.

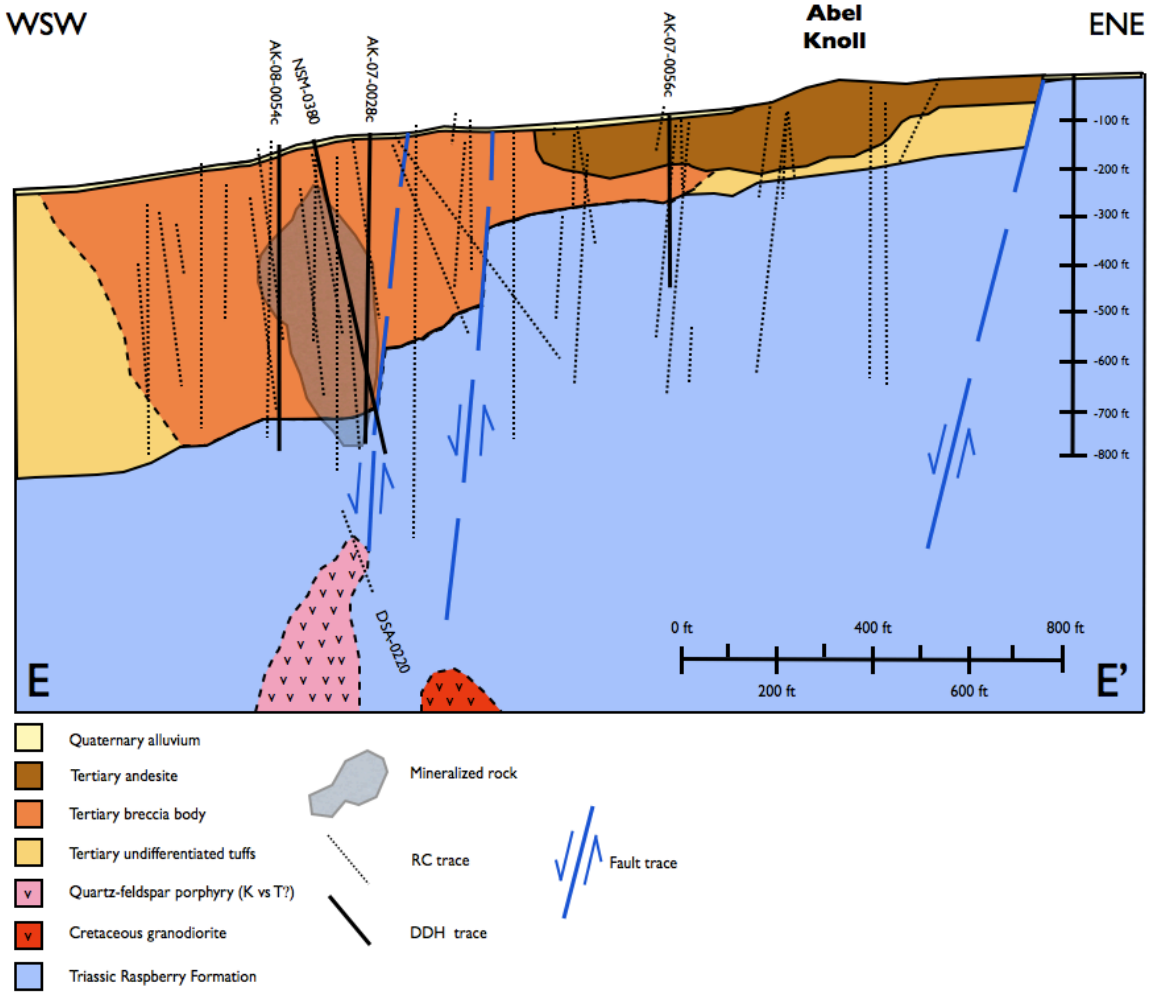

Figure 32: Generalized geologic cross section for the Abel Knoll deposit. Color differs slightly between key and figure for grade distribution and associated quartz-adularia alteration. Color differs slightly between key and figure for grade distribution and associated quartz-adularia alteration. See Fig. 5 for location, Fig. 15 for stratigraphic column, and Fig. 31 for surface geologic map. Modified from unpublished work by Newmont geologist Eric Lauha, Reed Kofoed, and Clay Postlethwaite.

Airfall, Ash-flow, Pyroclastic, and Epiclastic Tuffaceous Rocks

Tuffaceous rocks comprise a significant part of the Sandman stratigraphy and include abundant airfall tuffs, limited pyroclastic deposits, the distally sourced Nine Hill ash-flow tuff, and abundant epiclastics resulting from the weathering and reworking of primary tuffaceous deposits. Recognition of two tuffaceous marker horizons — the Red-Green Breccia pyroclastic package at Silica Ridge, Southeast Pediment and Abel Knoll, and the Nine Hill Tuff at North Hill and Silica Ridge — has allowed for the correlation of variable strata from deposit to deposit (see Fig. 15). The distribution of tuffaceous rocks across the property and within section show spatial and temporal variations, resulting from variability in deposition, preservation and changing volcanic input with time.

As discussed in the previous section on sedimentary rocks, fluvial rocks are prevalent in the north of the project area at North Hill, Silica Ridge, and Adularia Hill, recording the existence of a major Tertiary paleodrainage. Additionally, fluvial rocks are present at the base of the section at Southeast Pediment and a long-lived lacustrine environment is recorded towards the base of the section at Abel Knoll. At Abel Knoll the base of the section has not been drilled; however, it is possible that limited fluvial rocks are present here at the unconformity between Triassic basement rocks and the overlying Tertiary package. These fluvial depositional environments limited the preservation of many primary tuffaceous deposits through erosion. Fluvial channels may have also played a role in primary deposition, with pyroclastics and ash-flow tuffs deposited in paleotopographic lows (see later discussion on Nine Hill Tuff).

Temporal variations in the distribution of tuffaceous rocks within the Sandman stratigraphic section reflect increasing input and volume as well as changing composition

through time. While present at the base of the section, the volume of tuffaceous rocks is significantly less than that higher in the section. This reflects preservation rates within the lower fluvial sequence in the north of the property. Initial input also likely played a contributing factor with the thickest volume of tuffaceous rocks occurring in the middle of the section, and epiclastics dominating in upper portions of the stratigraphic column. Changes in composition of tuffaceous rocks also record temporal variations throughout the section (Figs. 12 and 23), with tuffs towards the base of the section being dacitic (NH deep tuff, Abel Knoll tuff, Burdgundy tuff) progressing up section to tuffs of rhyolitic composition (Red-Green Breccia tuff, SE Ped upper tuff, Silica Ridge-Adularia Hill unnamed tuff, Nine Hill Tuff). Sources for tuffaceous deposits have not been established and likely represent a combination of both local and distal sources.

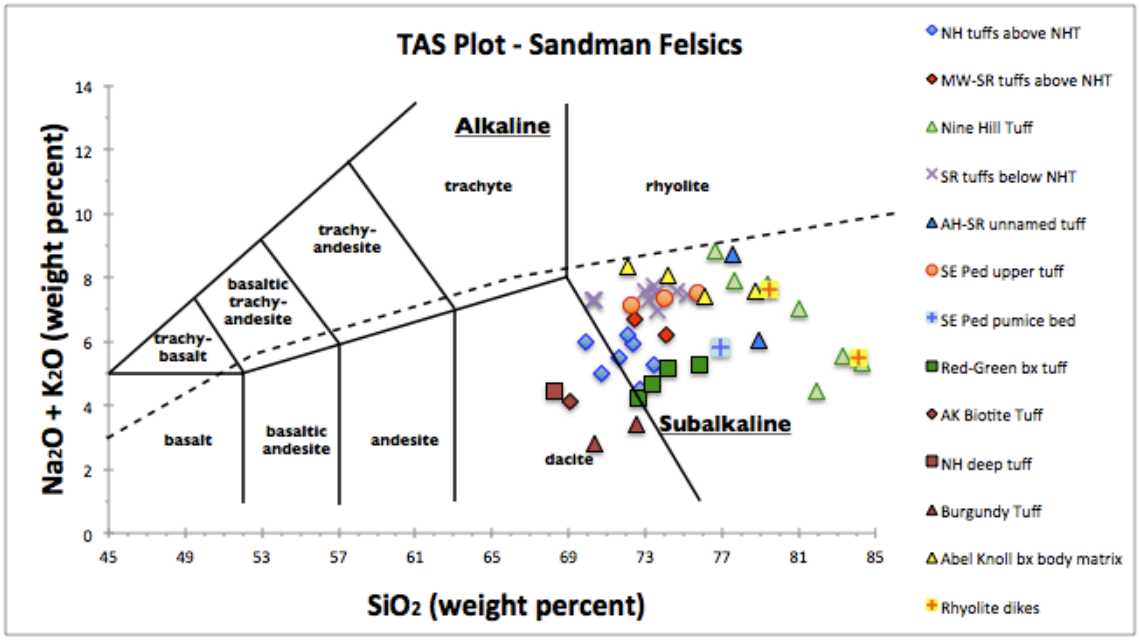

Figure 33: Total alkali versus silica plot for tuffaceous units in the Sandman stratigraphic section. See Fig. 15 for locations within stratigraphic column. Data for two rhyolite dikes (see Fig. 59 for locations) and altered matrix from Abel Knoll breccia body also plotted. See Appendices 2 through 12 for all geochemical data. Division between alkaline and subalkaline from Irvin and Baragar (1971).

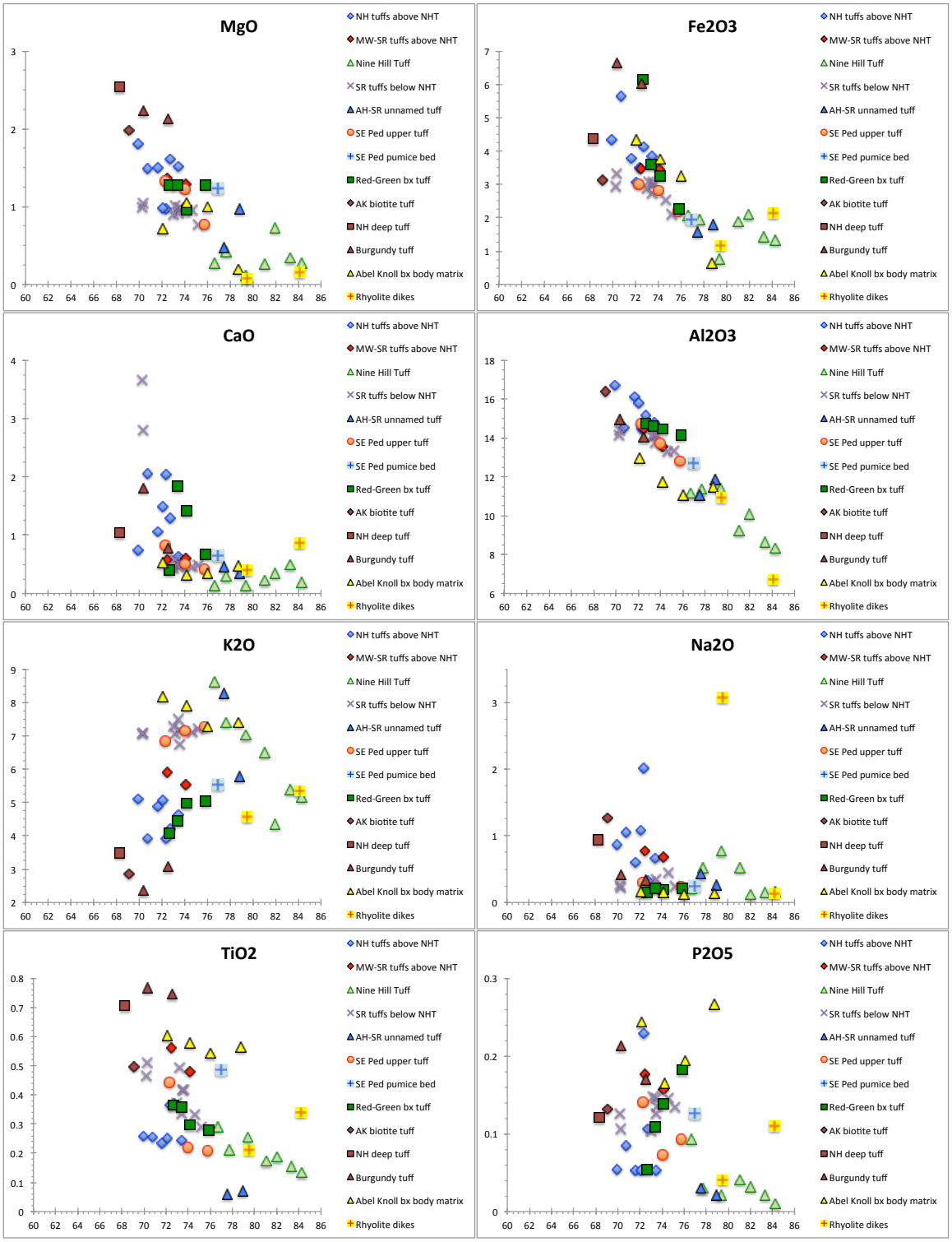

Figure 34: Harker diagram plots of whole rock analyses for all tuffaceous rock packages within the Sandman stratigraphic section.

Undifferentiated Tuffs and Epiclastics

In establishing stratigraphic columns within the Sandman project area, individual tuffaceous deposits and packages have been broken out where possible in an effort to correlate variable strata from deposit to deposit. A large portion of tuffaceous rocks within the stratigraphic package includes vitric to lapilli airfall tuffs and epiclastic deposits. Where notable discerning characteristics are lacking (i.e. fiamme, crystal and lithic contents) these rocks have not subdivided within columns as figures become far to busy. The following is a general description of undifferentiated tuffs and epiclastics, with subsequent sections describing notable and/or correlative tuffaceous deposits organized from the base to the top of the section.

Tuffs are typically beige, gray, light brown, green and in places pink. Consisting dominantly of vitric airfall tuffs, beds within these undifferentiated units range from less than one to several feet in thickness and are commonly finely laminated and normal graded, although rare instances show limited reverse grading. Predominantly composed of very fine-grained ash, matrix components also including variable percentages of shards, lapilli, and pumice. Limited crystal fragments and lithics may also present. Crystalline fragments include anorthoclase, beta quartz, biotite, and sanidine. Trace, very-fine grained, euhedral blue and blue-green topaz has also been observed locally in drill core. Lithics are commonly comprised of vitric and crystalline tuffs and volcaniclastics with lesser degrees of basement phyllite and quartzite clasts. Where the increased presence of basement lithics has been observed (i.e. at Southeast Pediment and Abel Knoll) these units have been sub-divided. Thin accretionary lapilli horizons have also been observed though have not served as a correlatable feature.

Interbedded within primary tuffaceous units, epiclastic tuffs are present throughout the entire section, resulting from limited weathering, simple sorting and winnowing of fines. With tuffaceous input increasing upwards through the section, epiclastic horizons also increase; however, epiclastic tuffs are typically thin and discontinuous features. Excluding thicker packages of epiclastic tuffs at the base and top of section at North Hill (also see later section on cold compaction fiamme package), and at the base of Southeast Pediment, epiclastics have not been distinguished elsewhere in the stratigraphic section.

Tuffs Low in Section (Abel Knoll Biotite Tuff, NH Burgundy Tuff, NH Deep Tuff)

As mentioned earlier, tuffs towards the base of the section plot within the dacitic compositional field. Distinguished by their typical maroon to burgundy coloration due to the oxidation of mafic crystal fragments and groundmass constituents, tuffs deeper in section are composed of ash, shards, and abundant lapilli sized pumice with euhedral biotite to 2mm a common constituent and variable percentages of basement phyllite lithics to 20%. Due to a lack of deep drilling, data for these deeper tuffaceous deposits is limited. Two holes pierce the lower section at North Hill, one at Abel Knoll, and none at Silica Ridge. Several holes pierce the base of the section at Southeast Pediment, although tuffaceous material is limited and no samples were collected here.

Comparisons of trace element geochemistry between a tuff towards the base of the section at North Hill and the Biotite Tuff present in the middle of the Abel Knoll section suggest the two may be correlative (Fig. 35). Four samples were compared. Samples NSM-00287-592.3 and NSM-00287-541.5 are from the Burgundy Tuff at North Hill. As mentioned earlier this unit is likely lacustrine in origin, although as composed dominantly

of tuffaceous ash, samples were taken for comparison. Sample NSM-00287-529 is from a thin dacitic tuff horizon above the Burgundy Tuff at North Hill, and sample AK-08-0057c-325 is from the Biotite Tuff horizon at Abel Knoll. Plotted on a Modified Spider Diagram for select trace element and REE geochemistry, the dacitic tuff present above the Burgundy Tuff at North Hill and the Biotite Tuff at Abel Knoll have near identical signatures for REE concentrations. With trace element geochemistry suggesting correlation of these two dacitic tuffs between North Hill and Abel Knoll, inferences into the relative age of the Burgundy Tuff can be made.

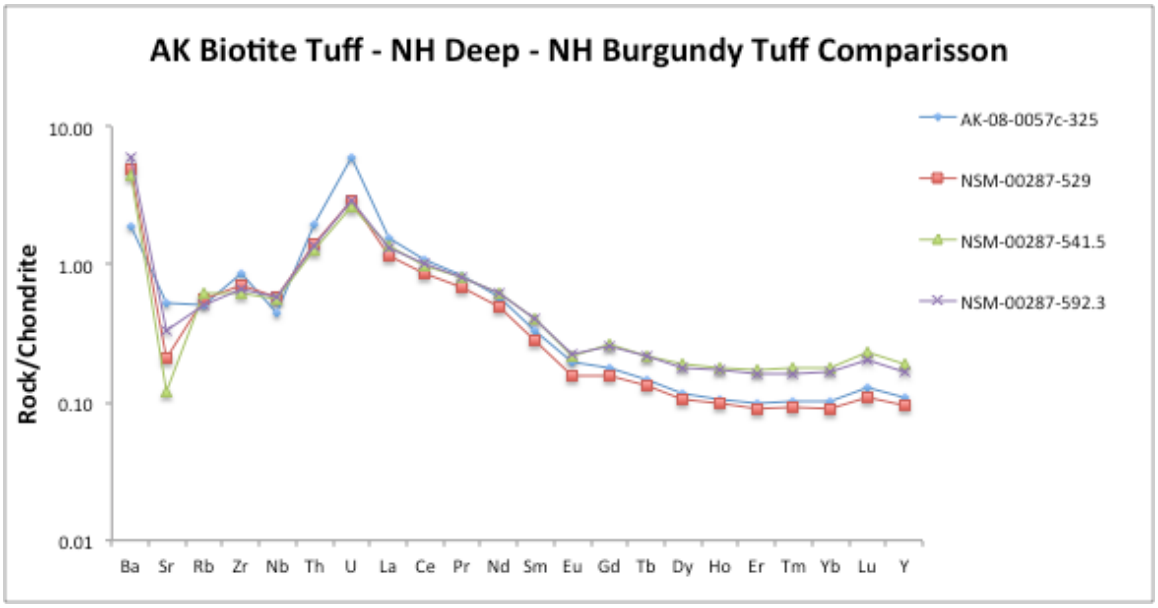

Figure 35: Modified spider diagram for select trace element and REE geochemistry for tuffs deeper in section. Sample AK-08-0057c-325 is from the dacitic Abel Knoll Biotite Tuff. Sample NSM-00287-529 is from a thin dacitic tuff above the North Hill Burgundy Tuff. Samples NSM-00287-541.5 and NSM-00287-592.3 are both from the Burgundy Tuff at North Hill. See Fig. 15 for stratigraphic relationships.

The Red-Green Breccia unit (see later discussion) has been used as one of two marker horizons linking the stratigraphy across the project area and is present at all deposits excluding North Hill and Ten Mile. With the Biotite Tuff occurring beneath the Red Green Breccia unit at Abel Knoll, and the Biotite Tuff of Abel Knoll being potentially correlative to a dacitic tuff above the Burgundy Tuff at North Hill, the Burgundy Tuff package is likely older than the Red-Green breccia marker unit. Probably lacustrine in origin, the Burgundy Tuff is potentially time equivalent to thick lacustrine sediments towards the base of the section at Abel Knoll, indicating a wetter depositional environment during this time period.

REE geochemical comparisons from samples within the Burgundy Tuff also suggest the same tuffaceous source for this thick lacustrine deposit through time. Concentrations and trend lines are near identical for samples from near the base and top of this unit. If the entirety of this deposit is from the same volcanic source, the approximately fifty feet thickness of the Burgundy Tuff represents a relatively short period of time. With rapid airfall sediment loads surpassing the deep fluvial sequence ability to remove this material, this tuffaceous material accumulated in topographic lows or potentially within river cutoffs and resulting Oxbow lakes. Enough deep drilling at North Hill has not been conducted to support or discredit this postulation.

Red-Green (Christmas Tree) Breccia Tuff Package

The Red-Green Breccia tuff package — present at Silica Ridge, Southeast Pediment, and Abel Knoll — is one of three pyroclastic marker units that has allowed for the correlation of variable stratigraphy from deposit to deposit (see Fig. 15). This tuffaceous package does not crop out within the project area and is best illustrated in drill

core from Southeast Pediment. Here thicknesses approach approximately eighty feet. At Southeast Pediment, the package consists of a basal polylithic breccia, a middle repetitive sequence of lapilli lithic, fiamme, and vitric tuffs, and an upper sequence of vitric airfall tuffs. To the south at Abel Knoll, a single core hole pierces the package with a thickness of approximately 25 feet. At Silica Ridge, two core holes have intercepted the basal volcanic breccia marker unit, although the upper extent of the package is unknown here due to structural complications and limited deep drilling (Fig. 27).

Recognized by a distinctive basal polylithic volcanic breccia, this marker horizon has been referred to both as the Red-Green Breccia and the Christmas Tree Breccia in drill logs by Newmont personnel. Most commonly seen in deeper drilling at Southeast Pediment, these names arise from the distinctive red and green color appearance resulting from increased chlorite, pyrite, and hematite due to propylitic alteration associated with the emplacement of an andesitic sill (Fig. 30). Where encountered in drill core at Silica Ridge and Abel Knoll, regional propylitic alteration and subsequent argillic alteration impart a fainter green coloration. At these locations, the basal breccia lacks abundant hematite — and the associated red coloration — although it is still recognizable as a marker unit. Thicknesses of the basal Red-Green breccia unit range from less than one foot to five feet thick at Silica Ridge, approximately four feet at Abel Knoll, and between four and ten feet thick at Southeast Pediment. Breccia clast percentages range from 25-50% and consist of mm-3cm, angular to subangular, crystalline and lithic volcanics ± trace quartzite and phyllite within a poor to moderately welded matrix of mm-4cm chloritized fiamme. Biotite is present to a few percent as is trace quartz and plagioclase crystal fragments.

At Southeast Pediment, the basal Red-Green breccia unit grades upwards into an approximately forty foot thick repetitive sequence of lapilli lithic, fiamme, and vitric airfall tuffs. Individual tuffaceous beds range from less than one to ten feet in thickness, and contacts may be sharp or gradational. Most beds are normal graded, although limited reverse grading has been observed within lapilli lithic beds. Overall, the entire package fines upward. Lapilli lithic horizons resemble the basal Red-Green breccia unit with similar crystalline and lithic volcanic breccia fragments; however, lithic clasts are less than 1cm — typically less than 5mm — and only approach 25% locally. As within the basal Red-Green breccia, abundant fiamme are absent and the groundmass is dominated by lapilli, pumice and fine-grained ash. Fiamme rich tuff beds are composed of lapilli, pumice, and fine-grained ash, with mm-3cm chloritized fiamme ranging from 10-30%. The upper 40 feet of the Red-Green breccia tuff package consists of numerous beds of upward fining vitric airfall tuffs.

It is not known if the entirety of the Red Green breccia tuffaceous package is related to a single event or combination of eruptive events from varying sources. Trace element geochemistry (see Fig. 36) indicates that at least the lower forty feet of this package is related. An upper boundary for the Red-Green tuffaceous package has been drawn where there is a 1-10 foot thick interval of organic and sulfur rich, gray to black, water-lain vitric tuffs that often exhibit soft sediment deformation. Above this horizon there is a return to upward fining vitric tuffs, lapilli tuffs, and a distinct 5-15 foot thick pumice dominant tuff occurring beneath a thick debri-flow package (see discussion on Southeast Pediment debri-flow in previous section on sedimentary rocks). This unit is 50-80% pumice fragments averaging 1cm with trace fragments up to 10cm within a

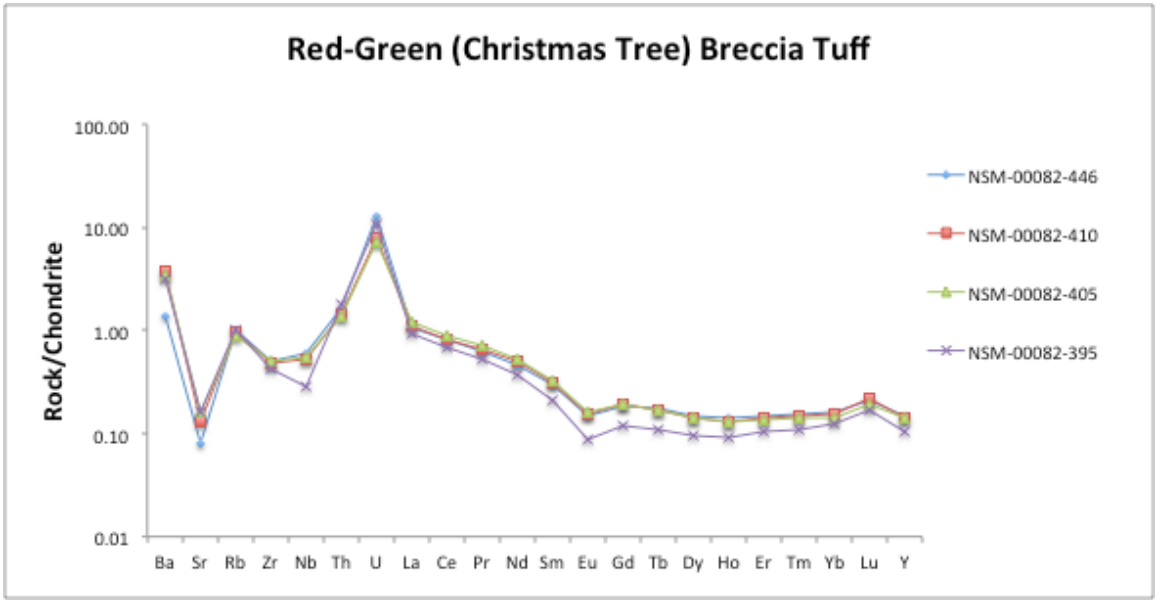

Figure 36: Modified spider diagram for select trace element and REE geochemistry for the Red-Green Breccia tuff package. The basal polylithic breccia occurs just beneath NSM-00082-446 and was not sampled due to contamination from abundant volcanic lithics. Only samples rich in ash and fiamme were sampled from within the Red-Green breccia tuff package. Note similar patterns between samples within the lower forty feet.

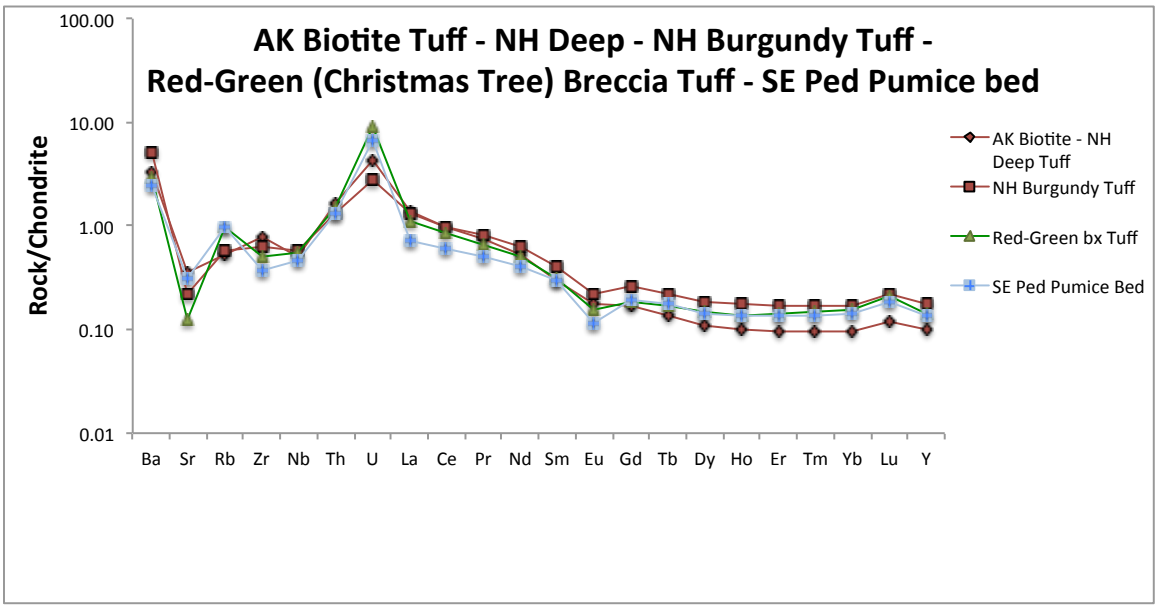

Figure 37: Modified spider diagram for select trace element and REE geochemistry comparing Southeast Pediment Pumice Bed, Red-Green breccia (NSM-00082-395 not used in average), and other tuffs low in the Sandman stratigraphic section. See Fig. 15 for stratigraphic relationships.

medium grained ash matrix. In core, this unit exhibits a characteristic pock marked pattern resulting from the plucking of pumice grains from the cores cut surface. The trace element geochemical signature of this unit shows differing patterns to other tuffs lower in the section (Fig. 37).

An exact age has not been established for the Red-Green Breccia tuffaceous package. Crystal content is very low within this package and no visible sanidine crystal fragments have been recognized in core or thin section. While biotite is present within the basal polylithic breccia, extensive propylitic and limited quartz-adularia alteration have hindered efforts to provide an exact age for this pyroclastic event. As the Red-Green breccia tuff package occurs beneath both the 25.4Ma Nine Hill Tuff and an unnamed tuff dated at 26.0 Ma Silica Ridge and geochemically correlated to Silica Ridge (see later discussion on these tuffs and Figs. 15 and 27 for stratigraphic relationships) a relative age of at least Oligocene or older can be established for this package.

Silica Ridge – Adularia Hill Tuff Package and Southeast Pediment Upper Tuff

Drilling at Silica Ridge has indicated an approximately 75 foot thick package of ash flow tuffs, airfall tuffs and pyroclastics within the middle of the stratigraphic section (Figs. 15 and 27). Composed of at least three, and likely more individual units, this package is bounded both upsection and downsection by fluvial conglomerates and tuffaceous sandstones indicating the role of paleotopography both in their deposition and preservation. The upper ten feet of this package consists of the widely distributed Nine Hill Tuff and will be discussed separately in the following section.

The base of the Silica Ridge tuff package is composed of several individual beds of laminated vitric airfall tuffs, becoming massive bedded lapilli and pumice rich tuffs

upsection with varying percentages of crystal fragments described as beta quartz and potassium feldspars in drill logs. A single mm topaz phenoocryst was also mentioned in DDH NSM-00164. Drill holes piercing the base of this section were not directly observed by the author and the previous descriptions are from core logs and photos of drill core.

Within the middle of the Silica Ridge tuff package is a thin—less than one to three feet thick—moderately welded pyroclastic horizon composed of 7-15%, 1-3mm, euhedral crystal fragments of sanidine with lesser anorthoclase, and 10-30% pumice and fiamme ranging from 5mm to 1.5cm in length, within an ash-shard-pumice matrix. Trace phyllite lithics, microscopic biotite crystals, and myrmekitic textured potassium feldspars have also been observed in thin section. Based on the distinctive appearance of abundant course grained potassium feldspar crystal fragments and abundant pumice fiamme observed both in hand sample and thin section, this pyroclastic has been correlated to the west with tuffs capping Adularia Hill. Additional supporting evidence for the correlation of this pyroclastic unit from Adularia Hill to Silica Ridge includes nearly identical trace element geochemical signatures (Fig. 38).

Above this fiamme and crystal rich tuff at Silica Ridge is an approximately 30 foot thick, massive tuff composed of 5-20%, 1-3mm euhedral crystal fragments of sanidine and lesser anorthoclase, and 10-25% pumice ranging from 2mm to trace 1cm within and ash-shard-pumice matrix. Thin intervals within this massive tuff also include abundant fiamme. The distinctive appearance of abundant course grained potassium feldspar crystal fragments and abundant pumice suggest this massive unit is the upper, non-welded portion of the Silica Ridge – Adularia Hill unnamed tuff.

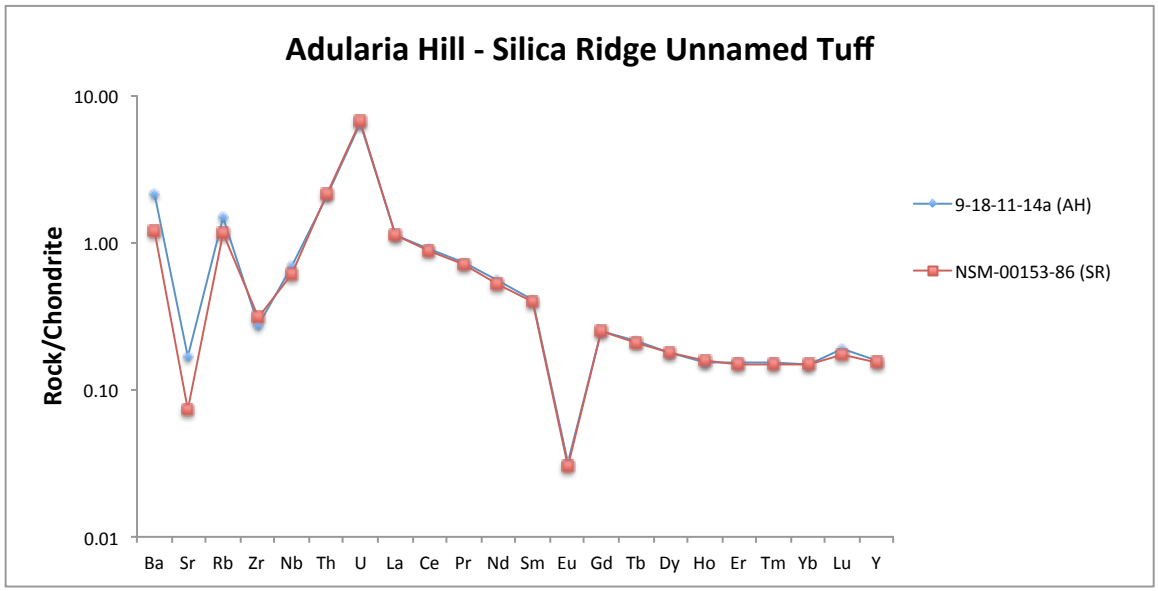

Figure 38: Modified spider diagram for select trace element and REE geochemistry comparing crystal and fiamme rich tuffs exposed at Adularia Hill and encountered in drill core in the middle of the Silica Ridge tuff package. Tuff in outcrop from Adularia Hill is dated at 26.01 ±0.07 Ma. Near identical signatures indicate the two are the same tuff unit. See Fig. 5 for location and Fig. 15 for stratigraphic relationships.

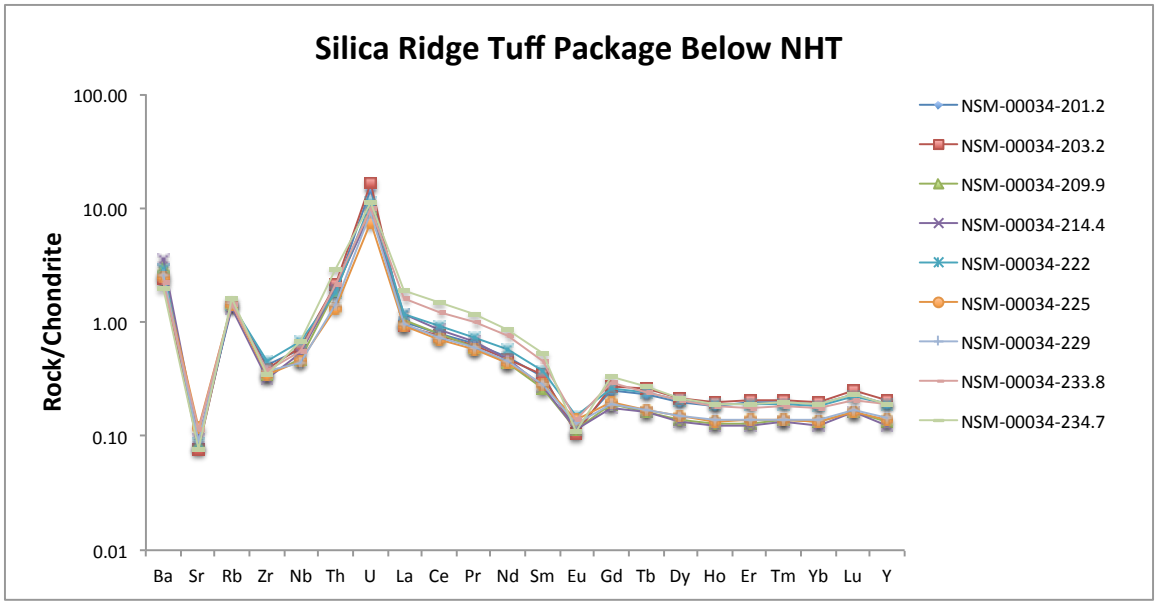

Figure 39: Modified spider diagram for select trace element and REE geochemistry for crystal and pumice rich tuffs beneath the Nine Hill Tuff at Silica Ridge.

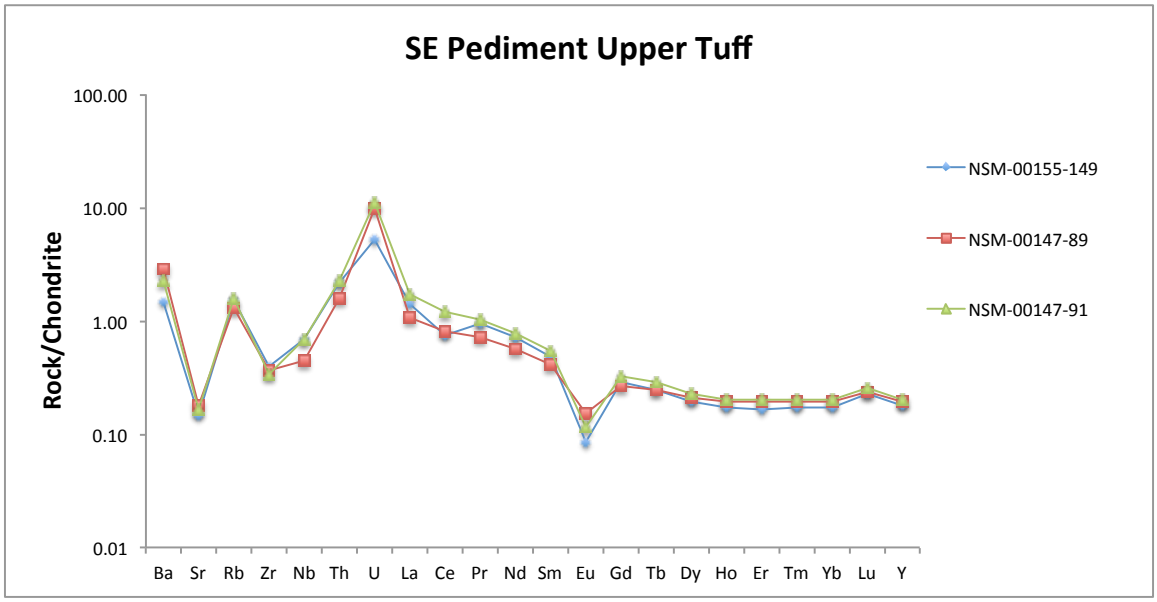

Figure 40: Modified spider diagram for select trace element and REE geochemistry for fiamme rich horizons in the Southeast Pediment Upper Tuff.

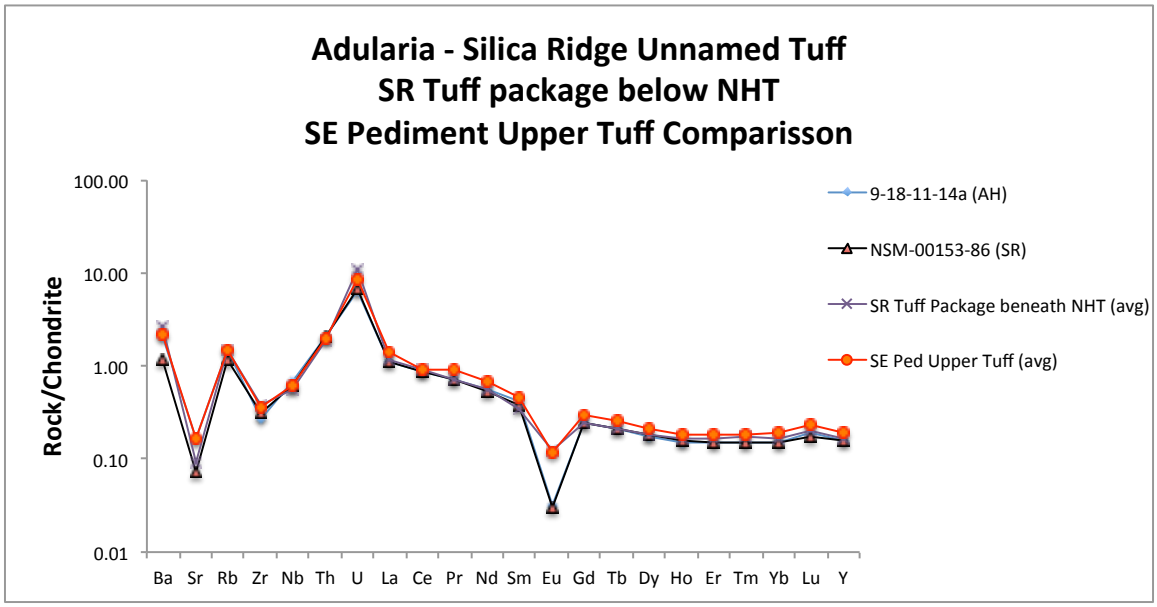

Figure 41: Modified spider diagram for select trace element and REE geochemistry comparing the crystal and pumice rich tuffs encountered in drill core at Southeast Pediment and Silica Ridge and exposed in outcrop at the top of Adularia Hill. Excluding variations in Eu depletion, the two have similar geochemical signatures. Based on geochemical similarities and petrologic characteristics, it is inferred the three tuff packages are related. This provides an upper age boundary of 26.0 Ma for the Southeast Pediment stratigraphic package. See Fig. 15 for stratigraphic relationships.

The Southeast Pediment Upper Tuff is also likely corelatable to the Adualria Hill-Silica Ridge unnamed tuff package. Ranging from five to sixty feet thick, this tuff is also composed of abundant coarse grained sanidine and anorthoclase and is also rich in pumice with thin fiamme dominant horizons. Disregarding the sharp Eu anomaly of the fiamme rich Silica Ridge – Adularia Hill unnamed tuff, the three tuffs have near identical trace element geochemical signatures (Fig. 41).

The crystal and fiamme rich tuff exposed at the top of Adularia Hill has been $^{40}Ar/^{39}Ar$ dated at 26.01±0.07 Ma. Tuffs of this age have been mapped in the Pine Forest and Black Rock Ranges (Colgan et al., 2006; Lerch et al., 2008), and include the Ashdown Tuff within both ranges, the tuff of Alder Creek within the Pine Forest Range, and an unnamed tuff within the Black Rock Range. With abundant pumice and course grained sanidine crystal fragments, the Ashdown Tuff—named for prominent exposures at the Ashdown Mine (Noble et al., 1970)—is petrographically similar to the Silica Ridge – Adularia Hill tuff; however trace element geochemical comparisons suggests the two tuffs are not correlative. Data presented in Colgan et al. (2006) gives Zr values ranging from 390-590 ppm and Nb values between 36-52 ppm. Values from the dated, weakly to moderately welded fiamme and crystal rich welded tuff at Silica Ridge and Adularia Hill are significantly lower with Zr ranging from 105-120 ppm and Nb ranging from 14-16 ppm. Assuming correlation of this unit to the Southeast Pediment Upper Tuff and the massive pumice and crystal rich tuff at Silica Ridge, Zr and Nb values are slightly higher ranging from 123-159 ppm and 11-16 ppm respectively; however, still significantly lower than that of the Ashdown Tuff. Geochemical data from this study were also compared to

the Tuff of Alder Creek (Colgan et al., 2006) and an unnamed Oligocene tuff within the Black Rock Range (Lerch et al., 2008). Provided descriptions of the two tuffs are petrographically unlike the 26.0 Ma tuff of Adularia Hill and Silica Ridge. Additionally, both have significantly higher Zr and Nb values—within the range of the Ashdown Tuff—than the tuff presented within this research.

Nine Hill Tuff (Fiamme Marker Unit of Newmont Geologists)

A distinctive fiamme-rich ash-flow tuff that crops out and is encountered in drillholes in the northwest part of the Sandman property is correlated with the regional Nine Hill tuff based on outcrop appearance, petrography, geochemical signature, and age (Deino, 1985; this study). The tuff is a key marker unit that ties stratigraphy between Silica Ridge, Adularia Hill, and North Hill (See Figs. 25 and 27 for cross sections and Fig. 15 for stratigraphic correlation).

Few outcrop exposures of the Nine Hill Tuff are within the Sandman project area. It has been mapped at the base of a prominent silicified and adularized conglomerate knob west of Silica Ridge, in float at the top of Adularia Hill, and within trench exposures at North Hill (Fig. 23). Drilling indicates an overall thickness for the Nine Hill Tuff at the Sandman property ranges from 10 feet at Silica Ridge (with complete erosion in the eastern footwall fault block) (Fig. 27), to as thick as 30 feet at North Hill (Fig. 25). The tuff is interbedded with fluvial deposits at North Hill and Silica Ridge, which suggests that it was deposited in a mid-Tertiary paleo-drainage. The Nine Hill Tuff has not been recognized to the south and east at the Southeast Pediment and Abel Knoll deposits, where fluvial rocks are largely absent.

The Nine Hill Tuff at Sandman contains 3-7% fine phenocrysts of sanidine, plagioclase, anorthoclase, beta quartz and biotite, 5-30% fiamme ranging from 1-6cm—decreasing in both percentage and size with depth—and trace 1-4cm lithic fragments including phyllite and quartzite, volcaniclastic sandstones, and tuffaceous material, in a fine grained ash-shard-lapilli matrix. Lithics were likely derived, scoured from the paleosurface and entrained in the ash flow during flow.

Trace element geochemistry also serves as an identifying characteristic for the Nile Hill Tuff. At Sandman, this tuff contains 248-385 ppm Zr (mostly ~300 ppm) and 20 to 26 ppm Nb, with all samples moderately to strongly quartz-adularia altered. Using the average values for SiO_2 and K_20 (72.82 and 5.33 weight % respectively) reported by Denio (1985) and Christiansen (2012), trace element data were adjusted to reflect original concentrations within samples of the Sandman Nine Hill Tuff (see Appendices 4 and 5). Zr and Nb in bulk rock glassy and devitrified samples and glass separates of the regional Nine Hill Tuff are ~300-400 ppm and ~25-35 ppm, respectively (Deino, 1985) (Figs. 43 and 44).

Sanidine $^{40}Ar/^{39}Ar$ age and K/Ca ratios are indistinguishable in regional samples of the Nine Hill Tuff. Sample H10-48 from outcrop west of Silica Ridge gave an age of 25.34 ± 0.11 Ma with a K/Ca ratio of 16.5 ± 5.5. Three regional samples of the Nine Hill Tuff gave 25.32 ± 0.07 Ma and 11.9 ± 2.7, 25.19 ± 0.06 Ma and 12.2 ± 3.6, and 25.27 ± 0.08 Ma and 9.5 ± 2.5 (Henry and Faulds, 2010). The slightly higher K/Ca ratio for sample H10-48 is likely the result of potassic alteration.

Named for the type locality in the hills just north of Carson City (Bingler, 1978), the Nine Hill Tuff is the most widespread Tertiary ash-flow tuff in the Great Basin,

stretching form the Sierra Nevada foothills in California, east to near Ely, NV (Deino, 1989; Best et al., 1989). Nine Hill Tuff at the Sandman project is the Farthest north known occurance (Fig. 42). No source caldera has been identified for the Nine Hill Tuff; however, regional distribution and facies suggest a source beneath the Carson Sink (Deino, 1989).

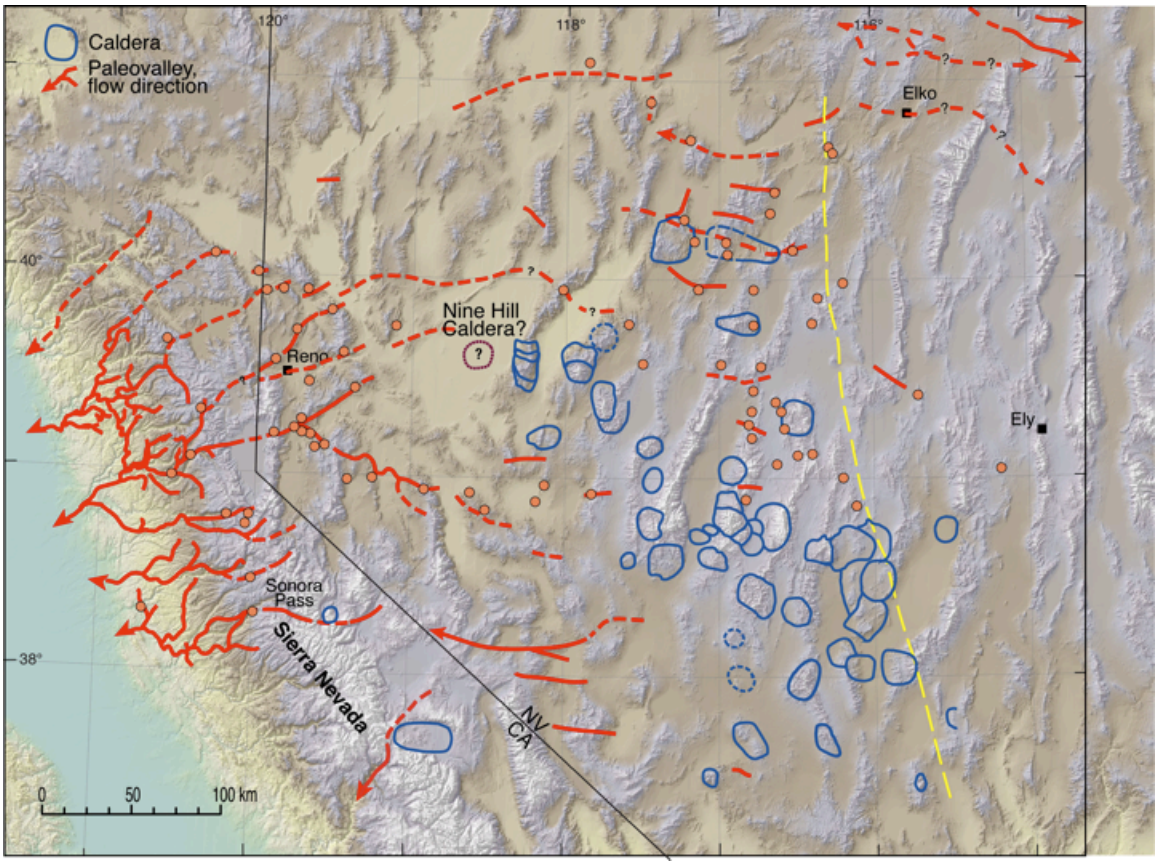

Figure 42: Digital elevation map of Nevada and eastern California showing known paleovalleys and a few segments (from Lindgren, 1911; Jenkins, 1932; Faulds et al., 2005a, 2005b; Garside et al., 2005; Henry and Faulds, 2010), a proposed paleodivide (Henry, 2008), known locations of tuffs of the Nine Hill paleovalley (locations with ? are uncertain correlations), and known or suspected mid-Tertiary calderas. The paleovalley system drained to the Pacific Ocean, in the Great Valley at the time. The discontinuously exposed paleovalleys in western Nevada probably were more irregular than shown, similar to those in the Sierra Nevada, which are continuously exposed and were mapped in detail. Modified from Henry and Faulds (2010).

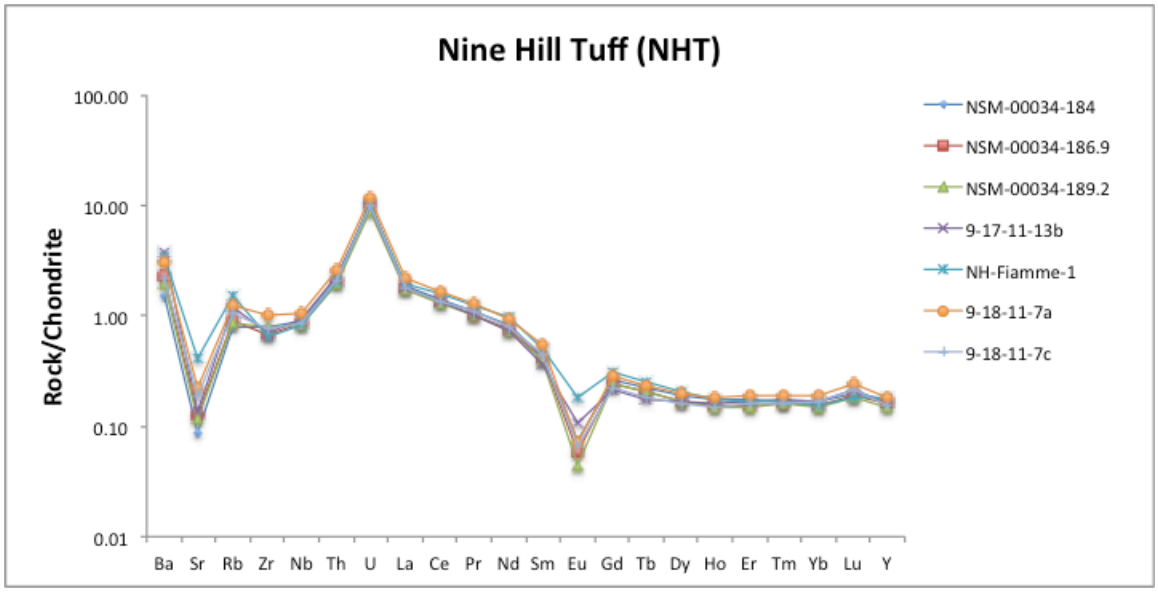

Figure 43: Modified spider diagram for select trace element and REE geochemistry for the Nine Hill Tuff. Data not adjusted for the addition of hydrothermal silica and potassium. NSM-00034-xxx samples are from Silica Ridge, samples 9-17-11-13b and NH-Fiamme-1 are from North Hill, and samples 9-18-11-7x are from float found at the top of Adularia Hill.

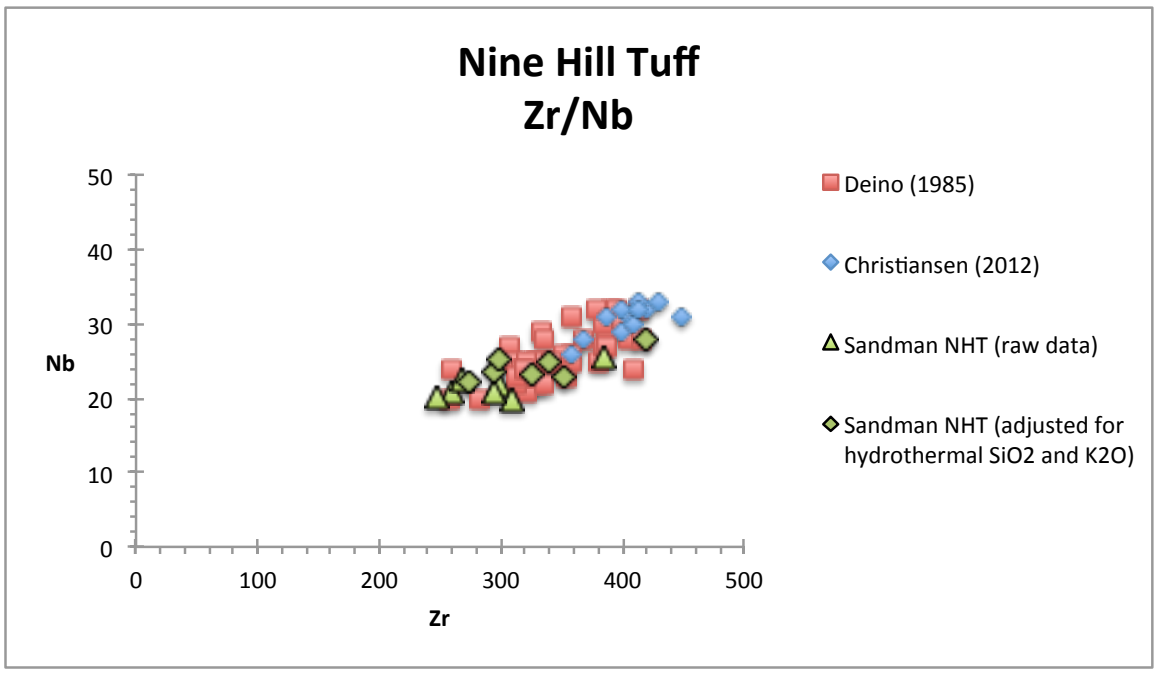

Figure 44: Zr/Nb plot for samples of the Nine Hill Tuff. Trace element geochemical values for samples from the Sandman project adjusted for the addition of hydrothermal silica and potassium (see Appendices 4 and 5). Deino (1985) reports Zr values between ~300-400 ppm and Nb values of ~ 25-35 ppm. Christiansen (2012) reports slightly higher values between ~350-450 for Zr.

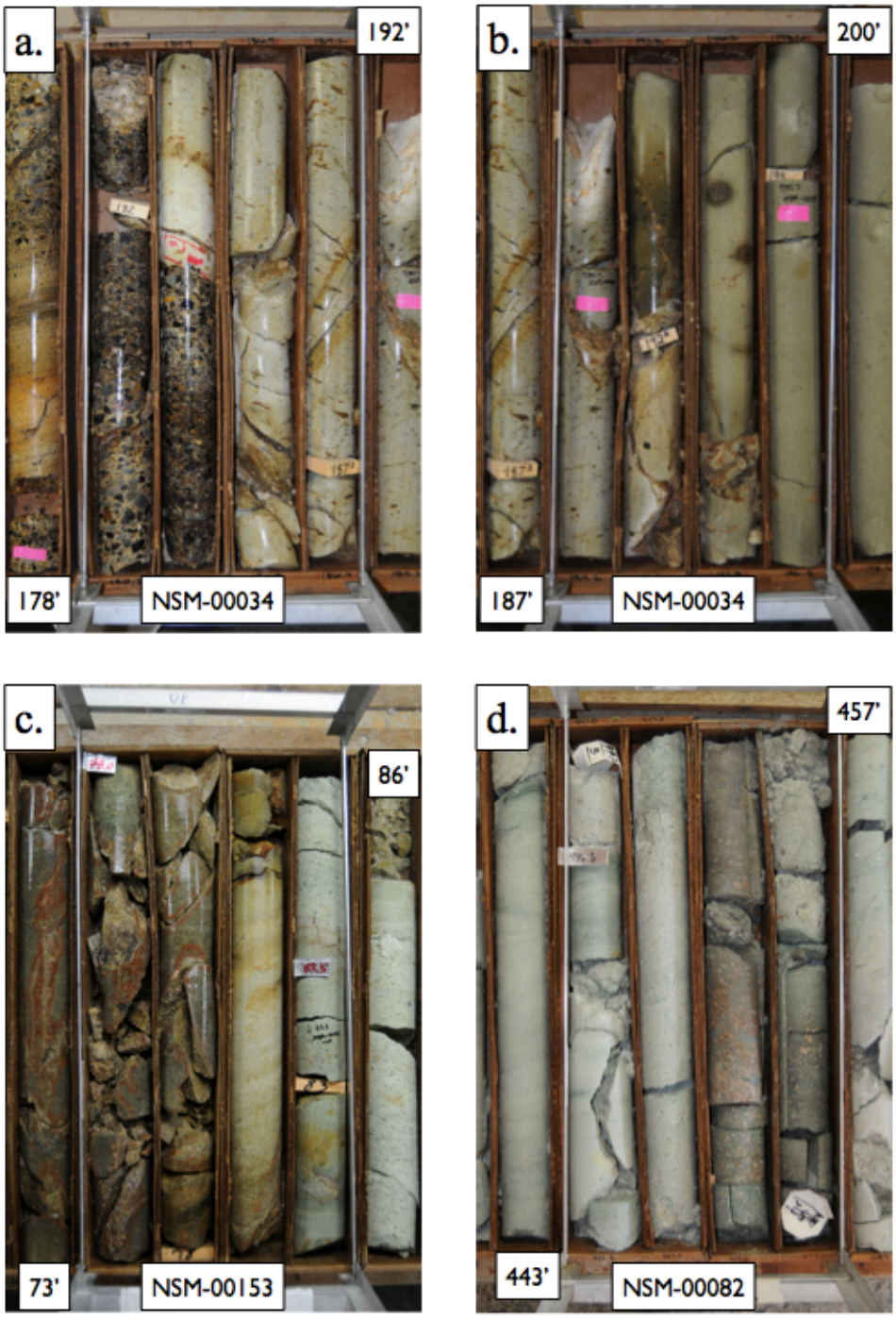

Figure 45: Drill core photos of correlative tuffs within the Sandman project area. A.) Intensely adularized and silicified Nine Hill Tuff and conglomerate at Silica Ridge. B.) Intensely adularized and silicified Nine Hill Tuff with rapidly decreasing alteration front into below moderately argically altered crystal lapilli lithic tuff. C.) Intensely adularized and silicified crystal lapilli lithic tuff grading into a prior argillically altered correlative 26.0 Ma Adularia-Silica Ridge unnamed tuff. D.) Strongly propylitically altered basal polylithic breccia of the Red-Green (Christmas Tree) Breccia tuff package at Southeast Pediment.

Additional Tuffs Higher in Section (North Hill and Silica Ridge)

The youngest tuffaceous deposits in the Sandman stratigraphic section are found at North Hill and Silica Ridge in the northwest part of the project area. Infill drilling between these two deposits is referred to as the Midway Zone by Newmont personnel. At North Hill, a distinct 20 to 25 foot package of thin bedded lapilli lithic tuffs, laminated vitric tuffs, fiamme and pumice rich tuffs, and trace accretionary lapilli tuffs are interbedded with tuffaceous sandstones and basement bearing tuffaceous conglomerates. A relative age for these tuffs is constrained by the lower 25.4 Ma Nine Hill Tuff and an upper basaltic trachy-andesite flow or sill at North Hill dated at 22.5 Ma (see Fig. 15). Individual tuff beds are less than four feet thick, with an average thickness of approximately one foot. Fiamme rich intervals are commonly pale green in color with abundant dark green chloritized fiamme and compacted pumice fragments ranging from 1mm to 1cm in length in an ash-pumice-lapilli matrix. As these fiamme rich intervals are very thin (generally a few to tens of cm) and interbedded with fluvial sandstones and conglomerates, apparent eutaxitic textures are not indicative of welding, but rather reflect diagenetic processes. Gifkins et al. (2005) have documented this process in the Miocene Green Tuff Belt of Japan, showing that apparent welding textures can result from alteration, dissolution, and mechanical compaction of pumice during diagenesis and lithification. These “cold compaction fiamme” have been observed higher in section above the lower basaltic trachy-andesite at North Hill and as cm thick beds within the Red-Green Breccia Tuff and other ash dominant tuffs higher in section at Southeast Pediment. Trace element comparisons between

In the Midway Zone north of Silica Ridge, drilling has encountered an upward

fining, massive lithic tuff with chaotic to imbricated cm vitric tuff clasts and variable pumice fragments in an ash-lapilli-pumice matrix preserved beneath a mafic flow. Unlike the North Hill tuff package, which exhibits an erosional contact with the Nine Hill Tuff, the Midway-Silica Ridge tuff has an apparent gradational contact obscured by intense quartz-adularia alteration in observed drill core. Trace element geochemical comparsions between the Nine Hill Tuff and the Midway-Silica Ridge tuff indicate the two are unrelated (Fig. 46).

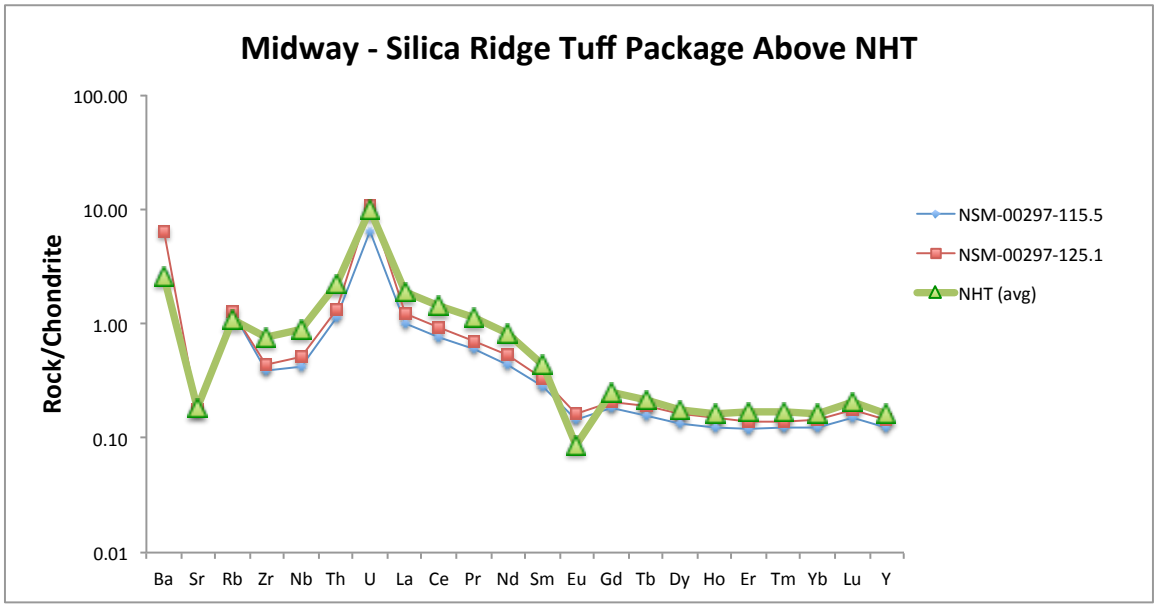

Figure 46: Modified spider diagram for select trace element and REE geochemistry from tuffs above the Nine Hill Tuff encountered in drill core in the southern extent of the Midway Zone near Silica Ridge. Geochemical data for the Nine Hill Tuff are plotted for comparison. See Fig. 15 for stratigraphic relationships.

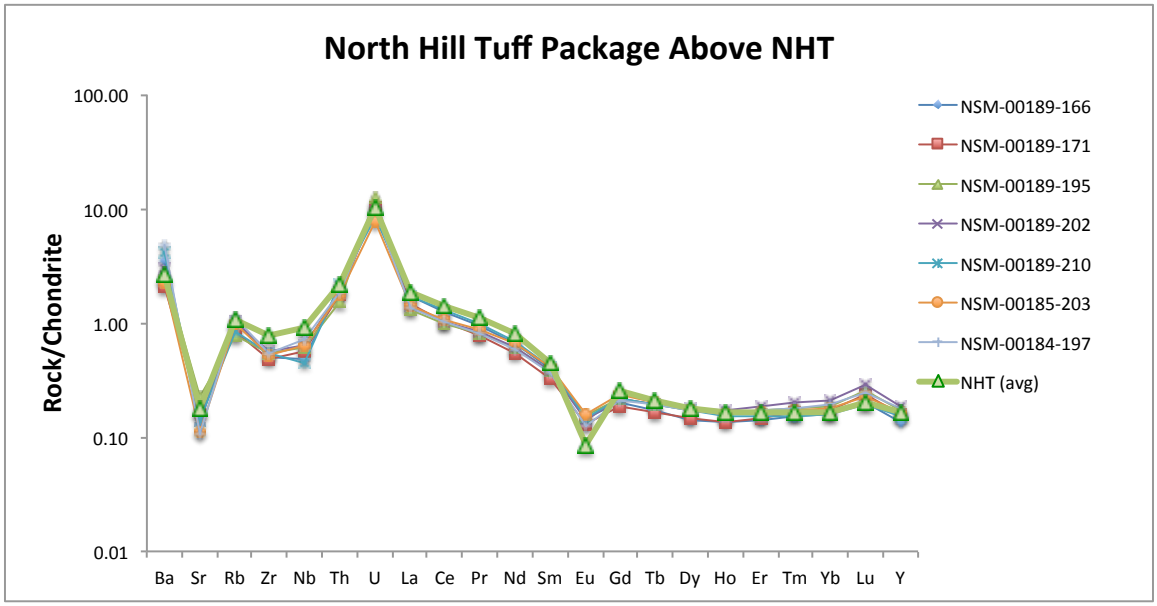

Figure 47: Modified spider diagram for select trace element and REE geochemistry from tuffs above the Nine Hill Tuff encountered in drill core at North Hill. Geochemical data for the Nine Hill Tuff are plotted for comparison. See Fig. 15 for stratigraphic relationships.

Rhyolite Dikes

Two rhyolite dikes have been observed within the vicinity of the Sandman project area. These include a 3-5 foot north-northwest striking dike intruding along regional basement foliations in Triassic phyllites within the Ten Mile Hills southeast of Southeast Pediment, and a 5-7 foot thick north-northwest striking dike intruding prominent ridge forming Tertiary mafics between Winnemucca Mountain and the Bloody Run Hills. Trace element geochemical comparisons (Fig. 48) do not suggest the two are related. Anomalous Au grade is encountered with the Rembrandt rhyolite dike as mm stringer quartz-adularia veinlets along its margins. An exact age is not known for these dikes; however, the Winni rhyolite dike intrudes mafic flows with an inferred age of ~22 Ma (see following discussion on mafics and Fig. 59 for outcrop locations).

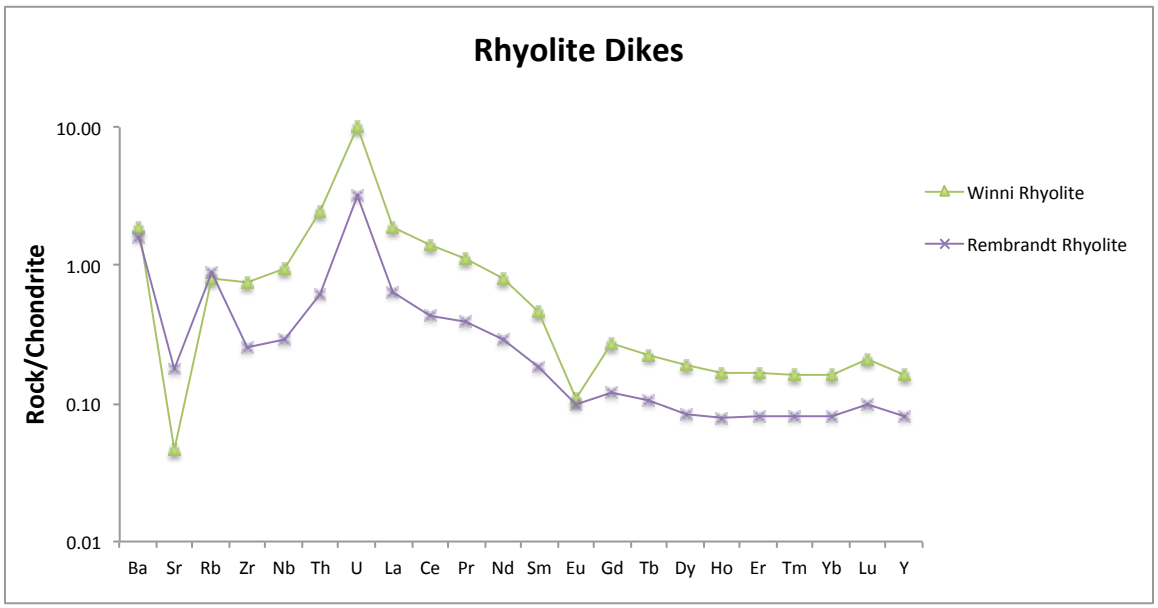

Figure 48: Modified spider diagram for select trace element and REE geochemistry of rhyolite dikes mapped within the vicinity of the Sandman project area. The Winni rhyolite dike intrudes assumed ~22.5 Ma mafics within the hills between Winnemucca Mountain and the Bloody Run Hills. The Rembrandt rhyolite dike intrudes Triassic phyllites within the Ten Mile Hills. See Fig. 59 for locations.

Mafic Flows, Sills, and Dikes

The youngest rocks exposed within the Sandman project include mafic flows, sills and dikes of a basaltic trachy-andesite, trachy-andesite, and lesser andesite composition (Fig. 49). Four $^{40}Ar/^{39}Ar$ age dates on groundmass separate indicate an age of ~22.5 Ma. These rocks have been informally referred to as the Ambien Basalt (Newmont nomenclature) and form subtle hills and north-northwest oriented ridges flanked by angular to platy talus. Outcrops are limited to ridges and along fault scarps. The largest exposures occur within the Basalt Hills and cover an area of approximately 8 square miles (see Fig. 5). Other exposures include the Little Basalt Hills, numerous ridges to the north of the Basalt Hills including Silica Ridge, isolated exposure at North Hill, and Abel Knoll, and a number of subtle ridges just north of the Krum Hills. Additionally an andesitic sill intrudes the stratigraphic section at Southeast Pediment.

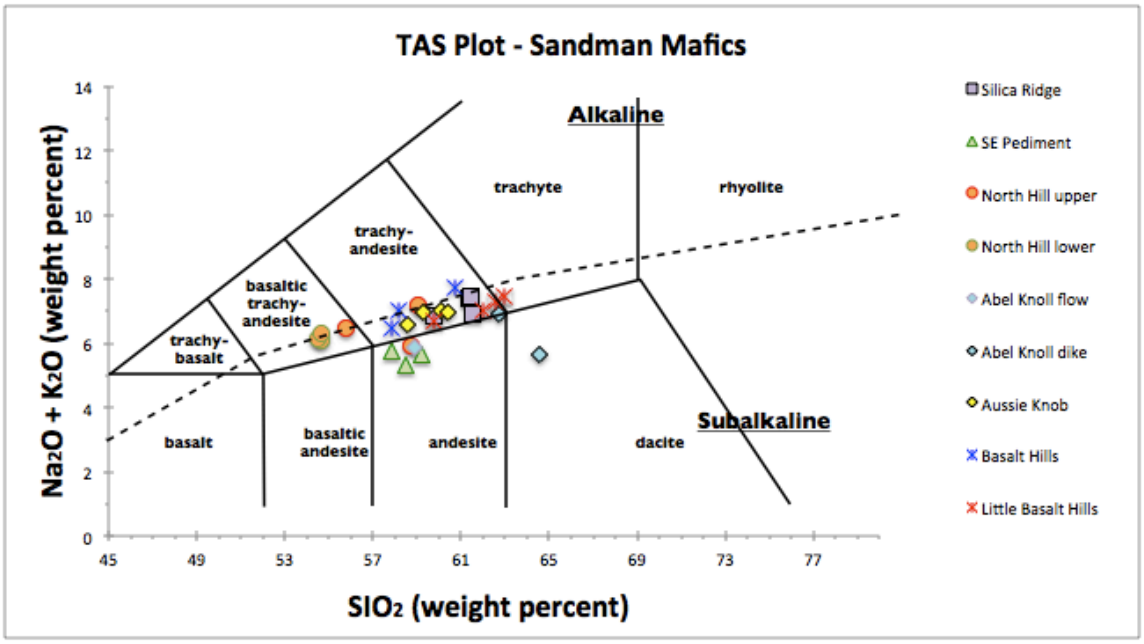

Figure 49: Total alkali versus silica plot for mafic units within the Sandman stratigraphic section. See Fig. 5 and 15 for sample locations. See Appendices 13 through 20 for all geochemical data. Division between alkaline and subalkaline from Irvin and Baragar (1971).

In the Basalt Hills, these rocks are dark gray to brick red, commonly vesicular, and locally approach thicknesses of 450 feet. Abruptly thinning margins likely reflect the role of topography in original distribution. Basal units are commonly platy in nature, with increasing vesicles up-section. Attitudes are variable, though have been mapped showing a general progression in strike from northeast, to east, to southeast— skirting a subtle inferred east-west oriented basement arch in the central portion of the property. Locally, pressure ridges have also been observed. Within the Basalt Hills, individual flows have been difficult to distinguish. At Aussie Knob to the north, at least four distinct, thin flows have been recognized. These include highly vesicular and in places auto-brecciated units separated by thin, brick-red, mafic derived sandstone horizons (Fig. 50). In the Little Basalt Hills, a medium gray, vitric and lapilli tuff—locally exposed in a central saddle—possibly indicates the presence of an upper and lower flow, although structural offsets are unclear here. Additionally, columnar jointing, a prominent northwest-southeast pressure ridge, and blocky flow tops are also preserved within the Little Basalt Hills (Fig. 50). Rocks within the Basalt Hills have been dated at 22.62 ± 0.29Ma while those in the Little Basalt Hills are 22.42 ± 0.23Ma (Peters, 2003). Given overlap in analytical uncertainties, relative ages can't be determined for the two.

The furthest north exposure of mafic rocks occurs at North Hill. Drilling and trenching (Figs. 23, 24, and 25) indicate two mafic units within a down to the west half graben, with one unit capping North Hill. The lower mafic unit has been dated at 22.53 ± 0.04 Ma. These mafic bodies are approximately one hundred feet thick. It is unclear if these units are shallow hypabyssal sills or surface flows. The North Hill capping basaltic trachy-andesite to trachy-andesite is highly vesicular with a thick basal auto breccia

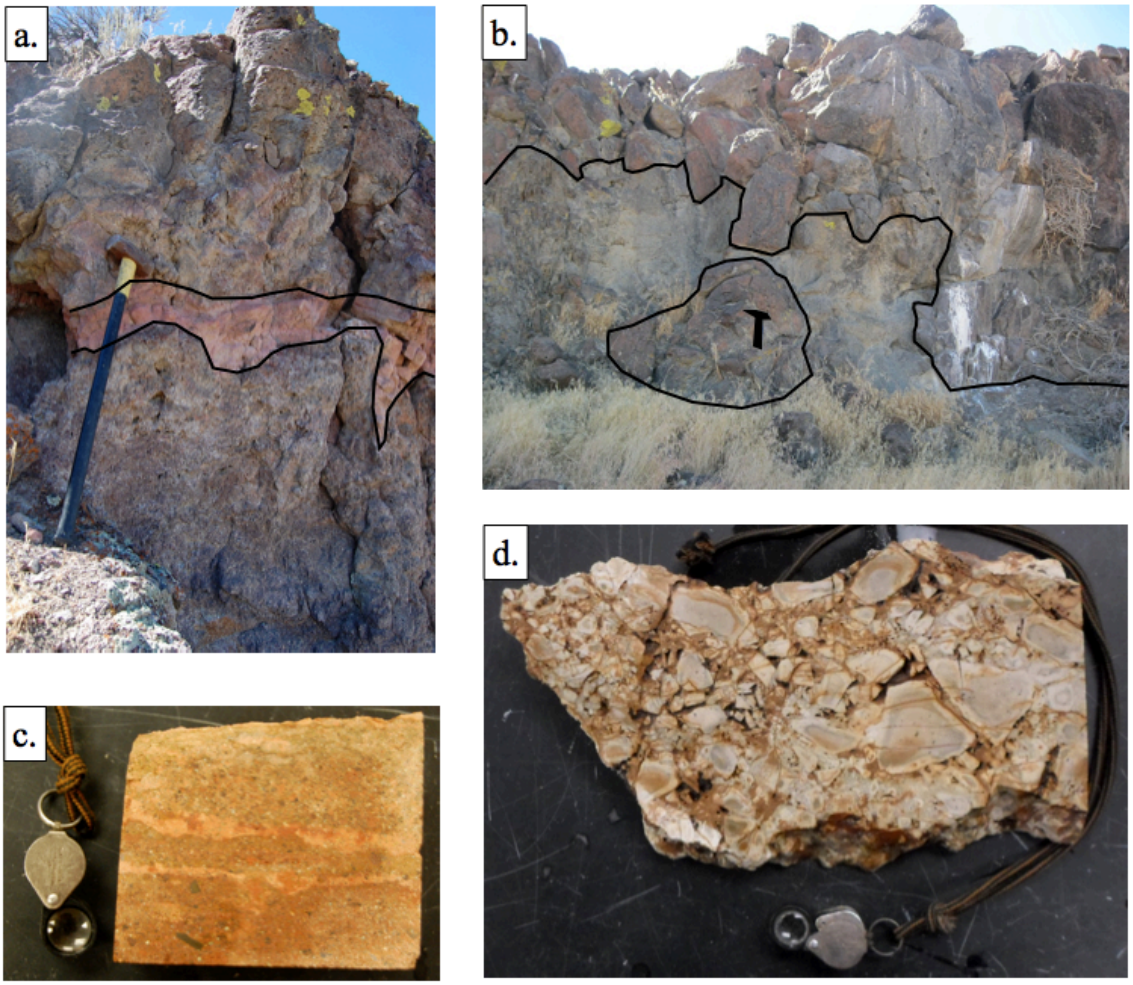

Figure 50: Outcrop and hand sample photos of mafic and mafic derived rocks within the Sandman project area. A.) Mafic derived sandstone separating individual flows at Aussie Knob. B.) Blocky flow top with locks entrained in more viscous interior flow exposed in the Little Basalt Hills. C.) Hand sample of mafic derived sandstone from image A.). D.) Moderately argillically altered autobreccia from base of flow at North Hill.

suggesting it is a surface flow (Fig. 50); however, contacts within drill core for the two basaltic trachy-andesite to trachy-andesite units to the west exhibit knife edge, non vesicular contacts in places, while elsewhere contacts are autobrecciated and highly vesicular.

To the south at Silica Ridge, the stratigraphic package is capped by approximately 100 feet of trachy-andesite flows thickening to 160 feet to the south. These rocks are highly vesicular, typically auto brecciated, and weathered upper contacts have been observed in drill core indicating at least two individual flows. These flows are sourced from a roughly east-west oriented dike as evident from drill data (Fig. 26).

Drilling at Southeast Pediment indicates a ~140 foot thick andesite directly beneath the Red-Green Breccia tuff. A relative age of >25.4 Ma is established as the Red-Green breccia is stratigraphically lower than the Nine Hill Tuff in the northwest part of the Sandman project area (Fig. 27). A date of 22.66 ± 0.07 Ma for the Southeast Pediment mafic indicates it is a hypabyssal sill rather than a surface flow. A feeder dike has not been recognized for the Southeast Pediment sill although it is likely sourced along the same structure that controlled later Middle Miocene low sulfidation mineralization. The upper 40 feet of this sill is commonly brecciated and hosts 0.0x opt Au mineralization. It appears that the intensely chloritized Red-Green Breccia Tuff acted as a aquitard to hydrothermal fluid flow, redirecting fluid flow from the feeder structure and out along the upper brecciated portion of the sill.

At the Abel Knoll deposit, an andesite flow caps a polylithic breccia body composed of basement phyllite and granodiorite, tuffaceous wall rocks, and abundant vesicular andesite breccia hosting Au mineralization. The breccia body also appears to

be intruded by a trachy-andesite dike (see Figs. 15 and 32). The Abel Knoll breccia body will be described separately in the following section.

In drill core, fresh mafic rocks have a dark blue-gray to black appearance with visible mm phenocrysts of plagioclase-olivine-magnetite in an aphanitic groundmass. Trachytic and amygdaloidal textures are common with open space in filled by chalcedony, zeolites, carbonates, and nontronite. In thin section, the groundmass is composed of abundant plagioclase microlites, clinopyroxene, olivine, oxide, and glass altering to clay. Altered samples have a range in colors from bleached beige white, light tan brown, purple, and variable shades of green dependent on type and intensity of hydrothermal alteration overprint. All mafic rocks observed in thin section exhibit similar mineral assemblages and textures. Combined with $^{40}Ar/^{39}Ar$ age data and trace element geochemistry, all mafic rocks within the Sandman project appear to be genetically related.

Whole rock and trace element geochemical data were collected from all mafic rocks in the Sandman project area to characterize and compare from deposit to deposit. All geochemical data can be found in Appendices 13 through 20. Whole rock geochemical data are summarized in Figure 55. As most samples have undergone some degree of hydrothermal alteration — propylitic, argillic, quartz-adularia or some combination of all — immobile incompatible elements were utilized in comparisons. All whole rock and trace element geochemistry were plotted against Zr to determine degree of immobility as outlined by MacLean and Kranidiotis (1987) (Figs. 56 and 57). Elements with R^2 values greater than 0.85—only Hf and Nb having 0.9 correlation—include Zr, Y, Nb, and the REE's. These elements in addition to Ba, Sr, R, Th, and U were compared (Fig. 51).

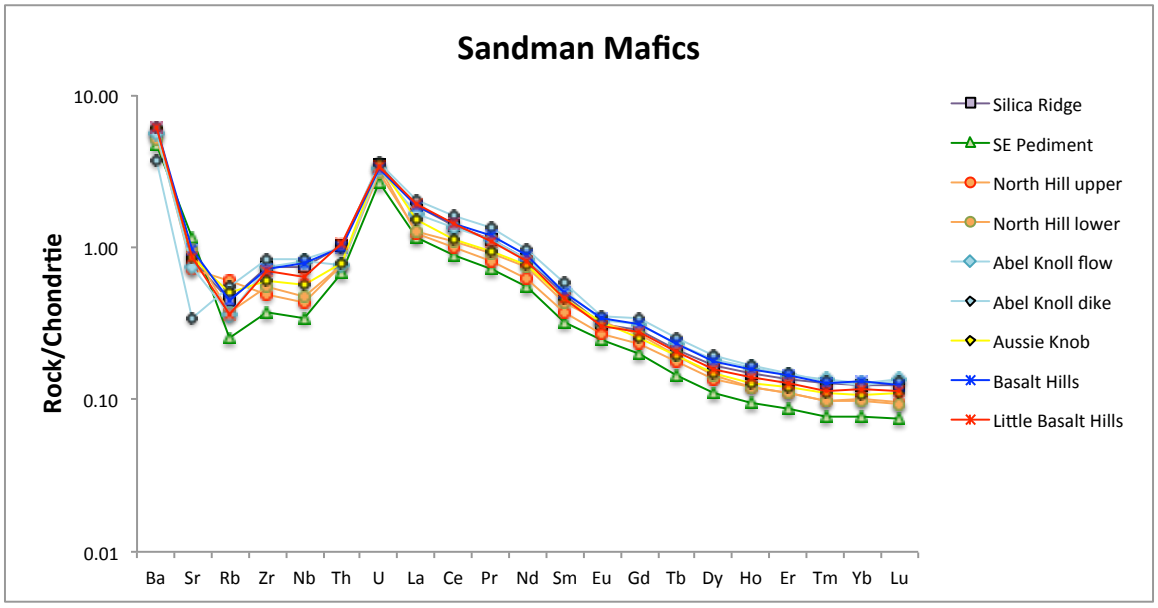

Figure 51: Modified spider diagram for select trace element and REE geochemistry for mafic flows, sills, and dikes within the Sandman project area. All units have similar show similar slopes and patterns indicating they are all sourced from the same parental melt. The Southeast Pediment sill is the least evolved with slight depletion in immobile incompatible elements and anomalous enrichment in Ca, Mg, Cr, Co, Cu, and Ni (Figs. 55 and 56). See Fig. 15 for stratigraphic relationships.

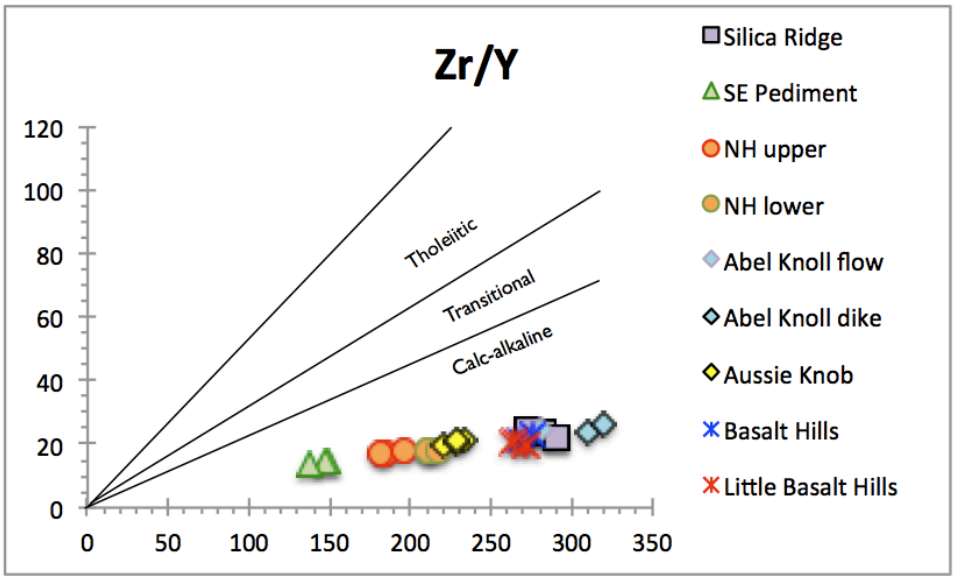

Figure 52: Zr/Y ratio plot showing calc-alkaline affinity of Sandman mafic flows, sills, and dikes. Method from MacLean and Barrett (1993).

MacLean and Barrett (1993) have also shown that immobile incompatible element ratio plots can be effective in discerning the magmatic affinity of hydrothermal altered mafic rocks. Zr/Y plots of geochemical data from the Sandman project indicate that mafic flows, sills and dikes are calc-alkaline (Fig. 52). Age, location, and elevated K within these rocks indicate they are part of the Western Andesite Assemblage of John (2001), constituting part of the subduction-related, continental margin arc of the ancestral cascades.

Individual mafic flows with depositionally conformable contacts have only been recognized at two locations—Silica Ridge and Aussie Knob. Trace element geochemical comparisons for these flows (Figs. 53 and 54) show nearly identical geochemical compositions. Plots comparing average geochemical data for all mafic units within the Sandman project area show similar slopes and patterns from unit to unit indicating they are all sourced from the same parental melt (Fig. 51). The Southeast Pediment sill is the least evolved of the Sandman mafics, with slight depletion in immobile incompatible elements and anomalous enrichment in Ca, Mg, Cr, Co, Cu, and Ni.

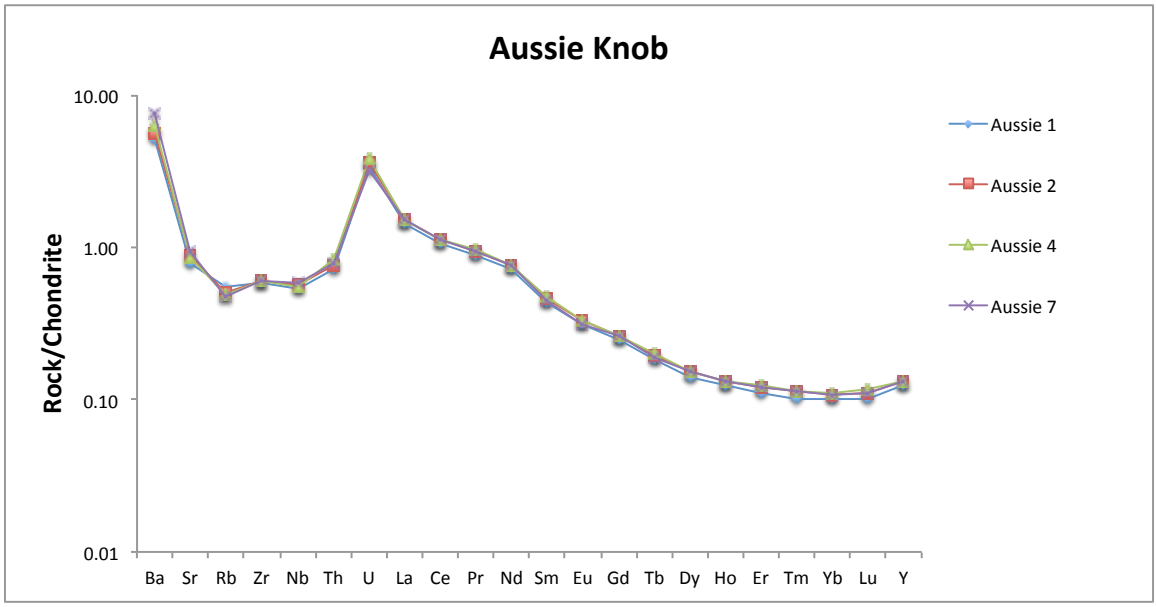

Figure 53: Modified spider diagram for select trace element and REE geochemistry comparing trachy-andesite flows exposed in outcrop at Aussie Knob. Individual flows are thin, highly vesicular, variably auto brecciated and separated by thin, mafic derived sandstone beds. See Fig. 5 for outcrop location.

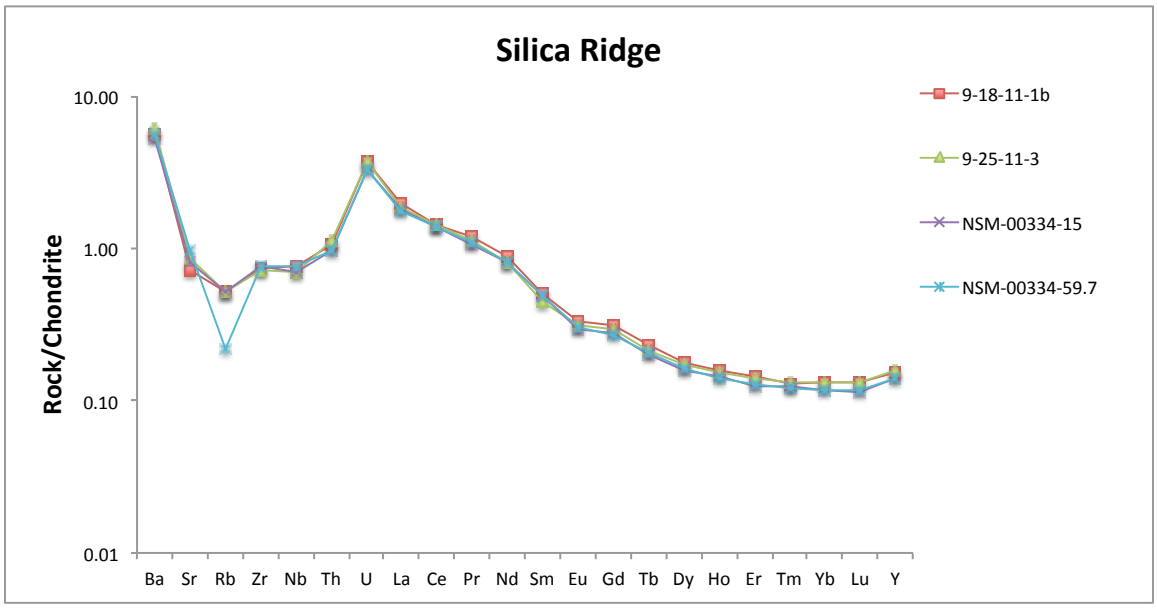

Figure 54: Modified spider diagram for select trace element and REE geochemistry from trachy-andesite flows within the southern portion of Silica Ridge. Samples 9-18-11-1b and 9-25-11-3 are from surface outcrops. Samples NSM-0033-xx are from drill core and represent two distinct flows with weathered contacts. Samples were not collected of the feeder dike due to intense hydrothermal alteration.

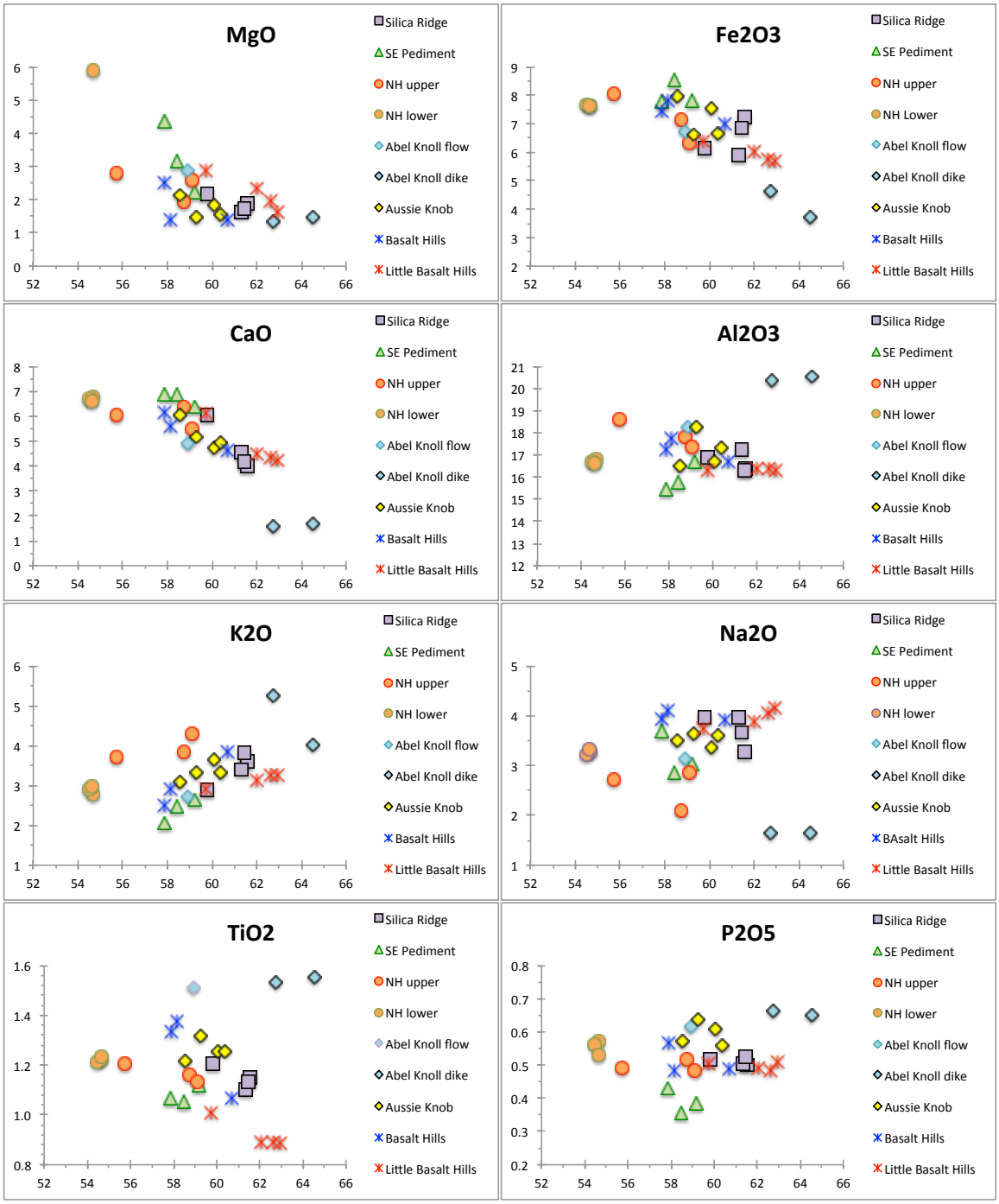

Figure 55: Harker diagram plots of whole rock analyses for all mafic units within the Sandman stratigraphic section.

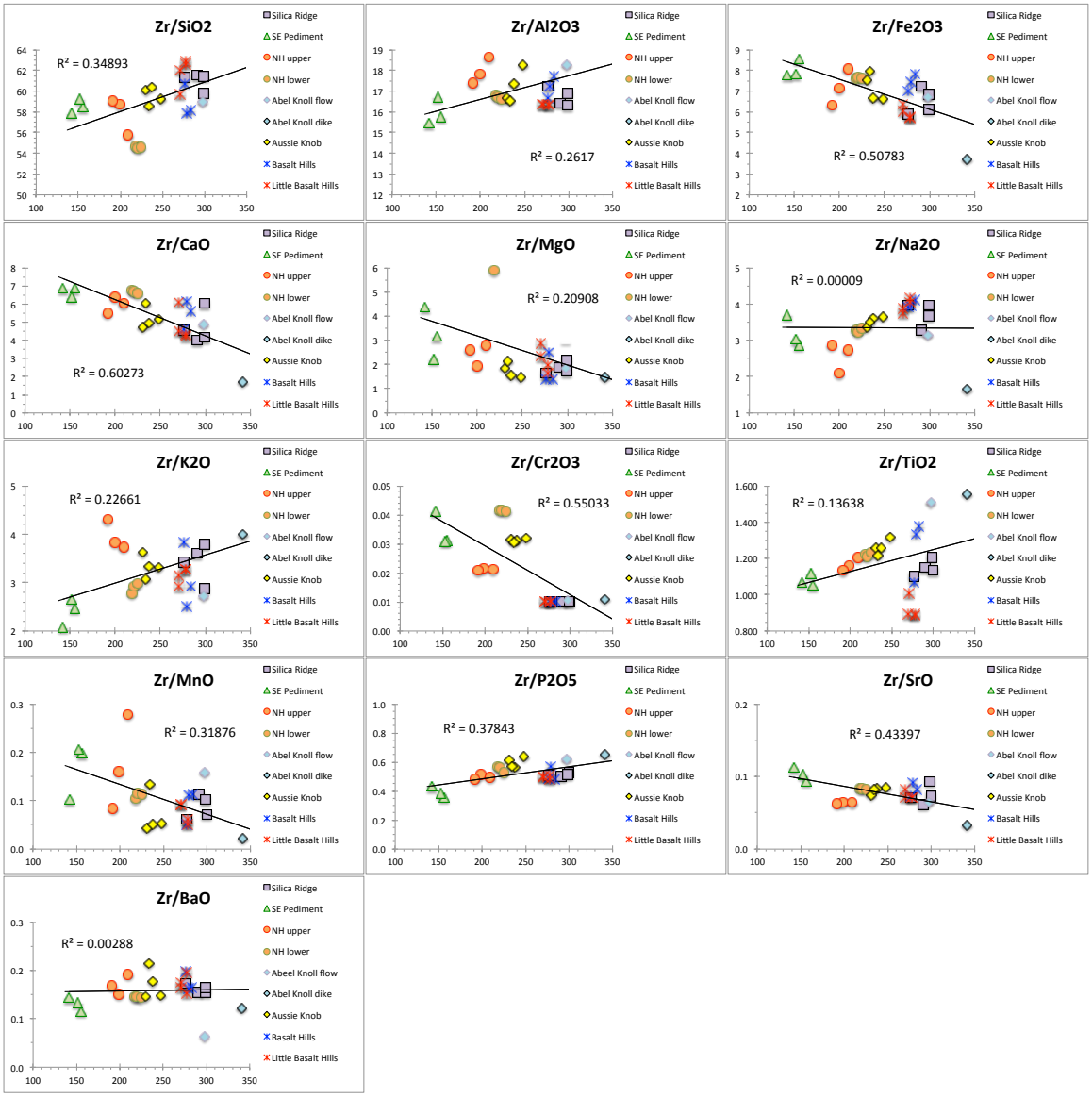

Figure 56: Whole rock oxides plotted against immobile Zr to determine degree of immobility as outlined by MacLean and Kranidiotis (1987). R^2 correlations may also reflect melt fractionation trends; however, error overlap in $^{40}Ar/^{39}Ar$ age dates does not allow for relative age relationships between mafic flows, sill, and dikes.

Figure 57: Trace element geochemistry plotted against immobile Zr to determine degree of immobility as outlined by MacLean and Kranidiotis (1987). R^2 correlations may also reflect melt fractionation trends; however, error overlap in $^{40}Ar/^{39}Ar$ age dates does not allow for relative age relationships between mafic flows, sill, and dikes.

Figure 57 continued: Trace element geochemistry plotted against immobile Zr to determine degree of immobility as outlined by MacLean and Kranidiotis (1987). R^2 correlations may also reflect melt fractionation trends; however, error overlap in $^{40}Ar/^{39}Ar$ age dates does not allow for relative age relationships between mafic flows, sill, and dikes.

The spatial association between Early Miocene mafic rocks and Mid-Miocene Au mineralization could provide a tool for further future exploration within and outside the project area. Dikes, sills, and flow bottoms appear to have acted as conduits for later low sulfidation mineralizing fluids. Examples include the feeder dike for flows at Silica Ridge and the polylithic breccia body at Abel Knoll. While a feeder dike has not been recognized at the Southeast Pediment deposit, it potentially occurs along the same structure that fed mineralizing fluids. At North Hill, contact relationships suggest the presence of mafic dikes proximal to the main fault zone, although structural complications and limited drill data hinder conclusive recognition.

Outside of the Sandman project area, Tertiary calc-alkaline mafic rocks are exposed along the eastern flanks of the Santa Rosa Range, the Bloody Run Hills, the Slumbering Hills, and in the hills between Winnemucca Mountain and the Bloody Run Hills (Fig. 59). Mellot (1987) reports K/Ar dates from mafic rocks in the Bloody Run Hills and Santa Rosa Range between 19.60 ± 0.90 Ma and 22.83 ± 1.12 Ma. More accurate $^{40}Ar/^{39}Ar$ age dates of 23.50 ± 0.24 Ma and 22.48 ± 0.08 Ma have been documented in andesites underlying the Santa Rosa-Calico volcanic field within the Santa Rosa Range (Brueseke and Hart, 2008).

Trace element geochemistry was compared between mafic rocks from the Sandman project area and analysis reran by Matheew Brueseke at the University of Nebraska on samples collected by Mellot (1987). Figure 58 indicates all mafics are genetically related. Mellot (1987) indicates $^{87}Sr/^{86}Sr@_{16\text{-}Ma} = 0.7040$ to 0.7050 for these rocks. Using geochemical and isotopic characteristics of these lava flows, Mellot concludes that they are derived from subduction-related mantle melting and

differentiation. Tectonomagmatism models of the northwestern U.S. (Christiansen and Yeats, 1992; Dickinson; 2004) have made similar interpretations for other temporally related, regionally exposed, calc-alkaline volcanic packages in western North America.

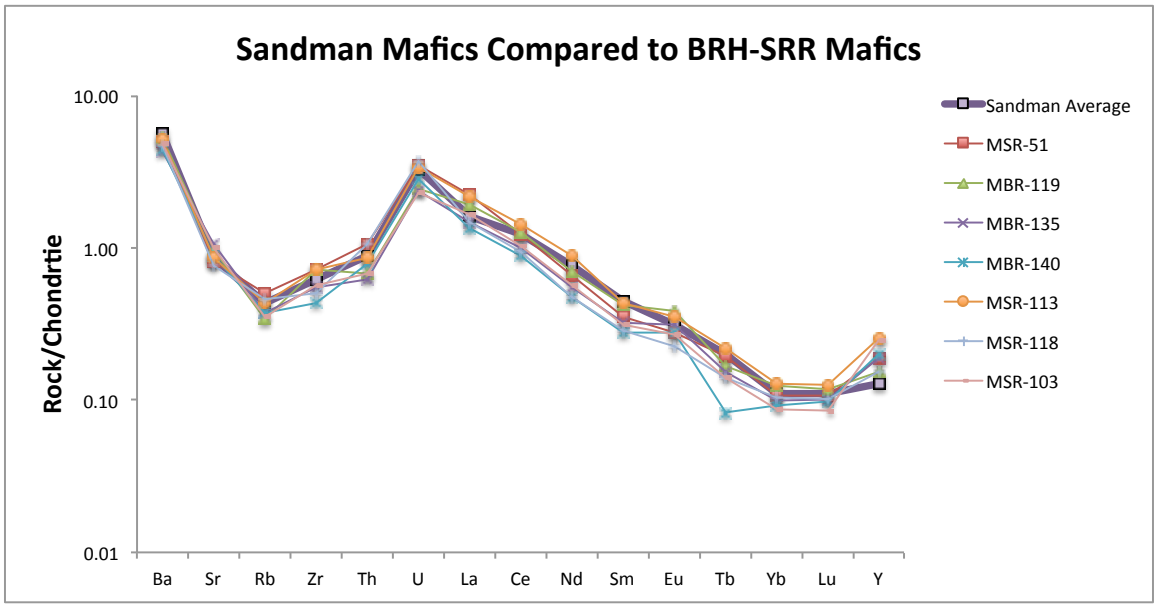

Figure 58: Modified spider diagram for select trace element and REE geochemistry comparing mafic rocks within the Sandman project are to mafic rocks exposed in the Bloody Run Hills and Santa Rosa Range. Average for all Sandman trace elements in thicker purple line. MSR-xx samples from the Santa Rosa Range, MBR-xx samples from the Bloody Run Hills. Trace element geochemical analysis reran by Mathew Brueseke on samples collected from study by Mellot (1987). See Appendix 22 for all geochemical data. From data set provided by M. Brueseke.

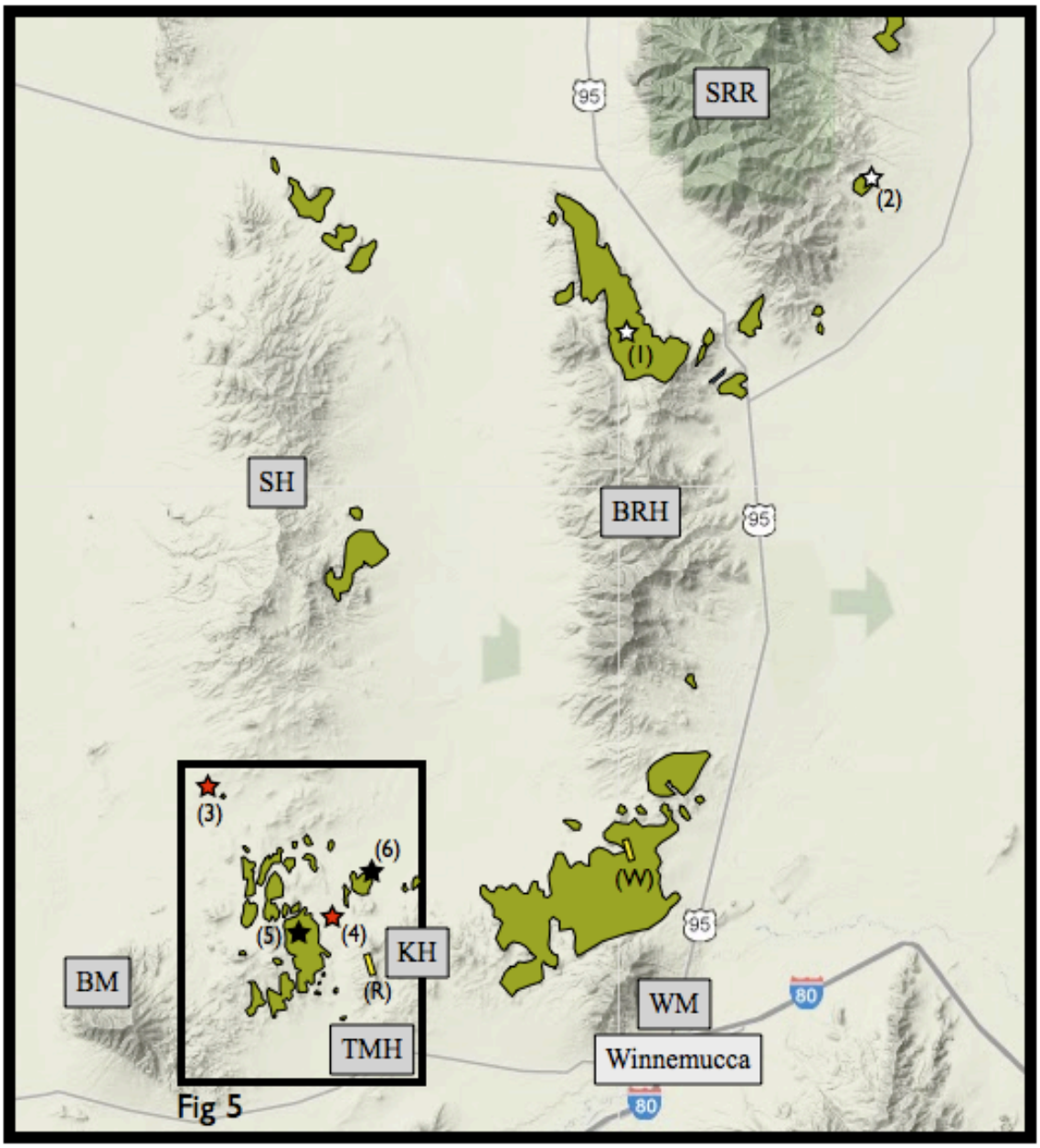

Figure 59: Regional distribution of Tertiary basalts and andesites modified from Willden (1964). Outcrops within the Sandman project area (Fig. 5) are from unpublished map by Newmont geologist Clay Postlethwaite. Stars indicate samples for which age data were obtained. White stars from Mellot (1987), red stars this study, black stars from Fronteer unpublished report (Peters, 2003), 1 = 22.83 ± 1.00 Ma (K/Ar), 2 = 20.55 ± 1.12 Ma (K/Ar), 3 = 22.53 ± 0.04 Ma (Ar/Ar), 4 = 22.66 ± 0.07 Ma (Ar/Ar), 5 = 22.62 ± 0.29 Ma (Ar/Ar), 6 = 22.42 ± 0.23 Ma (Ar/Ar) . Yellow outlines are for sample locations of rhyolite dikes, W = Winni Rhyolite, R = Rembrandt Rhyolite, SRR = Santa Rosa Range, BRH = Bloody Run Hills, SH = Slumbering Hills, BM = Blue Mountain, KH = Krum Hills, TMH = Ten Mile Hills, WM = Winnemucca Mountain.

Abel Knoll Breccia Body

Prior to Newmont's full ownership of the Sandman Au project, Fronteer drilled a total of 52 reverse circulation holes and 5 core holes into the Abel Knoll deposit. With a narrow, vertically elongate grade shell unsuitable to open pit mining methods, and Au grades not high enough to warrant underground extraction, only a few step out reverse circulation exploration holes, and one core hole into the center of the deposit were drilled by Newmont following their acquisition of the property. Surface mapping, historic drill logs, core photos, skeletonized core of AK-08-0057c (drilled by Fronteer), and drill hole NSM-00380 (drilled by Newmont) were used to generate a stratigraphic column and deposit cross section (see Fig. 15 for stratigraphic column, Fig. 31 for surface geologic map with drill hole locations and Fig. 32 for cross section).

Hosting low sulfidation Au mineralization at the Abel Knoll deposit is a polylithic breccia body composed of vesicular to aphanitic andesite, basement phyllites and quartzites, tuffaceous wall rocks, and trace Mesozoic granodiorite within an ash ± crystal fragment matrix. Crystal fragments are dominantly sanidine with lesser quartz and trace biotite. Clast percentages, compositions, and size are variable throughout the breccia body. Mafic dominant intervals are typically clast supported, while intervals rich in basement rocks are generally matrix supported. Breccia clasts range from 20-80%, with an average size between 1-8cm. Megablocks of basement phyllite were also encountered within the breccia body at depth in NSM-00380. Breccia clasts are typically sub rounded and fluidized textures are evident in thin section as linear concentrations of heavy minerals within an ashy matrix and along breccia clast margins.

Intruding the Abel Knoll breccia body is a trachy-andesite dike, which is

geochemically similar to surface flows at Abel Knoll (Fig. 60). Variations in Ba, Sr, and Rb, in addition to SiO_2 and K_2O (Figs. 49 and 55) are the result of hydrothermal alteration. Moderate to intense argillic alteration, overprinted by weak to intense quartz-adularia alteration affect most of the Abel Knoll breccia body. Mafic breccia clasts were not sampled, although it is presumed they are genetically related to the Abel knoll dike and surface flow. While mafics at Abel Knoll have not been dated, breccia clasts, the intrusive dike, and the Abel Knoll surface flow are all geochemically similar to mafic rocks dated at ~22.5 Ma elsewhere within the Sandman project area (Fig. 51). The Abel Knoll breccia body is likely of a similar age, recording a phreatomagmatic eruption resulting from the interaction of melt and groundwater.

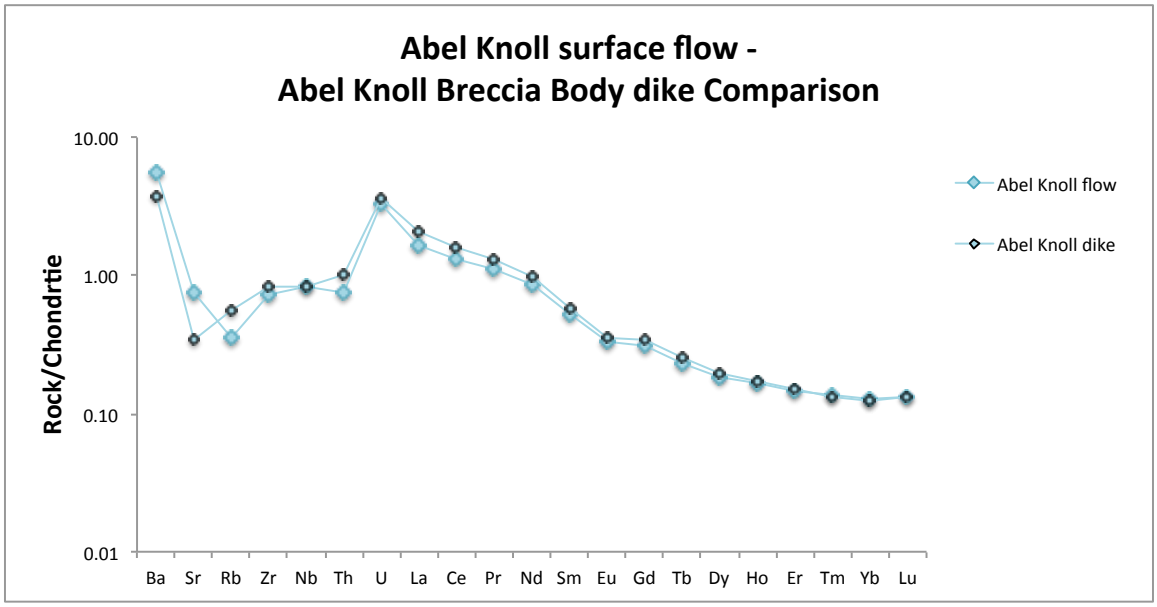

Figure 60: Modified spider diagram for select trace element and REE geochemistry comparing the Abel Knoll surface flow to a mafic dike within the Abel Knoll breccia body. Variations in Ba, Sr, and Rb are the result of quartz-adularia hydrothermal alteration. Similar trace element geochemistry between the two and other mafic rocks from the Sandman project (Fig. 39) provide a relative age of ~22.5 Ma for the Abel Knoll breccia body.

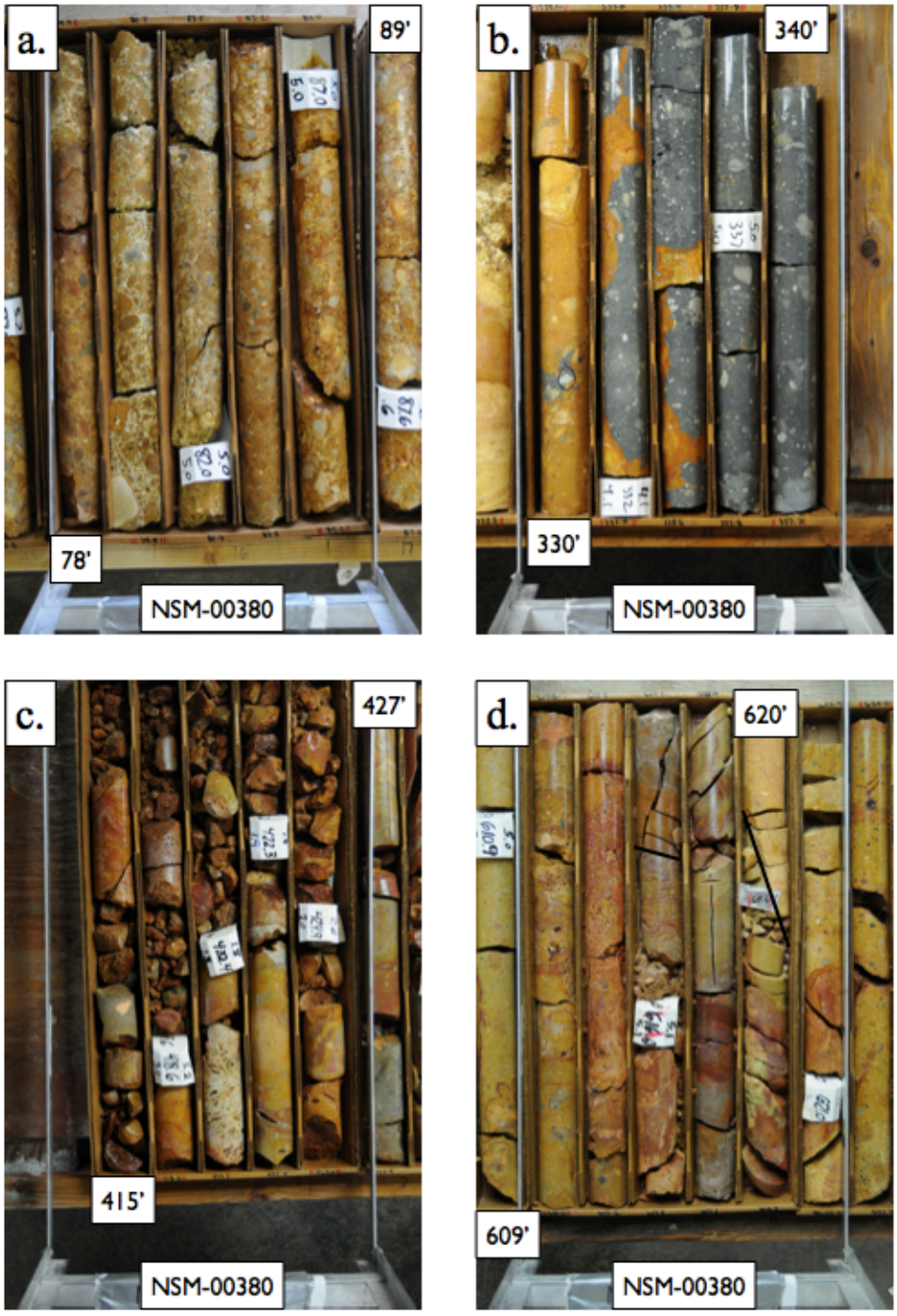

Figure 61: Drill core photos of the Abel Knoll polylithc breccia body composed of Triassic basement phyllite, trachy-andesite and trace Cretaceous granodiorite in a tuffaceous matrix. A.) Oxidized, argillically altered breccia with weak quartz-adularia alteration. B.) Oxidation front in strongly quartz-adualria altered breccia. C.) Oxidized fault breccia and quartz after bladed calcite vein. D.) Oxidized breccia with large megablock of Triassic basement phyllite.

As with other deposits within the Sandman project area, the intersection of north striking and east-northeast striking structures at Abel Knoll played a significant role in focusing mid-Miocene mineralizing fluids. These structural intersections also appear to have controlled the emplacement of the Abel Knoll breccia body (see Fig. 31). Deep basement drilling beneath the Abel Knoll breccia body is limited and a mafic intrusive source has not been encountered. Reverse circulation hole DSA-0220 (Fig 32) intercepted approximately 75 feet of rock described as rhyolite tuff based on the presence of quartz phenocrysts within drill chips. As these rocks are within the Triassic basement, they can not be tuff. Examination of these chips suggests they are quartz-feldspar porphyry; however, grain mount sections have not been prepared to confirm the actual composition. As quartz fragments are present within the Abel Knoll breccia body, the two may be genetically related; however, breccia clasts of quartz-feldspar porphyry have not been observed. The dominance of mafic breccia clasts within the Abel Knoll breccia body suggests a genetic relationship with a mafic intrusion rather than a felsic intrusion at depth. It is also possible that these chips are associated with late Mesozoic granitic intrusions rather than mid-Tertiary volcanics.

Resulting from limited core holes within the Abel Knoll deposit and structural offset within the Abel Knoll deposit, stratigraphic relationships are not definitively known between the Abel Knoll breccia body and its mid-Tertiary tuffaceous wall rocks. Excluding AK-08-0056c, all core holes at Abel Knoll are within the breccia body and only limited tuffaceous wall rocks are encountered. Basement pierce points in drill core AK-08-0056c and AK-08-0055c indicate approximately 350 feet of down to the south displacement across an east-northeast striking fault potentially bounding the Abel Knoll

breccia body. AK-08-0057c—approximately 400 feet to the south of the Abel Knoll breccia body within this down to the south structural block—was utilized in defining a mid-Tertiary stratigraphic column. The stratigraphic column for Abel Knoll (Fig. 15) is a composite of all available data and is conceptual in nature. AK-08-0057c was not drilled to basement and the lower stratigraphy is not known. Depth to basement at ~600 feet in Figure 15 is from reverse circulation and drill core occurring to the north of the east striking structure. As this block is up thrown approximately 350 feet, it is likely that the upper 350 feet of stratigraphy depicted in the stratigraphic column is missing within the Abel Knoll deposit area. Additional core holes to the south of the heavily drilled Abel Knoll corridor are needed for a better understanding of stratigraphic relationships and structural offset.

GEOCHRONOLOGY

Table 3 summarizes geochronological data for rocks and vein material within the vicinity of the Sandman project area. These include four new Ar/Ar age dates from this study, historical K/Ar age dates from an unpublished Kennecott internal report, and U/Pb, K/Ar, and Ar/Ar data from a number of thesis and published papers The oldest rocks in the project are basement metasedimentary rocks of the Luning Fencemaker allochthon. Biostratigraphy indicates they are mostly Norian (208.5-228 Ma), although locally some rocks within the basinal terrane are Carnian (235-228 Ma) and Early Jurassic (200-176 Ma) (Wyld, 2002). Inferred Cretaceous granitic stocks within the Ten Mile Hills have not been directly dated; however U-Pb zircon dating of zircons from stocks in the Slumbering Hills and Bloody Run Hills are 116 Ma and 98 Ma respectively (Colgan et al., 2006).

The oldest Tertiary rocks dated within the Sandman project area include a 26.0 unnamed tuff collected from outcrop at Adularia Hill, and the 25.4 Ma Nine Hill Tuff collected from outcrop just to the west of Silica Ridge. Standard thin sections were prepared and stained by sodium cobaltinitrite to determine degree of hydrothermal potassic alteration. Sanidine separates were prepared by Chris Henry with the Nevada Bureau of Mines and Geology and analyzed at the New Mexico Geochronology Research Laboratory by Ar/Ar methods. The youngest Tertiary rocks in the project area include basaltic trachy-andesite, trachy-andesite and andesite flows, sills, and dikes with an age of ~22.5 Ma. Two drill core samples, one from North Hill, and the other from Southeast Pediment were submitted to the University of Auburn Nobel Isotope Mass Analysis Lab. Groundmass serpaerates were prepared and analyzed by Dr. Willis Hames. These new

age dates of ~22.5 Ma agree with those from the Basalt Hills and Little Basalt Hills (Peters, 2003), and are similar in age to mafic rocks within the Northern Bloody Run Hills and along the east flanks of the Santa Rosa Range (Mellot, 1987; Brueseke and Hart, 2008). Regarding timing of mineralization, Unger (2008) dated adularia from vein outcrop at Adularia Hill and the Ten Mile Mine with respective ages of ~16.2 Ma and 16.5 Ma. See Figures 62 through 70 for plots and Appendices 23 through 27 for analytical data.

Lithology	Location	Age	Method	Source
Metasediments	Luning Fencemaker	Norian (208.5-228 Ma)	Biostratigraphy	Wyld (2002)
Granitic Stock	Slumbering Hills	116 Ma	U-Pb Zircon	Colgan et al. (2006)
Granitic Stock	Bloody Run Hills	98 Ma	U-Pb Zircon	Colgan et al. (2006)
Unnamed Tuff	Adularia Hill	26.01 ± 0.07 Ma	Ar/Ar Sanidine separate	This Study
Nine Hill Tuff	W of Silica Ridge	25.34 ± 0.11 Ma	Ar/Ar Sanidine separate	This Study
Mafic	Not given	26.40 ± 1.20 Ma	K/Ar groundmass	Kennecott Internal Report
Mafic	Basalt Hills	22.62 ± 0.29 Ma	Ar/Ar groundmass	Peters (2003)
Mafic	Little Basalt Hills	22.42 ± 0.23 Ma	Ar/Ar groundmass	Peters (2003)
Mafic	North Hill	22.53 ± 0.04 Ma	Ar/Ar groundmass	This Study
Mafic	SE Pediment Sill	22.66 ± 0.07 Ma	Ar/Ar groundmass	This Study
Mafic	N Bloody Run Hills	22.83 ± 1.00 Ma	K/Ar groundmass	Mellot (1987)
Mafic	SE Santa Rosa Range	20.55 ± 1.12 Ma	K/Ar groundmass	Mellot (1987)
Mafic	NE Santa Rosa Range	23.50 ± 0.24 Ma	K/ AR groundmass	Brueseke and Hart (2008)
Mafic	NE Santa Rosa Range	22.48 ± 0.08 Ma	K/ AR groundmass	Brueseke and Hart (2008)
Adularia-Silica Au Vein	Not given	17.10 ± 0.70 Ma	K/Ar adularia separate	Kennecott Internal Report
Adularia-Silica Au Vein	Not given	16.38 ± 0.13 Ma	Ar/Ar adularia separate	Peters (2003)
Adularia-Silica Au Vein	Ten Mile Mine	16.52 ± 0.04 Ma	Ar/Ar adularia separate	Unger (2008)
Adularia-Silcia Au Vein	Adularia Hill	16.17 ± 0.04 Ma	Ar/Ar adularia separate	Unger (2008)

Table 3: Summary of geochronological data for rocks and vein material within the vicinity of the Sandman project area.

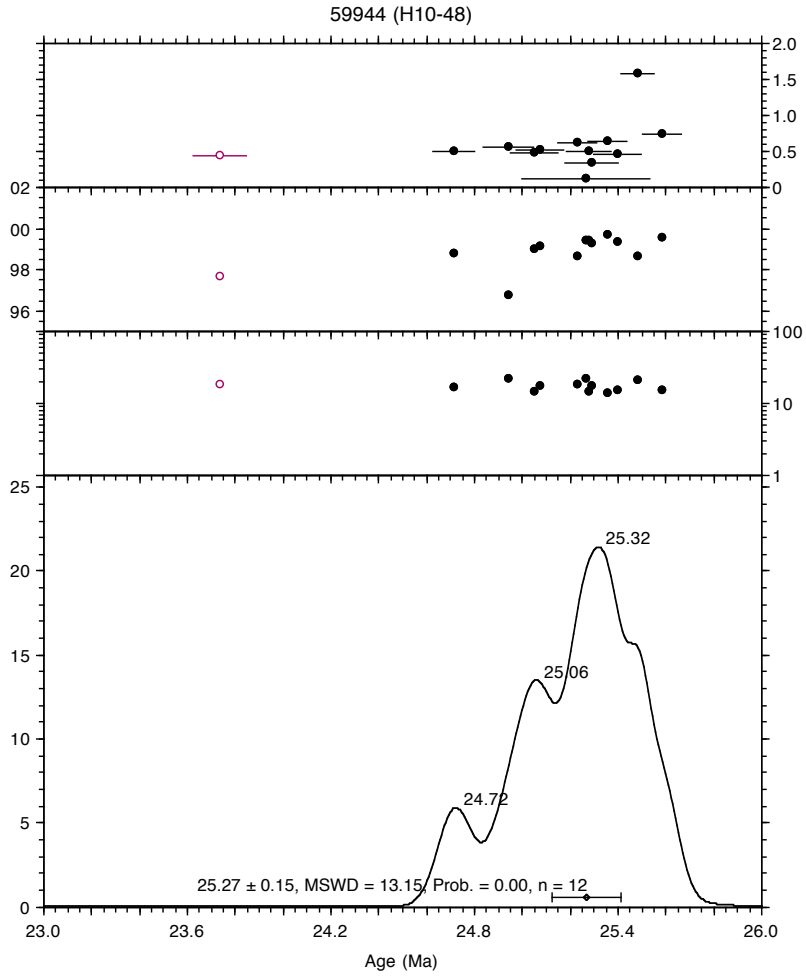

Figure 62: $^{40}Ar/^{39}Ar$ incremental heating curve plot for Nine Hill Tuff sample 5994 (H10-48). Sample collected in outcrop at base of conglomerate knob just west of Silica Ridge. The curve age of 25.27 ± 0.15 Ma is a mean of all 12 analyses. As the scatter of data is consistent with some Ar loss, the three youngest ages, two of which had the lowest radiogenic contents were eliminated for an age of 25.34 Ma. See Appendix 23 for analytical data.

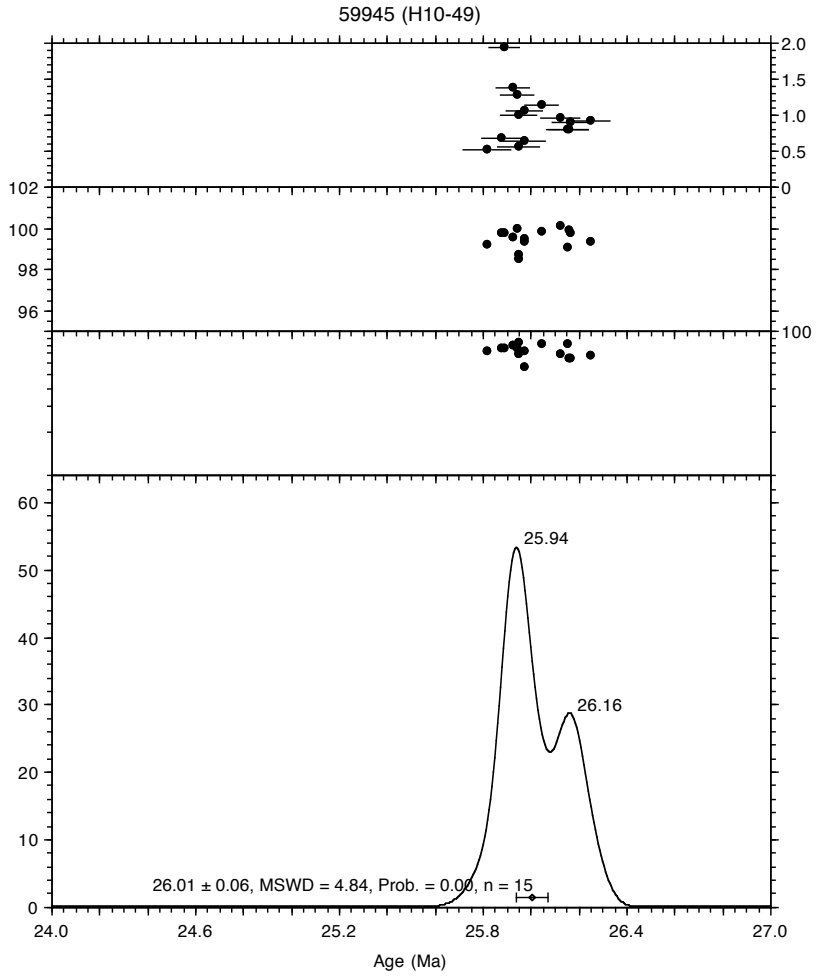

Figure 63: $^{40}Ar/^{39}Ar$ incremental heating curve plot for unnamed tuff sample 5995 (H10-49). Sample collected in outcrop at top of Adularia Hill. See Appendix 24 for analytical data.

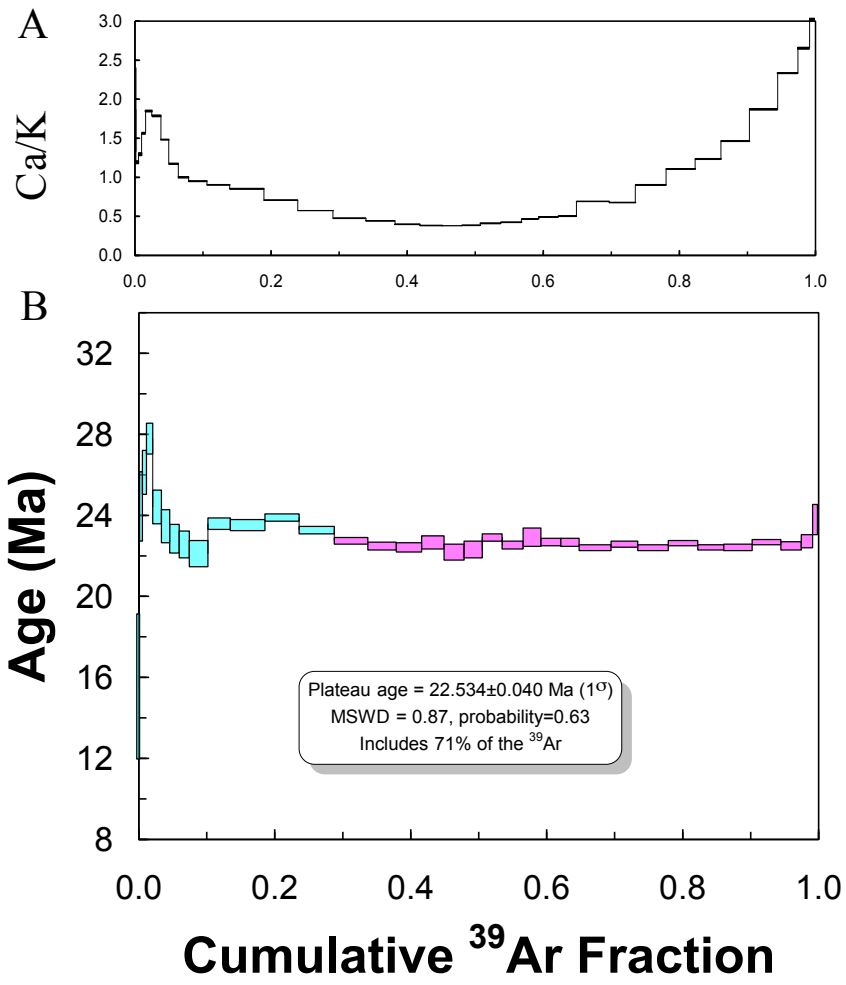

Figure 64: $^{40}Ar/^{39}Ar$ incremental heating release spectra with apparent Ca/K ratio (A) and age (B) for basalt sample NSM-00190-161 (au22.4l.whr). Sample from diamond drill core at North Hill. A plateau age of 22.534±0.040 Ma (1σ, precision of measurement only) is defined by higher temperature release steps comprising 71% of the ^{39}Ar released. Age variation over the first 30% of $^{39}Ar_K$ released is interpreted to result from a combination of extraneous, non-atmospheric argon and ^{39}Ar recoil within plagioclase. The plateau age defined by subsequent increments is interpreted to represent the crystallization age of the basalt. See Appendix 25 for analytical data.

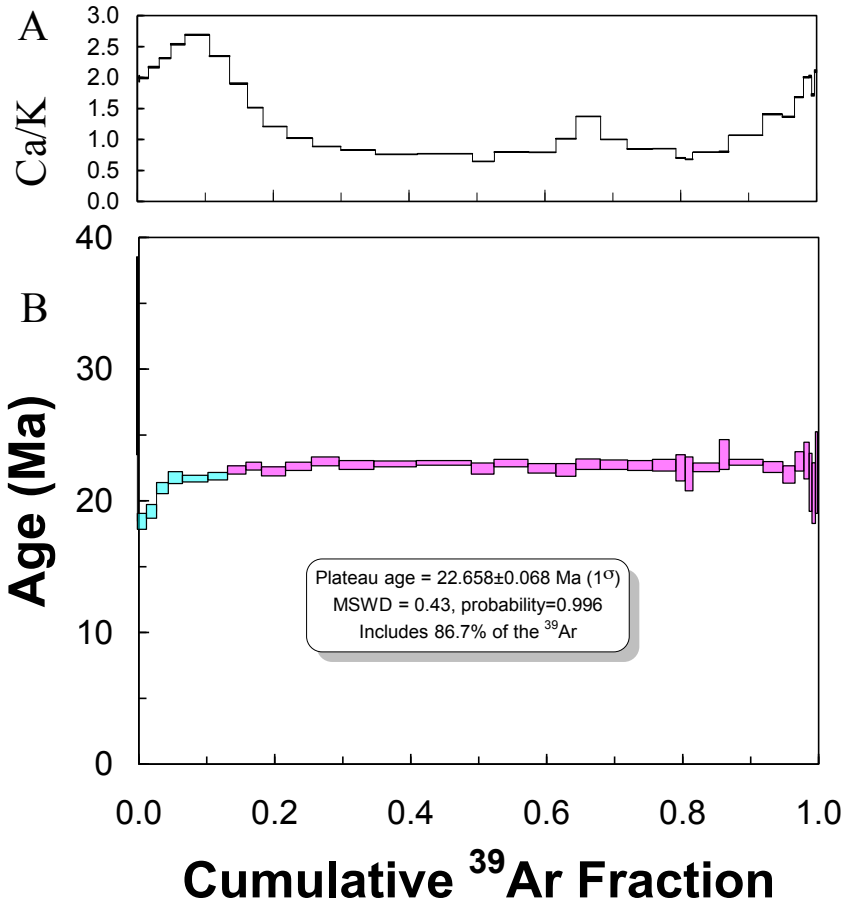

Figure 65: $^{40}Ar/^{39}Ar$ incremental heating release spectra with apparent Ca/K ratio (A) and age (B) for basalt sample NSM-00358-453 (au22.4m.whr). Sample collected from diamond drill core at Southeast Pediment. A plateau age of 22.658±0.068 Ma (1σ, precision of measurement only) is defined by higher temperature release steps comprising 86.7% of the ^{39}Ar released. The increase in age over the first 15% of ^{39}Ar release is interpreted to reflect some post-crystallization loss of radiogenic ^{40}Ar. The age defined by the plateau increments is interpreted to represent the crystallization age of the basalt. See Appendix 25 for analytical data.

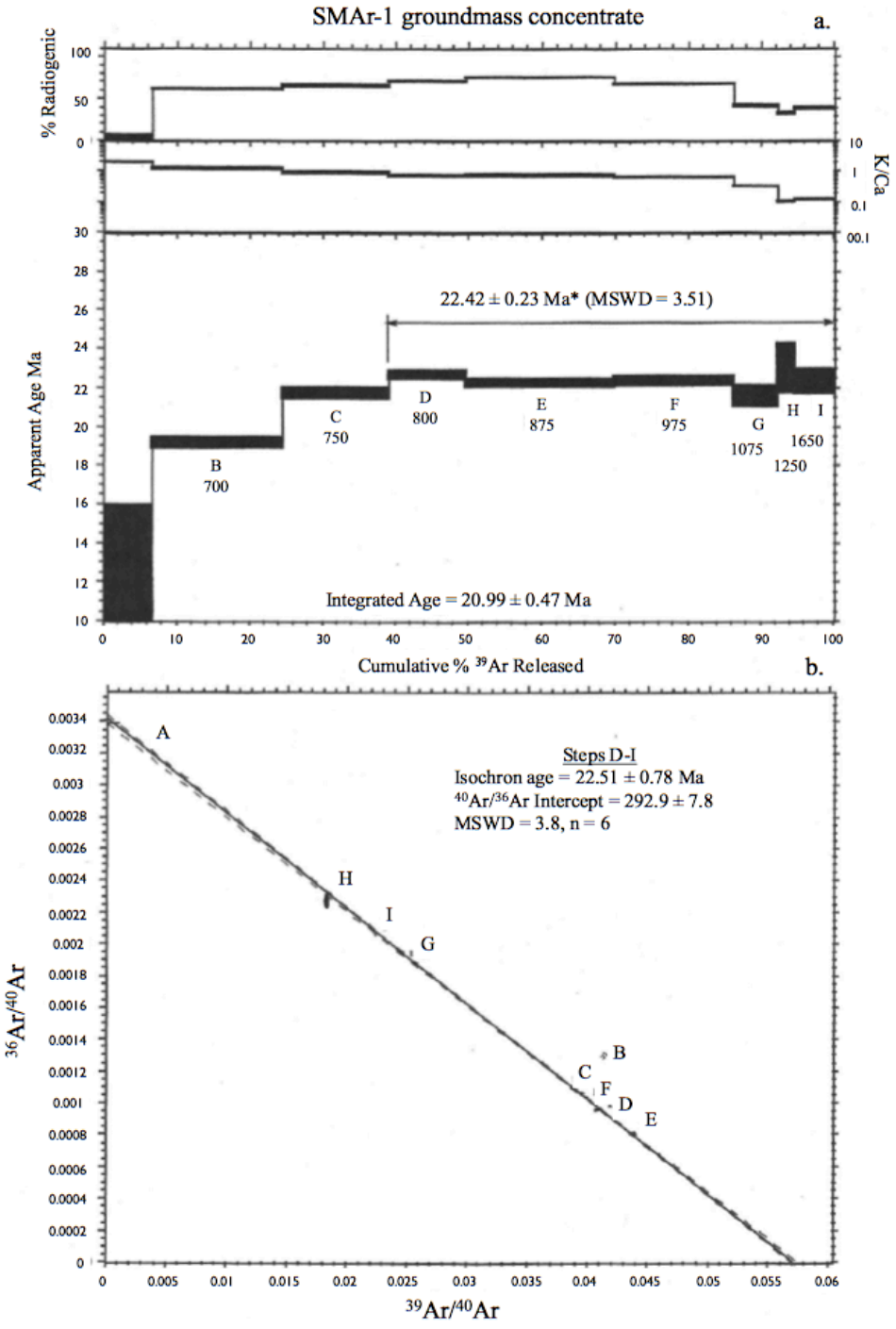

Figure 66: Age spectrum (1a) and isochrones (1b) for sample SAME-1 groundmass concentrate. Sample from outcrop in the Little Basalt Hills (Peters, 2003). See Appendix 26 for analytical data.

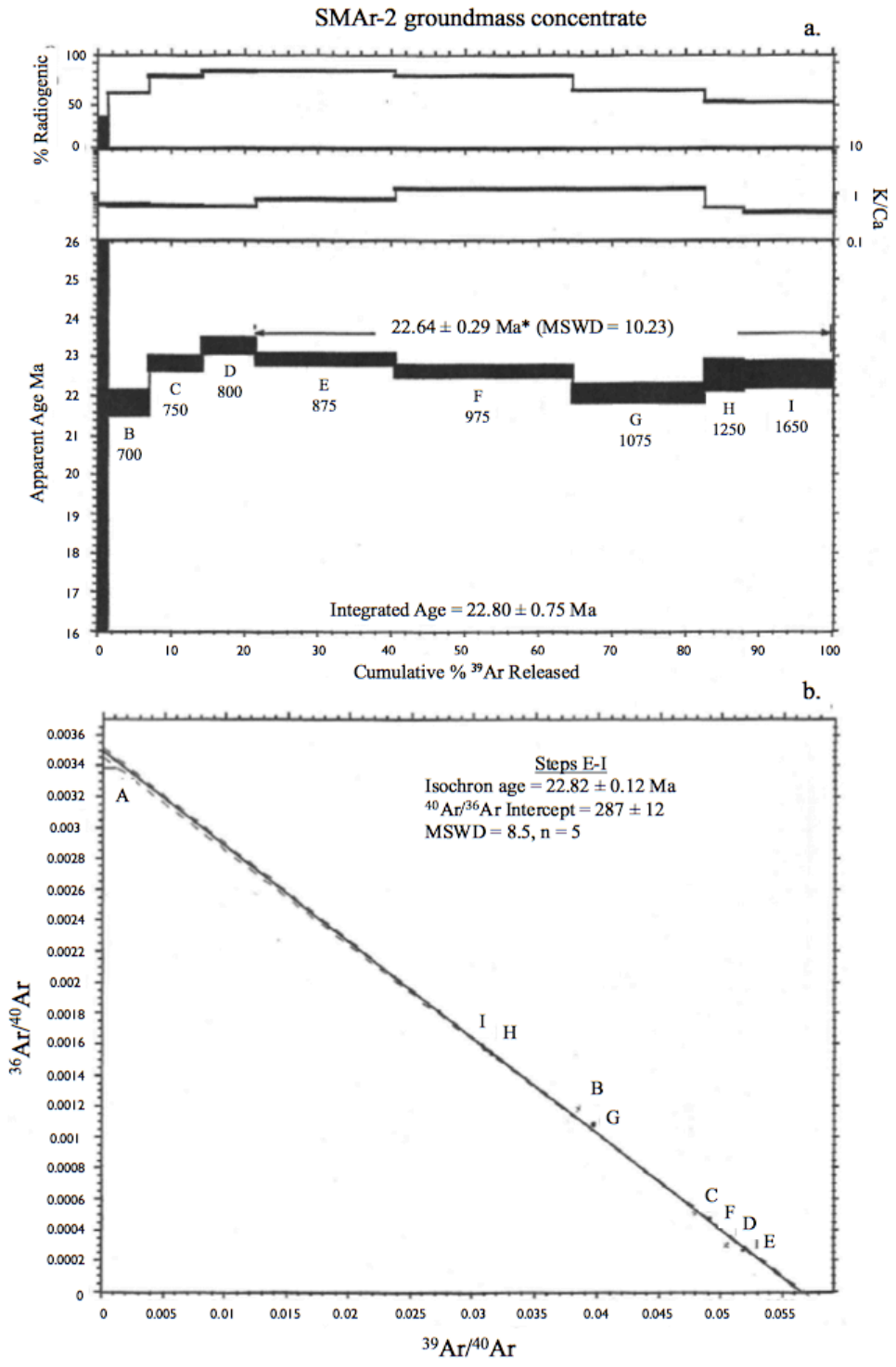

Figure 67: Age spectrum (1a) and isochrones (1b) for sample SAME-1 groundmass concentrate. Sample from outcrop in the Basalt Hills (Peters, 2003). See Appendix 26 for analytical data.

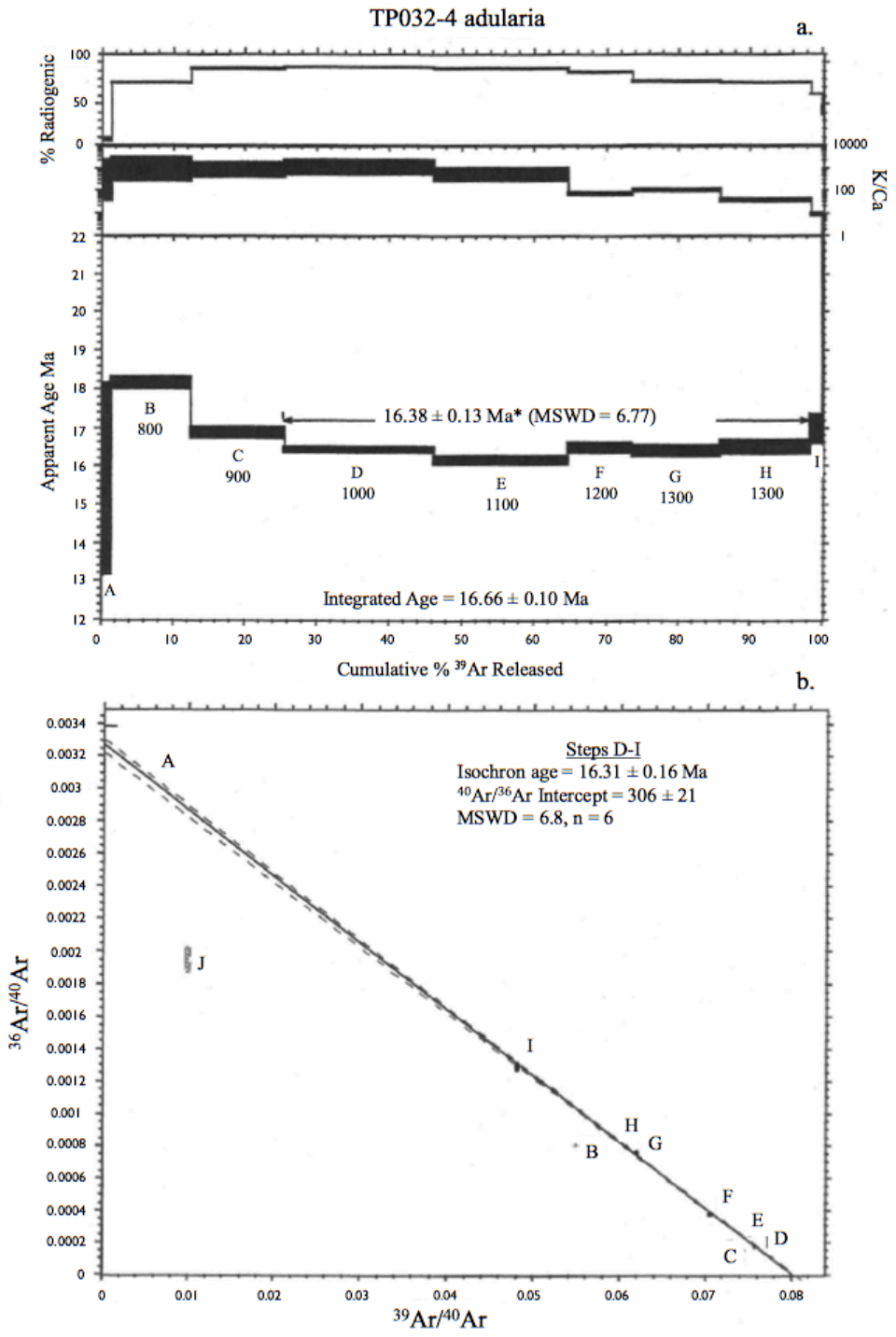

Figure 68: Age spectrum (1a) and isochrones (1b) for sample SAME-1 groundmass concentrate. Sample from outcrop in the Little Basalt Hills (Peters, 2003). See Appendix 26 for analytical data.

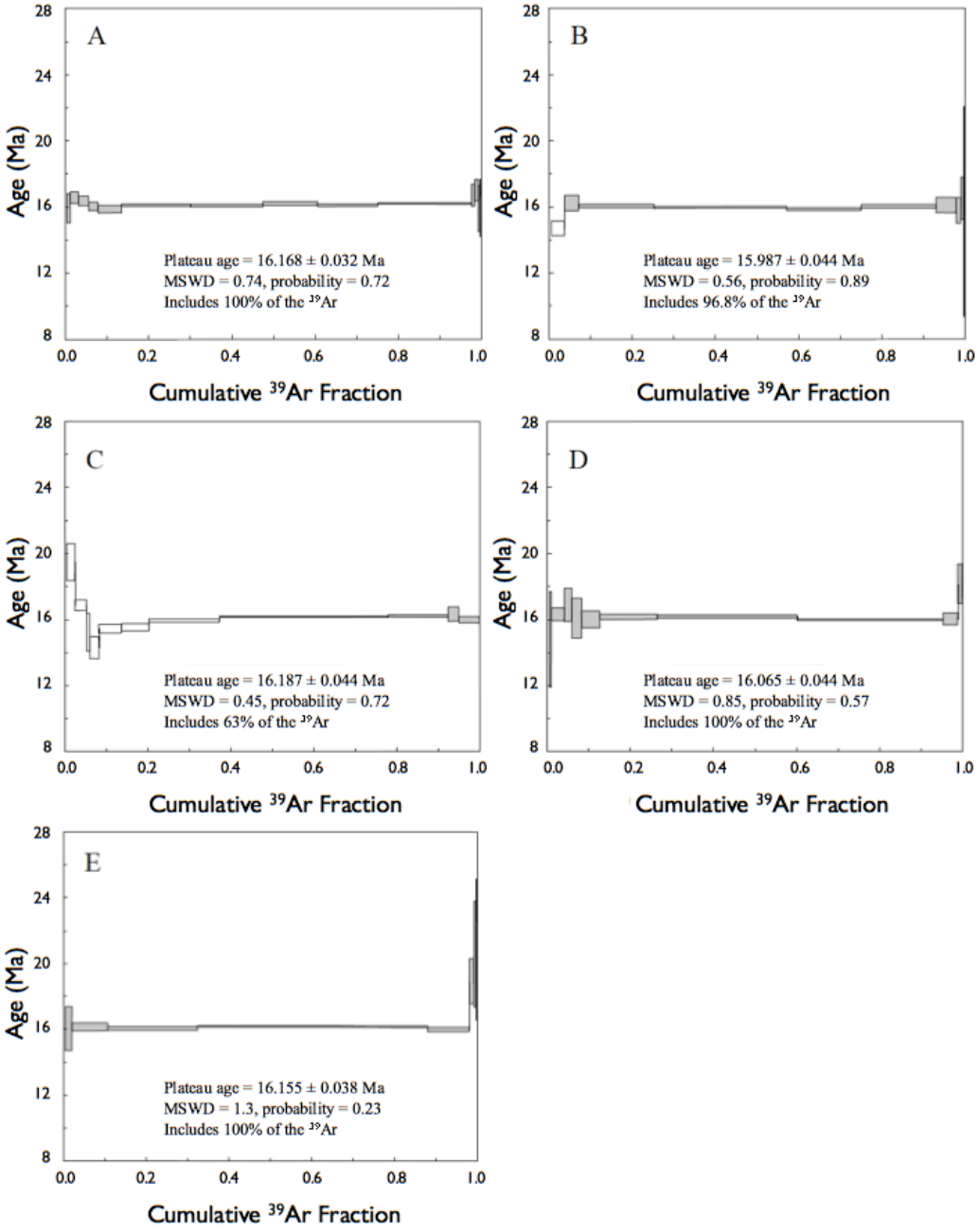

Figure 69: Release spectrum and plateau ages for five single adularia crystals (14-20 mesh size, 1.2-0.75 mm) of sample HCN-1 from the Sandman deposit. Steps used to define the plateau are shaded. Errors for individual steps and plateau ages are at 1σ. Irradiation filenames are as follows: A) au5.1a.adl.ih1, B) au5.1a.adl.ih2, C) au5.1a.adl.ih3,D) au5.1a.adl.ih4, and E) au5.1a.adl.ih1 (Unger, 2008). See Appendix 27 for analytical data.

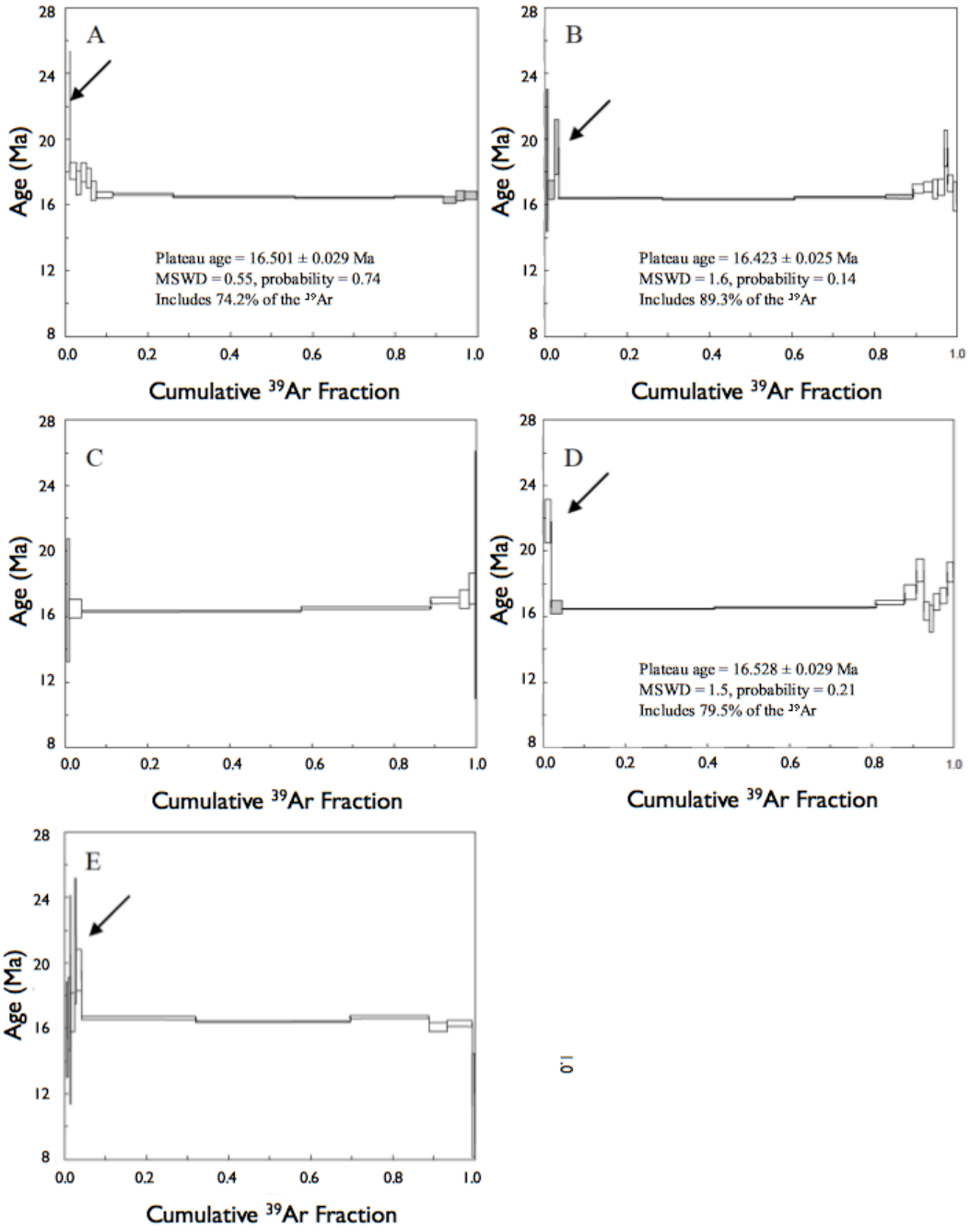

Figure 70: Release spectrum and plateau ages for five single adularia crystals (14-20 mesh size, 1.2-0.75 mm) of sample HCN-4 from the Ten Mile deposit. Steps used to define the plateau are shaded. Errors for individual steps and plateau ages are at 1σ. Irradiation filenames are as follows: A) au5.1h.adl.ih1, B) au5.1h.adl.ih2, C) au5.1h.adl.ih3, D) au5.1h.adl.ih4, and E) au5.1h.adl.ih1. Note anomalously old ages in initial or final increments of some analysis (arrows) consistent with release of extraneous ―excesse 40Ar (Unger, 2008). See Appendix 28 for analytical data.

Summary and Conclusion

Newmont Mining Corporation's Sandman Au project consists of five recognized, mid-Miocene low-sulfidation epithermal deposits hosted primarily in mid-Tertiary volcanic, volcaniclastic, and fluvial rocks, and to a lesser degree within basement Triassic rocks and late Mesozoic intrusions. These deposits include North Hill, Silica Ridge, Southeast Pediment, Abel Knoll and Ten Mile. Hosted entirely within mid-Tertiary volcanic, epiclastic, and fluvial rocks, the deposits of North Hill, Silica Ridge, and Southeast Pediment are both structurally and stratigraphically controlled. Abel Knoll is hosted within a mid-Tertiary polylithic breccia body composed of trachy-andesite to andesite, basement phyllites and trace granodiorite, and tuffaceous wall rocks. In the southeast of the project area, the Ten Mile deposit is structurally controlled and hosted dominantly within a late Mesozoic granodiorite stock.

Excluding the Ten Mile deposit, which is controlled by northeast-striking faults, deposits occur along north to north-northwest extensional structures. Intersections with northeast structures and the presence of Early Miocene mafic dikes also played a role as fluid conduits. Post-mineral structural offset affects all deposits. Older fault reactivation and movement along younger Basin and Range structures resulted in the development of north-south-striking grabens and half grabens and lesser intervening northeast grabens.

Basement lithologies consist of Triassic metasedimentary rocks dominated by phyllitic mudstones and siltstones with lesser degrees of quartzites and rare limestone units interbedded. Regional foliations strike northeast and dip moderately to the northwest. Basement rocks have been intruded by late Mesozoic granitic stocks to the east and southeast of the project in addition to local diking in phyllites on the flanks of

Blue Mountain to the west. Lying unconformably on basement rocks is an approximately 700->1300 foot thick package of Tertiary volcanic, epiclastic, and fluvial rocks. Lithologies consist of northeast striking, gently southeast dipping dacitic to rhyolitic airfall tuffs, pyroclastics and distally sourced ash flow tuffs with interbedded fluvial and lacustrine volcaniclastic siltstones, sandstones, and conglomerates. The presence of thick, distally sourced fluvial rocks in the northern portions of the property represent a major east-west (?) Oligocene to early Miocene paleodrainage. These rocks may be related to the inferred Cretaceous age Pansy Lee Conglomerate to the east, although this remains to be definitively proved. Additionally, further to the south drill intercepts have encountered approximately two hundred feet of organic and sulfur-rich, varved and laminated lacustrine sediments. Early Miocene basaltic trachy-andesite, trachy-andesite, and andesite sills and dikes intrude and cap the Sandman stratigraphic section.

Subtle topography limits outcrop exposures of mid-Tertiary rocks to capping mafic flows within the Basalt and Little Basalt Hills and more resistant quartz-adularia altered ridges occurring in the northwest of the Sandman project area. Additionally, extensive Quaternary deposits of the Crescent Dune Field cover much of the northern part of the property. Three field seasons were spent mapping surface exposures and trenches and logging drill core and reverse circulation chips from the project area leading to the recognition of three distinct tuff units within the Sandman stratigraphic section. Petrography, trace element geochemistry, and radiometric age dating was used to create a detailed stratigraphic column linking variable stratigraphy from deposit to deposit.

Within the northwest of the property, mapping and drilling has indicated a paleodrainage-controlled, marker fiamme unit—dated at ~25.4 Ma—linking the

stratigraphic section across Silica Ridge, Adularia Hill, and North Hill. Outcrop appearance with abundant large fiamme, a sparse phenocryst assemblage of sanidine-plagioclase-anorthoclase-beta quartz-biotite, radiometric age dating, and trace element geochemistry confirm this marker fiamme unit to be the regionally widespread rhyolitic Nine Hill Tuff. Named for the type locality in the Sierra Nevada foothills just north of Carson City, this pyroclastic unit is widespread and has been correlated with the "D" unit of the Bates Mountain Tuff in central Nevada near Austin. The Sandman project area is the furthest north documented location of the Nine Hill Tuff. No source caldera has yet been identified, though through regional distribution it has been suggested to lie beneath sediments within the Carson Sink.

Lower in section, a distinctive rhyolite tuff with coarse-grained sanidine-anorthoclase crystal fragments and abundant pumice ± fiamme has been dated at ~26.0 Ma. With a similar age, the Ashdown tuff—exposed to the west of the Sandman project in the Pine Forest and Black Ranges—is petrographically similar with abundant coarse-grained sanidine and pumice fragments; however, the two have differing trace element geochemistry, with the Ashdown Tuff being significantly enriched in Zr and Nb compared to the unnamed tuff found in outcrop at Adularia Hill and encountered in drill core at Silica Ridge and Southeast Pediment.

A dacitic to rhyolitic tuff of older—but unconfirmed age—has been encountered in drill core at Abel Knoll, Southeast Pediment, and Silica Ridge. Recognized by a distinctive, moderately welded, basal polylithic volcanic breccia, the Red-Green Breccia tuff package is composed of repetitive lapilli-lithic, fiamme, and vitric airfall tuffs. Excluding rare plagioclase and biotite within the basal polylithic breccia, crystal

fragments are largely absent. A lack of datable phenocrysts combined with extensive propylitic, argillic, and quartz-adularia overprints has hindered dating of this tuff unit.

The youngest rocks exposed within the Sandman project area include capping mafic flows and related sills and dikes of basaltic trachy-andesite, trachy-andesite, and lesser andesite. These rocks have been dated at ~22.5 Ma. Rocks of a similar age and composition have been documented to the northeast of the Sandman project area within the Bloody Run Hills and Santa Rosa Range. Similar rocks are also exposed to the east in the hills between Winnemucca Mountain and the Bloody Run Hills, and to the north in isolated exposures along the east flank of the Slumbering Hills. With abundant clasts of andesite, the Abel Knoll breccia body is also likely of a similar age. The spatial association of early Miocene dikes, sills, and mafic breccia bodies to middle Miocene low sulfidation Au mineralization may provide a useful tool for future exploration within and outside the project area.

REFERENCES

Best, M.G., Christiansen, E.H., Deino, A.L., Grommé, C.S., McKee, E.H., and Noble, D.C., 1989, Excursion 3A: Eocene through Miocene volcanism in the Great Basin of the western United States: New Mexico Bureau of Mines and Mineral Resources Memoir 47, p. 91-133.

Bingler, E.C., 1978, Abandonment of the name Hartford Hill Rhyolite Tuff and adoption of new formation names for middle Tertiary ash-flow tuffs in the Carson City-Silver City area, Nevada: U.S. Geological Survey Bulletin 1457-D, 19 p.

Bonham, Jr., H.F., Garside, L.J., Jones, R.B., Papke, K.G., Quade, J., and Tinglet, J.V., 1985, A Mineral Inventory of the Paradise-Denio and Sonoma-Gerlach Resources Areas, Winnemucca District, Nevada, NBMG Open File Report 85-3, 473 p.

Bowell, R.J., Hunerlach, M.P., Parshley, J., and Sears, S., 2000, The Ten Mile mining district, Winnemucca, Nevada: Geology, mineralogy and supergene gold enrichment, *in* Cluer, J.K., Price, J.G., Struhsacker, E.M., Hardyman, R.F., and Morris, C.L., eds., Geology and ore Deposits 2000: The Great Basin and Beyond: Geological Society of Nevada Symposium Proceedings, Reno/Sparks, May 2000, p. 349-363.

Brueseke, M.E., and Hart, W.K., 2008, Geology and petrology of the Mid-Miocene Santa Rosa-Calico volcanic field, northern Nevada: Nevada Bureau of Mines and Geology Bulletin 113, 46 p.

Brueseke, M.E., and Hart, W.K., 2009, Intermediate composition magma production in an intracontinental setting: Unusual andesites and dacites of the mid-Miocene Santa Rosa-Calico volcanic field, northern Nevada: *Journal of Volcanology and Geothermal Research,* v. 188, p. 197-213.

Burke, D.B., and Silberling, N.J., 1973, The Auld Lang Syne Group, of Late Triassic and Jurassic (?) age, north-central Nevada: U.S. Geological Survey Bulletin 1394-E, p. E1-E14.

Burke, D.B., and McKee, E.H., 1979, Mid-Cenozoic volcanotectonic troughs in central Nevada: Geological Society of America Bulletin, v. 90, no. Part 1, p. 181–184.

Christiansen, R.L., and Yeats, R.S., 1992, Post-Laramide geology of the U.S. Cordilleran region, *in* Burchfiel, B.C., Lipman, P.W., and Zoback, M.L., eds., The Cordilleran Orogen: conterminous U.S: The Geology of North America, Geological Society of America, v. G-3, p. 261–406.

Ciavarella, V.C., 2003, Mesozoic Deformation and Pluton Emplacement in the Northern Luning-Fencemaker Fold-and-Thrust Belt: New Evidence from the Bloody Run Hills, Nevada [M.S. thesis]: Athens, Georgia, University of Georgia, 131 p.

Ciavarella, V., and Wyld, S.J., 2008. Wall rocks as recorders of multiple pluton emplacement mechanisms-- Examples from Cretaceous intrusions of northwest Nevada: Geological Society of America Special Paper 438, 34 p.

Colgan, J.P., Dumitru, T.A., McWilliams, M., and Miller, E.L., 2005, Timing of Cenozoic volcanism and Basin and Range extension in northwestern Nevada: New constraints from the northern Pine Forest Range: Geological Society of America Bulletin, v. 118, p. 126-139.

Colgan, J.P., Dumitru, T.A., Reiners, P.W., Wooden, J.L, and Miller, E.L., 2006, Cenozoic Tectonic Evolution of the Basin and Range Province in Northwestern Nevada. American Journal of Science, v. 306, p. 616-654.

Compton, R.R., 1960, Contact metamorphism in Santa Rosa Range, Nevada: Geological Society of America Bulletin, v. 71, p. 1383–1416.

Conrad, J.E., McKee, E.H., Rytuba, J.J., Nash, J.T., and Utterback, W.C., 1993, Geochronology of the Sleeper deposit, Humboldt, County, Nevada: Epithermal gold-silver mineralization following silicic flow-dome complex: *Economic Geology*, v. 88, p. 317-327.

Conrad, J.E., and McKee, E.H., 1996, High-precision 40Ar/39Ar ages of rhyolitic host rock and mineralized veins at the Sleeper deposit, Humboldt County, Nevada: Geological Society of Nevada, Geology and Ore Deposits of the American Cordillera Symposium, Reno-Sparks, Nevada, April 1995, Proceedings, p. 257-262

Deino, A.L., 1985, Stratigraphy, chemistry, K-Ar dating, and paleomagnetism of the Nine Hill Tuff, California-Nevada [Ph.D. dissertation]: University of California, Berkeley, 457 p.

Deino, A.L., 1989, Single crystal 40Ar/39Ar dating as an aid in correlation of ash flows: Examples from the Chimney Springs/New Pass Tuffs and the Nine Hill/Bates Mountain Tuffs of California and Nevada: New Mexico Bureau of Mines and Mineral Resources, Continental Magmatism Abstracts Bulletin 131, p. 70.

Dianne Erwin, University of California Museum of Paleontology, personal communication

Dickinson, W.R., 2004, Evolution of the North American Cordillera: Annual Review of Earth and Planetary Sciences, v. 32, p. 13–45.

Elison, M.W., and Speed, R.C., 1989, Structural development during flysch basin collapse: The Fencemaker allochthon, East Range, Nevada: Journal of Structural Geology, v. 11, p. 523–538.

Faulds, J.E., Henry, C.D., and Hinz, N.H., 2005a, Kinematics of the northern Walker Lane: An incipient transform fault along the Pacific–North American plate boundary: Geology, v. 33, p. 505–508.

Faulds, J.E., Henry, C.D., Hinz, N.H., Drakos, P.S., and Delwiche, B., 2005b, Transect across the northern Walker Lane, northwest Nevada and northeast California: An incipient transform fault along the Pacific–North American plate boundary, *in* Pederson, J., and Debie, C.M., eds., Interior Western United States: Geological Society of America Field Guide 6, p. 129–150.

Ferguson, H.G., Muller, S.W., and Roberts, R.J., 1951, Geology of the Winnemucca Quadrangle, Nevada: U.S. Geol. Survey Geol. Quad. Map GQ-11.

Fosdick, J.C. and J.P. Colgan, 2008, Miocene extension in the East Range, Nevada: A two-stage history of normal faulting in the northern Basin and Range, GSA Bulletin, v. 120, no. 9/10, p. 1198–1213.

Garside, L.J., Henry, C.D., Faulds, J.E., and Hinz, N.H., 2005, The upper reaches of the Sierra Nevada auriferous gold channels, California and Nevada, *in* Rhoden, H.N., Steininger, R.C., and Vikre, P.G., eds., Geological Society of Nevada Symposium 2005: Window to the World, Reno, Nevada, May 2005, p. 209–235.

Gifkins, C.C., Allen, R.L., and McPhie, J., 2005, Apparent welding textures in altered pumice-rich rocks: Journal of Volcanology and Geothermal Research 142, p. 29-47.

Gopon, P.N., 2010, Sandman low-sulfidation epithermal Gold Deposits: Northern Great Basin, Nevada. [M.S. thesis]: University of Wisconsin. 88 p.

Grommé, C.S., McKee, E.H., and Blake, M.C., Jr., 1972, Paleomagnetic correlations and potassium-argon dating of middle Tertiary ash-flow sheets in the eastern Great Basin, Nevada and Utah: Geological Society of America Bulletin, v. 83, p. 1619–1638.

Gustin, M.M., Lanier, G., and Ashton, J., 2007, Updated Technical Report, Sandman Gold Project, Humboldt County, Nevada USA, 186 p.

Henry, C.D., Nevada Bureau of Mines and Geology, personal communication

Henry, C.D., 2008, Ash-flow tuffs and paleovalleys in northeastern Nevada: Implications for Eocene paleogeography and extension in the Sevier hinterland, northern Great Basin: Geosphere, v. 4, p. 1–35.

Henry, C.D., and Boden, D.R., 1998, Geologic map of the Mount Blitzen Quadrangle, Elko County, northeastern Nevada: Nevada Bureau of Mines and Geology Map 110.

Henry, C.D., Castor, S.B., and Boden, D.R., 1999, Geology of the Tuscarora Quadrangle, Elko County, Nevada: Nevada Bureau of Mines and Geology Map 116, p. 20.

Henry, C.D., and Faulds, J.E., 2010, Ash-flow tuffs in the Nine Hill, Nevada, Paleovalley and implications for tectonism and volcanism of the western Great Basin, USA: Geosphere, v. 6, no. 4. P 339-369.

Irvin, T.N., and Baragar, W.R., 1971, A guide to the chemical classification of the common volcanic rocks: Canadian Journal of Earth Sciences, v. 8. No. %, p. 523-548.

Jenkins, O.P., 1932, Geologic map of northern Sierra Nevada showing Tertiary river channels and mother lode belt: Sacramento, California Division of Mines and Geology.

John, D.A., 2001. Miocene and early Pliocene epithermal gold–silver deposits in the northern Great Basin, western United States: characteristics, distribution, and relationship to magmatism. Economic Geology 96, 1827–1853.

John, D.A., Henry, C.D., and Colgan, J.P., 2008, Magmatic and tectonic evolution of the Caetano Caldera, north-central Nevada: A tilted, md-Tertiary eruptive center and source of the Caetano Tuff: Geosphere, v. 4, no. 1, p. 75-106.

Kennecott Internal Company Memo, 1987

Koschmann, A.H., and Bergendahl, M.H., 1968, Principle Gold-Producing Districts of the United States, Geological Survey Professional Paper 610, p. 183.

Lauha, E.A., Postlethwaite, C., Reid, R.F. Vance, R.B., Blackmone, J.E., and Gopon, P.N., 2010, Geology of the Sandman epithermal gold vein prospects, Humboldt County, Nevada: 2010 Geological Society of Nevada Symposium, p. 813-824.

Lerch, D.W., Miller, E.L., McWilliams, M., and J.P. Colgan, 2008, Tectonic and magmatic evolution of the northwestern Basin and Range and its transition to unextended volcanic plateaus, Black Rock Range: Geological Society of America Bulletin, v. 120, p. 300-311.

Lindgren, W., 1911, The Tertiary gravels of the Sierra Nevada of California: U.S. Geological Survey Professional Paper 73, 226 p.

Ludington, S., Cox, D.P., Moring, B.C., and Leonard, K.W., 1996, Cenozoic volcanic geology of Nevada: Nevada Bureau of Mines and Geology Open-File Report 96-2, chapter 5, p. 5-1–5-10.

Lupe, R., and Silberling, N.J., 1985, Genetic relationship between Lower Mesozoic continental strata of the Colorado Plateau and marine strata of the western Great Basin: Signifi cance for accretionary history of Cordilleran lithotectonic terranes, *in* Howell, D.G., ed., Tectonostratigraphic Terranes of the Circum-Pacifi c Region: Earth Science Series 1: Houston, Texas, Circum-Pacifi c Council for Energy and Mineral Resources, p. 263–271.

MacLean, W.H., and Barret, T.J., 1993, Lithogeochemical techniques using immobile elements: Journal of Geochemical Exploration, 48, p. 109-133.

MacLean, W.H., and Kranidiotis, P., 1987, Immobile elements as monitors of mass transfer in hydrothermal alteration: Phelps Dodge massive sulfide deposit, Matagami, Quebec: Econ. Geol., 82, p. 951-962

Maffei, L., 1992, Petrogenesis of Staurolite in K-Poor Metapelites of the Santa Rosa Range Contact Aureoles, Nevada [M.S. thesis]: Seattle, Washington, University of Washington, 83 p.

Maher, K. A., 1989, Geology of the Jackson Mountains, northwest Nevada [Ph.D. dissert.]: Pasadena, California Institute of Technology, 491 p.

Martin, A.J., Wyld, S.J., Wright, J.E., and Bradford, J.H., 2009, The Lower Cretaceous King Lear Formation, northwest Nevada: Implications for Mesozoic orogenesis in the western U.S. Cordillera: GSA Bulletin, v. 122, no. ¾, p. 537-562

McDonough, W.F, and Sun, S.-s., 1994, The Composition of of the Earth: Chemical Geology 120, p. 223-253

McKee, E.H., 1970, Fish Creek Mountain Tuff And Volcanic Center, Lander County, Nevada: Geological Survey Professional Paper 651, 25 p.

Mellott, M.G., 1987. Geochemical, petrologic, and isotopic investigation of andesites and related volcanic rocks in the Santa Rosa Range and Bloody Run Hills, Nevada; tectonic implications [M.S. Thesis]: Miami University, Oxford, 164 p.

Neff, T.R., 1973, Emplacement of a Dike Swarm in the Buffalo Mountain Plution, Nevada: Geological Society of America Bulletine, v. 84, p. 3689-3696.

Noble, D.C., McKee, E.H., Smith, J.G., and Korringa, M.K., 1970, Stratigraphy and geochronology of Miocene volcanic rocks in northwestern Nevada: U.S. Geological Survey Professional Paper 700D, p. 23–32.

Oldow, J.S., 1984, Evolution of a late Mesozoic back-arc fold and thrust belt, northwestern Great Basin, U.S.A.: Tectonophysics, v. 102, p. 245–274.

Peters, L., 2003, 40Ar/39Ar Geochronology Results from the Winnemucca, Nevada Gold Project, Internal Report #: NMGRL-IR-332, Prepared by New Mexico Geochronological Research Laboratory for Western States Minerals Corp., 24 p.

Quinn, M. J., 1996, Pre-Tertiary stratigraphy, magmatism, and structural history of the central Jackson Mountains, Humboldt County, Nevada [Ph.D. dissert.]: Houston, Texas, Rice University, 243 p.

Quinn, M.J., Wright, J.E., and Wyld, S.J., 1997, Happy Creek igneous complex and tectonic evolution of the Early Mesozoic arc in the Jackson Mountains, northwest Nevada: GSA Bulletin, v. 109, no. 4, p. 461-482

Rogers, J.W., 1999, Jurassic-Cretaceous Deformation in the Santa Rosa Range, NV: Implications for the Development of the Northern Luning-Fencemaker Fold-and-Thrust Belt [M.S. thesis]: Athens, Georgia, University of Georgia, 195 p.

Russell, B. J., 1981, Pre-Tertiary paleogeography and tectonic history of the Jackson Mountains, northwestern Nevada [Ph.D. dissert.]: Evanston, Illinois, Northwestern University, 205 p.

Russell, B. J., 1984, Mesozoic geology of the Jackson Mountains, northwestern Nevada: Geological Society of America Bulletin, v. 95 p. 313–323.

Saunders, J.A., Unger, D.L., Kamenov, G.D., Hames, W.E., and Utterback, W.C., 2008, Genesis of mid-Miocene Yellowstone-hotspot-related bonanza epithermal Au-Ag deposits, Northern Great Basin region, USA: Mineralium Deposita, v. 43, p. 715-734.

Silberling, N.J., Jones, D.L., Blake, M.C., Jr., and Howell, D.G., 1987, Lithotectonic terranes of the western conterminous United States: U.S. Geological Survey Miscellaneous Field Studies Map MF-1874-C, scale 1:2,500,000.

Speed, R.C., 1978, Paleogeographic and plate tectonic evolution of the early Mesozoic marine province of the western Great Basin, *in* Howell, D.G., and McDougall, K.A., eds., Mesozoic Paleogeography of the Western United States: Sacramento, California, Society of Economic Paleontologists and Mineralogists, Pacifi c Coast Paleogeography Symposium 2, p. 253–270.

Thole, R.H., and Prihar, D.W., 1998, Geologic Map of the Eugene Mountains, Northwestern Nevada: Nevada Bureau of Mines and Geology Report 115, 12 p., 1:24,000 scale.

Unger, D.L., 2008, Geochronology and geochemistry of mid-Miocene bonanza low sulfidation epithermal ores of the northern Great Basin, USA. Unpublished MS thesis, Auburn University, 151 p.

Vanderburg, W.O., 1938a, Reconnaissance of mining districts in Humboldt County, Nevada: U.S. Bureau of Mines Information Circular 6995, 54 p.

Wallace, A.R., 2003a, Geologic map of the Willow Creek Reservoir SE Quadrangle, Elko Counties, Nevada: Nevada Bureau of Mines and Geology Map 136, scale 1:24,000.

Wallace, A.R., and McKee, E.H., 1994, Implications of Eocene through Miocene ages for volcanic rocks, Snowstorm Mountains and vicinity, northern Nevada: U.S. Geological Survey Bulletin 2081, p. 13-18.

Willden, R., 1958, Cretaceous and Tertiary orogeny in Jackson Mountains, Humboldt County, Nevada: American Association of Petroleum Geologists Bulletin, v. 42, p. 2378–2398.

Willden, R., 1963, General Geology of the Jackson Mountains, Humboldt County, Nevada: U.S. Geological Survey Bulletin 1141-D, 65 p. Willden, R., 1964, Geology and mineral deposits of Humboldt County, Nevada: Nevada Bureau of Mines and Geology Bulletin 59, 154 p.

Willden, R., 1964, Geology and mineral deposits of Humboldt County, Nevada: Nevada Bureau of Mines and Geology Bulletin 59, 154 p., 3 pl.

Wyld, S.J., 1996, Early Jurassic deformation in the Pine Forest Range, northwest Nevada, and implications for Cordilleran tectonics: Tectonics, v. 15, p. 566–583.

Wyld, S.J., 2000, Triassic evolution of the arc and backarc of northwest Nevada, and evidence for extensional tectonism: Geological Society of America Special Paper 347, 23 p.

Wyld, S.J., 2002, Structural evolution of a Mesozoic backarc fold-and thrust belt in the U.S. Cordillera: New evidence from northern Nevada: GSA Bulletin, v. 114, no. 11, p. 1452-1468.

Wyld, S.J., Rogers, J.W. and Wright, J.E, 2001, Structural evolution within the Luning-Fencemaker fold-thrust belt, Nevada: progression from back-arc basin closure to intraarc shortening: Journal of Structural Geology, v. 23, p. 1971-1995

Wyld, S.J., and Wright, J.E., 2005, Early Cretaceous, margin-parallel, dextral faulting and terrane translation in the U.S. Cordillera: Geological Society of America Abstracts with Programs, v. 37, no. 4, p. 102.

Appendix 1:

ALS Chemex Inc. Analytical Methods

Samples were crushed in a grinding mill to 85% passing 75 micron or better and split for separate analyses. For major oxides, a prepared sample (0.200 g) was added to lithium metaborate/lithium tetraborate flux (0.90 g), mixed well and fused in a furnace at 1000°C. The resulting melt was cooled and dissolved in 100 mL of 4% nitric acid/2% hydrochloric acid. This solution was then analyzed by ICP-AES and the results are corrected for spectral inter-element interferences. The total oxide content is determined from the ICP analyte concentrations and loss on Ignition (L.O.I.) values. A prepared sample (1.0 g) is placed in an oven at 1000°C for one hour, cooled and then weighed. The percent loss on ignition is calculated from the difference in weight.

For trace elements, a prepared sample (0.200 g) was added to lithium borate flux (0.90 g), mixed well and fused in a furnace at 1000°C. The resulting melt was then cooled and dissolved in 100 mL of 4% HNO3 / 2% HCl solution. This solution was then analyzed by inductively coupled plasma - mass spectrometry.

Major Oxides By ICP-AES				
Element	**Symbol**	**Units**	**Lower Limit**	**Upper Limit**
Aluminum	Al2O3	%	0.01	100
Barium	BaO	%	0.01	100
Calcium	CaO	%	0.01	100
Chromium	Cr2O3	%	0.01	100
Iron	Fe2O3	%	0.01	100
Magnesium	MgO	%	0.01	100
Manganese	MnO	%	0.01	100
Phosphorus	P2O5	%	0.01	100
Potassium	K2O	%	0.01	100
Silicon	SiO2	%	0.01	100
Sodium	Na2O	%	0.01	100
Strontium	SrO	%	0.01	100
Titanium	TiO	%	0.01	100
Loss on Ignition	LOI	%	0.01	100

Trace Elements By ICP=MS				
Element	**Symbol**	**Units**	**Lower Limit**	**Upper Limit**
Barium	Ba	ppm	0.5	10000
Cerium	Ce	ppm	0.5	10000
Cobalt	Co	ppm	0.5	10000
Chromium	Cr	ppm	10	10000
Cesium	Cs	ppm	0.01	10000
Dysporium	Dy	ppm	0.05	1000
Erbium	Er	ppm	0.03	1000
Europium	Eu	ppm	0.03	1000

Trace Elements By ICP=MS (cont.)				
Gallium	Ga	ppm	0.1	1000
Gadolinium	Gd	ppm	0.05	1000
Hafnium	Hf	ppm	0.2	10000
Holmium	Ho	ppm	0.01	1000
Lanthanum	La	ppm	0.5	10000
Lutetium	Lu	ppm	0.01	1000
Molybdenum	Mo	ppm	2	10000
Niobium	Nb	ppm	0.2	2500
Neodymium	Nd	ppm	0.1	10000
Praseodymium	Pr	ppm	0.03	1000
Rubidium	Rb	ppm	0.2	10000
Samarium	Sm	ppm	0.03	1000
Tin	Sn	ppm	1	10000
Strontium	Sr	ppm	0.1	10000
Tantalum	Ta	ppm	0.1	2500
Terbium	Tb	ppm	0.01	1000
Thorium	Th	ppm	0.05	1000
Thallium	Tl	ppm	0.5	1000
Thulium	Tm	ppm	0.01	1000
Uranium	U	ppm	0.05	10000
Vanadium	V	ppm	5	10000
Tungsten	W	ppm	1	10000
Yttrium	Y	ppm	0.5	10000
Ytterbium	Yb	ppm	0.03	1000
Zirconium	Zr	ppm	20	10000

Appendix 2:

North Hill Tuff Package Above NHT

Sample ID	NSM-00189-166	NSM-00189-171	NSM-00189-195	NSM-00189-202	NSM-00189-210	NSM-00185-203	NSM-00184-197	Average	STD DEV
Normalized 100% volatile free major elements (wt %)									
SiO2	71.65	70.75	72.34	72.05	69.93	72.70	73.44	71.84	1.19
Al2O3	16.09	14.51	14.44	15.79	16.68	15.14	14.77	15.35	0.86
Fe2O3	3.79	5.66	3.50	3.06	4.35	4.14	3.86	4.05	0.82
CaO	1.07	2.05	2.03	1.50	0.74	1.30	0.64	1.33	0.57
MgO	1.50	1.48	0.97	0.98	1.81	1.61	1.51	1.41	0.32
Na2O	0.60	1.06	2.01	1.09	0.86	0.33	0.66	0.94	0.54
K2O	4.87	3.93	3.93	5.08	5.11	4.19	4.62	4.53	0.52
Cr2O3	<0.01	<0.01	<0.01	<0.01	<0.01	<0.01	<0.01	NA	NA
TiO2	0.23	0.25	0.36	0.25	0.26	0.37	0.24	0.28	0.06
MnO	0.04	0.13	0.07	0.05	0.08	0.04	0.05	0.07	0.03
P2O5	0.05	0.08	0.23	0.05	0.05	0.11	0.05	0.09	0.06
SrO	0.01	0.02	0.02	0.01	0.01	0.01	0.01	0.01	0.01
BaO	0.09	0.06	0.08	0.08	0.12	0.06	0.14	0.09	0.03
LOI	6.14	6.17	4.93	5.03	6.23	6.66	5.93	5.87	0.65
Total-LOI	100.00	100.00	100.00	100.00	100.00	100.00	100.00	NA	NA
ICP-MS trace elements (ppm)									
Ba	830	496	678	713	980	547	1140	769.14	231.34
Ce	76	62.4	61.6	64.1	80.9	65.5	63.2	67.67	7.60
Co	3.3	4.8	4.6	1.9	8.1	3.1	5.7	4.50	2.03
Cr	10	10	10	<10	10	10	10	NA	NA
Cs	13	10.05	7.33	10.5	10.15	16.45	12.35	11.40	2.88
Cu	9	9	9	10	11	11	7	9.43	1.40
Dy	3.5	3.54	4.16	4.43	4.15	4.27	4.28	4.05	0.37
Er	2.23	2.36	2.72	2.92	2.46	2.61	2.77	2.58	0.24
Eu	0.83	0.72	0.87	0.79	0.84	0.89	0.7	0.81	0.07
Ga	23.1	21.2	20.2	27.2	26.5	22.6	26.3	23.87	2.79
Gd	3.94	3.75	4.39	4.28	4.38	4.65	4.25	4.23	0.30
Hf	6.2	5.1	6.2	6.4	6.6	6	6.2	6.10	0.48
Ho	0.73	0.75	0.86	0.94	0.83	0.87	0.88	0.84	0.07
La	40.5	35.3	31.3	33	41.5	33.9	32.4	35.41	4.02
Lu	0.41	0.47	0.51	0.57	0.38	0.45	0.5	0.47	0.06
Nb	11.5	13.6	14.9	15.4	10.5	15.3	17.4	14.09	2.40
Nd	30.7	24.9	27.6	27.7	32.1	29.7	26.9	28.51	2.46
Ni	22	16	<5	<5	17	7	25	NA	NA
Pb	8	13	21	7	39	12	16	16.57	10.97
Pr	8.77	7.08	7.42	7.71	9.25	8.1	7.42	7.96	0.79
Rb	243	192.5	181	238	196.5	231	259	220.14	29.79
Sm	5.84	4.83	5.6	5.68	6.01	6.12	5.38	5.64	0.43
Sr	96.9	126.5	162	103	103.5	79.2	76.5	106.80	29.55
Ta	1.5	1.3	1.3	1.4	1.6	1.3	1.4	1.40	0.12
Tb	0.61	0.59	0.71	0.71	0.7	0.73	0.7	0.68	0.05
Th	18.95	16.15	13.75	16.55	19.25	15.9	16.7	16.75	1.88
Tl	1	0.7	0.9	1.1	1	0.9	1.2	0.97	0.16
Tm	0.37	0.4	0.44	0.49	0.38	0.42	0.45	0.42	0.04
U	7.76	7.47	9.38	6.94	6.26	5.67	7.26	7.25	1.18
V	50	40	135	40	64	45	38	58.86	34.74
W	2	2	6	2	2	4	2	2.86	1.57
Y	21.5	24.8	27.3	28.8	24.4	25.5	27.7	25.71	2.46
Yb	2.52	2.8	3	3.39	2.5	2.86	3.08	2.88	0.31
Zn	72	84	85	81	97	79	85	83.29	7.59
Zr	191	184	207	213	210	200	204	201.29	10.48

Appendix 3:

Midway-Silica Ridge Tuff Package Above NHT

Sample ID	NSM-00297-115.5	NSM-00297-125.1	Average	STD DEV
Normalized 100% volatile free major elements (wt %)				
SiO2	74.13	72.49	73.31	1.16
Al2O3	13.57	14.46	14.01	0.62
Fe2O3	3.43	3.46	3.45	0.02
CaO	0.60	0.57	0.58	0.02
MgO	1.29	1.37	1.33	0.06
Na2O	0.68	0.77	0.72	0.06
K2O	5.53	5.90	5.72	0.26
Cr2O3	<0.01	<0.01	NA	NA
TiO2	0.48	0.56	0.52	0.06
MnO	0.02	0.03	0.03	0.01
P2O5	0.16	0.18	0.17	0.01
SrO	0.02	0.02	0.02	0.00
BaO	0.08	0.19	0.14	0.07
LOI	4.68	4.53	4.61	0.11
Total-LOI	100.00	100.00	NA	NA
ICP-MS trace elements (ppm)				
Ba	652	1535	1093.50	624.38
Ce	46.2	56.3	51.25	7.14
Co	4.3	5.4	4.85	0.78
Cr	40	50	45.00	7.07
Cs	32	28.6	30.30	2.40
Cu	17	21	19.00	2.83
Dy	3.27	3.97	3.62	0.49
Er	1.93	2.22	2.08	0.21
Eu	0.82	0.92	0.87	0.07
Ga	18	20.4	19.20	1.70
Gd	3.61	4.17	3.89	0.40
Hf	4.1	4.7	4.40	0.42
Ho	0.68	0.81	0.75	0.09
La	24.2	28.9	26.55	3.32
Lu	0.3	0.35	0.33	0.04
Nb	10.1	12.3	11.20	1.56
Nd	20.2	24.3	22.25	2.90
Ni	13	18	15.50	3.54
Pb	10	9	9.50	0.71
Pr	5.56	6.63	6.10	0.76
Rb	295	297	296.00	1.41
Sm	4.2	5	4.60	0.57
Sr	126	128	127.00	1.41
Ta	0.8	1	0.90	0.14
Tb	0.56	0.69	0.63	0.09
Th	10.25	12	11.13	1.24
Tl	1.3	1.4	1.35	0.07
Tm	0.31	0.34	0.33	0.02
U	4.81	7.83	6.32	2.14
V	71	70	70.50	0.71
W	7	5	6.00	1.41
Y	19.7	22.7	21.20	2.12
Yb	1.95	2.28	2.12	0.23
Zn	54	60	57.00	4.24
Zr	150	170	160.00	14.14

Appendix 4:

Nine Hill Tuff (NHT)

Sample ID	NSM-00034-184	NSM-00034-186.9	NSM-00034-189.2	9-17-11-13b	NH-Fiamme-1	9-18-11-7a	9-18-11-7c	Average	STD DEV
Normalized 100% volatile free major elements (wt %)									
SiO2	81.97	83.34	84.28	79.37	76.66	77.66	81.06	80.62	2.85
Al2O3	10.08	8.62	8.35	11.43	11.14	11.38	9.21	10.03	1.32
Fe2O3	2.12	1.42	1.32	0.76	2.08	1.96	1.88	1.65	0.50
CaO	0.35	0.49	0.20	0.13	0.14	0.29	0.23	0.26	0.13
MgO	0.73	0.34	0.28	0.11	0.28	0.42	0.26	0.35	0.19
Na2O	0.13	0.15	0.16	0.78	0.22	0.52	0.52	0.35	0.25
K2O	4.34	5.37	5.17	7.01	8.63	7.40	6.50	6.35	1.48
Cr2O3	<0.01	<0.01	<0.01	<0.01	<0.01	<0.01	<0.01	NA	NA
TiO2	0.19	0.15	0.13	0.26	0.29	0.21	0.17	0.20	0.06
MnO	0.01	0.01	0.03	<0.01	0.32	0.02	0.03	0.07	0.12
P2O5	0.03	0.02	0.01	0.02	0.09	0.03	0.04	0.04	0.03
SrO	0.01	0.01	0.01	0.01	0.04	0.02	0.02	0.02	0.01
BaO	0.04	0.06	0.06	0.11	0.10	0.08	0.06	0.07	0.03
LOI	3.91	2.41	2.08	1.81	1.8	2.47	1.56	2.29	0.79
Total-LOI	100.00	100.00	100.00	100.00	100.00	100.00	100.00	NA	NA
ICP-MS trace elements (ppm)									
Ba	362	550	478	918	846	722	534	630.00	203.56
Ce	87.7	81.3	78.9	83.2	96.7	101	83.3	87.44	8.32
Co	<0.5	0.6	1.9	<0.5	17.9	0.5	1.2	NA	NA
Cr	10	10	10	10	10	10	10	10.00	0.00
Cs	15.6	20.3	24.6	2.82	5.14	9.75	12.45	12.95	7.86
Cu	6	6	6	5	15	8	9	7.86	3.44
Dy	4.71	4.16	4.12	4.11	4.97	4.9	3.88	4.41	0.44
Er	2.81	2.47	2.42	2.72	2.72	3.03	2.55	2.67	0.21
Eu	0.41	0.33	0.25	0.6	1.02	0.4	0.37	0.48	0.26
Ga	18	14.1	13.4	12	10.5	17	9.6	13.51	3.14
Gd	5.32	4.81	4.81	4.2	6.15	5.56	4.45	5.04	0.68
Hf	8.3	7.3	8.4	7.5	6.9	10	7.8	8.03	1.02
Ho	0.95	0.85	0.82	0.87	0.96	0.99	0.82	0.89	0.07
La	45	41.9	40.5	43.2	46.7	51.3	42.6	44.46	3.64
Lu	0.4	0.38	0.36	0.42	0.37	0.48	0.43	0.41	0.04
Nb	21.9	20.8	20	22.7	20.1	25.7	21	21.74	1.99
Nd	37.2	34.5	33.2	34	44.2	43.2	35.7	37.43	4.48
Ni	<5	<5	<5	<5	27	<5	<5	NA	NA
Pb	9	9	25	9	23	12	11	14.00	6.95
Pr	10.3	9.51	9.3	9.58	11.75	11.95	10	10.34	1.08
Rb	179.5	203	196.5	278	353	289	244	249.00	61.89
Sm	6.41	6.12	5.92	5.47	7.55	8.16	6.6	6.60	0.94
Sr	62.5	89.6	84.1	99.3	293	160.5	135.5	132.07	78.25
Ta	1.6	1.5	1.5	1.6	1.6	1.9	1.6	1.61	0.13
Tb	0.82	0.73	0.73	0.64	0.92	0.85	0.65	0.76	0.10
Th	19.5	18.1	17.7	20.9	18.5	23.6	19.15	19.64	2.04
Tl	0.7	1.2	1.2	1.6	2.2	1.4	1.5	1.40	0.46
Tm	0.41	0.4	0.39	0.43	0.41	0.46	0.39	0.41	0.02
U	7.76	7.67	6.61	6.97	7.53	8.58	7.3	7.49	0.63
V	92	118	50	43	49	35	24	58.71	33.68
W	2	2	1	7	8	2	3	3.57	2.76
Y	27.2	25.1	23.3	25.2	28.9	28.2	23.9	25.97	2.15
Yb	2.66	2.43	2.34	2.73	2.45	3.01	2.68	2.61	0.23
Zn	51	44	35	20	85	57	45	48.14	20.15
Zr	298	260	308	268	248	385	294	294.43	45.53

Appendix 5:

Nine Hill Tuff (NHT)

Normalized 100% volatile free, all samples adjusted for hydrothermal silica, shaded samples adjusted for hydrothermal potassium Average 72.82% SiO2 and 5.33% K20, E.H Christiansen (2012); Deino (1985)

Sample ID	NSM-00034-184	NSM-00034-186.9	NSM-00034-189.2	9-17-11-13b	NH-Fiamme-1	9-18-11-7a	9-18-11-7c	Average	STD DEV
Major elements (wt%)									
SiO2	72.82	72.82	72.82	72.82	72.82	72.82	72.82	72.82	0.00
Al2O3	10.97	9.52	9.29	12.43	11.97	12.22	10.14	10.93	1.31
Fe2O3	2.30	1.57	1.46	0.82	2.24	2.11	2.07	1.80	0.54
CaO	0.38	0.54	0.22	0.14	0.16	0.32	0.25	0.29	0.14
MgO	0.80	0.37	0.31	0.12	0.30	0.45	0.29	0.38	0.21
Na2O	0.14	0.17	0.18	0.85	0.23	0.56	0.58	0.39	0.27
K2O	4.72	5.93	5.76	5.33	5.33	5.33	5.33	5.39	0.39
Cr2O3	<0.01	<0.01	<0.01	<0.01	<0.01	<0.01	<0.01	NA	NA
TiO2	0.21	0.17	0.15	0.28	0.31	0.23	0.19	0.22	0.06
MnO	0.01	0.01	0.03	<0.01	0.34	0.02	0.03	0.08	0.12
P2O5	0.03	0.02	0.01	0.02	0.10	0.03	0.04	0.04	0.03
SrO	0.01	0.01	0.01	0.01	0.04	0.02	0.02	0.02	0.01
BaO	0.05	0.07	0.07	0.12	0.11	0.09	0.07	0.08	0.03
ICP-MS trace elements (ppm)									
Ba	412.65	623.87	546.92	1023.36	937.60	787.67	591.94	703.43	220.64
Ce	99.97	92.22	90.28	92.75	107.17	110.19	92.34	97.84	8.05
Co	<0.5	0.68	2.17	<0.5	19.84	0.55	1.33	4.91	7.24
Cr	11.40	11.34	11.44	11.15	11.08	10.91	11.09	11.20	0.20
Cs	17.78	23.03	28.15	3.14	5.70	10.64	13.80	14.60	9.05
Cu	6.84	6.81	6.87	5.57	16.62	8.73	9.98	8.77	3.75
Dy	5.37	4.72	4.71	4.58	5.51	5.35	4.30	4.93	0.47
Er	3.20	2.80	2.77	3.03	3.01	3.31	2.83	2.99	0.21
Eu	0.47	0.37	0.29	0.67	1.13	0.44	0.41	0.54	0.29
Ga	20.52	15.99	15.33	13.38	11.64	18.55	10.64	15.15	3.58
Gd	6.06	5.46	5.50	4.68	6.82	6.07	4.93	5.65	0.73
Hf	9.46	8.28	9.61	8.36	7.65	10.91	8.65	8.99	1.09
Ho	1.08	0.96	0.94	0.97	1.06	1.08	0.91	1.00	0.07
La	51.30	47.53	46.34	48.16	51.76	55.97	47.22	49.75	3.43
Lu	0.46	0.43	0.41	0.47	0.41	0.52	0.48	0.45	0.04
Nb	24.96	23.59	22.88	25.31	22.28	28.04	23.28	24.33	1.96
Nd	42.41	39.13	37.99	37.90	48.99	47.13	39.57	41.87	4.51
Ni	<5	<5	<5	<5	29.92	<5	<5	29.92	11.31
Pb	10.26	10.21	28.60	10.03	25.49	13.09	12.19	15.70	7.89
Pr	11.74	10.79	10.64	10.68	13.02	13.04	11.09	11.57	1.06
Rb	204.62	230.27	224.83	309.91	391.22	315.29	270.48	278.09	65.54
Sm	7.31	6.94	6.77	6.10	8.37	8.90	7.32	7.39	0.96
Sr	71.25	101.63	96.23	110.70	324.72	175.10	150.20	147.12	85.71
Ta	1.82	1.70	1.72	1.78	1.77	2.07	1.77	1.81	0.12
Tb	0.93	0.83	0.84	0.71	1.02	0.93	0.72	0.85	0.11
Th	22.23	20.53	20.25	23.30	20.50	25.75	21.23	21.97	1.99
Tl	0.80	1.36	1.37	1.78	2.44	1.53	1.66	1.56	0.50
Tm	0.47	0.45	0.45	0.48	0.45	0.50	0.43	0.46	0.02
U	8.85	8.70	7.56	7.77	8.35	9.36	8.09	8.38	0.63
V	104.87	133.85	57.21	47.94	54.31	38.18	26.60	66.14	38.69
W	2.28	2.27	1.14	7.80	8.87	2.18	3.33	3.98	3.06
Y	31.01	28.47	26.66	28.09	32.03	30.77	26.49	29.07	2.20
Yb	3.03	2.76	2.68	3.04	2.72	3.28	2.97	2.93	0.22
Zn	58.14	49.91	40.05	22.30	94.20	62.18	49.88	53.81	22.11
Zr	339.70	294.92	352.41	298.76	274.85	420.02	325.90	329.51	48.24

Appendix 6:

Silica Ridge Tuff Package Below NHT

Sample ID	NSM-00034-201.2	NSM-00034-203.2	NSM-00034-209.9	NSM-00034-214.4	NSM-00034-222	NSM-00034-225	NSM-00034-229	NSM-00034-233.8	NSM-00034-234.7	Average	STD DEV
Normalized 100% volatile free major elements (wt %)											
SiO2	73.52	74.62	73.44	75.20	73.60	70.33	73.20	70.24	72.96	73.01	1.60
Al2O3	13.77	13.27	14.12	13.36	14.19	14.43	14.07	14.13	14.67	14.00	0.43
Fe2O3	3.00	2.55	2.72	2.11	3.07	3.32	3.06	2.94	2.87	2.85	0.33
CaO	0.49	0.45	0.46	0.49	0.51	2.80	0.59	3.65	0.44	1.10	1.16
MgO	0.99	0.96	0.91	0.77	0.98	1.05	1.01	0.99	0.90	0.95	0.08
Na2O	0.35	0.45	0.23	0.25	0.21	0.22	0.24	0.26	0.30	0.28	0.07
K2O	7.17	7.12	7.50	7.23	6.75	7.10	7.07	7.06	7.27	7.14	0.19
Cr2O3	<0.01	<0.01	<0.01	<0.01	<0.01	<0.01	<0.01	<0.01	<0.01	NA	NA
TiO2	0.42	0.33	0.33	0.29	0.42	0.51	0.49	0.46	0.37	0.40	0.07
MnO	0.05	0.03	0.05	0.05	0.04	0.05	0.03	0.06	0.05	0.05	0.01
P2O5	0.15	0.15	0.13	0.13	0.14	0.11	0.15	0.13	0.10	0.13	0.02
SrO	0.01	0.01	0.01	0.01	0.01	0.01	0.01	0.01	0.01	0.01	0.00
BaO	0.07	0.07	0.09	0.10	0.08	0.07	0.08	0.06	0.06	0.08	0.01
LOI	3.61	3.23	3.72	3.45	4.18	5.87	4.51	6.32	3.77	4.30	1.09
Total	100.00	100.00	100.00	100.00	100.00	100.00	100.00	100.00	100.00	NA	NA
ICP-MS trace elements (ppm)											
Ba	590	585	743	866	694	606	637	540	483	638.22	115.06
Ce	48.4	46.5	48.9	52.8	56	42.9	44.9	74.1	91.3	56.20	16.11
Co	4.2	4.5	4.8	4	4	4.4	3	3.9	4.1	4.10	0.50
Cr	20	20	20	20	20	20	10	10	10	16.67	5.00
Cs	8.95	8.07	13.3	14.75	13.65	8.98	10.05	9.83	11.4	11.00	2.39
Cu	17	17	14	12	16	14	10	9	10	13.22	3.11
Dy	4.96	5.39	3.44	3.32	5.16	3.68	3.71	5.04	5.35	4.45	0.88
Er	3.12	3.3	2.09	2	3.03	2.21	2.26	2.88	3.11	2.67	0.52
Eu	0.65	0.6	0.65	0.64	0.86	0.78	0.72	0.77	0.61	0.70	0.09
Ga	19.4	19.6	18.7	17	21.1	19.7	19.3	20.6	23.9	19.92	1.89
Gd	4.98	5.35	3.76	3.53	5.2	3.9	3.83	5.87	6.6	4.78	1.08
Hf	5.3	4.7	4.3	4.1	5.5	4.2	4.3	4.6	4.8	4.64	0.49
Ho	1.02	1.1	0.7	0.67	1.04	0.74	0.75	0.99	1.05	0.90	0.18
La	23.5	22.4	24.8	27.8	27.8	22.4	22.8	38.3	44.4	28.24	7.86
Lu	0.47	0.5	0.33	0.32	0.45	0.32	0.34	0.41	0.46	0.40	0.07
Nb	13.7	14.5	11.4	12.6	16.2	11.1	10.7	13.1	16	13.26	2.03
Nd	22.2	21.7	19.7	21.8	25.9	20.2	20.7	34.4	39.7	25.14	7.10
Ni	7	7	6	6	7	6	5	5	5	6.00	0.87
Pb	16	20	21	12	14	11	10	16	21	15.67	4.27
Pr	5.94	5.71	5.5	6.18	6.77	5.36	5.53	9.26	10.85	6.79	1.94
Rb	332	343	338	307	329	327	337	334	377	336.00	18.46
Sm	4.86	5.05	3.93	4.1	5.44	4.23	4.24	6.78	7.78	5.16	1.32
Sr	57.8	55.4	63.8	69	62.9	84.7	64.4	82.9	55.3	66.24	10.93
Ta	1.5	1.7	1.3	1.2	1.5	1	1	1.2	1.6	1.33	0.25
Tb	0.83	0.93	0.6	0.58	0.86	0.62	0.62	0.88	0.99	0.77	0.16
Th	17.35	19.3	16.75	18.05	16.6	11.8	13.15	19.25	25.9	17.57	4.03
Tl	1	1.1	1.2	1.2	1.1	1.1	1.1	1.1	1.3	1.13	0.09
Tm	0.5	0.51	0.34	0.33	0.48	0.35	0.35	0.46	0.49	0.42	0.08
U	10.95	12.35	7.4	6.91	8.33	5.61	6.75	7.24	8.24	8.20	2.15
V	61	55	71	59	61	64	55	76	97	66.56	13.36
W	5	4	3	2	6	7	7	5	5	4.89	1.69
Y	29.9	33.1	20.7	19.5	30.3	21.9	23.1	29.9	29.5	26.43	5.07
Yb	3.1	3.21	2.14	2	2.95	2.16	2.2	2.78	3.02	2.62	0.48
Zn	58	59	50	44	66	64	66	68	67	60.22	8.38
Zr	159	146	132	123	172	132	143	145	130	142.44	15.48

Appendix 7:

Adularia Hill-Silica Ridge Unnamed Tuff

Sample ID	9-18-11-14a (AH)	NSM-00153-86 (SR)	Average	STD DEV
Normalized 100% volatile free major elements (wt %)				
SiO2	77.52	78.88	78.20	0.96
Al2O3	11.07	11.85	11.46	0.56
Fe2O3	1.58	1.78	1.68	0.14
CaO	0.45	0.35	0.40	0.07
MgO	0.48	0.97	0.73	0.35
Na2O	0.43	0.26	0.34	0.12
K2O	8.28	5.77	7.03	1.77
Cr2O3	<0.01	<0.01	NA	NA
TiO2	0.06	0.07	0.07	0.01
MnO	0.02	0.01	0.02	0.01
P2O5	0.03	0.02	0.03	0.01
SrO	0.02	0.01	0.02	0.01
BaO	0.06	0.03	0.05	0.02
LOI	1.74	3.87	2.81	1.51
Total-LOI	100.00	100.00	NA	NA
ICP-MS trace elements (ppm)				
Ba	511	284	397.50	160.51
Ce	54.7	54.1	54.40	0.42
Co	0.8	1.6	1.20	0.57
Cr	<10	20	NA	NA
Cs	4.24	10.55	7.40	4.46
Cu	5	<5	NA	NA
Dy	4.32	4.41	4.37	0.06
Er	2.43	2.37	2.40	0.04
Eu	0.18	0.17	0.18	0.01
Ga	10.3	18.9	14.60	6.08
Gd	4.92	4.91	4.92	0.01
Hf	4.1	4.1	4.10	0.00
Ho	0.84	0.85	0.85	0.01
La	26.4	26.4	26.40	0.00
Lu	0.38	0.35	0.37	0.02
Nb	16.4	14.7	15.55	1.20
Nd	25.5	24	24.75	1.06
Ni	<5	7	NA	NA
Pb	10	13	11.50	2.12
Pr	6.76	6.64	6.70	0.08
Rb	339	263	301.00	53.74
Sm	6.12	5.77	5.95	0.25
Sr	121	52.5	86.75	48.44
Ta	1.5	1.5	1.50	0.00
Tb	0.78	0.76	0.77	0.01
Th	18.7	19.15	18.93	0.32
Tl	1.7	1.3	1.50	0.28
Tm	0.38	0.37	0.38	0.01
U	4.72	4.98	4.85	0.18
V	19	31	25.00	8.49
W	<1	<1	NA	NA
Y	24.7	24.3	24.50	0.28
Yb	2.4	2.36	2.38	0.03
Zn	28	56	42.00	19.80
Zr	105	120	112.50	10.61

Appendix 8:

	SE Pediment Upper Tuff					Pumice Bed
Sample ID	NSM-00155-149	NSM-00147-89	NSM-00147-91	Average	STD DEV	NSM-00082-315
Normalized 100% volatile free major elements (wt %)						
SiO2	74.00	72.26	75.76	74.01	1.75	76.94
Al2O3	13.73	14.70	12.80	13.74	0.95	12.68
Fe2O3	2.82	3.01	2.19	2.67	0.43	1.93
CaO	0.51	0.82	0.41	0.58	0.21	0.64
MgO	1.22	1.32	0.77	1.10	0.30	1.24
Na2O	0.20	0.30	0.24	0.25	0.05	0.24
K2O	7.15	6.83	7.29	7.09	0.23	5.55
Cr2O3	<0.01	<0.01	<0.01	NA	NA	<0.01
TiO2	0.22	0.44	0.21	0.29	0.13	0.49
MnO	0.02	0.05	0.17	0.08	0.08	0.05
P2O5	0.07	0.14	0.09	0.10	0.03	0.13
SrO	0.01	0.02	0.02	0.02	0.01	0.03
BaO	0.04	0.09	0.06	0.06	0.02	0.07
LOI	4.72	6.09	3.67	4.83	1.21	5.87
Total-LOI	100.00	100.00	100.00	NA	NA	100.00
ICP-MS trace elements (ppm)						
Ba	358	684	554	532.00	164.11	581
Ce	45.7	48.7	72.7	55.70	14.80	37.5
Co	1.2	2.4	4.2	2.60	1.51	4.6
Cr	10	10	<10	NA	NA	10
Cs	10.4	7.86	12.75	10.34	2.45	6.65
Cu	15	88	5	36.00	45.31	19
Dy	4.76	5.13	5.61	5.17	0.43	3.57
Er	2.64	3.06	3.22	2.97	0.30	2.16
Eu	0.48	0.85	0.65	0.66	0.19	0.65
Ga	23.7	19.9	22.7	22.10	1.97	15.3
Gd	5.64	5.36	6.45	5.82	0.57	3.86
Hf	5	4.3	4.7	4.67	0.35	4.3
Ho	0.93	1.04	1.08	1.02	0.08	0.73
La	33.4	25.4	40.5	33.10	7.55	17.3
Lu	0.45	0.47	0.51	0.48	0.03	0.37
Nb	16.7	10.9	16.4	14.67	3.27	10.9
Nd	32.4	25.5	34.8	30.90	4.83	18.6
Ni	<5	<5	<5	NA	NA	<5
Pb	13	19	31	21.00	9.17	16
Pr	8.87	6.62	9.6	8.36	1.55	4.78
Rb	344	302	366	337.33	32.52	225
Sm	7.03	6.02	7.92	6.99	0.95	4.45
Sr	107	129	121	119.00	11.14	222
Ta	1.4	1.1	1.7	1.40	0.30	1
Tb	0.87	0.88	1.03	0.93	0.09	0.63
Th	19.95	14	20.4	18.12	3.57	12.15
Tl	1.8	1.7	2	1.83	0.15	1.3
Tm	0.42	0.47	0.5	0.46	0.04	0.34
U	3.9	7.25	8.36	6.50	2.32	4.9
V	42	50	37	43.00	6.56	46
W	2	3	2	2.33	0.58	5
Y	28.2	30.7	32.2	30.37	2.02	21.1
Yb	2.72	3.05	3.26	3.01	0.27	2.29
Zn	82	69	53	68.00	14.53	37
Zr	151	137	131	139.67	10.26	141

Appendix 9:

SE Pediment Red-Green (Christmas Tree) Breccia Tuff Package

Sample ID	NSM-00082-446	NSM-00082-410	NSM-00082-405	NSM-00082-395	Average	STD DEV
Normalized 100% volatile free major elements (wt %)						
SiO2	72.66	74.15	73.37	75.84	74.01	1.37
Al2O3	14.75	14.44	14.62	14.12	14.48	0.27
Fe2O3	6.15	3.25	3.59	2.25	3.81	1.66
CaO	0.40	1.42	1.84	0.66	1.08	0.66
MgO	1.27	0.96	1.27	1.27	1.19	0.16
Na2O	0.15	0.19	0.22	0.21	0.19	0.03
K2O	4.08	4.98	4.43	5.03	4.63	0.45
Cr2O3	<0.01	<0.01	<0.01	<0.01	NA	NA
TiO2	0.37	0.30	0.36	0.28	0.33	0.04
MnO	0.06	0.05	0.08	0.05	0.06	0.01
P2O5	0.05	0.14	0.11	0.18	0.12	0.05
SrO	0.01	0.01	0.01	0.01	0.01	0.00
BaO	0.04	0.12	0.11	0.09	0.09	0.03
LOI	6.31	5.62	7.57	6.58	6.52	0.81
Total-LOI	100.00	100.00	100.00	100.00	NA	NA
ICP-MS trace elements (ppm)						
Ba	334	907	852	757	712.50	259.83
Ce	49.1	50.6	55.5	42.1	49.33	5.54
Co	10.6	3	2.8	3.4	4.95	3.77
Cr	20	10	10	10	12.50	5.00
Cs	24.6	16.35	16.65	16.1	18.43	4.12
Cu	5	20	12	32	17.25	11.59
Dy	3.73	3.5	3.53	2.37	3.28	0.62
Er	2.33	2.25	2.18	1.67	2.11	0.30
Eu	0.82	0.88	0.93	0.49	0.78	0.20
Ga	29.8	23.4	21.2	18.1	23.13	4.95
Gd	3.6	3.78	3.83	2.41	3.41	0.67
Hf	6	5.6	5.5	4.6	5.43	0.59
Ho	0.77	0.72	0.71	0.5	0.68	0.12
La	24.7	26.6	28.4	21.7	25.35	2.86
Lu	0.42	0.44	0.38	0.34	0.40	0.04
Nb	14.5	12.8	13	6.9	11.80	3.35
Nd	21.3	22.7	24.5	16.8	21.33	3.29
Ni	34	5	<5	<5	NA	NA
Pb	31	20	19	19	22.25	5.85
Pr	5.89	6.12	6.6	4.81	5.86	0.76
Rb	231	227	205	230	223.25	12.28
Sm	4.49	4.64	4.93	3.18	4.31	0.78
Sr	57.9	92.7	115	115.5	95.28	27.09
Ta	1.2	1.1	1.1	0.6	1.00	0.27
Tb	0.63	0.6	0.62	0.39	0.56	0.11
Th	14.85	13.1	12.7	16.45	14.28	1.72
Tl	1.5	1.1	1	1.1	1.18	0.22
Tm	0.38	0.37	0.35	0.27	0.34	0.05
U	9.36	5.97	5.29	7.92	7.14	1.86
V	75	31	37	39	45.50	19.96
W	3	2	2	2	2.25	0.50
Y	22.9	22.3	22.2	16.4	20.95	3.05
Yb	2.63	2.53	2.32	1.98	2.37	0.29
Zn	101	84	84	52	80.25	20.47
Zr	195	186	190	161	183.00	15.12

Appendix 10:

Abel Knoll Tuff		NH Deep Tuff		NH Burgundy Tuff		
Sample ID	AK-08-0057c-325	NSM-00287-529	NSM-00287-541.5	NSM-00287-592.3	Average	STD DEV
Normalized 100% volatile free major elements (wt %)						
SiO2	69.04	68.28	72.52	70.33	71.43	1.55
Al2O3	16.38	18.28	14.02	14.95	14.49	0.65
Fe2O3	3.13	4.36	6.04	6.64	6.34	0.43
CaO	4.53	1.04	0.77	1.81	1.29	0.74
MgO	1.98	2.54	2.13	2.23	2.18	0.07
Na2O	1.28	0.95	0.34	0.41	0.38	0.05
K2O	2.85	3.47	3.07	2.37	2.72	0.49
Cr2O3	<0.01	0.01	0.01	0.01	0.01	0.00
TiO2	0.49	0.70	0.75	0.77	0.76	0.01
MnO	0.07	0.06	0.03	0.05	0.04	0.01
P2O5	0.13	0.12	0.17	0.21	0.19	0.03
SrO	0.05	0.02	0.01	0.03	0.02	0.02
BaO	0.05	0.15	0.13	0.18	0.15	0.04
LOI	9.06	8.39	5.8	6.96	6.38	0.82
Total-LOI	100.00	100.00	100.00	100.00	NA	NA
ICP-MS trace elements (ppm)						
Ba	450	1165	1055	1445	1250.00	275.77
Ce	65.7	52	60.5	61.1	60.80	0.42
Co	5.4	8.5	9.2	12.5	10.85	2.33
Cr	40	60	70	80	75.00	7.07
Cs	7.97	10	20.2	17.6	18.90	1.84
Cu	17	14	69	38	53.50	21.92
Dy	2.87	2.57	4.68	4.43	4.56	0.18
Er	1.57	1.44	2.79	2.57	2.68	0.16
Eu	1.1	0.88	1.21	1.25	1.23	0.03
Ga	19.8	22.8	18.8	20.3	19.55	1.06
Gd	3.51	3.15	5.19	5.03	5.11	0.11
Hf	7.3	6.4	5.9	6.1	6.00	0.14
Ho	0.57	0.53	0.97	0.93	0.95	0.03
La	36.8	27.5	31.7	31.3	31.50	0.28
Lu	0.26	0.22	0.46	0.41	0.44	0.04
Nb	10.8	13.8	13.4	13.9	13.65	0.35
Nd	26.5	22.1	27.8	28.5	28.15	0.49
Ni	13	17	28	30	29.00	1.41
Pb	20	20	36	13	24.50	16.26
Pr	7.7	6.25	7.44	7.52	7.48	0.06
Rb	115	127.5	143.5	118	130.75	18.03
Sm	4.87	4.13	5.97	6	5.99	0.02
Sr	375	150.5	86.1	238	162.05	107.41
Ta	0.9	0.8	0.9	1	0.95	0.07
Tb	0.53	0.47	0.79	0.77	0.78	0.01
Th	17.6	12.65	11.4	12.25	11.83	0.60
Tl	0.7	0.6	0.7	0.7	0.70	0.00
Tm	0.25	0.23	0.44	0.4	0.42	0.03
U	4.37	2.11	1.96	2.13	2.05	0.12
V	63	85	106	112	109.00	4.24
W	2	1	3	2	2.50	0.71
Y	16.8	15	29.7	26.2	27.95	2.47
Yb	1.64	1.44	2.82	2.67	2.75	0.11
Zn	59	70	104	117	110.50	9.19
Zr	330	270	240	250	245.00	7.07

Appendix 11:

Abel Knoll Breccia Body Matrix

Sample ID	NSM-00380-171.8	NSM-00380-239.8	NSM-00380-335.7	NSM-00380-622.4	Average	STD DEV
Normalized 100% volatile free major elements (wt %)						
SiO2	72.12	78.72	74.19	76.06	75.27	2.81
Al2O3	12.97	11.45	11.73	11.06	11.80	0.83
Fe2O3	4.34	0.65	3.76	3.26	3.00	1.63
CaO	0.52	0.47	0.32	0.35	0.41	0.10
MgO	0.71	0.19	1.05	0.99	0.74	0.39
Na2O	0.17	0.13	0.15	0.12	0.15	0.02
K2O	8.17	7.41	7.90	7.28	7.69	0.42
Cr2O3	0.01	0.01	0.01	0.01	0.01	0.00
TiO2	0.60	0.56	0.58	0.54	0.57	0.03
MnO	0.01	0.01	0.04	0.04	0.03	0.02
P2O5	0.24	0.27	0.17	0.19	0.22	0.05
SrO	0.05	0.02	0.02	0.03	0.03	0.02
BaO	0.07	0.09	0.07	0.07	0.08	0.01
LOI	3.92	1.76	2.85	2.01	2.64	0.98
Total-LOI	100.00	100.00	100.00	100.00	NA	NA
ICP-MS trace elements (ppm)						
Ba	605	724	581	584	623.50	67.85
Ce	63.7	34.8	48.8	41.3	47.15	12.43
Co	2.8	0.9	12.8	3.9	5.10	5.28
Cr	50	40	50	60	50.00	8.16
Cs	8.73	5.19	3.84	3.54	5.33	2.38
Cu	24	<5	33	33	NA	NA
Dy	4.72	2.29	3.33	3.17	3.38	1.01
Er	2.88	1.58	1.93	1.77	2.04	0.58
Eu	1.23	0.54	1.03	0.9	0.93	0.29
Ga	15.1	10.2	12.6	10.5	12.10	2.27
Gd	5.49	2.28	4.07	3.5	3.84	1.33
Hf	4.9	4.2	4.1	3.8	4.25	0.47
Ho	1.01	0.52	0.69	0.63	0.71	0.21
La	33.8	18.3	24.8	20.8	24.43	6.80
Lu	0.44	0.26	0.3	0.27	0.32	0.08
Nb	12.6	10.3	10.4	9.7	10.75	1.27
Nd	34.3	14.2	22.6	19.9	22.75	8.46
Ni	15	7	24	21	16.75	7.50
Pb	15	10	25	12	15.50	6.66
Pr	9.45	4.22	6.23	5.3	6.30	2.25
Rb	355	336	310	260	315.25	41.19
Sm	6.32	2.55	4.66	4.38	4.48	1.54
Sr	425	197	155.5	198.5	244.00	122.30
Ta	0.9	0.8	0.7	0.7	0.78	0.10
Tb	0.83	0.36	0.59	0.53	0.58	0.19
Th	9.11	7.26	7.85	9.07	8.32	0.92
Tl	3.1	3	3.2	2.3	2.90	0.41
Tm	0.42	0.25	0.29	0.26	0.31	0.08
U	5.48	3.73	2.55	3.57	3.83	1.22
V	209	58	85	73	106.25	69.38
W	2	2	2	2	2.00	0.00
Y	28	14	18.2	17.7	19.48	5.98
Yb	2.74	1.59	1.87	1.72	1.98	0.52
Zn	103	16	31	30	45.00	39.27
Zr	180	160	160	150	162.50	12.58

Appendix 12:

	Pansy Lee Conglomerate Tuff Clasts				Rhyolite Dikes	
Sample ID	8-09-12-1	8-09-12-2	8-09-12-3	8-09-12-4	Winni Rhyolite	Rembrandt Rhyolite
Normalized 100% volatile free major elements (wt %)						
SiO2	70.85	68.53	75.66	65.88	79.49	84.13
Al2O3	15.65	15.81	11.58	17.86	10.94	6.70
Fe2O3	0.43	0.80	0.86	0.76	1.16	2.12
CaO	0.11	0.79	1.46	0.14	0.41	0.87
MgO	0.07	0.22	0.43	0.08	0.07	0.15
Na2O	0.42	0.05	0.29	0.35	3.07	0.14
K2O	11.36	12.80	8.70	13.58	4.56	5.36
Cr2O3	<0.01	<0.01	<0.01	<0.01	<0.01	<0.01
TiO2	0.43	0.53	0.49	0.68	0.21	0.34
MnO	0.01	0.01	0.02	0.01	0.01	0.01
P2O5	0.03	0.05	0.14	0.04	0.04	0.11
SrO	0.01	0.01	0.02	0.01	<0.01	<0.01
BaO	0.61	0.40	0.34	0.59	0.05	0.04
LOI	1.51	2.09	2.63	1.52	1.59	1.56
Total-LOI	100.00	100.00	100.00	100.00	100.00	100.00
ICP-MS trace elements (ppm)						
Ba	4960	3310	2720	4650	451	384
Ce	74	38.4	36	65.3	86	26.6
Co	0.8	0.6	1.3	0.6	<0.5	3.8
Cr	20	30	20	40	<10	20
Cs	30.5	18.35	14.85	23.2	5.65	1.69
Cu	5	10	11	7	<5	74
Dy	2.66	1.37	1.35	2.44	4.6	2.06
Er	0.99	0.62	0.49	0.9	2.63	1.29
Eu	1.63	0.46	0.71	1.37	0.61	0.56
Ga	10.2	6.3	8.2	10.4	18.9	5.5
Gd	4.92	2.16	2.43	4.73	5.5	2.38
Hf	4.9	4.2	4	5.2	8	2.6
Ho	0.44	0.24	0.23	0.39	0.9	0.43
La	34.7	17.4	15.5	28	45	15.2
Lu	0.13	0.09	0.08	0.12	0.42	0.2
Nb	13.6	7.3	13.5	13.1	22.7	6.9
Nd	32.5	17.5	15.9	32.6	36.4	13.4
Ni	8	7	8	7	<5	5
Pb	11	8	10	8	18	20
Pr	9.13	4.83	4.5	8.62	10.2	3.58
Rb	427	561	325	517	184	203
Sm	6.48	3.07	3.15	6.78	6.91	2.71
Sr	98.8	52.4	149.5	65	33.1	130.5
Ta	1.2	0.6	0.7	0.9	1.7	0.5
Tb	0.63	0.28	0.31	0.58	0.82	0.38
Th	19.05	11.15	9.65	14	22.1	5.5
Tl	8.4	8.5	4.3	9.1	<0.5	1.2
Tm	0.15	0.1	0.08	0.14	0.4	0.2
U	8.73	1.25	2.16	3.31	7.37	2.37
V	61	30	51	51	19	25
W	62	28	54	84	1	3
Y	11	7.1	6	10.3	25.5	12.8
Yb	0.89	0.54	0.5	0.78	2.58	1.28
Zn	17	14	11	16	22	39
Zr	200	180	160	210	291	97

Appendix 13:

Abel Knoll Mafics

	flow	dike	dike		
Sample ID	AK-08-0056c-76.5	NSM-00380-544.6	NSM-00380-543.9	Average (dike)	STD DEV (dike)
Normalized 100% volatile free major elements (wt %)					
SiO2	58.92	64.54	62.75	63.65	1.27
Al2O3	18.24	20.54	20.36	20.45	0.13
Fe2O3	6.70	3.71	4.65	4.18	0.67
CaO	4.88	1.69	1.60	1.64	0.06
MgO	2.88	1.46	1.33	1.40	0.09
Na2O	3.14	1.65	1.66	1.65	0.00
K2O	2.71	4.01	5.27	4.64	0.89
Cr2O3	0.01	0.01	0.01	0.01	0.00
TiO2	1.51	1.55	1.53	1.54	0.01
MnO	0.16	0.02	0.02	0.02	0.00
P2O5	0.62	0.65	0.66	0.65	0.01
SrO	0.06	0.03	0.03	0.03	0.00
BaO	0.17	0.12	0.11	0.12	0.01
LOI	6.88	9.97	8.9	9.44	0.76
Total-LOI	100.00	100.00	100.00	NA	NA
ICP-MS trace elements (ppm)					
Ba	1355	894	905	899.50	7.78
Ce	81.7	89.9	104.5	97.20	10.32
Co	18.1	7.6	7.9	7.75	0.21
Cr	100	90	100	95.00	7.07
Cs	3	2.29	2.67	2.48	0.27
Cu	29	19	21	20.00	1.41
Dy	4.55	4.66	4.89	4.78	0.16
Er	2.34	2.33	2.42	2.38	0.06
Eu	1.87	1.76	2.19	1.98	0.30
Ga	20.2	22.4	22.9	22.65	0.35
Gd	6.22	6.43	7.01	6.72	0.41
Hf	6.3	7.3	7.4	7.35	0.07
Ho	0.9	0.9	0.95	0.93	0.04
La	39.3	44.4	53	48.70	6.08
Lu	0.33	0.32	0.32	0.32	0.00
Nb	19.7	20	20.5	20.25	0.35
Nd	38.6	41.6	47.6	44.60	4.24
Ni	31	13	12	12.50	0.71
Pb	9	12	13	12.50	0.71
Pr	10.5	11.65	13.15	12.40	1.06
Rb	82.6	103.5	151	127.25	33.59
Sm	7.72	8.15	9.08	8.62	0.66
Sr	538	253	245	249.00	5.66
Ta	1.2	1.2	1.2	1.20	0.00
Tb	0.84	0.89	0.96	0.93	0.05
Th	6.87	8.99	8.99	8.99	0.00
Tl	0.5	0.6	1	0.80	0.28
Tm	0.34	0.32	0.33	0.33	0.01
U	2.42	2.68	2.7	2.69	0.01
V	166	149	157	153.00	5.66
W	1	3	3	3.00	0.00
Y	24.2	23.6	25.8	24.70	1.56
Yb	2.04	1.97	1.98	1.98	0.01
Zn	110	184	154	169.00	21.21
Zr	280	310	320	315.00	7.07

Appendix 14:

Aussie Knob Mafics

Sample ID	Aussie 1	Aussie 2	Aussie 4	Aussie 7	Average	STD DEV
Normalized 100% volatile free major elements (wt %)						
SiO2	60.07	59.26	60.40	58.54	59.57	0.84
Al2O3	16.67	18.25	17.33	16.50	17.19	0.79
Fe2O3	7.53	6.64	6.65	7.97	7.20	0.66
CaO	4.74	5.15	4.94	6.05	5.22	0.58
MgO	1.85	1.47	1.57	2.14	1.75	0.30
Na2O	3.37	3.64	3.60	3.49	3.52	0.12
K2O	3.63	3.32	3.34	3.07	3.34	0.23
Cr2O3	0.03	0.03	0.03	0.03	0.03	0.00
TiO2	1.26	1.32	1.26	1.22	1.26	0.04
MnO	0.04	0.05	0.05	0.13	0.07	0.04
P2O5	0.61	0.64	0.56	0.57	0.59	0.04
SrO	0.07	0.09	0.08	0.08	0.08	0.01
BaO	0.15	0.15	0.18	0.21	0.17	0.03
LOI	5.43	4.29	4.07	3.85	4.41	0.70
Total-LOI	100.00	100.00	100.00	100.00	NA	NA
ICP-MS trace elements (ppm)						
Ba	1235	1365	1505	1800	1476.25	242.36
Ce	65.2	68.4	69.3	69.9	68.20	2.09
Co	19.9	21.8	22.3	24.4	22.10	1.85
Cr	200	220	240	220	220.00	16.33
Cs	4.79	4.65	4.36	3.68	4.37	0.49
Cu	37	39	34	36	36.50	2.08
Dy	3.48	3.73	3.77	3.79	3.69	0.14
Er	1.76	1.94	1.98	1.95	1.91	0.10
Eu	1.74	1.86	1.86	1.77	1.81	0.06
Ga	20.6	22.2	21.4	21.2	21.35	0.66
Gd	4.88	5.16	5.21	5.16	5.10	0.15
Hf	5.1	5.5	5.6	5.4	5.40	0.22
Ho	0.67	0.71	0.72	0.71	0.70	0.02
La	33.7	35.7	36.1	36.1	35.40	1.15
Lu	0.25	0.27	0.29	0.27	0.27	0.02
Nb	13	13.7	13.1	14	13.45	0.48
Nd	33	35.2	35.3	34.5	34.50	1.06
Ni	112	150	98	105	116.25	23.21
Pb	8	8	9	9	8.50	0.58
Pr	8.31	8.79	8.87	8.73	8.68	0.25
Rb	128	114.5	113.5	108	116.00	8.50
Sm	6.47	6.91	6.97	6.63	6.75	0.24
Sr	563	636	630	685	628.50	50.14
Ta	0.8	0.8	0.8	0.8	0.80	0.00
Tb	0.67	0.7	0.73	0.69	0.70	0.03
Th	6.52	6.97	7.61	7.08	7.05	0.45
Tl	<0.5	<0.5	<0.5	<0.5	<0.5	NA
Tm	0.25	0.28	0.28	0.28	0.27	0.02
U	2.49	2.66	2.82	2.33	2.58	0.21
V	157	185	171	152	166.25	14.86
W	1	2	2	1	1.50	0.58
Y	19.7	21	20.8	20.9	20.60	0.61
Yb	1.62	1.74	1.77	1.73	1.72	0.07
Zn	93	131	93	102	104.75	18.01
Zr	220	233	229	229	227.75	5.50

Appendix 15:

Basalt Hills Mafics

Sample ID	2010-006	2010-017	2010-018	Average	STD DEV
Normalized 100% volatile free major elements (wt %)					
SiO2	60.71	57.89	58.15	58.91	1.56
Al2O3	16.68	17.27	17.72	17.22	0.52
Fe2O3	7.02	7.43	7.84	7.43	0.41
CaO	4.59	6.16	5.63	5.46	0.80
MgO	1.38	2.52	1.41	1.77	0.65
Na2O	3.91	3.93	4.11	3.98	0.11
K2O	3.83	2.52	2.92	3.09	0.67
Cr2O3	0.01	0.01	0.01	0.01	0.00
TiO2	1.07	1.33	1.38	1.26	0.17
MnO	0.05	0.11	0.11	0.09	0.03
P2O5	0.49	0.57	0.48	0.51	0.05
SrO	0.07	0.09	0.08	0.08	0.01
BaO	0.20	0.16	0.16	0.17	0.02
LOI	2.49	2.89	2.30	2.56	0.30
Total-LOI	100.00	100.00	100.00	NA	NA
ICP-MS trace elements (ppm)					
Ba	1690	1375	1410	1491.67	172.65
Ce	85.9	88.1	91.3	88.43	2.72
Co	17.1	21	21	19.70	2.25
Cr	80	80	90	83.33	5.77
Cs	5.42	2.2	1.63	3.08	2.04
Cu	23	28	25	25.33	2.52
Dy	3.98	4.49	4.7	4.39	0.37
Er	2.09	2.41	2.39	2.30	0.18
Eu	1.69	1.97	2.05	1.90	0.19
Ga	20.7	20.6	21.5	20.93	0.49
Gd	5.69	6.28	6.66	6.21	0.49
Hf	6.4	6.6	6.6	6.53	0.12
Ho	0.79	0.88	0.9	0.86	0.06
La	43.4	44.3	45.9	44.53	1.27
Lu	0.29	0.32	0.31	0.31	0.02
Nb	16.3	19.7	20.1	18.70	2.09
Nd	36.7	39.9	44	40.20	3.66
Ni	31	28	32	30.33	2.08
Pb	13	12	12	12.33	0.58
Pr	10.2	10.7	11.95	10.95	0.90
Rb	155.5	67.8	81.6	101.63	47.16
Sm	6.75	7.52	8.23	7.50	0.74
Sr	647	742	732	707.00	52.20
Ta	1	1.2	1.2	1.13	0.12
Tb	0.76	0.84	0.9	0.83	0.07
Th	9.85	8.46	8.43	8.91	0.81
Tl	<0.5	<0.5	<0.5	<0.5	NA
Tm	0.29	0.32	0.33	0.31	0.02
U	2.76	2.16	2.3	2.41	0.31
V	136	141	147	141.33	5.51
W	1	1	2	1.33	0.58
Y	21.1	22.9	22.5	22.17	0.95
Yb	1.97	2.12	2.22	2.10	0.13
Zn	90	103	89	94.00	7.81
Zr	267	275	276	272.67	4.93

Appendix 16:

Little Basalt Hills Mafics

Sample ID	9-18-11-20	9-18-11-21	9-18-11-22	9-18-11-23	Average	STD DEV
Normalized 100% volatile free major elements (wt %)						
SiO2	59.75	62.58	62.02	62.94	61.82	1.24
Al2O3	16.35	16.36	16.37	16.35	16.36	0.01
Fe2O3	6.37	5.72	6.03	5.70	5.96	0.27
CaO	6.09	4.33	4.49	4.24	4.79	0.76
MgO	2.89	1.97	2.32	1.66	2.21	0.46
Na2O	3.75	4.04	3.90	4.17	3.97	0.15
K2O	2.93	3.27	3.14	3.27	3.15	0.14
Cr2O3	0.01	0.01	0.01	0.01	0.01	0.00
TiO2	1.01	0.89	0.89	0.89	0.92	0.05
MnO	0.09	0.06	0.09	0.05	0.07	0.02
P2O5	0.50	0.48	0.49	0.51	0.50	0.01
SrO	0.08	0.07	0.07	0.07	0.07	0.00
BaO	0.17	0.19	0.16	0.15	0.17	0.02
LOI	3.06	1.63	1.71	2.09	2.12	0.66
Total-LOI	100.00	100.00	100.00	100.00	NA	NA
ICP-MS trace elements (ppm)						
Ba	1490	1680	1370	1360	1475.00	148.88
Ce	83.1	84.8	96	82.7	86.65	6.30
Co	16.6	12.3	14.1	13	14.00	1.89
Cr	80	70	70	70	72.50	5.00
Cs	1.92	3.39	1.92	2.43	2.42	0.69
Cu	32	40	30	36	34.50	4.43
Dy	3.91	3.73	4.28	3.75	3.92	0.25
Er	2.07	1.97	2.08	2.02	2.04	0.05
Eu	1.72	1.57	1.98	1.58	1.71	0.19
Ga	20.3	20.1	19.9	19.9	20.05	0.19
Gd	5.63	5.24	6.11	5.14	5.53	0.44
Hf	6.3	6.4	6.3	6.5	6.38	0.10
Ho	0.76	0.72	0.81	0.75	0.76	0.04
La	42.7	44.9	50.3	43.3	45.30	3.46
Lu	0.29	0.27	0.28	0.28	0.28	0.01
Nb	15.7	15	15.9	14.7	15.33	0.57
Nd	35.6	35.5	40.3	35	36.60	2.48
Ni	29	26	28	25	27.00	1.83
Pb	12	13	15	13	13.25	1.26
Pr	9.84	9.96	11.15	9.7	10.16	0.67
Rb	75.6	92.1	81.5	89.3	84.63	7.50
Sm	6.74	6.5	7.46	6.31	6.75	0.50
Sr	672	613	612	598	623.75	32.89
Ta	1	0.9	0.9	0.9	0.93	0.05
Tb	0.75	0.7	0.83	0.71	0.75	0.06
Th	8.32	9.04	11.95	8.97	9.57	1.62
Tl	<0.5	<0.5	<0.5	<0.5	<0.5	NA
Tm	0.29	0.27	0.29	0.27	0.28	0.01
U	2.61	2.47	2.42	2.51	2.50	0.08
V	120	101	107	94	105.50	11.03
W	1	1	1	1	1.00	0.00
Y	20	19.9	21.3	19.8	20.25	0.70
Yb	1.9	1.86	1.95	1.84	1.89	0.05
Zn	94	90	93	88	91.25	2.75
Zr	263	271	264	273	267.75	4.99

Appendix 17:

North Hill Upper Mafic

Sample ID	NSM-00198-19	NSM-00198-60	NSM-00198-112	Average	STD DEV
Normalized 100% volatile free major elements (wt %)					
SiO2	58.74	59.08	55.74	57.86	1.84
Al2O3	17.80	17.40	18.63	17.95	0.63
Fe2O3	7.13	6.33	8.07	7.18	0.87
CaO	6.38	5.49	6.02	5.96	0.45
MgO	1.94	2.59	2.81	2.44	0.45
Na2O	2.09	2.86	2.73	2.56	0.41
K2O	3.84	4.30	3.73	3.96	0.30
Cr2O3	0.02	0.02	0.02	0.02	0.00
TiO2	1.16	1.14	1.21	1.17	0.04
MnO	0.16	0.08	0.28	0.17	0.10
P2O5	0.52	0.48	0.49	0.50	0.02
SrO	0.06	0.06	0.06	0.06	0.00
BaO	0.15	0.17	0.19	0.17	0.02
LOI	7.29	5.42	7.46	6.72	1.13
Total-LOI	100.00	100.00	100.00	NA	NA
ICP-MS trace elements (ppm)					
Ba	1205	1370	1575	1383.33	185.36
Ce	59.5	58.6	63.5	60.53	2.61
Co	19.3	21.7	23.7	21.57	2.20
Cr	150	140	160	150.00	10.00
Cs	3.82	5.36	5.99	5.06	1.12
Cu	29	29	32	30.00	1.73
Dy	3.31	3.29	3.53	3.38	0.13
Er	1.73	1.72	1.83	1.76	0.06
Eu	1.55	1.47	1.59	1.54	0.06
Ga	18.9	18.6	20.7	19.40	1.14
Gd	4.5	4.45	4.97	4.64	0.29
Hf	4.8	4.6	5	4.80	0.20
Ho	0.65	0.62	0.69	0.65	0.04
La	29.3	28.3	30.4	29.33	1.05
Lu	0.23	0.23	0.25	0.24	0.01
Nb	10.4	10.2	11	10.53	0.42
Nd	27.6	27.2	30.1	28.30	1.57
Ni	39	48	52	46.33	6.66
Pb	10	9	10	9.67	0.58
Pr	7.41	7.24	7.96	7.54	0.38
Rb	139	134	138	137.00	2.65
Sm	5.32	5.37	5.93	5.54	0.34
Sr	517	527	544	529.33	13.65
Ta	0.7	0.6	0.7	0.67	0.06
Tb	0.62	0.62	0.68	0.64	0.03
Th	6.65	6.6	7.15	6.80	0.30
Tl	0.8	0.8	0.8	0.80	0.00
Tm	0.24	0.23	0.26	0.24	0.02
U	2.77	2.29	2.5	2.52	0.24
V	167	151	176	164.67	12.66
W	2	1	2	1.67	0.58
Y	17	16.8	18.2	17.33	0.76
Yb	1.57	1.56	1.69	1.61	0.07
Zn	81	85	96	87.33	7.77
Zr	185	182	196	187.67	7.37

Appendix 18:

North Hill Lower Mafic

Sample ID	NSM-00190-161	NSM-00251-274	NSM-00184-168	Average	STD DEV
Normalized 100% volatile free major elements (wt %)					
SiO2	54.68	54.47	54.63	54.59	0.11
Al2O3	16.81	16.70	16.61	16.70	0.10
Fe2O3	7.64	7.67	7.63	7.64	0.02
CaO	6.75	6.72	6.59	6.69	0.09
MgO	5.89	6.13	6.10	6.04	0.13
Na2O	3.28	3.23	3.32	3.28	0.04
K2O	2.78	2.92	2.98	2.89	0.10
Cr2O3	0.04	0.04	0.04	0.04	0.00
TiO2	1.22	1.21	1.23	1.22	0.01
MnO	0.10	0.11	0.11	0.11	0.01
P2O5	0.57	0.56	0.53	0.55	0.02
SrO	0.08	0.08	0.08	0.08	0.00
BaO	0.15	0.15	0.14	0.15	0.001
LOI	3.13	3.35	2.93	3.14	0.21
Total-LOI	100.00	100.00	100.00	NA	NA
ICP-MS trace elements (ppm)					
Ba	1235	1190	1250	1225.00	31.22
Ce	65.8	65.4	67.1	66.10	0.89
Co	30.5	30.5	30.8	30.60	0.17
Cr	300	310	310	306.67	5.77
Cs	27.6	20.3	28.6	25.50	4.53
Cu	29	29	29	29.00	0.00
Dy	3.53	3.59	3.66	3.59	0.07
Er	1.73	1.81	1.78	1.77	0.04
Eu	1.86	1.78	1.85	1.83	0.04
Ga	19.5	18.7	19.4	19.20	0.44
Gd	5.37	5.38	5.32	5.36	0.03
Hf	5.6	5.6	5.7	5.63	0.06
Ho	0.64	0.65	0.68	0.66	0.02
La	30.2	30.3	30.9	30.47	0.38
Lu	0.23	0.23	0.23	0.23	0.00
Nb	11.3	11.3	11.7	11.43	0.23
Nd	33.2	33	34.5	33.57	0.81
Ni	129	129	132	130.00	1.73
Pb	8	7	8	7.67	0.58
Pr	8.45	8.5	8.7	8.55	0.13
Rb	63.6	92.6	100.5	85.57	19.43
Sm	6.45	6.47	6.62	6.51	0.09
Sr	728	667	694	696.33	30.57
Ta	0.7	0.7	0.8	0.73	0.06
Tb	0.7	0.68	0.72	0.70	0.02
Th	6.92	6.91	6.95	6.93	0.02
Tl	<0.5	0.5	0.5	NA	NA
Tm	0.24	0.24	0.24	0.24	0.00
U	2.28	2.26	2.35	2.30	0.05
V	168	172	173	171.00	2.65
W	1	1	1	1.00	0.00
Y	17.7	17.9	18	17.87	0.15
Yb	1.61	1.55	1.64	1.60	0.05
Zn	86	84	87	85.67	1.53
Zr	210	211	217	212.67	3.79

Appendix 19:

Silica Ridge Mafic

Sample ID	9-18-11-1b	9-25-11-3	NSM-00334-15	NSM-00334-59.7	Average	STD DEV
Normalized 100% volatile free major elements (wt %)						
SiO2	61.54	61.34	61.45	59.79	61.03	0.83
Al2O3	16.41	17.26	16.32	16.91	16.72	0.44
Fe2O3	7.23	5.90	6.86	6.13	6.53	0.62
CaO	4.02	4.56	4.19	6.05	4.71	0.92
MgO	1.91	1.64	1.73	2.18	1.86	0.24
Na2O	3.29	3.97	3.68	3.97	3.73	0.32
K2O	3.61	3.41	3.80	2.88	3.42	0.40
Cr2O3	0.01	0.01	0.01	0.01	0.01	0.00
TiO2	1.15	1.10	1.14	1.21	1.15	0.04
MnO	0.11	0.06	0.07	0.10	0.09	0.02
P2O5	0.50	0.51	0.53	0.52	0.51	0.01
SrO	0.06	0.07	0.07	0.09	0.07	0.01
BaO	0.15	0.17	0.15	0.16	0.16	0.01
LOI	4.43	3.11	3.54	4.73	3.95	0.76
Total-LOI	100.00	100.00	100.00	100.00	NA	NA
ICP-MS trace elements (ppm)						
Ba	1335	1490	1265	1365	1363.75	94.02
Ce	87.9	86.6	83.7	84	85.55	2.04
Co	17.6	17.5	15.9	18.1	17.28	0.95
Cr	90	80	90	90	87.50	5.00
Cs	5.16	5.68	4.84	4.43	5.03	0.53
Cu	24	29	28	27	27.00	2.16
Dy	4.37	4.25	3.92	3.95	4.12	0.22
Er	2.3	2.27	1.99	2.02	2.15	0.16
Eu	1.86	1.77	1.65	1.72	1.75	0.09
Ga	21.1	21.2	20.8	21	21.03	0.17
Gd	6.2	5.79	5.49	5.38	5.72	0.37
Hf	6.6	6.4	6.4	6.4	6.45	0.10
Ho	0.85	0.83	0.78	0.76	0.81	0.04
La	46.9	44.8	43	42.2	44.23	2.09
Lu	0.32	0.32	0.28	0.29	0.30	0.02
Nb	18.2	16.8	16.9	18.3	17.55	0.81
Nd	40	37.4	37.2	37.5	38.03	1.32
Ni	43	36	37	34	37.50	3.87
Pb	13	11	13	13	12.50	1.00
Pr	11	10.4	9.93	10.1	10.36	0.47
Rb	119.5	118.5	121	50.9	102.48	34.40
Sm	7.45	6.71	7.16	7.22	7.14	0.31
Sr	520	624	592	710	611.50	78.76
Ta	1.1	1	1	1	1.03	0.05
Tb	0.85	0.77	0.73	0.75	0.78	0.05
Th	9.67	10.1	8.7	8.84	9.33	0.67
Tl	0.6	<0.5	0.7	<0.5	NA	NA
Tm	0.32	0.33	0.31	0.3	0.32	0.01
U	2.76	2.77	2.46	2.43	2.61	0.19
V	140	137	116	126	129.75	10.97
W	1	1	1	1	1.00	0.00
Y	23.8	24.7	21.8	22.1	23.10	1.38
Yb	2.14	2.11	1.9	1.88	2.01	0.14
Zn	93	122	95	102	103.00	13.24
Zr	283	273	290	290	284.00	8.04

Appendix 20:

South East Pediment Mafic

Sample ID	NSM-00358-453	NSM-00358-481	NSM-00073-248	Average	STD DEV
Normalized 100% volatile free major elements (wt %)					
SiO2	58.45	59.21	57.86	58.51	0.68
Al2O3	15.76	16.72	15.47	15.98	0.65
Fe2O3	8.56	7.83	7.77	8.05	0.44
CaO	6.86	6.37	6.86	6.70	0.29
MgO	3.18	2.24	4.39	3.27	1.08
Na2O	2.86	3.02	3.69	3.19	0.44
K2O	2.47	2.65	2.07	2.40	0.30
Cr2O3	0.03	0.03	0.04	0.03	0.01
TiO2	1.05	1.12	1.07	1.08	0.03
MnO	0.20	0.21	0.10	0.17	0.06
P2O5	0.35	0.38	0.43	0.39	0.04
SrO	0.09	0.10	0.11	0.10	0.01
BaO	0.11	0.13	0.14	0.13	0.01
LOI	5.11	5.10	2.99	4.40	1.00
Total-LOI	100.00	100.00	100.00	NA	NA
ICP-MS trace elements (ppm)					
Ba	1025	1125	1200	1116.67	71.69
Ce	55.3	56.1	53	54.80	1.31
Co	32.4	25.5	29	28.97	2.82
Cr	280	270	270	273.33	4.71
Cs	6.38	8.17	5.67	6.74	1.05
Cu	70	48	64	60.67	9.29
Dy	2.76	2.71	2.61	2.69	0.06
Er	1.45	1.43	1.3	1.39	0.07
Eu	1.43	1.4	1.35	1.39	0.03
Ga	20.8	20.9	19.7	20.47	0.54
Gd	4.04	4	3.9	3.98	0.06
Hf	3.8	3.8	3.6	3.73	0.09
Ho	0.55	0.52	0.49	0.52	0.02
La	28	28.4	26.3	27.57	0.91
Lu	0.19	0.19	0.17	0.18	0.01
Nb	8.4	8.3	7.8	8.17	0.26
Nd	25.6	25.9	24.5	25.33	0.60
Ni	135	104	124	121.00	12.83
Pb	12	13	12	12.33	0.47
Pr	6.75	6.84	6.53	6.71	0.13
Rb	60	69	45.1	58.03	9.86
Sm	4.9	4.94	4.66	4.83	0.12
Sr	785	829	906	840.00	50.01
Ta	0.5	0.5	0.5	0.50	0.00
Tb	0.52	0.54	0.5	0.52	0.02
Th	6.41	6.26	5.81	6.16	0.25
Tl	<0.5	<0.5	<0.5	NA	NA
Tm	0.2	0.19	0.18	0.19	0.01
U	2.04	2.01	1.95	2.00	0.04
V	175	171	169	171.67	2.49
W	1	1	1	1.00	0.00
Y	14.7	14.2	13.4	14.10	0.54
Yb	1.3	1.3	1.18	1.26	0.06
Zn	100	103	94	99.00	3.74
Zr	149	147	138	144.67	4.78

Appendix 21:

Sandman Mafics Data Summary

	Average	STD DEV	Zr ratio R2
Normalized 100% volatile free major elements (wt %)			
SiO2	59.26	2.66	0.34893
Al2O3	17.12	1.18	0.26170
Fe2O3	6.91	1.09	-0.50783
CaO	5.34	1.39	-0.60273
MgO	2.72	1.52	-0.20908
Na2O	3.34	0.67	-0.00009
K2O	3.24	0.66	0.22661
Cr2O3	0.02	0.01	-0.55033
TiO2	1.19	0.17	0.13638
MnO	0.11	0.06	-0.31876
P2O5	0.52	0.08	0.37843
SrO	0.08	0.02	-0.43397
BaO	0.16	0.02	0.00288
LOI	4.33	2.09	NA
Total-LOI	100.00	NA	NA
ICP-MS trace elements (ppm)			
Ba	1335.70	216.28	0.00999
Ce	75.83	14.01	0.88868
Co	20.36	6.64	-0.61820
Cr	157.41	87.78	-0.57907
Cs	6.53	7.13	-0.10882
Cu	33.19	11.55	-0.52466
Dy	3.82	0.59	0.84553
Er	1.97	0.30	0.84187
Eu	1.74	0.20	0.45572
Ga	20.56	1.06	0.23853
Gd	5.39	0.80	0.78710
Hf	5.78	1.01	0.95830
Ho	0.74	0.12	0.86507
La	38.23	7.78	0.84317
Lu	0.27	0.04	0.85745
Nb	14.52	3.92	0.90819
Nd	35.06	5.64	0.86270
Ni	65.26	45.98	-0.49699
Pb	11.00	2.18	0.13346
Pr	9.38	1.69	0.88850
Rb	99.86	30.62	0.04511
Sm	6.69	1.05	0.81207
Sr	622.56	143.73	-0.31923
Ta	0.88	0.22	0.88400
Tb	0.73	0.11	0.81213
Th	7.96	1.46	0.55853
Tl	NA	NA	NA
Tm	0.27	0.04	0.85949
U	2.45	0.25	0.32635
V	149.04	25.04	-0.34210
W	1.33	0.62	0.07260
Y	20.14	3.22	0.86612
Yb	1.78	0.27	0.82737
Zn	101.56	22.75	0.18731
Zr	240.04	50.33	NA

Appendix 22:

Bloody Run Hills and Santa Rosa Range Mafics

Sample ID	MSR-51	MBR-119	MBR-135	MBR-140	MSR-113	MSR-118	MSR-103
Normalized 100% major elements (wt %)							
SiO2	63.72	58.23	58.03	61.09	59.74	62.31	60.04
Al2O3	16.57	16.76	17.11	16.72	16.43	16.29	17.13
Fe2O3	3.38	3.21	3.59	2.11	2.94	2.95	3.17
TiO2	0.72	1.29	1.08	0.86	1.14	0.80	0.92
CaO	4.02	5.63	5.70	4.97	5.20	4.66	5.55
MgO	1.77	3.36	3.46	3.04	3.31	2.64	3.03
Na2O	3.75	3.46	3.98	3.69	3.47	4.10	3.83
K2O	3.52	3.07	2.77	3.22	3.29	3.25	2.91
Cr2O3	NA	NA	NA	NA	NA	NA	NA
MnO	0.06	0.12	0.12	0.09	0.11	0.06	0.09
P2O5	0.38	0.56	0.47	0.36	0.50	0.32	0.43
SrO	NA	NA	NA	NA	NA	NA	NA
BaO	NA	NA	NA	NA	NA	NA	NA
LOI	1.5	1.84	1.3	1.32	2.03	0.48	2
Total	100.00	100.00	100.00	100.00	100.00	100.00	100.00
ICP-MS trace elements (ppm)							
Ba	1207	1257	1020	1061	1250	1132	1151
Ce	75	78	60.5	54	88	57	63
Co	13	20	20	17	19	16	16
Cr	49	73	84	71	67	75	58
Cs	1.6	1.2	1.15	1.6	1.6	1.8	1
Cu	NA	NA	NA	NA	NA	NA	NA
Dy	NA	NA	NA	NA	NA	NA	NA
Eu	1.55	2.14	1.785	1.54	2	1.26	1.51
Ga	NA	NA	NA	NA	NA	NA	NA
Gd	NA	NA	NA	NA	NA	NA	NA
Hf	6.2	5.7	4.75	4.3	6.2	5	4.8
Ho	NA	NA	NA	NA	NA	NA	NA
La	53.2	44.9	34.5	32	50.9	35.1	38.9
Lu	0.26	0.29	0.245	0.24	0.31	0.25	0.21
Nb	NA	NA	NA	NA	NA	NA	NA
Nd	30	32	25.5	22	40	22	26
Ni	28	33	40	35	25	37	25
Pb	NA	NA	NA	NA	NA	NA	NA
Pr	NA	NA	NA	NA	NA	NA	NA
Rb	117	79	85	86	101	105	82
Sm	5.24	6.18	4.79	4.05	6.51	4.18	4.61
Sr	589	693	759	634	628	562	727
Ta	1.2	1.1	0.6	0.5	1.1	1	0.6
Tb	0.7	0.6	0.55	0.3	0.8	0.5	0.5
Th	9.5	6.1	5.5	7.1	7.8	9.5	6.1
Tl	NA	NA	NA	NA	NA	NA	NA
Tm	NA	NA	NA	NA	NA	NA	NA
U	2.6	1.8	1.75	2.1	2.5	2.7	1.7
V	101	140	121	110	120	110	117
W	NA	NA	NA	NA	NA	NA	NA
Y	30	24	30	31	40	24	39
Yb	1.75	2	1.6	1.49	2.08	1.67	1.4
Zn	NA	NA	NA	NA	NA	NA	NA
Zr	273	271	212	164	272	194	216
Sc	10.5	14.3	13.85	12.9	13.6	13	13.1

Appendix 23:

ID	$^{40}Ar/^{39}Ar$	$^{38}Ar/^{39}Ar$	$^{37}Ar/^{39}Ar$	$^{36}Ar/^{39}Ar$ (x 10^{-3})	$^{39}Ar_K$ (x 10^{-15} mol)	K/Ca	$^{40}Ar^*$ (%)	Age (Ma)	±1σ (Ma)
H10-48, Nine Hill Tuff Sanidine, J=0.0021228±0.05%, D=1.001±0.001, NM-240A, Lab#=59944									
6	*6.403*	*0.0137*	*0.0287*	*0.5258*	*4.277*	*17.7*	*97.6*	*23.741*	*0.090*
5	*6.591*	*0.0135*	*0.0318*	*0.2877*	*4.947*	*16.0*	*98.7*	*24.717*	*0.071*
7	*6.790*	*0.0133*	*0.0240*	*0.7563*	*5.473*	*21.3*	*96.7*	*24.946*	*0.083*
8	6.669	0.0136	0.0358	0.2515	4.797	14.2	98.9	25.053	0.080
10	6.666	0.0128	0.0307	0.2165	5.053	16.6	99.1	25.081	0.074
4	6.740	0.0136	0.0287	0.3279	6.078	17.8	98.6	25.235	0.063
13	6.695	0.0122	0.0234	0.1439	1.038	21.8	99.4	25.27	0.25
11	6.699	0.0132	0.0356	0.1466	4.912	14.3	99.4	25.284	0.070
12	6.715	0.0129	0.0298	0.1893	3.284	17.1	99.2	25.295	0.090
1	6.704	0.0138	0.0383	0.0927	6.236	13.3	99.6	25.364	0.060
9	6.738	0.0138	0.0344	0.1717	4.400	14.8	99.3	25.404	0.078
3	6.809	0.0136	0.0255	0.3330	15.632	20.0	98.6	25.490	0.048
2	6.772	0.0136	0.0349	0.1195	7.338	14.6	99.5	25.590	0.062
Mean age ± 2σ		n=10		MSWD=6.16		16.5 ±5.5		25.34	0.11
H10-49, Unknown tuff, Sanidine, J=0.0021278±0.05%, D=1.001±0.001, NM-240A, Lab#=59945									
23	6.842	0.0132	0.0071	0.1973	5.167	71.7	99.2	25.818	0.078
17	6.821	0.0132	0.0069	0.0688	6.624	74.4	99.7	25.882	0.058
15	6.823	0.0136	0.0068	0.0675	19.328	74.6	99.7	25.894	0.044
2	6.847	0.0131	0.0065	0.1136	13.680	78.1	99.5	25.930	0.045
13	6.822	0.0131	0.0068	0.0147	12.740	75.6	99.9	25.947	0.046
1	6.909	0.0132	0.0074	0.3045	5.524	68.8	98.7	25.953	0.069
12	6.927	0.0133	0.0062	0.3623	9.837	81.9	98.5	25.955	0.053
16	6.862	0.0132	0.0071	0.1232	10.496	72.1	99.5	25.978	0.053
18	6.872	0.0134	0.0092	0.1575	6.230	55.5	99.3	25.978	0.065
11	6.857	0.0133	0.0063	0.0460	11.293	80.6	99.8	26.046	0.051
14	6.863	0.0133	0.0075	-0.0098	9.578	68.3	100.1	26.129	0.061
19	6.942	0.0137	0.0063	0.2319	7.978	80.7	99.0	26.158	0.065
20	6.886	0.0132	0.0080	0.0380	7.998	63.7	99.8	26.166	0.060
21	6.894	0.0138	0.0080	0.0608	8.815	63.5	99.7	26.170	0.054
22	6.948	0.0134	0.0076	0.1679	9.125	67.1	99.3	26.252	0.060
Mean age ± 2σ		n=15		MSWD=4.75		71.8 ±14.8		26.010	0.068

Notes:

Isotopic ratios corrected for blank, radioactive decay, and mass discrimination, not corrected for interfering reactions.

Errors quoted for individual analyses include analytical error only, without interfering reaction or J uncertainties.

Mean age is weighted mean age of Taylor (1982). Mean age error is weighted error of the mean (Taylor, 1982), multiplied by the root of the MSWD where MSWD>1, and also incorporates uncertainty in J factors and irradiation correction uncertainties.

Decay constants and isotopic abundances after Steiger and Jäger (1977).

symbol preceding sample ID denotes analyses excluded from mean age calculations.

Ages calculated relative to FC-2 Fish Canyon Tuff sanidine interlaboratory standard at 28.201 Ma

Decay Constant (LambdaK (total)) = 5.543e-10/a

Correction factors:

$(^{39}Ar/^{37}Ar)_{Ca}$ = 0.0007 ± 5e-05

$(^{36}Ar/^{37}Ar)_{Ca}$ = 0.00028 ± 2e-05

$(^{38}Ar/^{39}Ar)_{K}$ = 0.013

$(^{40}Ar/^{39}Ar)_{K}$ = 0.01 ± 0.002

Appendix 24:

ID	Temp (°C)	$^{40}Ar/^{39}Ar$	$^{37}Ar/^{39}Ar$	$^{36}Ar/^{39}Ar$ (x 10^{-3})	$^{39}Ar_K$ (x 10^{-15} mol)	K/Ca	$^{40}Ar^*$ (%)	^{39}Ar (%)	Age (Ma)	±1σ (Ma)
SMAR-1, N2:160, 29.87 mg groundmass concentrate, J=0.000718±0.11%, D=1.00743±0.00124, NM-160, Lab#=53802-01										
A	*625*	*314.4*	*0.2581*	*1034.7*	*8.7*	*2.0*	*2.7*	*6.5*	*11.2*	*2.4*
B	*700*	*24.14*	*0.4013*	*31.47*	*24.1*	*1.3*	*61.6*	*24.4*	*19.17*	*0.14*
C	*750*	*25.64*	*0.5505*	*29.73*	*19.6*	*0.93*	*65.9*	*39.0*	*21.77*	*0.14*
D	800	24.57	0.7061	23.68	14.3	0.72	71.8	49.6	22.70	0.11
E	875	22.79	0.6490	18.69	27.1	0.79	76.0	69.8	22.31	0.10
F	975	25.31	0.7925	27.02	21.9	0.64	68.7	86.1	22.40	0.12
G	1075	39.43	1.536	77.06	8.12	0.33	42.6	92.2	21.64	0.27
H	1250	54.20	4.746	124.3	3.13	0.11	32.9	94.5	23.06	0.62
I	1650	44.60	4.157	93.46	7.37	0.12	38.8	100.0	22.36	0.30
Integrated age ± 2σ		n=9		MSWD=63.06	134.3				20.99	0.47
Plateau ± 2σ steps D-I		n=6		MSWD=3.51	81.9	0.61		61.0	22.42	0.23
SMAR-2, N3:160, 32.92 mg groundmass concentrate, J=0.0007193±0.11%, D=1.00743±0.00124, NM-160, Lab#=53803-01										
A	*625*	*2380.4*	*0.8452*	*7957.5*	*2.84*	*0.60*	*1.2*	*1.4*	*37*	*23*
B	*700*	*26.00*	*0.8950*	*31.01*	*10.9*	*0.57*	*65.0*	*6.8*	*21.82*	*0.16*
C	*750*	*20.86*	*0.9129*	*10.93*	*14.9*	*0.56*	*84.9*	*14.2*	*22.85*	*0.09*
D	*800*	*19.81*	*0.9514*	*6.192*	*14.6*	*0.54*	*91.2*	*21.5*	*23.30*	*0.10*
E	*875*	*19.29*	*0.6501*	*5.277*	*38.1*	*0.78*	*92.2*	*40.4*	*22.94*	*0.08*
F	975	20.40	0.3803	9.759	48.5	1.3	86.0	64.5	22.63	0.07
G	1075	25.24	0.3983	27.65	36.3	1.3	67.8	82.6	22.06	0.12
H	1250	31.83	1.0140	48.92	10.6	0.50	54.8	87.9	22.52	0.19
I	1650	32.38	1.267	50.83	24.4	0.40	53.9	100.0	22.54	0.17
Integrated age ± 2σ		n=9		MSWD=13.98	201.1				22.80	0.75
Plateau ± 2σ steps E-I		n=5		MSWD=10.23	157.9	0.99		78.5	22.64	0.29
TP032-4, G12:160, 9.56 mg adularia, J=0.0007286±0.11%, D=1.0054±0.001, NM-160, Lab#=53743-01										
A	*650*	*160.4*	*0.0018*	*502.2*	*2.82*	*283.1*	*7.5*	*1.4*	*15.7*	*1.2*
B	*800*	*18.21*	*0.0006*	*14.65*	*21.8*	*917.6*	*76.2*	*12.4*	*18.16*	*0.08*
C	*900*	*13.71*	*0.0006*	*2.775*	*25.9*	*815.4*	*94.0*	*25.4*	*16.87*	*0.06*
D	*1000*	*13.21*	*0.0005*	*2.219*	*41.1*	*1111.8*	*95.0*	*46.1*	*16.43*	*0.04*
E	1100	13.29	0.0010	3.161	36.4	521.0	93.0	64.5	16.17	0.05
F	1200	14.16	0.0067	5.266	17.9	76.2	89.0	73.5	16.49	0.06
G	1300	16.17	0.0047	12.36	24.5	107.5	77.4	85.8	16.38	0.07
H	1380	16.48	0.0135	13.23	24.7	37.9	76.5	98.3	16.49	0.08
I	*1450*	*20.77*	*0.0604*	*26.40*	*3.27*	*8.4*	*62.5*	*99.9*	*16.97*	*0.19*
J	*1700*	*101.2*	*5.899*	*198.90*	*0.15*	*0.086*	*42.4*	*100.0*	*55.8*	*3.2*
Integrated age ± 2σ		n=10		MSWD=70.62	198.60				16.66	0.10
Plateau ± 2σ steps D-H		n=5		MSWD=6.77	144.70	481.30		72.8	16.38	0.13

Notes:

Isotopic ratios corrected for blank, radioactive decay, and mass discrimination, not corrected for interfering reactions.

Ages calculated relative to FC-1 Fish Canyon Tuff sanidine interlaboratory standard at 27.84 Ma.

Errors quoted for individual analysis include analytical error only, without interferring reaction or J uncerttainties

Intergrated age calculated by recombining isotopic measurements of all steps

Integrated age error calculated by recombining errors of isotopic measurements of all steps

Plateau age is inverse-variance-weighted mean of selected steps

Plateau age error is inverse-variance-weighted mean error (Taylor, 1982) times square root MSWD where MSWD>1.

Plateau and integrated ages incorporates uncerntainties in interferring reaction corrections and J factors.

Decay constants and isotopic abundances after Steiger and Jaeger (1977)

Italics denote analyses excluded from plateau age calculations

Discrimination = 1.00743 ± 0.00124

Correction factors:

$(^{38}Ar/^{37}Ar)_{Ca}$ = 0.0007 ± 2e-05

$(^{36}Ar/^{37}Ar)_{Ca}$ = 0.00028 ± 2e-06

$(^{38}Ar/^{39}Ar)_{K}$ = 0.01077

$(^{40}Ar/^{39}Ar)_{K}$ = 0.0002 ± 0.0003

Appendix 25:

Sample NSM-00190-161, North Hill mafic-2, step heating increments for whole rock, 60-80 mesh size

Irradiation filename: au22.4l.whr.1a-1ai

P	40Ar (*±atm)	39Ar (K)	38Ar (Cl±atm)	37Ar (Ca)	36Ar (Atm)	Moles 40Ar*	%Rad	R	Age (Ma)
0.5	0.01416 ± 0.000334	0.00074 ± 0.000203	0.00000 ± 0.000050	0.00138 ± 0.000114	0.000079 ± 0.000020	9.92E-17	-63.22%	-12.1558	-146.373 -± 156.308
0.7	0.80735 ± 0.001042	0.04918 ± 0.000277	0.00125 ± 0.000052	0.05871 ± 0.000711	0.002525 ± 0.000047	5.65E-15	8.19%	1.3451	15.491 ± 3.590
0.8	0.73384 ± 0.000946	0.05575 ± 0.000235	0.00106 ± 0.000057	0.07225 ± 0.000895	0.002103 ± 0.000025	5.14E-15	16.13%	2.1253	24.416 ± 1.723
0.9	0.78625 ± 0.001595	0.07401 ± 0.000206	0.00127 ± 0.000048	0.11594 ± 0.000645	0.002124 ± 0.000021	5.51E-15	21.38%	2.2739	26.110 ± 1.086
1	0.93762 ± 0.001265	0.11511 ± 0.000318	0.00188 ± 0.000050	0.21310 ± 0.001012	0.002291 ± 0.000023	6.57E-15	29.68%	2.4207	27.782 ± 0.766
1.05	1.06151 ± 0.001040	0.16705 ± 0.000584	0.00267 ± 0.000068	0.29920 ± 0.001050	0.002477 ± 0.000038	7.43E-15	33.37%	2.1237	24.396 ± 0.839
1.1	0.74700 ± 0.000657	0.14964 ± 0.000330	0.00202 ± 0.000050	0.22183 ± 0.000733	0.001559 ± 0.000035	5.23E-15	40.80%	2.0392	23.432 ± 0.818
1.15	0.71187 ± 0.000643	0.17712 ± 0.000487	0.00230 ± 0.000040	0.20771 ± 0.000923	0.001279 ± 0.000037	4.99E-15	49.35%	1.9851	22.815 ± 0.717
1.2	0.66876 ± 0.001164	0.18905 ± 0.000498	0.00250 ± 0.000054	0.18911 ± 0.001056	0.001063 ± 0.000036	4.68E-15	55.38%	1.9604	22.533 ± 0.669
1.3	1.34012 ± 0.001574	0.34086 ± 0.000859	0.00456 ± 0.000076	0.32344 ± 0.001628	0.002412 ± 0.000064	9.39E-15	48.83%	1.9212	22.084 ± 0.657
1.4	1.48605 ± 0.001955	0.42205 ± 0.000856	0.00579 ± 0.000101	0.38090 ± 0.000634	0.002209 ± 0.000032	1.04E-14	58.19%	2.0504	23.561 ± 0.279
1.5	2.53850 ± 0.002296	0.63472 ± 0.000704	0.00855 ± 0.000086	0.53932 ± 0.002301	0.004353 ± 0.000050	1.78E-14	51.09%	2.0445	23.493 ± 0.276
1.6	2.21943 ± 0.002093	0.63159 ± 0.000585	0.00825 ± 0.000066	0.44599 ± 0.000968	0.003198 ± 0.000033	1.55E-14	59.09%	2.0774	23.868 ± 0.186
1.7	1.90871 ± 0.002414	0.65375 ± 0.000948	0.00846 ± 0.000147	0.37425 ± 0.001102	0.002091 ± 0.000030	1.34E-14	69.25%	2.0228	23.246 ± 0.171
1.8	1.53110 ± 0.001091	0.61309 ± 0.000933	0.00802 ± 0.000147	0.28915 ± 0.001093	0.001163 ± 0.000028	1.07E-14	79.12%	1.9767	22.718 ± 0.165
1.85	1.29555 ± 0.001004	0.53711 ± 0.000765	0.00674 ± 0.000060	0.23635 ± 0.000636	0.000902 ± 0.000029	9.07E-15	80.95%	1.9531	22.449 ± 0.187
1.9	1.02629 ± 0.001162	0.46134 ± 0.000451	0.00601 ± 0.000107	0.18218 ± 0.001077	0.000485 ± 0.000030	7.19E-15	87.52%	1.9474	22.385 ± 0.227
1.95	0.90685 ± 0.001004	0.41629 ± 0.000685	0.00515 ± 0.000030	0.15831 ± 0.000653	0.000341 ± 0.000039	6.35E-15	90.33%	1.9684	22.623 ± 0.325
2	0.78371 ± 0.001542	0.36854 ± 0.000791	0.00450 ± 0.000048	0.13871 ± 0.000735	0.000287 ± 0.000042	5.49E-15	90.64%	1.9280	22.163 ± 0.396
2.05	0.70606 ± 0.001096	0.33738 ± 0.000837	0.00454 ± 0.000090	0.12928 ± 0.000895	0.000214 ± 0.000041	4.94E-15	92.58%	1.9380	22.277 ± 0.421
2.1	0.78763 ± 0.000922	0.37763 ± 0.000632	0.00489 ± 0.000081	0.15416 ± 0.001237	0.000165 ± 0.000018	5.52E-15	95.44%	1.9913	22.886 ± 0.173
2.2	0.79664 ± 0.001419	0.38623 ± 0.000682	0.00480 ± 0.000049	0.16315 ± 0.000759	0.000184 ± 0.000020	5.58E-15	94.88%	1.9577	22.502 ± 0.189
2.3	0.66660 ± 0.000794	0.32355 ± 0.000735	0.00411 ± 0.000070	0.15027 ± 0.000986	0.000118 ± 0.000044	4.67E-15	96.66%	1.9922	22.895 ± 0.462
2.4	0.73815 ± 0.001030	0.36169 ± 0.000668	0.00456 ± 0.000067	0.17773 ± 0.000767	0.000136 ± 0.000018	5.17E-15	96.55%	1.9712	22.656 ± 0.175
2.5	0.69098 ± 0.000768	0.34035 ± 0.000438	0.00439 ± 0.000084	0.16966 ± 0.000802	0.000118 ± 0.000020	4.84E-15	96.99%	1.9698	22.640 ± 0.200
2.7	1.20592 ± 0.001537	0.60031 ± 0.000727	0.00755 ± 0.000064	0.41287 ± 0.001662	0.000244 ± 0.000023	8.45E-15	96.86%	1.9467	22.376 ± 0.136
2.9	0.99064 ± 0.000877	0.49322 ± 0.000920	0.00625 ± 0.000073	0.33238 ± 0.001888	0.000174 ± 0.000021	6.94E-15	97.60%	1.9614	22.544 ± 0.151
3.1	1.13633 ± 0.001125	0.56819 ± 0.000934	0.00706 ± 0.000126	0.51202 ± 0.001687	0.000249 ± 0.000024	7.96E-15	97.26%	1.9465	22.374 ± 0.148
3.3	1.07936 ± 0.000866	0.53781 ± 0.000782	0.00694 ± 0.000059	0.59553 ± 0.001770	0.000244 ± 0.000021	7.56E-15	97.90%	1.9665	22.603 ± 0.135
3.5	0.96052 ± 0.000852	0.48005 ± 0.001005	0.00628 ± 0.000102	0.59270 ± 0.001969	0.000256 ± 0.000018	6.73E-15	97.25%	1.9477	22.387 ± 0.139
3.7	1.05519 ± 0.000858	0.52694 ± 0.001240	0.00695 ± 0.000099	0.77285 ± 0.002297	0.000318 ± 0.000021	7.39E-15	97.18%	1.9481	22.392 ± 0.148
3.9	1.05951 ± 0.001225	0.52646 ± 0.000981	0.00693 ± 0.000136	0.98587 ± 0.002754	0.000356 ± 0.000020	7.42E-15	97.78%	1.9707	22.650 ± 0.139
4.1	0.76260 ± 0.001338	0.37907 ± 0.000563	0.00491 ± 0.000091	0.88642 ± 0.001611	0.000327 ± 0.000022	5.34E-15	97.00%	1.9547	22.468 ± 0.205
4.3	0.43292 ± 0.000722	0.21486 ± 0.000547	0.00270 ± 0.000046	0.57101 ± 0.002052	0.000193 ± 0.000020	3.03E-15	97.81%	1.9746	22.695 ± 0.324
4.5	0.18571 ± 0.000610	0.09171 ± 0.000270	0.00112 ± 0.000042	0.27778 ± 0.000916	0.000066 ± 0.000020	1.30E-15	101.91%	2.0685	23.766 ± 0.752

Note: %P = percentage of total laser output (60W)

Sample NSM-00358-453, SE Pediment mafic, step heating increments for whole rock, 60-80 mesh size

Irradiation filename: au22.4m.whr.3a-3ai

P	40Ar (*±atm)	39Ar (K)	38Ar (Cl±atm)	37Ar (Ca)	36Ar (Atm)	Moles 40Ar*	%Rad	R	Age (Ma)
0.5	0.10626 ± 0.000665	0.00880 ± 0.000201	0.00009 ± 0.000047	0.01705 ± 0.000239	0.000284 ± 0.000016	7.44E-16	22.36%	2.7032	30.997 ± 7.549
0.7	0.44209 ± 0.000766	0.11083 ± 0.000486	0.00172 ± 0.000052	0.21609 ± 0.001029	0.000959 ± 0.000017	3.10E-15	39.98%	1.5971	18.378 ± 0.584
0.8	0.42083 ± 0.000867	0.13630 ± 0.000331	0.00180 ± 0.000055	0.29000 ± 0.001712	0.000740 ± 0.000020	2.95E-15	53.77%	1.6630	19.132 ± 0.521
0.9	0.45088 ± 0.000546	0.15271 ± 0.000503	0.00204 ± 0.000071	0.34751 ± 0.000820	0.000685 ± 0.000018	3.16E-15	61.49%	1.8185	20.912 ± 0.411
1	0.53173 ± 0.000520	0.18045 ± 0.000643	0.00219 ± 0.000052	0.45210 ± 0.001273	0.000775 ± 0.000022	3.72E-15	63.97%	1.8887	21.713 ± 0.439
1.05	0.89019 ± 0.000789	0.31510 ± 0.000485	0.00397 ± 0.000046	0.83876 ± 0.001992	0.001245 ± 0.000023	6.23E-15	66.49%	1.8823	21.640 ± 0.252
1.1	0.62540 ± 0.001014	0.25646 ± 0.000443	0.00317 ± 0.000054	0.59275 ± 0.001905	0.000638 ± 0.000020	4.38E-15	77.72%	1.8987	21.827 ± 0.276
1.15	0.52941 ± 0.000389	0.23088 ± 0.000679	0.00277 ± 0.000039	0.42844 ± 0.001703	0.000399 ± 0.000021	3.71E-15	84.46%	1.9394	22.293 ± 0.325
1.2	0.43460 ± 0.000803	0.19869 ± 0.000534	0.00241 ± 0.000067	0.29007 ± 0.000923	0.000231 ± 0.000017	3.04E-15	89.84%	1.9673	22.612 ± 0.301
1.3	0.67037 ± 0.001171	0.30692 ± 0.000637	0.00358 ± 0.000058	0.35234 ± 0.001494	0.000365 ± 0.000030	4.69E-15	88.29%	1.9300	22.186 ± 0.338
1.4	0.71281 ± 0.001131	0.32935 ± 0.000601	0.00394 ± 0.000052	0.31488 ± 0.001755	0.000313 ± 0.000032	4.99E-15	90.70%	1.9644	22.578 ± 0.336
1.5	0.78661 ± 0.000999	0.36166 ± 0.000714	0.00423 ± 0.000048	0.29545 ± 0.000948	0.000303 ± 0.000035	5.51E-15	91.73%	1.9963	22.942 ± 0.332
1.6	0.96721 ± 0.001146	0.44561 ± 0.000669	0.00539 ± 0.000093	0.33748 ± 0.001585	0.000397 ± 0.000045	6.77E-15	90.78%	1.9715	22.659 ± 0.344
1.7	1.15498 ± 0.000735	0.53655 ± 0.001212	0.00676 ± 0.000106	0.36876 ± 0.001212	0.000418 ± 0.000032	8.09E-15	91.95%	1.9803	22.760 ± 0.209
1.8	1.51702 ± 0.001765	0.70806 ± 0.001070	0.00877 ± 0.000082	0.49412 ± 0.001530	0.000515 ± 0.000033	1.06E-14	92.66%	1.9864	22.829 ± 0.166
1.85	0.60054 ± 0.000619	0.28024 ± 0.000770	0.00335 ± 0.000055	0.16057 ± 0.000682	0.000231 ± 0.000035	4.21E-15	90.88%	1.9483	22.394 ± 0.427
1.9	0.94139 ± 0.001537	0.43748 ± 0.000581	0.00564 ± 0.000095	0.31785 ± 0.001193	0.000338 ± 0.000036	6.59E-15	92.20%	1.9850	22.814 ± 0.286
1.95	0.75429 ± 0.000917	0.35220 ± 0.000810	0.00435 ± 0.000063	0.25393 ± 0.000999	0.000300 ± 0.000036	5.28E-15	91.02%	1.9505	22.419 ± 0.351
2	0.55526 ± 0.000496	0.25828 ± 0.000556	0.00322 ± 0.000040	0.24449 ± 0.001082	0.000253 ± 0.000035	3.89E-15	90.17%	1.9398	22.297 ± 0.470
2.05	0.67599 ± 0.000902	0.31402 ± 0.000509	0.00387 ± 0.000066	0.41261 ± 0.000774	0.000304 ± 0.000038	4.73E-15	91.76%	1.9773	22.726 ± 0.411
2.1	0.74358 ± 0.001176	0.34312 ± 0.000555	0.00448 ± 0.000088	0.32085 ± 0.000778	0.000315 ± 0.000035	5.21E-15	91.07%	1.9751	22.700 ± 0.350
2.2	0.70136 ± 0.001076	0.32799 ± 0.000720	0.00426 ± 0.000084	0.25439 ± 0.000736	0.000259 ± 0.000035	4.91E-15	92.11%	1.9707	22.651 ± 0.369
2.3	0.64561 ± 0.001503	0.29754 ± 0.000730	0.00382 ± 0.000051	0.23299 ± 0.000746	0.000267 ± 0.000037	4.52E-15	90.79%	1.9712	22.656 ± 0.427
2.4	0.25793 ± 0.000545	0.11787 ± 0.000349	0.00161 ± 0.000058	0.07392 ± 0.000551	0.000115 ± 0.000035	1.81E-15	89.24%	1.9538	22.458 ± 1.006
2.5	0.20298 ± 0.000700	0.09371 ± 0.000480	0.00120 ± 0.000042	0.05673 ± 0.000422	0.000096 ± 0.000035	1.42E-15	88.36%	1.9149	22.013 ± 1.295
2.7	0.75191 ± 0.001510	0.34626 ± 0.000618	0.00441 ± 0.000066	0.25050 ± 0.000866	0.000322 ± 0.000031	5.27E-15	90.11%	1.9577	22.502 ± 0.310
2.9	0.24978 ± 0.000608	0.11322 ± 0.000381	0.00132 ± 0.000044	0.08301 ± 0.000797	0.000087 ± 0.000038	1.75E-15	92.51%	2.0421	23.465 ± 1.131
3.1	0.97557 ± 0.000905	0.44122 ± 0.000703	0.00547 ± 0.000061	0.44208 ± 0.001313	0.000458 ± 0.000029	6.83E-15	89.90%	1.9892	22.862 ± 0.225
3.3	0.57041 ± 0.000762	0.25284 ± 0.000670	0.00309 ± 0.000053	0.34091 ± 0.001745	0.000352 ± 0.000030	3.99E-15	86.72%	1.9583	22.508 ± 0.415
3.5	0.35260 ± 0.000838	0.15451 ± 0.000410	0.00184 ± 0.000054	0.20246 ± 0.001056	0.000252 ± 0.000030	2.47E-15	83.62%	1.9102	21.959 ± 0.676
3.7	0.26795 ± 0.000499	0.11462 ± 0.000367	0.00140 ± 0.000052	0.18707 ± 0.000892	0.000186 ± 0.000025	1.88E-15	85.32%	1.9970	22.951 ± 0.748
3.9	0.15851 ± 0.000404	0.06755 ± 0.000240	0.00081 ± 0.000046	0.13254 ± 0.000544	0.000116 ± 0.000028	1.11E-15	85.23%	2.0030	23.019 ± 1.401
4.1	0.09286 ± 0.000453	0.03804 ± 0.000230	0.00044 ± 0.000044	0.07508 ± 0.000540	0.000096 ± 0.000025	6.50E-16	76.03%	1.8588	21.372 ± 2.215
4.3	0.08882 ± 0.000467	0.03754 ± 0.000245	0.00043 ± 0.000051	0.06266 ± 0.000609	0.000092 ± 0.000026	6.22E-16	75.37%	1.7857	20.535 ± 2.323
4.5	0.07100 ± 0.000435	0.02836 ± 0.000200	0.00035 ± 0.000055	0.05847 ± 0.000418	0.000072 ± 0.000026	4.97E-16	76.71%	1.9239	22.115 ± 3.114

Note: %P = percentage of total laser output (60W)

Monitor Data

Sample	%P	40Ar(*+atm)	39Ar(K)	38Ar(Cl+atm)	37Ar(Ca)	36Ar(Atm)	Moles 40Ar*	%Rad	36/37	36/37 error	39/37	39/37 Error
au22.4d.caf.3a.txt	1.8	0.02606 0.00033	0.00415 0.00007	-0.00020 0.00003	5.64565 0.00634	0.001621 0.000019	1.83E-16	182.06%	0.0002715	3.0492E-07	0.00073473	1.2919E-05
au22.4d.caf.4a.txt	1.8	0.00201 0.00023	0.00245 0.00008	-0.00014 0.00003	3.26801 0.00395	0.000939 0.000015	1.41E-17	699.19%	0.0002853	3.4527E-07	0.00074854	2.5268E-05
au22.4d.caf.5a.txt	1.8	0.04347 0.00029	0.00596 0.00016	-0.00023 0.00004	7.74597 0.00595	0.002266 0.000021	3.04E-16	138.93%	0.0002735	2.1044E-07	0.00076923	2.0203E-05
au22.4d.caf.6a.txt	1.8	0.00612 0.00022	0.00208 0.00009	-0.00010 0.00003	2.75795 0.00458	0.000780 0.000016	4.28E-17	327.42%	0.0002753	4.572E-07	0.00075318	3.3273E-05
au22.4d.caf.7a.txt	1.8	0.06736 0.00036	0.00844 0.00010	-0.00030 0.00003	11.21896 0.00631	0.003490 0.000045	4.72E-16	44.81%	0.0002908	1.6399E-07	0.00075263	8.8027E-06
au22.4d.caf.8a.txt	1.8	0.05456 0.00032	0.00244 0.00011	-0.00019 0.00005	3.21104 0.00509	0.001045 0.000015	3.82E-16	55.42%	0.0002680	4.2519E-07	0.00076136	3.3788E-05

Air Standard Data

Date		40Ar(*+atm)	39Ar(K)	38Ar(Cl+atm)	37Ar(Ca)	36Ar(Atm)	Moles 40Ar*	(40/36)m	(40/38)m	M. Fract
10/2/12 19:33	a	12.70549 0.00849	0.00026 0.00015	0.00832 0.00006	0.00026 0.00002	0.0435300 0.0001787	8.90E-14	291.9	1527	0.9969
	aa	13.02344 0.00620	0.00020 0.00021	0.00845 0.00007	0.00031 0.00002	0.0444810 0.0001693	9.12E-14	292.8	1542	0.9977
	b	13.10036 0.00759	0.00022 0.00016	0.00852 0.00010	0.00034 0.00002	0.0447700 0.0001894	9.17E-14	292.6	1537	0.9976
10/3/12 9:36	a	7.55343 0.00259	-0.00035 0.00008	0.00502 0.00006	-0.00012 0.00004	0.0259086 0.0001242	5.29E-14	291.5	1505	0.9967
	b	7.76217 0.00624	-0.00050 0.00010	0.00499 0.00006	-0.00010 0.00006	0.0263810 0.0001520	5.44E-14	294.2	1557	0.9989
	c	13.11682 0.00641	0.00057 0.00012	0.00862 0.00010	0.00020 0.00005	0.0449412 0.0001857	9.19E-14	291.9	1521	0.9969
10/6/12 10:50	b	20.90309 0.01481	0.00392 0.00024	0.01502 0.00012	0.00081 0.00011	0.0718204 0.0002076	1.46E-13	291.0	1392	0.9962

Appendix 26:

ID	Temp (°C)	$^{40}Ar/^{39}Ar$	$^{37}Ar/^{39}Ar$	$^{36}Ar/^{39}Ar$ (x 10^{-3})	$^{39}Ar_K$ (x 10^{-15} mol)	K/Ca	$^{40}Ar^*$ (%)	^{39}Ar (%)	Age (Ma)	±1σ (Ma)
SMAR-1, N2:160, 29.87 mg groundmass concentrate, J=0.000718±0.11%, D=1.00743±0.00124, NM-160, Lab#=53802-01										
A	*625*	*314.4*	*0.2581*	*1034.7*	*8.7*	*2.0*	*2.7*	*6.5*	*11.2*	*2.4*
B	*700*	*24.14*	*0.4013*	*31.47*	*24.1*	*1.3*	*61.6*	*24.4*	*19.17*	*0.14*
C	*750*	*25.64*	*0.5505*	*29.73*	*19.6*	*0.93*	*65.9*	*39.0*	*21.77*	*0.14*
D	800	24.57	0.7061	23.68	14.3	0.72	71.8	49.6	22.70	0.11
E	875	22.79	0.6490	18.69	27.1	0.79	76.0	69.8	22.31	0.10
F	975	25.31	0.7925	27.02	21.9	0.64	68.7	86.1	22.40	0.12
G	1075	39.43	1.536	77.06	8.12	0.33	42.6	92.2	21.64	0.27
H	1250	54.20	4.746	124.3	3.13	0.11	32.9	94.5	23.06	0.62
I	1650	44.60	4.157	93.46	7.37	0.12	38.8	100.0	22.36	0.30
Integrated age ± 2σ		n=9		MSWD=63.06	134.3				20.99	0.47
Plateau ± 2σ steps D-I		n=6		MSWD=3.51	81.9	0.61		61.0	22.42	0.23
SMAR-2, N3:160, 32.92 mg groundmass concentrate, J=0.0007193±0.11%, D=1.00743±0.00124, NM-160, Lab#=53803-01										
A	*625*	*2380.4*	*0.8452*	*7957.5*	*2.84*	*0.60*	*1.2*	*1.4*	*37*	*23*
B	*700*	*26.00*	*0.8950*	*31.01*	*10.9*	*0.57*	*65.0*	*6.8*	*21.82*	*0.16*
C	*750*	*20.86*	*0.9129*	*10.93*	*14.9*	*0.56*	*84.9*	*14.2*	*22.85*	*0.09*
D	*800*	*19.81*	*0.9514*	*6.192*	*14.6*	*0.54*	*91.2*	*21.5*	*23.30*	*0.10*
E	*875*	*19.29*	*0.6501*	*5.277*	*38.1*	*0.78*	*92.2*	*40.4*	*22.94*	*0.08*
F	975	20.40	0.3803	9.759	48.5	1.3	86.0	64.5	22.63	0.07
G	1075	25.24	0.3983	27.65	36.3	1.3	67.8	82.6	22.06	0.12
H	1250	31.83	1.0140	48.92	10.6	0.50	54.8	87.9	22.52	0.19
I	1650	32.38	1.267	50.83	24.4	0.40	53.9	100.0	22.54	0.17
Integrated age ± 2σ		n=9		MSWD=13.98	201.1				22.80	0.75
Plateau ± 2σ steps E-I		n=5		MSWD=10.23	157.9	0.99		78.5	22.64	0.29
TP032-4, G12:160, 9.56 mg adularia, J=0.0007286±0.11%, D=1.0054±0.001, NM-160, Lab#=53743-01										
A	*650*	*160.4*	*0.0018*	*502.2*	*2.82*	*283.1*	*7.5*	*1.4*	*15.7*	*1.2*
B	*800*	*18.21*	*0.0006*	*14.65*	*21.8*	*917.6*	*76.2*	*12.4*	*18.16*	*0.08*
C	*900*	*13.71*	*0.0006*	*2.775*	*25.9*	*815.4*	*94.0*	*25.4*	*16.87*	*0.06*
D	*1000*	*13.21*	*0.0005*	*2.219*	*41.1*	*1111.8*	*95.0*	*46.1*	*16.43*	*0.04*
E	1100	13.29	0.0010	3.161	36.4	521.0	93.0	64.5	16.17	0.05
F	1200	14.16	0.0067	5.266	17.9	76.2	89.0	73.5	16.49	0.06
G	1300	16.17	0.0047	12.36	24.5	107.5	77.4	85.8	16.38	0.07
H	1380	16.48	0.0135	13.23	24.7	37.9	76.5	98.3	16.49	0.08
I	*1450*	*20.77*	*0.0604*	*26.40*	*3.27*	*8.4*	*62.5*	*99.9*	*16.97*	*0.19*
J	*1700*	*101.2*	*5.899*	*198.90*	*0.15*	*0.086*	*42.4*	*100.0*	*55.8*	*3.2*
Integrated age ± 2σ		n=10		MSWD=70.62	198.60				16.66	0.10
Plateau ± 2σ steps D-H		n=5		MSWD=6.77	144.70	481.30		72.8	16.38	0.13

Notes:

Isotopic ratios corrected for blank, radioactive decay, and mass discrimination, not corrected for interfering reactions.

Ages calculated relative to FC-1 Fish Canyon Tuff sanidine interlaboratory standard at 27.84 Ma.

Errors quoted for individual analysis include analytical error only, without interferring reaction or J uncerttainties

Intergrated age calculated by recombining isotopic measurements of all steps

Integrated age error calculated by recombining errors of isotopic measurements of all steps

Plateau age is inverse-variance-weighted mean of selected steps

Plateau age error is inverse-variance-weighted mean error (Taylor, 1982) times square root MSWD where MSWD>1.

Plateau and integrated ages incorporates uncerntainties in interferring reaction corrections and J factors.

Decay constants and isotopic abundances after Steiger and Jaeger (1977)

Italics denote analyses excluded from plateau age calculations

Discrimination = 1.00743 ± 0.00124

Correction factors:

$(^{38}Ar/^{37}Ar)_{Ca}$ = 0.0007 ± 2e-05

$(^{36}Ar/^{37}Ar)_{Ca}$ = 0.00028 ± 2e-06

$(^{38}Ar/^{39}Ar)_{K}$ = 0.01077

$(^{40}Ar/^{39}Ar)_{K}$ = 0.0002 ± 0.0003

Appendix 27:

Sandman deposit step heating increments for 5 single adularia crystals (14-20, 1.2-0.75 mm) of sample: HCN-1
Irradiation filename: au5.1a.ad1.ih1

%P	40Ar(*±atm)	39Ar(K)	38Ar(Cl±atm)	37Ar(Ca)	36Ar(Atm)	%Rad	R	Age (Ma)
3.0	3.64E-15 ± 3.38E-18	1.14E-17 ± 4.38E-19	2.5E-18 ± 2.7E-19	-1.5E-18 ± 5.9E-19	1.24E-17 ± 1.48E-19	0%	-1.2771	-6.45 ± -90
3.3	1.10E-15 ± 6.15E-18	1.61E-16 ± 1.18E-18	7.5E-19 ± 6.5E-20	5.6E-19 ± 3.9E-19	2.01E-18 ± 8.83E-20	46%	3.1759	15.93 ± 0.88
3.6	1.81E-15 ± 4.98E-18	4.08E-16 ± 9.36E-19	1.1E-18 ± 6.9E-20	-3.0E-19 ± 5.0E-19	1.55E-18 ± 9.60E-20	75%	3.3040	16.57 ± 0.36
4.0	1.65E-15 ± 5.31E-18	4.78E-16 ± 1.45E-18	1.3E-18 ± 5.3E-20	-1.3E-19 ± 4.7E-19	2.91E-19 ± 9.23E-20	95%	3.2630	16.37 ± 0.30
4.3	1.58E-15 ± 4.98E-18	4.64E-16 ± 1.49E-18	1.4E-18 ± 3.8E-20	5.7E-20 ± 5.6E-19	3.35E-19 ± 8.15E-20	94%	3.1987	16.05 ± 0.27
4.5	3.97E-15 ± 4.84E-18	1.17E-15 ± 3.14E-18	2.7E-18 ± 4.7E-20	3.5E-19 ± 4.4E-19	9.35E-19 ± 1.72E-19	93%	3.1654	15.88 ± 0.22
4.8	1.23E-14 ± 1.29E-17	3.39E-15 ± 6.30E-18	8.6E-18 ± 1.4E-19	-3.0E-20 ± 4.6E-19	4.78E-18 ± 1.77E-19	89%	3.2123	16.11 ± 0.09
5.0	1.31E-14 ± 1.07E-17	3.56E-15 ± 5.70E-18	8.9E-18 ± 1.0E-19	-8.9E-19 ± 5.0E-19	5.54E-18 ± 1.80E-19	87%	3.2071	16.09 ± 0.08
5.3	9.43E-15 ± 1.11E-17	2.69E-15 ± 8.12E-18	6.2E-18 ± 7.2E-20	1.3E-19 ± 4.7E-19	2.42E-18 ± 1.64E-19	92%	3.2343	16.22 ± 0.11
5.5	1.02E-14 ± 1.35E-17	2.95E-15 ± 8.41E-18	6.1E-18 ± 7.8E-20	9.7E-20 ± 4.4E-19	2.59E-18 ± 9.99E-20	93%	3.2121	16.11 ± 0.07
5.8	1.56E-14 ± 1.50E-17	4.61E-15 ± 9.84E-18	1.0E-17 ± 7.5E-20	-1.1E-18 ± 5.8E-19	2.19E-18 ± 1.00E-19	96%	3.2352	16.23 ± 0.05
6.0	5.39E-16 ± 2.84E-18	1.58E-16 ± 1.03E-18	2.9E-19 ± 3.4E-20	-7.5E-19 ± 4.0E-19	4.43E-20 ± 6.96E-20	98%	3.3345	16.72 ± 0.67
6.5	6.30E-16 ± 3.20E-18	1.82E-16 ± 1.10E-18	4.4E-19 ± 4.3E-20	-6.5E-19 ± 3.6E-19	3.70E-20 ± 7.92E-20	98%	3.3938	17.02 ± 0.66
7.0	2.76E-16 ± 3.07E-18	7.99E-17 ± 7.49E-19	1.7E-19 ± 4.0E-20	2.5E-20 ± 4.2E-19	7.48E-20 ± 7.36E-20	92%	3.1721	15.91 ± 1.39
8.0	1.89E-16 ± 3.02E-18	5.58E-17 ± 7.17E-19	-5.2E-20 ± -2.4E-20	-1.1E-18 ± 4.3E-19	3.96E-20 ± 6.37E-20	94%	3.1826	15.97 ± 1.73
9.0	1.90E-16 ± 3.18E-18	5.48E-17 ± 5.27E-19	-3.5E-19 ± -4.0E-19	-4.6E-19 ± 3.7E-19	4.70E-20 ± 6.96E-20	93%	3.2073	16.09 ± 1.91
10.0	3.37E-17 ± 2.03E-18	8.76E-18 ± 3.62E-19	-5.3E-19 ± -2.2E-19	-5.5E-20 ± 3.3E-19	2.64E-20 ± 8.13E-20	77%	2.9501	14.80 ± 13
11.0	1.13E-17 ± 2.12E-18	2.88E-18 ± 3.86E-19	-3.6E-19 ± -2.1E-19	9.5E-20 ± 4.6E-19	-2.35E-19 ± -1.17E-19	715%	28.0900	136.26 ± 60
12.0	1.27E-17 ± 2.25E-18	2.37E-18 ± 3.75E-19	-4.9E-19 ± -1.9E-19	-3.5E-19 ± 4.2E-19	-1.43E-19 ± -1.33E-19	432%	23.0992	112.79 ± 82
14.0	1.83E-16 ± 2.34E-18	1.57E-18 ± 3.48E-19	-2.1E-19 ± -2.0E-19	5.7E-19 ± 4.1E-19	5.35E-19 ± 8.63E-20	13%	15.6469	77.17 ± 186

Note: %P = percentage of total laser output (60 w).

Irradiation filename: au5.1a.ad1.ih2

%P	40Ar(*±atm)	39Ar(K)	38Ar(Cl±atm)	37Ar(Ca)	36Ar(Atm)	%Rad	R	Age (Ma)
3.0	1.07E-15 ± 3.91E-18	4.63E-18 ± 4.01E-19	7.6E-19 ± 1.6E-19	2.5E-19 ± 3.4E-19	3.85E-18 ± 1.21E-19	-7%	-14.9832	-77.12 ± -154
3.3	1.12E-15 ± 3.86E-18	1.23E-16 ± 8.68E-19	8.8E-19 ± 8.6E-20	1.0E-19 ± 5.3E-19	2.84E-18 ± 1.25E-19	25%	2.2698	11.40 ± 1.57
3.6	1.44E-15 ± 3.49E-18	4.08E-16 ± 1.50E-18	1.2E-18 ± 5.0E-20	9.0E-19 ± 5.2E-19	8.11E-19 ± 1.19E-19	83%	2.9324	14.72 ± 0.44
4.0	1.50E-15 ± 6.75E-18	4.49E-16 ± 1.58E-18	1.4E-18 ± 5.0E-20	2.5E-19 ± 3.1E-19	1.46E-19 ± 1.40E-19	97%	3.2366	16.24 ± 0.47
4.3	8.09E-15 ± 6.48E-18	2.34E-15 ± 3.28E-18	6.6E-18 ± 1.1E-19	7.3E-19 ± 4.0E-19	2.01E-18 ± 1.62E-19	93%	3.2042	16.07 ± 0.11
4.5	1.50E-14 ± 1.63E-17	4.11E-15 ± 6.46E-18	1.0E-17 ± 1.1E-19	-1.7E-19 ± 4.4E-19	6.47E-18 ± 1.81E-19	87%	3.1853	15.98 ± 0.07
4.8	7.89E-15 ± 5.62E-18	2.30E-15 ± 4.91E-18	5.8E-18 ± 9.1E-20	1.0E-19 ± 4.2E-19	2.03E-18 ± 1.33E-19	92%	3.1603	15.85 ± 0.09
5.0	8.07E-15 ± 9.30E-18	2.33E-15 ± 3.52E-18	5.6E-18 ± 1.3E-19	1.4E-19 ± 4.4E-19	2.08E-18 ± 1.32E-19	92%	3.1983	16.04 ± 0.09
5.3	2.14E-15 ± 5.15E-18	6.17E-16 ± 1.50E-18	1.9E-18 ± 5.3E-20	2.7E-19 ± 3.7E-19	5.26E-19 ± 1.87E-19	93%	3.2121	16.11 ± 0.45
5.5	4.94E-16 ± 4.67E-18	1.43E-16 ± 7.53E-19	4.4E-20 ± 6.9E-21	3.0E-19 ± 3.9E-19	1.53E-19 ± 7.16E-20	91%	3.1469	15.79 ± 0.77
5.8	3.35E-16 ± 3.89E-18	9.69E-17 ± 1.19E-18	2.0E-19 ± 3.1E-20	1.9E-19 ± 4.4E-19	5.16E-20 ± 8.12E-20	95%	3.2972	16.54 ± 1.28
6.0	6.76E-17 ± 2.53E-18	1.78E-17 ± 4.14E-19	1.1E-19 ± 6.9E-20	-2.0E-19 ± 4.7E-19	3.92E-20 ± 7.57E-20	83%	3.1358	15.73 ± 6.35
6.5	2.09E-17 ± 2.73E-18	2.08E-18 ± 3.00E-19	-1.0E-21 ± -8.7E-21	-2.5E-19 ± 3.7E-19	-2.77E-19 ± -1.48E-19	492%	49.3967	233.17 ± 103.3
7.0	3.28E-17 ± 2.92E-18	3.61E-18 ± 2.53E-19	-7.4E-20 ± -3.8E-19	1.7E-19 ± 4.4E-19	2.54E-20 ± 7.50E-20	77%	7.0108	34.99 ± 31.09
8.0	2.12E-17 ± 2.36E-18	2.50E-18 ± 3.38E-19	2.4E-19 ± 1.3E-19	-1.6E-19 ± 4.1E-19	3.80E-20 ± 7.46E-20	47%	3.9613	19.85 ± 44.85
9.0	7.15E-19 ± 1.51E-18	1.07E-19 ± 2.99E-19	-2.0E-19 ± -2.2E-19	7.9E-19 ± 4.4E-19	5.00E-20 ± 6.86E-20	-1966%	-131.7752	-827.99 ± -2712.
10.0	2.17E-18 ± 2.24E-18	6.34E-19 ± 3.35E-19	-1.7E-19 ± -1.9E-19	-7.8E-20 ± 5.0E-19	-7.15E-20 ± -7.36E-20	1074%	36.7539	176.30 ± 185.9
11.0	1.15E-19 ± 1.94E-18	-9.15E-19 ± -4.02E-19	-2.9E-19 ± -1.9E-19	2.3E-19 ± 3.5E-19	-2.91E-19 ± -1.25E-19	74925%	-94.2096	-550.87 ± -337
12.0	1.33E-17 ± 1.83E-18	6.26E-19 ± 3.16E-19	-2.6E-19 ± -1.9E-19	5.8E-19 ± 4.9E-19	-8.17E-20 ± -6.85E-20	282%	59.8454	278.85 ± 183
14.0	2.98E-16 ± 2.65E-18	5.29E-19 ± 3.19E-19	-1.7E-19 ± -1.9E-19	2.9E-19 ± 4.7E-19	8.64E-19 ± 8.17E-20	14%	79.8724	363.30 ± 2041

Appendix 27 (continued):

Irradiation filename: au5.1a.adl.ih3

%P	40Ar(*±atm)	39Ar(K)	38Ar(Cl±atm)	37Ar(Ca)	36Ar(Atm)	%Rad	R	Age (Ma)
3.0	1.58E-15 ± 4.96E-18	2.17E-18 ± 4.14E-19	7.6E-19 ± 2.3E-19	2.4E-19 ± 4.4E-19	5.26E-18 ± 1.30E-19	2%	11.2053	55.60 ± 9
3.3	9.66E-16 ± 4.29E-18	1.66E-17 ± 4.22E-19	7.3E-19 ± 1.5E-19	-5.0E-21 ± 4.3E-19	3.04E-18 ± 8.48E-20	7%	4.0022	20.05 ± 12
3.6	1.93E-15 ± 6.71E-18	2.86E-16 ± 1.23E-18	1.2E-18 ± 6.5E-20	2.6E-19 ± 5.5E-19	2.79E-18 ± 2.13E-19	57%	3.8886	19.49 ± 1.12
4.0	1.98E-15 ± 5.23E-18	3.92E-16 ± 1.97E-18	1.3E-18 ± 5.5E-20	1.5E-19 ± 4.6E-19	2.24E-18 ± 7.73E-20	67%	3.3681	16.89 ± 0.33
4.3	4.89E-16 ± 4.32E-18	1.14E-16 ± 5.03E-19	2.5E-19 ± 3.8E-20	8.7E-19 ± 4.8E-19	4.78E-19 ± 8.72E-20	71%	3.0387	15.25 ± 1.15
4.5	1.31E-15 ± 5.09E-18	3.04E-16 ± 8.22E-19	1.1E-18 ± 5.4E-20	7.5E-19 ± 4.4E-19	1.48E-18 ± 1.37E-19	67%	2.8536	14.32 ± 0.68
4.8	2.89E-15 ± 3.96E-18	7.88E-16 ± 2.74E-18	2.3E-18 ± 5.5E-20	-3.6E-19 ± 4.1E-19	1.54E-18 ± 1.25E-19	84%	3.0817	15.46 ± 0.24
5.0	3.25E-15 ± 2.81E-18	9.26E-16 ± 2.21E-18	2.1E-18 ± 7.3E-20	-7.3E-20 ± 4.7E-19	1.27E-18 ± 1.32E-19	88%	3.0999	15.55 ± 0.22
5.3	8.95E-15 ± 1.02E-17	2.42E-15 ± 7.17E-18	6.7E-18 ± 5.1E-20	-2.4E-19 ± 5.1E-19	4.29E-18 ± 1.51E-19	86%	3.1760	15.93 ± 0.11
5.5	2.15E-14 ± 1.58E-17	5.77E-15 ± 9.92E-18	1.7E-17 ± 1.6E-19	-4.2E-19 ± 5.2E-19	9.70E-18 ± 1.74E-19	87%	3.2252	16.18 ± 0.06
5.8	7.20E-15 ± 5.77E-18	2.07E-15 ± 4.60E-18	5.3E-18 ± 1.0E-19	7.1E-20 ± 4.9E-19	1.66E-18 ± 8.88E-20	93%	3.2346	16.23 ± 0.08
6.0	1.25E-15 ± 4.30E-18	3.56E-16 ± 1.84E-18	1.4E-18 ± 6.0E-20	-2.7E-19 ± 4.4E-19	3.12E-19 ± 1.01E-19	93%	3.2592	16.35 ± 0.43
6.5	2.49E-15 ± 8.55E-18	7.13E-16 ± 2.49E-18	1.6E-18 ± 5.1E-20	1.2E-19 ± 5.9E-19	7.41E-19 ± 8.49E-20	91%	3.1892	16.00 ± 0.20
7.0	4.35E-17 ± 1.66E-18	1.17E-17 ± 3.59E-19	1.4E-19 ± 1.1E-19	-4.0E-19 ± 5.1E-19	8.78E-20 ± 9.20E-20	40%	1.4982	7.53 ± 11
8.0	2.01E-17 ± 1.79E-18	9.40E-18 ± 3.27E-19	-2.5E-19 ± -3.4E-19	-1.6E-19 ± 5.1E-19	-6.71E-20 ± -7.99E-20	199%	4.2490	21.28 ± 12
9.0	5.99E-18 ± 2.05E-18	1.48E-18 ± 2.91E-19	1.4E-19 ± 2.0E-19	4.8E-20 ± 4.9E-19	8.40E-20 ± 7.76E-20	-314%	-12.7128	-65.22 ± -81
10.0	2.98E-18 ± 1.55E-18	1.16E-18 ± 3.70E-19	-6.8E-20 ± -2.3E-19	4.0E-19 ± 4.7E-19	1.11E-19 ± 8.86E-20	-998%	-25.6109	-133.90 ± -127

Irradiation filename: au5.1a.adl.ih4

%P	40Ar(*±atm)	39Ar(K)	38Ar(Cl±atm)	37Ar(Ca)	36Ar(Atm)	%Rad	R	Age (Ma)
3.0	6.66E-16 ± 4.41E-18	7.80E-19 ± 3.32E-19	1.4E-19 ± 1.7E-19	2.5E-19 ± 4.7E-19	2.06E-18 ± 2.05E-19	9%	74.4690	340.90 ± 2285
3.3	2.50E-16 ± 3.00E-18	1.25E-17 ± 4.56E-19	-7.6E-20 ± -3.3E-19	1.0E-19 ± 5.4E-19	1.01E-18 ± 8.37E-20	-19%	-3.7349	-18.92 ± -12
3.6	2.48E-16 ± 1.93E-18	4.51E-17 ± 5.07E-19	-2.5E-19 ± -2.5E-19	-2.9E-21 ± 4.7E-19	3.88E-19 ± 8.69E-20	54%	2.9538	14.82 ± 2.89
4.0	1.08E-15 ± 2.21E-18	3.17E-16 ± 1.18E-18	4.3E-19 ± 2.4E-20	9.1E-20 ± 3.6E-19	1.42E-19 ± 7.85E-20	96%	3.2550	16.33 ± 0.37
4.3	5.75E-16 ± 3.67E-18	1.76E-16 ± 1.57E-18	9.0E-19 ± 8.5E-20	-2.6E-20 ± 4.6E-19	-5.81E-20 ± -1.17E-19	103%	3.3699	16.90 ± 1.00
4.5	7.77E-16 ± 3.78E-18	2.38E-16 ± 1.49E-18	3.9E-19 ± 2.6E-20	-5.0E-19 ± 6.1E-19	4.98E-20 ± 1.92E-19	98%	3.2070	16.09 ± 1.20
4.8	1.43E-15 ± 4.25E-18	4.30E-16 ± 1.01E-18	8.3E-19 ± 5.5E-20	-4.5E-19 ± 4.4E-19	1.71E-19 ± 1.46E-19	96%	3.1946	16.03 ± 0.51
5.0	4.64E-15 ± 6.10E-18	1.39E-15 ± 2.12E-18	2.3E-18 ± 4.7E-20	-3.2E-19 ± 4.5E-19	4.97E-19 ± 1.39E-19	97%	3.2236	16.17 ± 0.15
5.3	1.14E-14 ± 8.80E-18	3.36E-15 ± 1.26E-17	7.0E-18 ± 5.2E-20	2.3E-19 ± 4.5E-19	1.70E-18 ± 1.78E-19	96%	3.2276	16.19 ± 0.10
5.5	1.17E-14 ± 8.80E-18	3.52E-15 ± 7.00E-18	7.7E-18 ± 7.4E-20	2.3E-19 ± 3.8E-19	1.62E-18 ± 9.51E-20	96%	3.1906	16.01 ± 0.05
5.8	1.17E-15 ± 5.35E-18	3.51E-16 ± 8.28E-19	7.0E-19 ± 3.8E-20	-6.6E-20 ± 4.2E-19	1.70E-19 ± 8.32E-20	96%	3.2009	16.06 ± 0.36
6.0	3.64E-16 ± 2.11E-18	1.05E-16 ± 9.21E-19	3.9E-19 ± 6.5E-20	1.7E-19 ± 3.4E-19	-5.42E-20 ± -8.43E-20	104%	3.6244	18.17 ± 1.21
6.5	7.57E-18 ± 2.12E-18	1.50E-18 ± 4.70E-19	4.1E-19 ± 1.8E-19	-3.5E-19 ± 4.2E-19	-8.96E-20 ± -9.11E-20	450%	22.7664	111.22 ± 92
7.0	2.72E-17 ± 2.58E-18	6.74E-18 ± 4.21E-19	6.1E-20 ± 1.0E-19	-3.4E-19 ± 3.9E-19	-1.29E-19 ± -9.06E-20	240%	9.6663	48.06 ± 19
8.0	7.49E-18 ± 2.08E-18	7.54E-19 ± 3.71E-19	2.4E-19 ± 1.9E-19	1.8E-19 ± 4.0E-19	-4.52E-20 ± -8.42E-20	279%	27.6782	134.34 ± 167
9.0	7.24E-18 ± 1.90E-18	1.80E-18 ± 4.92E-19	1.6E-19 ± 1.9E-19	-3.2E-19 ± 3.5E-19	-1.17E-19 ± -8.53E-20	578%	23.2122	113.33 ± 73
10.0	9.97E-18 ± 2.29E-18	-3.40E-19 ± -4.38E-19	-6.7E-21 ± -1.3E-19	-4.0E-19 ± 3.8E-19	-3.44E-19 ± -1.42E-19	1121%	-329.1044	-4538.78 ± -5618

Irradiation filename: au5.1a.adl.ih5

%P	40Ar(*±atm)	39Ar(K)	38Ar(Cl±atm)	37Ar(Ca)	36Ar(Atm)	%Rad	R	Age (Ma)
3.0	1.16E-15 ± 3.57E-18	4.26E-18 ± 3.49E-19	7.7E-19 ± 2.1E-19	-8.3E-19 ± 3.8E-19	4.07E-18 ± 1.51E-19	-3%	-9.4739	-48.38 ± -173
3.3	4.26E-16 ± 3.41E-18	8.81E-17 ± 8.09E-19	4.3E-19 ± 5.5E-20	5.1E-21 ± 4.8E-19	5.74E-19 ± 1.50E-19	60%	2.9068	14.59 ± 2.54
3.6	6.43E-16 ± 4.31E-18	1.65E-16 ± 8.15E-19	1.7E-19 ± 1.9E-20	1.6E-19 ± 4.9E-19	3.91E-19 ± 1.49E-19	82%	3.1958	16.03 ± 1.35
4.0	3.21E-15 ± 6.72E-18	9.35E-16 ± 3.31E-18	1.8E-18 ± 5.0E-20	-5.1E-19 ± 4.3E-19	6.90E-19 ± 1.42E-19	94%	3.2185	16.15 ± 0.24
4.3	8.16E-15 ± 6.66E-18	2.34E-15 ± 4.74E-18	5.9E-18 ± 1.2E-19	-1.3E-18 ± 5.7E-19	2.25E-18 ± 1.61E-19	92%	3.2007	16.06 ± 0.11
4.5	2.02E-14 ± 2.01E-17	6.02E-15 ± 1.01E-17	1.5E-17 ± 1.2E-19	4.1E-19 ± 4.2E-19	2.65E-18 ± 1.11E-19	96%	3.2254	16.18 ± 0.04
4.8	3.55E-15 ± 4.17E-18	1.08E-15 ± 4.72E-18	2.1E-18 ± 4.4E-20	-2.5E-19 ± 3.9E-19	3.49E-19 ± 8.42E-20	97%	3.1935	16.02 ± 0.14
5.0	4.10E-16 ± 2.89E-18	1.21E-16 ± 1.05E-18	-8.1E-20 ± -1.7E-20	5.3E-19 ± 3.5E-19	-1.69E-19 ± -1.12E-19	112%	3.7820	18.96 ± 1.38
5.3	1.83E-16 ± 2.76E-18	5.44E-17 ± 7.19E-19	-4.1E-19 ± -6.2E-19	1.7E-19 ± 3.3E-19	-1.38E-19 ± -1.17E-19	122%	4.1078	20.58 ± 3.21
5.5	8.98E-17 ± 1.99E-18	2.69E-17 ± 5.03E-19	-7.5E-20 ± -8.3E-20	1.3E-19 ± 3.4E-19	-7.54E-20 ± -7.73E-20	125%	4.1659	20.87 ± 4.28
5.8	2.40E-17 ± 2.04E-18	6.69E-18 ± 3.47E-19	-2.0E-19 ± -3.1E-19	3.2E-19 ± 4.0E-19	-2.56E-19 ± -1.38E-19	416%	14.9177	73.64 ± 30.38
6.0	8.97E-17 ± 2.66E-18	2.41E-17 ± 3.53E-19	4.3E-20 ± 2.4E-20	-4.1E-19 ± 3.8E-19	-3.22E-20 ± -8.67E-20	111%	4.1162	20.62 ± 5.36
6.5	3.93E-17 ± 2.51E-18	1.01E-17 ± 3.89E-19	-5.1E-20 ± -2.4E-19	-5.4E-19 ± 2.7E-19	-3.45E-19 ± -1.08E-19	359%	14.0192	69.29 ± 15
7.0	1.84E-17 ± 2.11E-18	5.09E-18 ± 2.49E-19	4.7E-20 ± 7.7E-20	-2.2E-19 ± 4.2E-19	-5.61E-22 ± -8.28E-20	101%	3.6509	18.30 ± 24
8.0	1.12E-17 ± 1.71E-18	1.28E-18 ± 3.01E-19	-6.6E-20 ± -2.0E-19	-3.4E-19 ± 2.8E-19	-3.74E-19 ± -1.45E-19	1082%	95.1714	425.26 ± 175
9.0	8.19E-18 ± 2.46E-18	1.03E-18 ± 3.87E-19	-3.2E-19 ± -1.8E-19	-9.4E-19 ± 2.5E-19	-4.46E-20 ± -7.88E-20	261%	20.8243	101.99 ± 115

Appendix 28:

Ten Mile deposit step heating increments for 5 single adularia crystals (14-20 mesh size, 1.2-0.75 mm) of sample: HCN-4
Irradiation filename: au5.1h.adl.ih1

%P	40Ar(*±atm)	39Ar(K)	38Ar(Cl±atm)	37Ar(Ca)	36Ar(Atm)	%Rad	R	Age (Ma)
3.0	3.30E-15 ± 4.23E-18	3.86E-18 ± 4.06E-19	2.0E-18 ± 1.5E-19	-6.9E-19 ± 3.3E-19	1.11E-17 ± 1.58E-19	0%	2.3137	11.62 ± 640
3.3	3.19E-15 ± 5.21E-18	2.28E-17 ± 6.49E-19	1.8E-18 ± 1.6E-19	-4.5E-19 ± 4.2E-19	1.02E-17 ± 1.26E-19	5%	7.4235	37.02 ± 28
3.6	1.88E-15 ± 2.69E-18	1.19E-16 ± 7.25E-19	1.2E-18 ± 7.9E-20	2.8E-19 ± 4.0E-19	4.19E-18 ± 1.98E-19	34%	5.3753	26.88 ± 2.54
4.0	2.02E-15 ± 4.68E-18	3.19E-16 ± 1.23E-18	1.1E-18 ± 5.5E-20	-1.9E-19 ± 4.3E-19	2.94E-18 ± 1.05E-19	57%	3.6060	18.08 ± 0.51
4.3	1.04E-15 ± 1.68E-18	2.02E-16 ± 1.66E-18	4.9E-19 ± 4.5E-20	-1.0E-20 ± 3.6E-19	1.14E-18 ± 9.53E-20	67%	3.4610	17.36 ± 0.74
4.5	1.34E-15 ± 3.96E-18	2.42E-16 ± 1.45E-18	1.0E-18 ± 5.9E-20	1.2E-19 ± 3.2E-19	1.60E-18 ± 9.21E-20	65%	3.5858	17.98 ± 0.60
4.8	8.89E-16 ± 3.59E-18	2.25E-16 ± 2.51E-18	5.3E-19 ± 3.8E-20	3.4E-19 ± 4.3E-19	3.29E-19 ± 8.39E-20	89%	3.5184	17.64 ± 0.60
5.0	1.10E-15 ± 4.13E-18	2.41E-16 ± 1.26E-18	1.2E-18 ± 6.8E-20	4.5E-19 ± 4.5E-19	9.86E-19 ± 9.27E-20	74%	3.3659	16.88 ± 0.59
5.3	3.23E-15 ± 3.78E-18	7.71E-16 ± 2.18E-18	2.7E-18 ± 6.1E-20	4.4E-19 ± 4.4E-19	2.27E-18 ± 8.65E-20	79%	3.3143	16.62 ± 0.18
5.5	1.01E-14 ± 9.27E-18	2.78E-15 ± 2.71E-18	7.1E-18 ± 8.3E-20	-1.3E-19 ± 4.6E-19	2.98E-18 ± 1.03E-19	91%	3.3229	16.67 ± 0.06
5.8	1.91E-14 ± 2.07E-17	5.63E-15 ± 1.55E-17	1.3E-17 ± 1.4E-19	1.1E-19 ± 4.0E-19	1.63E-18 ± 1.00E-19	97%	3.2967	16.54 ± 0.06
6.0	1.54E-14 ± 1.15E-17	4.61E-15 ± 8.85E-18	1.2E-17 ± 1.1E-19	-4.8E-19 ± 3.4E-19	8.99E-19 ± 8.33E-20	98%	3.2815	16.46 ± 0.04
6.5	7.57E-15 ± 8.82E-18	2.27E-15 ± 2.61E-18	4.5E-18 ± 6.2E-20	-4.1E-19 ± 3.5E-19	2.81E-19 ± 7.93E-20	99%	3.2985	16.54 ± 0.06
7.0	1.94E-15 ± 3.32E-18	5.77E-16 ± 2.75E-18	7.5E-19 ± 3.3E-20	-1.3E-19 ± 3.5E-19	2.09E-19 ± 7.51E-20	97%	3.2547	16.33 ± 0.21
8.0	1.35E-15 ± 3.43E-18	4.00E-16 ± 3.34E-18	4.9E-19 ± 2.3E-20	-8.2E-20 ± 3.6E-19	8.42E-20 ± 7.71E-20	98%	3.3041	16.57 ± 0.32
9.0	1.95E-15 ± 5.89E-18	5.86E-16 ± 3.54E-18	1.5E-18 ± 5.4E-20	-2.9E-19 ± 4.2E-19	3.76E-20 ± 8.97E-20	99%	3.3115	16.61 ± 0.25

Irradiation filename: au5.1h.adl.ih2

%P	40Ar(*±atm)	39Ar(K)	38Ar(Cl±atm)	37Ar(Ca)	36Ar(Atm)	%Rad	R	Age (Ma)
3.0	9.51E-16 ± 2.68E-18	1.66E-19 ± 4.10E-19	1.2E-18 ± 2.9E-19	-6.9E-19 ± 4.0E-19	3.11E-18 ± 8.97E-20	3%	196.9579	790.78 ± 7936
3.3	4.08E-15 ± 7.99E-18	6.26E-18 ± 3.49E-19	3.2E-18 ± 3.2E-19	-3.0E-19 ± 3.4E-19	1.36E-17 ± 1.75E-19	1%	7.1064	35.46 ± 258
3.6	1.79E-15 ± 4.37E-18	6.84E-17 ± 1.36E-18	1.8E-18 ± 2.1E-19	-5.1E-19 ± 3.3E-19	5.19E-18 ± 1.20E-19	14%	3.7373	18.73 ± 4.33
4.0	1.37E-15 ± 2.72E-18	2.57E-16 ± 1.75E-18	1.4E-18 ± 1.1E-19	-4.8E-19 ± 3.8E-19	1.71E-18 ± 9.43E-20	63%	3.3759	16.93 ± 0.58
4.3	1.04E-15 ± 5.16E-18	1.54E-16 ± 7.69E-19	6.0E-19 ± 1.1E-19	-7.7E-19 ± 4.5E-19	1.47E-18 ± 1.73E-19	58%	3.8997	19.54 ± 1.68
4.5	1.60E-14 ± 2.12E-17	4.16E-15 ± 4.77E-18	1.2E-17 ± 1.3E-19	5.6E-19 ± 4.4E-19	8.04E-18 ± 1.31E-19	85%	3.2781	16.44 ± 0.06
4.8	1.75E-14 ± 1.57E-17	5.28E-15 ± 6.13E-18	1.2E-17 ± 6.5E-20	4.3E-19 ± 4.4E-19	1.03E-18 ± 8.71E-20	98%	3.2636	16.37 ± 0.03
5.0	1.21E-14 ± 9.48E-18	3.66E-15 ± 8.29E-18	8.6E-18 ± 6.7E-20	3.9E-19 ± 4.3E-19	2.64E-19 ± 7.64E-20	99%	3.2892	16.50 ± 0.05
5.3	3.57E-15 ± 5.45E-18	1.08E-15 ± 3.09E-18	2.4E-18 ± 4.0E-20	2.9E-20 ± 3.9E-19	4.42E-20 ± 8.69E-20	100%	3.2934	16.52 ± 0.13
5.5	1.50E-15 ± 2.69E-18	4.50E-16 ± 2.93E-18	7.9E-19 ± 2.3E-20	1.2E-19 ± 3.6E-19	-8.97E-20 ± -7.58E-20	102%	3.3922	17.01 ± 0.27
5.8	1.24E-15 ± 3.62E-18	3.66E-16 ± 1.80E-18	9.3E-19 ± 4.7E-20	1.8E-19 ± 4.3E-19	-5.46E-20 ± -7.37E-20	101%	3.4145	17.12 ± 0.31
6.0	6.17E-16 ± 5.11E-18	1.85E-16 ± 9.80E-19	2.0E-19 ± 1.7E-20	-8.8E-21 ± 4.0E-19	-3.02E-20 ± -7.22E-20	101%	3.3880	16.99 ± 0.60
6.5	8.43E-16 ± 4.48E-18	2.49E-16 ± 1.52E-18	4.2E-19 ± 3.5E-20	-2.2E-19 ± 3.9E-19	-2.39E-20 ± -8.07E-20	101%	3.4113	17.11 ± 0.50
7.0	4.63E-16 ± 4.71E-18	1.38E-16 ± 9.96E-19	-4.2E-20 ± -6.6E-21	-5.7E-19 ± 4.1E-19	-2.53E-19 ± -1.02E-19	116%	3.8842	19.47 ± 1.11
8.0	7.72E-16 ± 4.89E-18	2.27E-16 ± 1.17E-18	3.3E-19 ± 2.9E-20	-3.9E-20 ± 3.6E-19	-5.00E-20 ± -7.56E-20	102%	3.4576	17.34 ± 0.51
9.0	4.70E-16 ± 2.68E-18	1.43E-16 ± 1.23E-18	1.9E-20 ± 2.2E-21	-4.2E-19 ± 3.5E-19	-8.42E-21 ± -8.33E-20	101%	3.3012	16.56 ± 0.88

Irradiation filename: au5.1h.adl.ih3

%P	40Ar(*±atm)	39Ar(K)	38Ar(Cl±atm)	37Ar(Ca)	36Ar(Atm)	%Rad	R	Age (Ma)
3.0	1.23E-15 ± 3.42E-18	2.62E-18 ± 3.39E-19	9.6E-19 ± 1.2E-19	5.6E-19 ± 4.3E-19	4.22E-18 ± 1.06E-19	-1%	-5.6097	-28.49 ± -444
3.3	8.08E-16 ± 3.77E-18	4.59E-17 ± 4.85E-19	5.9E-19 ± 9.5E-20	7.8E-19 ± 4.9E-19	2.21E-18 ± 1.10E-19	19%	3.3909	17.01 ± 3.76
3.6	1.20E-15 ± 2.58E-18	2.66E-16 ± 2.23E-18	6.6E-19 ± 4.5E-20	3.2E-19 ± 4.3E-19	1.10E-18 ± 9.37E-20	73%	3.2899	16.50 ± 0.56
4.0	1.65E-14 ± 1.47E-17	4.67E-15 ± 7.83E-18	1.1E-17 ± 1.0E-19	-1.0E-19 ± 5.0E-19	4.28E-18 ± 1.15E-19	92%	3.2577	16.34 ± 0.05
4.3	9.17E-15 ± 9.73E-18	2.76E-15 ± 5.99E-18	6.1E-18 ± 8.7E-20	6.5E-19 ± 4.5E-19	1.74E-19 ± 1.43E-19	99%	3.3001	16.55 ± 0.09
4.5	2.09E-15 ± 4.96E-18	6.20E-16 ± 1.67E-18	1.5E-18 ± 5.9E-20	-5.8E-19 ± 3.7E-19	-3.68E-20 ± -7.39E-20	101%	3.3913	17.01 ± 0.19
4.8	6.91E-16 ± 2.70E-18	2.08E-16 ± 1.05E-18	2.5E-19 ± 2.1E-20	-7.4E-19 ± 3.0E-19	-6.18E-20 ± -7.80E-20	103%	3.4070	17.09 ± 0.57
5.0	4.18E-16 ± 2.37E-18	1.22E-16 ± 9.79E-19	-4.0E-19 ± -1.1E-19	-1.9E-20 ± 4.4E-19	-4.93E-20 ± -7.66E-20	103%	3.5326	17.71 ± 0.94
5.3	5.62E-17 ± 2.46E-18	1.62E-17 ± 3.48E-19	1.2E-19 ± 1.0E-19	-5.1E-19 ± 3.4E-19	-1.23E-20 ± -8.18E-20	106%	3.7019	18.56 ± 7.55
5.5	5.77E-18 ± 1.81E-18	1.29E-19 ± 3.57E-19	6.0E-21 ± 1.6E-19	-8.3E-19 ± 4.1E-19	-1.00E-19 ± -7.69E-20	613%	274.8279	1027.65 ± 2516
5.8	4.91E-18 ± 1.75E-18	-8.98E-20 ± -2.80E-19	4.9E-20 ± 2.1E-19	-4.8E-19 ± 3.8E-19	3.73E-20 ± 8.34E-20	-124%	68.7209	316.77 ± 2312
6.0	7.96E-19 ± 2.26E-18	8.72E-20 ± 3.07E-19	-1.1E-19 ± -2.0E-19	3.7E-19 ± 3.5E-19	1.57E-19 ± 1.99E-19	-5747%	-525.8438	n/a ± n/a
6.5	3.42E-18 ± 1.97E-18	1.14E-19 ± 2.31E-19	-1.1E-19 ± -2.2E-19	3.9E-19 ± 4.4E-19	4.35E-19 ± 1.28E-19	-3661%	-1096.3408	n/a ± n/a
7.0	1.51E-18 ± 2.15E-18	-9.21E-19 ± -4.27E-19	-4.0E-20 ± -1.9E-19	3.5E-19 ± 4.5E-19	5.05E-19 ± 1.33E-19	-9807%	160.3184	667.56 ± 359
8.0	1.36E-18 ± 1.97E-18	-3.16E-19 ± -3.06E-19	-1.8E-19 ± -2.0E-19	-1.4E-19 ± 4.4E-19	3.50E-19 ± 1.33E-19	-7479%	323.4493	1161.19 ± 1226
9.0	1.31E-18 ± 2.08E-18	6.47E-20 ± 2.61E-19	-2.6E-19 ± -2.1E-19	-2.9E-19 ± 3.5E-19	4.10E-19 ± 1.32E-19	-9125%	-1852.5235	n/a ± na

Appendix 28 (continued):

Irradiation filename: au5.1h.adl.ih4

%P	40Ar(*±atm)	39Ar(K)	38Ar(Cl±atm)	37Ar(Ca)	36Ar(Atm)	%Rad	R	Age (Ma)
3.0	1.25E-15 ± 7.03E-18	2.82E-18 ± 3.21E-19	6.2E-19 ± 1.7E-19	-7.5E-19 ± 4.9E-19	4.12E-18 ± 1.12E-19	3%	12.1610	60.26 ± 353
3.3	4.87E-16 ± 3.11E-18	2.07E-17 ± 4.11E-19	3.4E-19 ± 6.4E-20	-1.1E-18 ± 3.8E-19	1.29E-18 ± 8.56E-20	22%	5.1477	25.75 ± 6.83
3.6	3.89E-16 ± 3.20E-18	7.82E-17 ± 5.83E-19	8.3E-20 ± 1.7E-20	-1.1E-18 ± 4.1E-19	-1.58E-20 ± -1.34E-19	101%	5.0290	25.16 ± 2.55
4.0	1.97E-15 ± 3.75E-18	2.14E-16 ± 1.15E-18	1.2E-18 ± 4.4E-20	-7.7E-19 ± 4.0E-19	3.50E-18 ± 1.88E-19	47%	4.3608	21.84 ± 1.33
4.3	3.18E-15 ± 3.14E-18	4.33E-16 ± 1.06E-18	2.2E-18 ± 9.7E-20	1.5E-18 ± 5.1E-19	5.92E-18 ± 1.11E-19	45%	3.3074	16.59 ± 0.40
4.5	2.01E-14 ± 1.95E-17	5.78E-15 ± 9.83E-18	1.2E-17 ± 9.6E-20	3.1E-19 ± 4.6E-19	3.61E-18 ± 1.05E-19	95%	3.2837	16.47 ± 0.04
4.8	2.02E-14 ± 9.99E-18	6.12E-15 ± 6.81E-18	1.4E-17 ± 1.4E-19	1.2E-19 ± 5.4E-19	5.73E-20 ± 1.39E-19	100%	3.3043	16.57 ± 0.04
5.0	3.72E-15 ± 2.63E-18	1.11E-15 ± 2.80E-18	2.9E-18 ± 4.7E-20	-1.6E-19 ± 4.8E-19	-5.66E-20 ± -8.24E-20	100%	3.3622	16.86 ± 0.12
5.3	1.50E-15 ± 4.72E-18	4.46E-16 ± 1.03E-18	2.2E-18 ± 1.4E-19	-6.7E-20 ± 5.2E-19	-1.94E-19 ± -1.33E-19	104%	3.4894	17.50 ± 0.45
5.5	9.26E-16 ± 3.80E-18	2.80E-16 ± 2.01E-18	3.2E-19 ± 2.4E-20	1.6E-19 ± 5.2E-19	-4.29E-19 ± -1.28E-19	114%	3.7588	18.84 ± 0.69
5.8	7.19E-16 ± 3.91E-18	2.15E-16 ± 1.13E-18	2.9E-19 ± 2.7E-20	-3.9E-19 ± 4.7E-19	6.04E-20 ± 8.10E-20	98%	3.2603	16.35 ± 0.57
6.0	5.12E-16 ± 3.08E-18	1.54E-16 ± 8.13E-19	3.0E-19 ± 3.6E-20	-2.5E-19 ± 3.9E-19	8.50E-20 ± 8.41E-20	95%	3.1658	15.88 ± 0.82
6.5	8.34E-16 ± 2.86E-18	2.47E-16 ± 1.42E-18	4.8E-19 ± 4.8E-20	-5.5E-19 ± 5.2E-19	6.75E-21 ± 8.31E-20	100%	3.3682	16.89 ± 0.51
7.0	8.71E-16 ± 4.67E-18	2.57E-16 ± 1.06E-18	-1.7E-19 ± -1.8E-20	-2.9E-19 ± 2.6E-19	-6.10E-20 ± -8.05E-20	102%	3.4496	17.30 ± 0.48
8.0	8.60E-16 ± 2.72E-18	2.53E-16 ± 1.25E-18	6.2E-19 ± 3.9E-20	-2.7E-19 ± 3.7E-19	-2.94E-19 ± -1.02E-19	110%	3.7359	18.73 ± 0.60
9.0	2.62E-16 ± 2.41E-18	7.60E-17 ± 6.55E-19	2.0E-19 ± 3.7E-20	-3.0E-19 ± 3.8E-19	5.95E-20 ± 8.46E-20	93%	3.2063	16.08 ± 1.66

Irradiation filename: au5.1h.adl.ih5

%P	40Ar(*±atm)	39Ar(K)	38Ar(Cl±atm)	37Ar(Ca)	36Ar(Atm)	%Rad	R	Age (Ma)
3.0	1.17E-15 ± 5.06E-18	3.26E-18 ± 2.13E-19	1.1E-18 ± 1.6E-19	-4.1E-20 ± 4.0E-19	3.69E-18 ± 1.08E-19	7%	24.6500	120.12 ± 163
3.3	7.90E-16 ± 3.56E-18	5.45E-17 ± 6.40E-19	8.6E-19 ± 1.3E-19	-1.9E-20 ± 4.3E-19	2.09E-18 ± 9.81E-20	22%	3.1822	15.96 ± 2.90
3.6	2.72E-16 ± 3.46E-18	5.22E-17 ± 5.08E-19	5.5E-19 ± 9.9E-20	-6.6E-19 ± 4.0E-19	3.23E-19 ± 7.71E-20	65%	3.3737	16.92 ± 2.23
4.0	5.44E-17 ± 3.00E-18	1.53E-17 ± 3.56E-19	9.2E-19 ± 2.3E-19	6.5E-19 ± 7.1E-19	7.68E-22 ± 6.47E-20	100%	3.5449	17.77 ± 6.36
4.3	5.96E-16 ± 3.01E-18	1.11E-16 ± 1.17E-18	7.7E-19 ± 8.6E-20	3.6E-19 ± 3.6E-19	7.48E-19 ± 8.56E-20	63%	3.3899	17.00 ± 1.20
4.5	1.60E-16 ± 2.79E-18	4.43E-17 ± 5.87E-19	3.4E-19 ± 8.0E-20	4.4E-20 ± 3.3E-19	-1.09E-19 ± -1.24E-19	120%	4.3303	21.69 ± 4.16
4.8	5.79E-16 ± 3.63E-18	1.50E-16 ± 6.80E-19	1.4E-19 ± 2.1E-20	-8.3E-19 ± 4.2E-19	-2.57E-20 ± -1.27E-19	101%	3.9086	19.59 ± 1.27
5.0	1.12E-14 ± 1.13E-17	3.17E-15 ± 4.85E-18	8.2E-18 ± 8.8E-20	-3.1E-19 ± 4.2E-19	2.23E-18 ± 2.01E-19	94%	3.3241	16.67 ± 0.10
5.3	1.44E-14 ± 2.14E-17	4.30E-15 ± 8.94E-18	1.1E-17 ± 7.1E-20	-5.7E-19 ± 4.0E-19	9.13E-19 ± 8.72E-20	98%	3.2771	16.44 ± 0.05
5.5	7.34E-15 ± 6.24E-18	2.20E-15 ± 4.53E-18	6.8E-18 ± 2.1E-19	-2.7E-20 ± 4.2E-19	1.18E-20 ± 1.33E-19	100%	3.3338	16.72 ± 0.10
5.8	1.67E-15 ± 4.45E-18	4.96E-16 ± 1.83E-18	1.8E-18 ± 1.2E-19	-4.0E-19 ± 3.6E-19	2.61E-19 ± 8.58E-20	95%	3.2087	16.10 ± 0.27
6.0	2.36E-15 ± 3.54E-18	7.08E-16 ± 2.51E-18	1.1E-18 ± 5.3E-20	-6.7E-19 ± 3.4E-19	1.87E-19 ± 8.74E-20	98%	3.2571	16.34 ± 0.19
6.5	2.13E-16 ± 2.32E-18	6.26E-17 ± 4.90E-19	3.7E-19 ± 7.8E-20	6.9E-19 ± 3.9E-19	2.44E-19 ± 1.33E-19	66%	2.2546	11.33 ± 3.16
7.0	1.45E-17 ± 1.81E-18	3.81E-18 ± 2.93E-19	1.4E-19 ± 1.6E-19	2.1E-19 ± 3.5E-19	3.56E-19 ± 1.32E-19	-623%	-23.7740	-123.96 ± -54
8.0	1.55E-17 ± 1.46E-18	2.93E-18 ± 2.82E-19	1.7E-19 ± 1.7E-19	2.6E-19 ± 3.4E-19	-1.23E-19 ± -1.69E-19	334%	17.7467	87.28 ± 83
9.0	7.61E-18 ± 1.68E-18	1.08E-18 ± 3.78E-19	5.8E-20 ± 1.9E-19	2.6E-19 ± 3.5E-19	3.17E-19 ± 1.35E-19	-1131%	-79.9909	-456.17 ± -274
10.0	5.54E-18 ± 2.32E-18	2.07E-19 ± 3.26E-19	8.8E-20 ± 1.8E-19	9.6E-19 ± 3.5E-19	-1.28E-19 ± -1.68E-19	780%	209.5503	831.25 ± 1487

Appendix 29: Thin Section Inventory

Box 1	Location	Box 2	Location	Box 3	Location
NSM-00010-13.7	SE Pediment	NSM-00003-299	SE Pediment	NWRA-10433	SE Pediment
NSM-00010-44	SE Pediment	NSM-00010-333	SE Pediment	NWRA-10440	SE Pediment
NSM-00021-47.3	SE Pediment	NSM-00010-384.9	SE Pediment	NWRA-10437	SE Pediment
NSM-00050-7	SE Pediment	NSM-00010-412	SE Pediment	NWRA-10446	SE Pediment
NSM-00010-83.3	SE Pediment	NSM-00010-433.4	SE Pediment	NWRA-10445	SE Pediment
NSM-00010-89.7	SE Pediment	NSM-00010-436.1	SE Pediment	NSM-00021-150	SE Pediment
NSM-00021-101	SE Pediment	NSM-00010-451.4	SE Pediment	NSM-10-130.5	SE Pediment
NSM-00010-107.3	SE Pediment	NSM-00010-460.3	SE Pediment		
NSM-00009-129	SE Pediment	NSM-00010-491.3	SE Pediment	NSM-00175-40.5	Silica Ridge
NSM-00014-130	SE Pediment	NSM-00010-494.7	SE Pediment	NSM-00175-42.1	Silica Ridge
NSM-00010-142.4	SE Pediment	NSM-00010-507.8	SE Pediment	NSM-00175-51.5	Silica Ridge
NSM-00013-152	SE Pediment	NSM-00010-514.6	SE Pediment	NSM-00175-62	Silica Ridge
NSM-00010-148	SE Pediment	NSM-00010-527.4	SE Pediment	NSM-00175-65.7	Silica Ridge
NSM-00010-155	SE Pediment	NSM-00010-527.4	SE Pediment	NSM-00175-68	Silica Ridge
NSM-00011-156.4	SE Pediment	NSM-00010-561	SE Pediment		
NSM-00011-157.6	SE Pediment	NSM-00010-609.5	SE Pediment	H10-48	Adularia Hill
NSM-00010-178.6	SE Pediment	NSM-00010-629.5	SE Pediment	H10-49	Silica Ridge
NSM-00010-205	SE Pediment	NSM-00043-186	Silica Ridge		
NSM-00011-225	SE Pediment	NSM-00004-77	SE Pediment	**Box 7**	**Location**
NSM-00011-225,6	SE Pediment	NSM-00032-121	SE Pediment	NSM-00380-543.9	Abel Knoll
NSM-00010-230	SE Pediment	NSM-00043-261	Silica Ridge	NSM-00380-59.6	Abel Knoll
NSM-00010-247	SE Pediment	NSM-00043-24	Silica Ridge	NSM-00380-622.4	Abel Knoll
NSM-00010-263.3	SE Pediment	NSM-00015-265	SE Pediment	NSM-00380-706.7	Abel Knoll
NSM-10-276	SE Pediment	NSM-00015-268	SE Pediment	8-09-12-1	Pansy Lee
NSM-0003-292.7	SE Pediment	NSM-00004-93	SE Pediment	8-09-12-3	Pansy Lee

Box 4	Location	Box 5	Location	Box 6	Location
NSM-00176-30.2	North Hill	NSM-00034-1	Silica Ridge	9-18-11-9b	Aularia Hill
NSM-00177-92.8	North Hill	NSM-00034-186.9	Silica Ridge	AK-08-0057C-325	Abel Knoll
NSM-00182-32.6	North Hill	NSM-00034-189.2	Silica Ridge	NSM-00082-225.2	SE Pediment
NSM-00183-30.2	North Hill	NSM-00034-193.5	Silica Ridge	NSM-00082-405	SE Pediment
NSM-00177-214.7	North Hill	NSM-00034-203.2	Silica Ridge	NSM-00082-446	SE Pediment
NSM-00177-51.3	North Hill	NSM-00034-214.4	Silica Ridge	NSM-00153-86	SE Pediment
NWRA-10697	North Hill	NSM-00034-222	Silica Ridge	NSM-00185-203	North Hill
19D-NH-bx	North Hill	NSM-00034-234.2	Silica Ridge	NSM-00189-171	North Hill
GXF-20005	North Hill	NSM-00034-240.5	Silica Ridge	NSM-00189-195	North Hill
NSM-00182-288.4	North Hill	NSM-00189-225.4	Silica Ridge	NSM-00270-54	SE Pediment
NSM-00184-196.6	North Hill	9-18-11-7a	Adularia Hill	NSM-00270-76	SE Pediment
NSM-00182-405.4	North Hill	9-18-11-7C	Adularia Hill	NSM-00292-76	North Hill
NSM-00182-552.3	North Hill	9-18-11-14a	Adularia Hill	NSM-00296-30.5	North Hill
16B-Bslt Hills	Basalt Hills	9-25-11-7	Silica Ridge	NSM-00296-502	North Hill
NSM-00182-152.6	North Hill	9-25-11-8	Silica Ridge	NSM-00334-15	Abel Knoll
NSM-00182-223,8	North Hill	9-25-11-9	Silica Ridge	NSM-00334-59.7	Abel Knoll
NSM-00182-114.6	North Hill	9-25-11-10	Silica Ridge	NSM-00380-118.3	Abel Knoll
Aussie 1	Aussie Knob	9-25-11-11	Silica Ridge	NSM-00380-152	Abel Knoll
Aussie 10	Aussie Knob	9-25-11-12	Silica Ridge	NSM-00380-171.8	Abel Knoll
Aussie 20	Aussie Knob	9-25-11-12b	Silica Ridge	NSM-00380-225.3	Abel Knoll
Aussie 4	Aussie Knob	9-25-11-13	Silica Ridge	NSM-00380-239.8	Abel Knoll
Aussie 5	Aussie Knob	NSM-00175-2.5	Silica Ridge	NSM-00380-335.8	Abel Knoll
L Bslt 1	Little Basalt Hills	NSM-00175-9	Silica Ridge	NSM-0038-339.8	Abel Knoll
		NSM-00175-22.5	Silica Ridge	NSM-00380-461.8	Abel Knoll
		NSM-00175-25	Silica Ridge	NSM-00380-492	Abel Knoll

Appendix 30:

Samples collected by Elizabeth Cassel for possible U-Pb Zr dating

Newmont Sample Number	Unversity of Texas Sample #	Location	Lithology	Age inferred from dated units
NSM-00153 (51.7-69.6)	NV12-072SM	Southeast Pediment	Crystal tuff	26.0 Ma (?)
NSM-00189 (225.4-226)	NV12-073SM	North Hill	Nine Hill Tuff	25.4 Ma
NSM-00082 (333-333.4)	NV12-074SM	Southeast Pediment	Pumice tuff	<26.0 Ma
NSM-00297 (497.6-500.6)	NV12-075SM	N of Silica Ridge	Conglomerate	<26.0 Ma
NSM-00297 (459.7-461.5)	NV12-076SM	N of Silica Ridge	Tuffaceous sandstone	<26.0 Ma
NSM-00297 (392.2-394.4)	NV12-077SM	N of Silica Ridge	Conglomerate	<26.0 Ma
NSM-00297 (371.1-373)	NV12-078SM	N of Silica Ridge	Conglomerate	<26.0 Ma
NSM-00297 (287.3-289.3)	NV12-079SM	N of Silica Ridge	Conglomerate and Sandstone	<26.0 Ma
NSM-00297 (249-250.7)	NV12-080SM	N of Silica Ridge	Conglomerate	<25.4 Ma (?)
NSM-00189 (249.2-249.6)	NV12-081SM-A	North Hill	Nine Hill Tuff	25.4 Ma
NSM-00182 (405.1-405.5)	NV12-082SM-B	North Hill	Nine Hill Tuff	25.4 Ma
NSM-00287 (719.3-720.7)	NV12-082SM	S of North Hill	Graphitic phyllite	208.5-228 Ma
NSM-00287 (689.6-691.0)	NV12-083SM	S of North Hill	Quartzite	208.5-228 Ma
NSM-00287 (681-681.5)	NV12-084SM-A	S of North Hill	Quartzite	208.5-228 Ma
NSM-00287 (678-678.5)	NV12-084SM-B	S of North Hill	Phyllitic sharpstone at unconformity	<25.4 Ma
NSM-00287 (649-651)	NV12-085SM	S of North Hill	Conglomerate	<25.4 Ma
NSM-00287 (643.5-645.4)	NV12-086SM	S of North Hill	Phyllitic sharpstone	<25.4 Ma
NSM-00287 (618.2-619.9)	NV12-087SM	S of North Hill	Tuffaceous sandstone	<25.4 Ma
NSM-00287 (590-591.6)	NV12-088SM	S of North Hill	Carbonaceous lacustrine/floodplain	<25.4 Ma
NSM-00287 (553.3-555.3)	NV12-089SM	S of North Hill	Tuffaceous sandstone	<25.4 Ma
NSM-00287 (496.2-498.2)	NV12-090SM	S of North Hill	Conglomerate	<25.4 Ma
NSM-00287 (421.0-422.5)	NV12-091SM	S of North Hill	Phyllitic sharpstone	<25.4 Ma
NSM-00287 (533.5-535.0)	NV12-092SM	S of North Hill	Tuff	<25.4 Ma